

FROM TEST TUBE TO THE HUMAN CELL NUCLEUS: THE NATURE
OF “INVISIBLE” DAMAGE SEARCH TRANSITION STATES OF
HUMAN DNA GLYCOSYLASES

by
Shannen Lee Cravens

A dissertation submitted to Johns Hopkins University in conformity with the
requirements for the degree of Doctor of Philosophy

Baltimore, Maryland

July, 2016

Abstract

The integrity of the genetic code is preserved by maintenance of DNA by glycosylases. These remarkable proteins efficiently repair infrequent lesions amongst a sea of nonspecific target sites. It is well accepted that glycosylases utilize DNA to accelerate their search through DNA chain translocation or “facilitated diffusion”, which reduces dimensionality of the search process. Although DNA translocation has been studied for over 50 years, little attention has been given to how the environment of the cell nucleus affects DNA translocation. It is therefore the goal of my thesis to determine the impact of physiological ions, macromolecular crowding and high concentrations of bystander DNA chains on this important aspect of DNA damage recognition in cells. It is essential to understand the effects of these variables to interpret future *in vivo* experiments of damage recognition in cells.

I began by investigating the effects of high ionic strength on the interactions of human uracil DNA glycosylase (hUNG) with DNA. One salient finding was that shielding of non-specific electrostatic interactions by physiological concentration of salt enhanced the specificity of hUNG for damaged DNA. Nevertheless, the fundamental aspects of DNA translocation by hUNG did not change in the presence of a physiological concentration of salt. I then explored the same question with another paradigm enzyme, human 8-oxoguanine DNA glycosylase (hOGG1). In contrast to hUNG, hOGG1’s non-specific interactions with DNA were not electrostatic in nature, and accordingly, salt had no effect on its specificity for 8-oxoguanine lesions in DNA. These findings revealed that different DNA glycosylases can use entirely distinct non-specific DNA interactions during a damage search process that involves facilitated diffusion.

I then moved to a comprehensive study of the effects of molecular crowding on the DNA interactions of both hUNG and hOGG1 using crowding conditions similar to that found in the cell nucleus. Although crowded solutions have high macroscopic viscosity, which is expected to slow translational diffusion, crowding had no effect on the rate of protein-DNA association. This is attributed to the caging effect of large crowders, which increases the efficiency of macromolecule association once both molecules enter the same caged environment. In addition, the cage provided by macromolecular crowders significantly increases the DNA chain translocation efficiency of both enzymes. Overall, the cage provided by crowders plays an important role in increasing DNA chain translocation under physiological conditions of high salt by introducing a barrier to escape of the enzyme to bulk solution.

Finally, I probed the combined effects of salt, crowding, and high concentrations of bulk DNA chains in damage recognition and translocation. In the presence of excess DNA chains, the rate of repair by hOGG1 was insensitive to solution ionic strength, while the activity of hUNG was greatly stimulated by high salt. These opposite effects are directly related to the different contributions of electrostatics to the binding of non-specific DNA by both enzymes. The general effect of crowding was to promote chain translocation just as observed in the absence of bulk DNA. Overall these studies show that cellular crowding and ion concentrations have important effects on the rate and mechanism of DNA damage search and repair.

Thesis Advisor: James Stivers

Thesis Committee: Scott Bailey, Jungsan Sohn, Albert Lau, Dominique Frueh

Acknowledgements

I have to start by thanking my parents, Mitra and Jim. They have been such avid supporters of my love of science for as long as it can remember. I know it hasn't been easy for them having their youngest daughter on the other side of the country, but it's their belief in making the most of life that brought me here. I thank my sister, Tiffany, and cousins for always being in my corner. Special thanks go to Kathleen for always increasing the age she thought I would graduate each time she saw me. The fact that I'm way younger than her last guess is an accomplishment! To my Aunt Haydeh and Uncle Kuimars for never letting the distance between us hinder their support. To my Aunt Carol and Uncle Bob for welcoming me during a memorable spur of the moment getaway trip. And especially, a huge thank you goes out to my Aunt Pat and Uncle Jim who were my closest family during these past 5 years and my new Thanksgiving home. Being able to get out of Baltimore and away from the stress of graduate school by visiting them has been such a blessing.

I thank one last Jim – my boss, for being an incredible mentor and always pushing me to never accept my current understanding and skill as the limit of my abilities. I am a better scientist and a more confident person for having known him. To my labmates, past and present, for all of the jokes and support that made those failed experiments easier to swallow. To all of my Hopkins friends– they were an incredible support system and I know these friendships will follow us after we leave Baltimore. Thanks are due to my USD family of friends and faculty who have always make me feel at home when I'm back on campus.

To my best friend Alyssa, I thank her for never flinching when I said I was moving away and for never letting our friendship dwindle. Our phone conversations during her commute home were often the highlight of my day.

I thank the man I love, Harman, for being my rock and a voice of encouragement since the day we met in 2012. Finding him here will always be the fondest part of my time in graduate school. He helped me find the strength I needed to tackle the hurdles that came my way, whether it be when an experiment failed (even though biochemistry isn't his thing) or my knee failed. All of our adventures together made it possible for a Southern California girl to love Baltimore and be happy here.

I cannot write my thesis without thanking the women who inspired this journey. I thank Marjan, my high school chemistry teacher, who made me fall in love with atoms. I'm so blessed to call her a friend so many years later. To Debbie, I thank her for getting me involved in research at USD and for providing much needed reality checks. I thank Tammy, the woman who took me under her wing at USD for 4 years and who has inspired me every day since. She helped me find the courage to even consider graduate school.

Though it might be odd, I thank the City of Baltimore for opening the eyes of a privileged Southern California girl to the realities of life's struggles. I am a better human being for having lived here.

I dedicate this thesis to my grandma, Malihe Parsa Scudieri, who passed away earlier this year. Her belief in always reaching your potential was passed on to my mother, who passed it on to me. I know that is why I am here today. This is for you, Grandma!

Table of Contents

Chapter 1. Introduction.	1
1.1. The Biological Context of DNA Repair	2
1.2. A historical perspective on facilitated diffusion	6
1.3. Theoretical and Experimental Basis for Associative ‘Sliding’ Transfers	9
1.4. Theoretical and Experimental Basis for Dissociative ‘Hopping’ Transfers	13
1.5. Ensemble Biochemical Assays Developed to Probe Facilitated Diffusion.....	15
1.6. Counter-ion Condensation Theory	18
1.7. Macromolecular Crowding: Excluded Volume and Solution Viscosity Effects	22
1.8. General Summary of Thesis Chapters	26
1.9. References	33
Chapter 2. Electrostatic properties of complexes along a DNA glycosylase damage search pathway	38
2.1. Introduction	39
2.2. Results	43
2.2.1. Ion Effects on Non-specific DNA Binding	43
2.2.2. Ion Effects on the Binding Equilibrium for Specific DNA	51
2.2.3. Salt Effects on the Kinetics for Binding and Dissociation from Specific DNA	55
2.2.4. Salt Effects on Steady-State Kinetics of hUNG Catalyzed Uracil Excision	60
2.2.5. Increased Salt Concentrations Reduce Probability of Intramolecular Site Transfer	65
2.3. Discussion	69
2.3.1. Electrostatic Contribution to Non-specific DNA Binding is Entropy Driven..	69
2.3.2. Specific DNA Binding is Driven by Non-electrostatic Interactions	73
2.3.3. Association of hUNG with DNA is Accelerated by Electrostatics	74
2.3.4. Dissociation of the Specific Complex is a Multi-step Process.....	75
2.3.5. The Dissociative Facilitated Diffusion Pathway Involves Escape of hUNG from the DNA Ion Cloud	76
2.4. Methods	78
2.4.1. Characterization of 1-[2-Deoxy-5- <i>O</i> -(4,4'-dimethoxytrityl)-2-fluoro-1- β -arabinofuranosyl]uracil.....	78
2.4.2. Oligonucleotide Reagents	79
2.4.3. Expression and Purification of hUNG	80
2.4.4. Oligonucleotide Preparation	81
2.4.5. Experimental Conditions.....	82
2.4.6. Dissociation Constants for DNA Binding using Fluorescence Measurements	82
2.4.7. Stopped-Flow Kinetic Measurements	83
2.4.8. Steady-State Kinetic Measurements.....	84
2.4.9. Intramolecular Site Transfer Assay	85
2.5. References	86

Chapter 3. Consequences of limited electrostatic interactions between repair enzymes and undamaged DNA: The case of human 8-oxoguanine DNA glycosylase.....91

3.1. Introduction	92
3.2. Results	95
3.2.1. Ion Effects on Non-specific DNA Binding	95
3.2.2. Ion Effects on the Binding Equilibrium for Specific DNA	96
3.2.3. Ion Effects on Binding of hOGG1 to DNA containing 8-oxoguanine	104
3.3. Discussion	106
3.3.1. Salt Effects on DNA Binding in the Absence of Crowding or Bulk DNA ...	106
3.3.2. Relating Salt Effects to the Efficiency of Damage Recognition	106
3.4. Methods	108
3.4.1. Experimental Conditions	108
3.4.2. Oligonucleotide Reagents	109
3.4.3. hOGG1 Equilibrium DNA Binding Measurements	80
3.4.4. Salt Dependence of DNA Binding	81
3.4.5. K249Q Activity Assay	82
3.5. References	86

Chapter 4. Molecular crowding enhances facilitated diffusion of two human DNA glycosylases115

4.1. Introduction	116
4.2. Results	118
4.2.1. Crowding Effects on DNA Translocation	118
4.2.2. Crowding Primarily Enhances the Associative Transfer Pathway.....	127
4.2.3. Crowding Effects on Translocation of hOGG1	130
4.2.4. Effects of a Protein Crowder on Translocation	135
4.2.5. Crowding Decreases Turnover of hUNG with Large DNA Substrates	136
4.2.6. Crowding has Little Effect on Non-specific DNA Binding	142
4.2.7. Crowding Effects on the Association Rate with a Specific Site	144
4.2.8. Crowding Effects on the Dissociation Rate from a Specific Site (D^s)	149
4.3. Discussion	152
4.3.1. Translational Diffusion from Bulk Solution to DNA.....	152
4.3.2. Associative Transfer Steps	153
4.3.3. Dissociative Transfer Steps	154
4.3.4. Departure to Bulk Solution.....	155
4.3.5. Damage Search and Repair in the Cell Nucleus.....	155
4.4. Methods	158
4.4.1. Experimental Conditions	158
4.4.2. hOGG1 Expression and Purification.....	158
4.4.3. Measurement of hOGG1 Reaction Rates	160
4.4.4. Site Transfer Assay.....	160
4.4.5. hUNG Equilibrium DNA Binding Measurements	162

4.4.6. hUNG Stopped Flow Measurements	162
4.4.7. hUNG Steady-State Kinetic Measurements	164
4.4.8. Ion Activity Measurements	165
4.4.9 DNA Sequences	165
4.4.10. Calculation of Depletion Layer Sizes	167
4.4.11. Effect of Hemoglobin on Translocation of hUNG	168
4.5. References	172
Chapter 5. Differential Effects of Ions, Molecular Crowding, and Solution DNA Density on the Damage Search Mechanism of hOGG1 and hUNG	176
5.1. Introduction	177
5.2. Results	179
5.2.1. Environmental Effects on DNA Translocation by hOGG1	179
5.2.2. Environmental Effects on Steady-State Turnover of hOGG1	185
5.2.3. Environmental Effects on DNA Translocation of hUNG	188
5.2.4. Environmental Effects on Steady-State Turnover of hUNG	193
5.3. Discussion	196
5.3.1. Salt Effects on DNA Translocation in the Absence of Crowding or Bulk DNA	196
5.3.2. Salt Effects on Turnover in the Absence of Crowding or Bulk DNA	197
5.3.3. Impacts of Inert Macromolecule Crowding on the Salt Effect	198
5.3.4. Bulk DNA Effects on Translocation and Turnover	199
5.3.5. Glycosylase Activity in a Cellular Environment	203
5.4. Methods	204
5.4.1. Experimental Conditions	204
5.4.2. Oligonucleotide Reagents	205
5.4.3. Site Transfer Assay	206
5.4.4. Turnover Rate Determination	207
5.4.5. hUNG Transfer Bias at High Salt	208
5.5. References	210
Chapter 6. Concluding Remarks	213
Chapter 7. Appendix	218
7.1. Overview of hOGG1+APE1 investigation	219
7.2. Literature Review of hOGG1 interactions with APE1	220
7.3. Preliminary Data	221
7.4. Generation of inducible hOGG1 cell line	232
7.5. References	235
Curriculum Vitae	236

List of Figures

Figure 1.1. The Base Excision Repair Pathway.....	27
Figure 1.2. Facilitated Diffusion: Associative and Dissociative Translocation	28
Figure 1.3. Mathematical Representation of Associative Transfers	29
Figure 1.4. Schematic of the Molecular Clock assay	30
Figure 1.5. The Site Transfer assay	31
Figure 1.6. Representations of molecular crowding agents in solution	32
Figure 2.1. The hUNG DNA search and repair pathway	42
Figure 2.2. Salt dependence of the non-specific DNA (D^N) equilibrium binding affinity	46
Figure 2.3. Salt dependence of the non-specific DNA (D^N) equilibrium binding affinity at high salt concentrations.....	47
Figure 2.4. Salt dependences of the specific DNA (D^S) association and dissociation constants and equilibrium binding affinity determined by stopped-flow fluorescence	53
Figure 2.5. Binding affinity (K_D) of the specific substrate determined by fluorescence titration at varying salt concentrations.....	54
Figure 2.6. Salt dependence of the association (k_{on}) and dissociation (k_{off}) kinetics of hUNG binding to specific DNA (D^S)	58
Figure 2.7. Michaelis-Menten curves of the initial rates of reaction with PUA-30 as a function of DNA concentration	62
Figure 2.8. Salt dependences of k_{cat} , K_m , and k_{cat}/K_m	63
Figure 2.9. Salt dependence of the intramolecular dissociative transfer probability of hUNG between two uracil sites spaced 20 bp apart (P_{diss}).....	67
Figure 2.10. Salt dependence of the nonspecific DNA binding affinity at various temperatures	71
Figure 2.11. Summary of the salt dependences of each measured thermodynamic and kinetic parameter (X).....	72
Figure 3.1. Schematics of undamaged and damaged DNA bound to hOGG1	99
Figure 3.2. Salt dependence of the non-specific and specific DNA binding affinity determined by fluorescence anisotropy	100

Figure 3.3. Salt dependence of the non-specific DNA binding affinity of hOGG1 at various salt concentrations using the indicated DNA sequences	101
Figure 3.4. Salt dependence of the non-specific DNA binding affinity of K249Q at various salt concentrations	105
Figure 4.1. Approach for measuring site transfer probabilities of hUNG and hOGG1 ..	123
Figure 4.2. Effect of molecular crowding agents on the site transfer probability (P_{trans}) of hUNG between uracil lesions spaced 20 bp apart	124
Figure 4.3. Molecular trap concentration control	128
Figure 4.4. Effect of 20% PEG 8K on the intramolecular site transfer probability between uracil sites of variable spacing	129
Figure 4.5. Reaction rates in dilute buffer, 20% (w/v) PEG 8K, and 5% (w/v) hemoglobin	132
Figure 4.6. Effect of 20% PEG 8K and 5% hemoglobin on the site transfer probability of hOGG1 over a 20 bp spacing (P_{trans})	133
Figure 4.7. The effect of molecular crowding agents on the steady-state kinetics of hUNG acting on short and long duplex DNA substrates.....	139
Figure 4.8. Binding affinity (K_D) of hUNG for nonspecific DNA (D^N , 100 nM) in the presence and absence of 20% PEG 8K.....	143
Figure 4.9. Influence of PEG 8K on association kinetics of hUNG from specific DNA (D^S) determined by stopped-flow 2-aminopurine fluorescence measurements at 20 °C.....	146
Figure 4.10. General schematic of how the introduction of molecular crowders can influence individual steps in the DNA glycosylase damage search pathway.....	156
Figure 4.11. Effect of hemoglobin on the site transfer probability (P_{trans}) of hUNG between uracil lesions spaced 20 bp apart	171
Figure 5.1. Site transfer probabilities and kinetic activity of hOGG1 in the presence of variable cosolutes	183
Figure 5.2. Example gels of hOGG1 reacting with S20 ^{oxoG} under various solution conditions.....	186
Figure 5.3. Site transfer probabilities and kinetic activity of hUNG in the presence of variable cosolutes.....	190

Figure 5.4. Effect of salt concentration on the site transfer probability of hUNG between uracil lesions spaced 5 bp apart	191
Figure 5.5. Example gels of hUNG reacting with S20 ^U under various solution conditions	194
Figure 5.6. Summary of the effects of salt, molecular crowding, and bulk DNA on each measured thermodynamic and kinetic parameter	201
Figure 6.1. Model of the DNA Search-and-Repair Pathways of hUNG and hOGG1 in the Cellular Environment.....	217
Figure 7.1. hOGG1 remains tightly bound to product DNA	221
Figure 7.2. Reactions containing APE1 require buffer devoid of EDTA and a minimum of 1mM MgCl ₂	222
Figure 7.3. Addition of APE1 rescues hOGG1 regardless of ionic strength	223
Figure 7.4. Addition of APE1 has no effect on P_{trans}	224
Figure 7.5 Example gels of hOGG1 reacting with S20 ^{oxoG} with and without APE1.....	225
Figure 7.6. Reaction scheme for hOGG1-DNA covalent complex trapping.....	226
Figure 7.7. Controls to determine appropriate NaBH ₄ concentration and timing of SDS quench addition	227
Figure 7.8. Addition of 100 nM APE1 is sufficient for maximal effect on hOGG1	228
Figure 7.9. Addition of APE1 reduces the lifetime of the hOGG1 covalent complex ...	229
Figure 7.10. Effect of active and inactive APE1 on turnover and covalent complex lifetime	230
Figure 7.11. Covalent complex trapping using hOGG1 and pre-formed abasic DNA ...	231
Figure 7.12. Digestion of pCW57.1 before and after homologous recombination step .	233
Figure 7.13. Test induction of hOGG1 expression using doxycycline	234

List of Tables

Table 2.1. Analysis of the salt dependences of the thermodynamic and kinetic parameters using eq 2.1	48
Table 2.2. Binding affinities of hUNG and non-specific DNA ($1/K_a^N$) at variable salt concentration.....	49
Table 2.3. Electrostatic (ΔG_{elec}) and non-electrostatic (ΔG_{non}) contributions to the binding free energy (ΔG_{bind}) for non-specific (D^N) and specific (D^S) hUNG complexes in the presence of 150 mM K^+	50
Table 2.4. Specific DNA binding affinities ($1/K_a^S$) and association (k_{on}) and dissociation (k_{off}^S) rate constants for hUNG as a function of $[K^+]$	59
Table 2.5. Steady-state kinetic parameters of hUNG and specific DNA at various salt concentrations	64
Table 2.6. Probability of site transfer (P_{trans}) between two uracils with 20 base pair spacing at varying salt concentrations	68
Table 3.1 Binding affinities ($K_D = 1/K_a$) of hOGG1 for nonspecific DNA and specific DNA sequences at various concentrations of potassium ions	102
Table 3.2. Analysis of the salt dependences of non-specific and specific binding of hOGG1	102
Table 3.3. Binding affinities ($K_D = 1/K_a$) of hOGG1 for multiple nonspecific DNA sequences at various concentrations of potassium ions	103
Table 3.4. Electrostatic (ΔG_{elec}) and non-electrostatic (ΔG_{non}) contributions to the binding free energy (ΔG_{bind}) for non-specific (D^S , D^{TATA} , D^{GC} , D^{GCCG}) and specific (D^S) hOGG1 complexes in the presence of 150 mM K^+	103
Table 4.1. Solution viscosities at 25 °C for varying amounts of EG, PEG 600, PEG 3350, and PEG 8K	125
Table 4.2. P_{trans} , P_{assoc} , and P_{diss} for hUNG in the presence and absence of 20% PEG 8K	126
Table 4.3. Sodium ion activity in the presence and absence of 20% PEG 8K	126
Table 4.4. Effect of 20% PEG 8K on P_{trans} , P_{assoc} , and P_{diss} for hOGG1 ($S20^{oG}$)	134
Table 4.5 Effects of EG and PEG 8K on the steady-state kinetic parameters of hUNG with short and long DNA substrates	141
Table 4.6. Specific DNA association rates (k_{on}) for hUNG in the presence of a variety of molecular crowding agents compared to the predicted rate from the Stokes-Einstein relation (k_{on}^{SE}).....	148

Table 4.7. Rate constants and amplitudes for slow and fast kinetic phases for the biphasic dissociation of hUNG from specific DNA in the presence of various amounts of PEG 8K	151
Table 5.1. Effect of 20% PEG 8K, and salmon sperm DNA (salDNA) on the site transfer probability (P_{trans}) of hOGG1 at 30 mM potassium ions	184
Table 5.2. Effect of 20% PEG 8K, and salmon sperm DNA (salDNA) on the site transfer probability (P_{trans}) of hOGG1 at 150 mM potassium ions	184
Table 5.3. Reaction rates (k_{obs}) with S20 ^{oxoG} in the presence of salt, 20% PEG 8K, and salmon sperm DNA (salDNA) for hOGG1	187
Table 5.4. Effect of salt, 20% PEG 8K, and salmon sperm DNA (salDNA) on the site transfer probability (P_{trans}) of hUNG at 22 mM potassium ions	192
Table 5.5. Effect of salt, 20% PEG 8K, and salmon sperm DNA (salDNA) on the site transfer probability (P_{trans}) of hUNG at 150 mM potassium ions	192
Table 5.6. Reaction rates (k_{obs}) in the presence of salt, 20% PEG 8K, and salmon sperm DNA (salDNA) for hUNG	195

Chapter 1: Introduction

1.1 The Biological Context of DNA Repair

DNA is under constant assault by errors in replication and a variety of chemical insults that result in a plethora of base lesions including alkylation, oxidation, deamination, and numerous other modifications^{1, 2}. While the frequency of these damaged bases is minimal within the vast background of billions of base pairs that make up cellular DNA, the persistence of these modifications poses an intolerable threat to the stability and preservation of the genomic DNA code. It is therefore of utmost importance that the information content of DNA be protected from persistent damage.

The central mechanism by which the genomic DNA sequence is maintained is through a cellular processes called base excision repair (BER)^{1, 2, 3}. The first step in this pathway is an exhaustive search of DNA by specialized enzymes known as DNA glycosylases that are responsible for scanning genomic DNA for infrequent lesion sites. Upon recognition of their target lesion, these enzymes catalyze cleavage of the glycosidic bond. The resultant abasic sites within the DNA trigger a cascade of additional enzymes that repair the nucleic acid in a step-wise fashion. Endonucleases incise the phosphate backbone at the abasic site, polymerases fill in the correct nucleotide, and ligases finish the job by resealing the break in the DNA strand (**Figure 1.1**).

Uracil, which is a standard RNA base, is a commonly observed form of damage when found within a DNA sequence^{4, 5}. Misincorporation of dUTP instead of dTTP by DNA polymerases and the spontaneous deamination of cytosine can result in steady-state levels of $10^3 - 10^6$ uracils per genome depending on the cell type, though the higher levels detected originate from studies conducted using perturbations such as thymidylate synthase inhibitors and inactive dUTPase mutants to elevate dUTP levels and increase the likelihood

of uracil misincorporation^{5,6,7,8}. Uracil that persists within DNA due to misincorporation typically results in U:A pairs, while deamination of cytosine generates U:G mispairs^{4,5}. The persistence of U:G pairs eventually leads to C:G → T:A transition mutation as polymerases efficiently incorporate an adenine across from uracil bases encountered in the template strand during replication. In order to prevent the possibility of this mechanism of mutagenesis, efficient repair of uracil damage is necessary. The more prevalent form of uracil damage within DNA is in the context of U:A base pairs, which is primarily dictated by the ratio of dUTP:dTTP pool levels since DNA polymerases cannot distinguish between these two deoxynucleotides. While not mutagenic in nature, U:A pairs still require efficient repair due to the fact that they directly lead to genomic instability from strand breaks produced during BER^{9,10,11,12}.

The removal of uracil from genomic DNA is handled by the UDG superfamily of glycosylases. In mammals, four enzymes are responsible: UNG, SMUG1, TDG, and MBD4. Each enzyme is tailored to primarily recognize uracil within specific sequence contexts. UNG and SMUG1 preferentially cleave uracil within single-stranded DNA, but do have efficient reactivity within the context of a DNA duplex. In contrast, TDG and MBD4 only recognize uracil within double-stranded DNA (dsDNA). UNG also displays preferential activity on the more prevalent form of uracil damage, the U:A pair, caused by errant processing of dUTP by polymerases. It has been proposed that SMUG1 primarily repairs uracil damage arising from spontaneous deamination. The activity of TDG and MBD4 is potentially relegated to repair of mismatches involving uracil, thymine, and other damaged pyrimidines within dsDNA¹³. UNG is considered to be the primary uracil-acting

glycosylase given that it is the most active and most heavily conserved across the vast majority of living organisms^{14, 15}.

Oxidation of DNA is another common form of damage that results from reaction with reactive oxygen species (ROS)¹⁶. In living cells, ROS arise from both metabolic reactions and external factors, generating a vast array of oxidative modifications to DNA bases (including uracil) and single- and double-strand breaks. Of the many potential oxidative adducts, 8-oxoguanine (8-oxoG or ^{oxo}G) is the most abundant in the cell with a steady-state level ranging from 0.07 – 147 adducts per 10⁶ nucleotides in human cells¹⁷. During DNA replication, 8-oxoG has been found to preferentially pair with adenine, resulting in G:C → T:A transversion mutations if the damaged base persists within the template strand¹⁶.

Much like uracil, 8-oxoG is recognized by a variety of glycosylases that preferentially excise the damaged base depending on its sequence context. In humans, repair of 8-oxoG is carried out by hOGG1, MYH, hOGG2, and NEIL1^{18, 19, 20}. With the exception of hOGG1, 8-oxoG-recognizing glycosylases primarily target the oxidized base when mispaired with either adenine or guanine. hOGG1 is considered to be the major repair enzyme for 8-oxoG:C pairs, has no activity toward 8-oxoG:A or G:C pairs, and works primarily on non-transcribed sequences. Unlike hUNG, hOGG1 has been deemed a bifunctional glycosylase due to its apparent AP-lyase activity and is constitutively expressed^{18, 19, 20}. Glycosylases that recognize oxidized DNA damage are conserved across all kingdoms of life, much like the uracil repair machinery.

The importance of DNA repair is made clear by the dire consequences of persistent damage and the presence of glycosylases in all species. It is therefore of great interest to

understand the fundamental principles of the search-and-repair mechanism used by these essential enzymes. In order to devise a comprehensive model of glycosylase functionality, I have developed a comparative study of hUNG and hOGG1. These enzymes were chosen in particular as they are the most well studied human representatives of the two largest glycosylase superfamilies – the UDG superfamily (hUNG) and Helix-hairpin-Helix GPD (HhH-GPD) superfamily (hOGG1). These enzymes are structurally very distinct and have independently evolved to perform the same daunting task of perusing the genome for infrequent, but lethal DNA lesions²¹.

The “DNA search problem” is encountered by all enzymes that must localize to specific, low-frequency target sites within the high background of genomic DNA. Additional complexity is added to the search embarked on by glycosylases due to the fact that these enzymes are not targeting a consensus sequence, but rather a single base that can exist within any sequence context. It has been historically accepted that glycosylases enhance their searching capabilities by reducing the dimensionality of the search through a process known as “facilitated diffusion.” The two primary mechanisms of this process are “associative transfer” (historically called sliding) and “dissociative transfer” (historically called hopping) steps along the DNA chain (**Figure 1.2**)²². The associative transfer pathway refers to a state in which the enzyme remains associated with the DNA chain as it processes in a random walk. The dissociative transfer pathway involves dissociation of the enzyme from the DNA chain and diffusion outside of the DNA ion cloud before reassociation. The terms “associative” and “dissociative” transfer are used throughout this thesis in place of the historical “sliding” and “hopping”, respectively to account for recent discoveries involving intramolecular translocation by DNA glycosylases

that deviates from the criteria established by the older terminology^{23, 24, 25}. While facilitated diffusion was first observed nearly 50 years ago, our knowledge of the microscopic details of these pathways and the effects of macroscopic solution properties on the search-and-repair mechanism is limited.

The majority of studies conducted on DNA glycosylases utilize low ionic strength, dilute buffer conditions that are easy to work with, but fail to model the environment encountered within the cell^{26, 27, 28, 29}. It is not beyond reason to believe that the significant concentration of monovalent cations and macromolecules within the cell nucleus could have a dramatic effect on both the thermodynamic and kinetic aspects of the DNA search-and-repair pathway. The goal of my thesis is to build off of the fundamental knowledge of uracil and 8-oxoG repair developed in the Stivers' lab by systematically investigating the influence of ionic strength, macromolecular crowding, solution viscosity, and undamaged DNA density on the search and repair pathways of hUNG and hOGG1. The detailed comparison between these two distinct glycosylases will serve as a means to develop a model of how the cellular environment modulates DNA repair.

1.2 A Historical Perspective on Facilitated Diffusion

The magnitude of the search problem encountered by glycosylases can be quantified by considering the number of DNA glycosylase molecules in the cell and the frequency of their target lesions. Both hUNG and hOGG1 exist in a relatively high copy number ($\sim 10^5$) and the average steady-state levels of uracil and 8-oxoG are $\sim 10^4$ per genome. Given that the human genome size is on the order of 10^9 base pairs, each glycosylase molecule is charged with searching $\sim 10,000$ bases within which one lesion site

might be encountered. While copy number alone already reduces the size of the search, the scanning of those 10,000 bases must be done within the timeframe of the cell cycle.

The rate of a biomolecular reaction is in principle limited by the rate at which two species will diffuse freely in solution and encounter one another. The encounter probability of two species, A and B, can be quantified from the relationship between the size of the interacting species, represented as spheres, and the fractional reactive surface area. This relationship is summarized by the Smoluchowski equation (eq. 1.1)^{30, 31, 32}

$$k_{A+B \rightarrow AB} = \frac{N_o 4\pi(D_A + D_B)(r_A + r_B)}{1000} \quad (1.1)$$

where D_a and D_b are the diffusion constants of A and B in $\text{cm}^2 \text{s}^{-1}$, r_a and r_b are the hydrodynamic radii of the spherical models in cm, N_o is Avagadro's number, and the factor of 1000 normalizes the rate constant to units of $\text{M}^{-1} \text{s}^{-1}$. The diffusion constants for each species can be theoretically calculated based on size, temperature, and solution viscosity (η) using the Stokes-Einstein relation (eq 1.2).

$$D = \frac{kT}{6\pi r \eta} \quad (1.2)$$

The Smoluchowski equation is a simplified model that does not fully characterize the nature of diffusion for biological macromolecules. Modifications to the equation are required in order to include consequences of i) non-uniform reactive surface area, ii) the non-spherical nature of biological particles, iii) electrostatic attractive and repulsive forces between molecules, and iv) that the interaction distance may not be simply the sum of the hydrodynamic radii of A and B. With these correction factors in place, theoretical target searching rates by DNA-binding proteins utilizing only 3D diffusion can be estimated. This

was done previously for the lac repressor, which resulted in a diffusion-controlled reaction rate of $\sim 10^8 \text{ M}^{-1} \text{ s}^{-1}$ ²².

In 1968, Riggs *et al* experimentally measured an association rate of lac repressor with its target operator DNA sequence on the order of $10^{10} \text{ M}^{-1} \text{ s}^{-1}$. The large, reproducible discrepancy between the theoretical association rate and the experimentally derived value indicated an additional mechanism to the search process not accounted for by 3D diffusion. The fact that the experiments with lac repressor were carried out using DNA in which the operator site was buried within 50,000 base pairs of non-cognate DNA created initial suspicion that the enzyme was utilizing the excess DNA to accelerate its search process. Riggs and others proposed that lac repressor was able to translocate along the non-cognate DNA it initially encountered in a 1-dimensional search, rather than relying solely on 3D diffusion^{33, 34, 35}.

The process of utilizing non-target DNA sites as a guiding conduit to reduce the dimensionality of the search process and enhance the association rate is known as “facilitated diffusion.” Since its proposal nearly 50 years ago, a large body of work has been generated by numerous labs to describe a variety of searching mechanisms, including the *sliding* and *hopping* translocation pathways²². *Sliding* was the first proposed by Adam and Delbruck³⁶, mathematically formulated by Richter and Eigen³⁴, and experimentally characterized by Berg and von Hippel^{22, 37}. The sliding process is best described as a one-dimensional search carried out by a loosely associated enzyme molecule diffusing along the DNA chain. The sliding process is facilitated by the use of thermal energy to overcome the relatively small activation barrier of translocation. *Hopping* was defined by Berg as a *microscopic* dissociation event of a protein from DNA in which the protein molecule

remains near the original site and, though it is free to diffuse in any direction, reassociates with a nearby site with a high probability. This process allows a protein molecule to explore longer stretches of DNA within its *macroscopic* bound lifetime. These two mechanisms are not viewed as mutually exclusive as Berg and others proposed that the most efficient search process would involve a combination of sliding and hopping^{22, 31, 37, 38}. The 1D sliding mechanism allows for close inspection of short, DNA fragments that leads to eventual recognition while the 3D hopping pathway limits the potential redundancy of the sliding model by promoting search over longer stretches of DNA (**Figure 1.2**).

Our understanding of facilitated diffusion is rooted in decades of theoretical and experimental dissection for a number of DNA-binding proteins, including glycosylases; however, our knowledge is limited primarily to ideal solution conditions. Dilute, low ionic strength buffers promote favorable interactions between proteins and DNA and are easy to work with given their low solution viscosity, but they fail to mimic the environment encountered by these enzymes within the cell nucleus. It is, therefore, of great interest to investigate how components of the cellular environment might modulate both the kinetic and thermodynamic aspects of the search-and-repair process individually and cooperatively. In the following sections, I describe our current fundamental understanding of various facilitated transfer mechanisms and provide the theoretical basis for how I will test if our current model of facilitated diffusion can persist within the complex solution conditions encountered in the cell.

1.3 Theoretical and Experimental Basis for Associative ‘Sliding’ Transfer

Associative transfer involves a one-dimensional search in which an enzyme molecule ‘slides’ along the contour length of a DNA helix. In this mechanism, an enzyme

will sample linearly contiguous binding sites with no preferential bias to step left or right from its initial position. This random walk is then interrupted either by a conformational change in the enzyme upon recognition of a target site or the dissociation of the enzyme molecule. The probability of an enzyme associatively transferring (P_{assoc}) along the DNA is therefore a kinetic interplay between the rate of 1D translocation (k_{assoc}) and the rate at which it falls off the DNA chain (k_{off}) (eq 1.3).

$$P_{\text{assoc}} = \frac{k_{\text{assoc}}}{k_{\text{off}} + k_{\text{assoc}}} \quad (1.3)$$

In order for rapid sliding to be possible, the transition from one site on the DNA chain to the next must have a negligible energetic barrier ($\sim 1-2 \text{ k}_b\text{T}$)^{30, 39}. An unbiased random walk would also require the energy landscape of the DNA surface to be relatively flat. This is an unlikely scenario given that charged phosphate groups distributed along the DNA chain create a non-uniform interaction surface. To overcome this caveat, von Hippel proposed that “out of register” charged moieties along the enzyme binding surface would generate an isopotential interaction surface that would allow the enzyme to slide without friction regardless of its position on the DNA²².

According to Schurr in 1979, a theoretical upper limit of the 1D diffusion rate of an enzyme sliding along DNA can be calculated simply from hydrodynamic considerations. Associative translocation requires that the enzyme rotate 360° around the helical pitch of the duplex every 10 basepairs in order for the interacting face of the enzyme to remain in contact with the phosphate backbone. This spiraling motion impacts a hydrodynamic drag on the enzyme molecule and has been shown to have a substantial effect on the diffusion rate. Indeed, the theoretical maximal ‘rotation-coupled’ diffusion

rate of an enzyme was calculated to be $\sim 10^7 \text{ bp}^2 \text{ s}^{-1}$ which is slower than the typical free translational diffusion rate by two orders of magnitude^{40, 41}.

In the case of DNA glycosylases, an upper limit of the associative diffusion rate can be calculated from the bound lifetime of the enzyme (τ_{bind}) and the average length it slides (L_{slide}) along the chain before dissociating (eq 1.4).

$$D_1 = \frac{L_{\text{slide}}^2}{\tau_{\text{bind}}} \quad (1.4)$$

For hUNG, the bound lifetime on undamaged DNA ($\tau_{\text{bind}} = 3 \text{ ms}$) and mean sliding length ($L_{\text{slide}} = 4.2 \text{ bp}$) results in a 1D diffusion rate of $6 \times 10^3 \text{ bp}^2 \text{ s}^{-1}$, which is lower than the theoretical limit proposed by Schurr⁴². In the case of hOGG1, single molecule studies have reported a diffusion rate of $2\text{-}5 \times 10^6 \text{ bp}^2 \text{ s}^{-1}$ ²⁶. Translocation by hOGG1 has been assumed to be frictionless due to the fact that the 1D diffusion rate approaches the maximal value proposed by Schurr. It must be noted that the limited spatial resolution of single molecule imaging results in a rate estimation that also includes cycles of 3D dissociative transfer events that are “blurred” together with the 1D associative transfer steps. The inclusion of indistinguishable 3D diffusion events in the 1D diffusion rate causes D_1 to be estimated as faster than reality given the more rapid nature of 3D diffusion relative to 1D diffusion.

It is not entirely surprising that experimentally derived associative transfer rates deviate substantially from the theoretical upper limit. The assumption that DNA behaves as an isoenergetic, frictionless surface is not easily reconcilable with the fact that the energetics of non-specific DNA-protein binding interactions are on the order of 10-15 $k_B T$ and that numerous hydrogen bonding donors and acceptors are found throughout a DNA

molecule^{30, 39}. The formation of even a single hydrogen bond, which contributes to the large interaction potential with undamaged DNA, would produce a significant energetic barrier to rapid translocation. It is therefore necessary to hypothesize an additional state of the protein that deviates substantially from its bound form. It has previously been proposed that an enzyme molecule undergoing associative sliding events occupies two potential conformations: a loosely bound ‘search’ mode and a ‘recognition’ mode consistent with the tightly bound crystallographic models^{30, 39, 43}. Previous work in the Stivers lab by Friedman *et al* showed by NMR that free hUNG in solution has no intrinsic dynamics (nanosecond – millisecond time scales); however, binding to nonspecific DNA induces dynamic motions on the millisecond timescale. These motions have been attributed to the transition of the enzyme between a closed conformation and a loosely bound, open conformation⁴⁴. It has also been shown that the introduction of methyl phosphonate linkages to reduce the phosphate backbone charge density between damage sites did not affect the ability of hUNG to translocate, which is consistent with the mobile form of the enzyme being loosely associated with the DNA²³. Associative transfers are therefore best defined as free diffusion along the DNA chain during the transition state for dissociation. The completion of an associative transfer event occurs when the open enzyme molecule closes on the DNA chain rather than diffusing into bulk solution.

The discussion of the nature of a sliding enzyme molecule up to this point does not take into consideration the possible effects of the cellular environment. Given that nonspecific interactions between proteins and DNA are largely electrostatic in nature, the counterion cloud that surrounds the polyanionic DNA chain could mediate the ability of a glycosylase to productively translocate. In principle, ions needing to be displaced from the

DNA by the loosely associated ‘search’ state of a DNA glycosylase could render the enzyme sensitive to local fluctuations in the counterion content surrounding the DNA. These ions would technically re-condense behind the enzyme as it continues traversing along the DNA chain, resulting in a zero net ion displacement, which could in fact render the associative transfer pathway impervious to changes in ionic strength²². Additional nuclear solution features that must also be considered are molecular crowding and excluded volume. The presence of significant concentrations of other species that limit the volume available to the DNA and glycosylase could potentially favor the associative transfer mechanism due to the compact nature of sliding search states. It is thus of great relevance to investigate how this transient search mode responds to changes in the ionic strength and the crowded state of its solution environment in order to better understand translocation in a relevant context.

1.4 Theoretical and Experimental Basis for Dissociative ‘Hopping’ Transfers

While associative translocation along DNA is rather complex, a rather simple model is sufficient to characterize the nature of three-dimensional dissociative ‘hopping’ transfers. Short-range dissociation and re-association events are largely governed by diffusion as the probability of productively executing a dissociative transfer (P_{diss}) is defined by the likelihood that a dissociated enzyme molecule will re-bind the DNA chain rather than diffuse into bulk solution. The kinetic description of this model is captured in eq 1.5⁴²

$$P_{\text{diss}} = \left(\frac{k_{\text{off}}}{k_{\text{assoc}} + k_{\text{off}}} \right) \left(\frac{k_{\text{return}}}{k_{\text{bulk}} + k_{\text{return}}} \right) \quad (1.5)$$

where k_{bulk} is the translational diffusion rate of the enzyme in bulk solution and k_{return} is the association rate of the enzyme with the initial DNA strand. The first term represents the likelihood that the enzyme will dissociate from the DNA chain, rather than undergoing an associative transfer step, and the second term represents the likelihood of the enzyme returning to the DNA strand.

Theoretical calculations supported by Monte Carlo simulations have been used in the Stivers lab to predict the length scales that best characterize dissociative transfer events of both hUNG and hOGG1²⁵. In the case of hUNG, the maximal distance of a hopping event (r_{diss}) was calculated based on the experimentally derived lifetime of a hop (τ_{diss}) and the 3D diffusion rate (D_3) using **eq 1.6**.

$$\langle r_{\text{diss}} \rangle = \sqrt{6D_3\tau_{\text{diss}}} \quad (1.6)$$

hUNG was determined to hop a maximum distance of 7 nm from the DNA, which requires that the enzyme molecule fully remove itself from the condensed ion environment surrounding the nucleic acid prior to reassociating⁴². This same calculation predicted a ~3 nm distance for hOGG1, which was substantiated by simulations predicting hOGG1 would move ~5 nm on average during a dissociative transfer event²⁵. Should an enzyme molecule move beyond 10-20 nm, it is unlikely that it will return to its initial DNA target and will instead continue to freely diffuse through bulk solution. The finite lifetime of the free enzyme prior to reassociation (nanoseconds to microseconds) also indicates that hopping distances along the DNA chain are only on the order of a few nanometers. Dissociative transfers are best described as rapid, short-range movements in three dimensions along a DNA chain.

Unlike associative transfer, dissociative transfers require an enzyme molecule to move away from its initial target strand and sample both the highly condensed ionic environment of the DNA periphery and the surrounding bulk solution. A potentially significant net ion displacement upon reassociation with the DNA chain could render searching enzyme molecules very sensitive to the surrounding counterion concentrations. It is also possible that the large volume occupied by the dissociated state of the enzyme molecule would be inhibited by the introduction of volume excluding crowding agents. It is likely that this transient search state would be sensitive to both ionic strength and molecular crowding conditions encountered inside the nucleus, though this avenue has yet to be explored with any degree of detail.

1.5 Ensemble Biochemical Assays Developed to Probe Facilitated Diffusion

While the historic observation of a rapid target localization and slower than predicted diffusion rate of *lac repressor* was suggestive of facilitated diffusion, recent decades have led to the development of biochemical assays to characterize translocation in detail. I will limit my discussion to just the origin of a vital assay utilized in my thesis.

In 1985, Paul Modrich published a study on EcoRI that provided strong evidence of this DNA-modifying enzyme's ability to processively track along a DNA chain⁴⁵. The assay developed utilized a DNA substrate with two target sites. The very early encounters of EcoRI with the two-site substrate revealed a preferential generation of DNA fragments consistent with EcoRI cutting both sites. Significantly low concentrations of enzyme used in the study ruled out the possibility that the two-site reaction was due to two separate enzyme molecules acting on the DNA and suggested a more likely model where a single enzyme processively moves to the second site after the first cleavage event. This 'site

transfer' assay has been used to identify and characterize facilitated diffusion of numerous DNA-binding proteins.

A variation of the site transfer assay was used by Stanford and co-authors to provide more explicit experimental evidence for the presence of associative slides and dissociative hops by EcoRV along DNA⁴⁶. This was accomplished by simply using multiple DNA substrates in which the two specific sites were placed further and further apart. Theoretical calculations based on a 1-D Brownian search can then be used to predict the probability of an enzyme sliding the number of base pairs between the two sites by using a modification of equation 1.3 (**eq 1.7**), which states that an enzyme translocating linearly along DNA with no directional bias will have a probability of sliding N base pairs that is proportional to N^2 .

$$P_N = \left(\frac{k_{\text{assoc}}}{k_{\text{off}} + k_{\text{assoc}}} \right) N^2 \quad (1.7)$$

A protein that can only undergo associative transfer ($k_{\text{assoc}} \gg k_{\text{off}}$) is expected to display intermolecular transfer probabilities between two target sites that scale with N^2 (**Figure 1.3**). This is due to the simple fact that the significantly faster rate of associative transfer over dissociation would lead to very few enzyme molecules falling off the DNA chain before reaching the second site. A second trend can be envisioned from eq 1.7 in which the k_{assoc} is still faster than k_{off} , but only by a small margin (**Figure 1.3**). This would result in a significant number of enzyme molecules dissociating at least once prior to reaching the next target site (dissociative transfer) and the probability of transfer would follow an a/r dependence where a is the maximum length of DNA the enzyme can slide ($a = 1$ for enzyme's that only hop) and r is the mean distance between the target sites in 3-D

space. What Stanford *et al* observed for EcoRV was an intermediate dependence of the transfer probability on site spacing length, which indicated a combination of both ~50 bp associative slides and numerous dissociative hops giving rise to productive intermolecular translocation. Similar observations have been made for other DNA-searching proteins^{28, 29, 38, 47}, including the E. coli form of UNG (eUNG) by Porecha *et al* who found the eUNG slides ~10bp before undergoing dissociative transfer²⁸.

While the use of theoretical models to discriminate between translocation mechanisms is a useful tool, it is limited in its relevance due to the fact that it is an indirect method for discriminating against associative and dissociative transfer events. Efforts have been made to provide more direct evidence of each transfer pathway, which have culminated in the assay heavily utilized in this thesis. In 2012, Schonhoft *et al* designed a modification to Modrich's site transfer assay, which involved the addition of a molecular clock⁴² (**Figure 1.4**). 'Molecular clocks' are small molecules that have a known lifetime that can be used to 'clock' the lifetime of transient reaction intermediates. The design of the 'clock' molecule follows 3 major principles: (1) it binds weakly to the enzyme such that not all enzyme molecules are sequestered in the bound state, (2) it is soluble enough to be present in high enough concentrations to densely populate the solution and rapidly diffuse to the enzyme active site during the lifetime of a hopping event, (3) it must not perturb the ability of an enzyme to undergo associative transfers along the DNA chain. Satisfying these requirements allows the 'clock' molecule to effectively trap any enzyme molecules attempting to undergo the dissociative transfer pathway and provides a way by which associative and dissociative translocation events can be distinguished experimentally. The site transfer assay is carried out in the absence of the trapping molecule

to determine the overall transfer probability (P_{trans}) and conducted again in the presence of the trap. Transfer events that persist are all associative in nature (P_{assoc}) and the probability of the enzyme undergoing dissociative transfer is determined through a simple calculation:

$$P_{\text{trans}} = P_{\text{assoc}} + P_{\text{diss}}.$$

In the Stivers lab, extensive work preceding this thesis was done to characterize the mechanistic details of facilitated diffusion for hUNG and hOGG1 under ideal solution conditions using the ‘molecular clock’ site transfer assay^{23, 24, 25, 42}(**Figure 1.5**). Uracil and 2-amino-6-chloropurine were found to be sufficient trapping molecules for hUNG and hOGG1, respectively. A summary of the most salient findings follows. (i) hUNG and hOGG1 both utilize a combination of associative and dissociative transfers until damage sites are beyond 10 bp and 40 bp, respectively^{25, 42} and (ii) the associatively translocating intermediate of both enzymes is only loosely associated with the DNA and is therefore capable of bypassing roadblocks along the backbone^{25, 42}. The experiments provide a fundamental framework for how glycosylases localize to target lesions, though little is known with regards to how these pathways respond to non-ideal solution conditions encountered in the cell.

In the following sections, I will introduce the two key features of the cellular environment investigated in this thesis: high ionic strength and macromolecular crowding. A detailing of the physiological significance of these solution components and the theoretical models used to interpret the effects of each on the glycosylase search-and-repair pathway will be presented.

1.6 Counter-ion Condensation Theory

The ion content of the intercellular environment is heavily regulated by movement of ions across the plasma membrane and organelle membranes through transport proteins such as symporters, antiporters, and ion channels⁴⁸. Differing concentrations of individual ions between the intercellular and extracellular fluid produces a gradient of electrochemical potential along which an ion will naturally diffuse in or out of the cell through passive transport. The potential energy stored by ion gradients can be converted to other forms of energy required to power numerous biological processes.

One major source of electrochemical potential originates from the disparity in potassium ion concentrations across the plasma membrane. Within the cell, potassium is the most prevalent monovalent cation at a concentration of ~150 mM, which is 30 times that of its extracellular concentration⁴⁸. Potassium ions thus have a tendency to flow out of the cell along their concentration gradient; however, the negative potential of the plasma membrane (-70 to -90 mV) produces an electrical counteracting force that drags potassium back. The end result is an essentially fixed concentration of intercellular potassium due to no net movement of potassium ions across the membrane.

High concentrations of monovalent ions are known to effect the stability of nucleic acid helices (DNA only for our purposes) and their complexes with proteins in solution^{49, 50, 51, 52, 53, 54, 55}. The origin of this effect arises from the structural properties of DNA, which can be simplified to a uniform rod with a large number of negative like charges from the phosphate backbone and a high helical charge density. Many historical theoretical models and experiments have predicted and proven that cations will condense to form a concentrated layer surrounding a polyion rod in solution^{52, 53, 54, 56, 57}. This “ion cloud” surrounding the DNA maintains a constant local concentration that is insensitive to changes

in the ion content of the surrounding bulk solution^{51, 56}. G.S. Manning first proposed that the effect of this condensed ion layer on the thermodynamic activity of the DNA would have a logarithmic dependence on the bulk solution salt concentration and would be heavily dependent on the helical charge density^{54, 58}. Interactions with DNA that perturb the charge density (i.e. conformational changes, protein binding, etc.) could thus be facilitated or inhibited by small changes in the surrounding salt concentration.

This “counter-ion condensation” theory (CC theory) was experimentally implemented by T.M. Record to more quantitatively describe the nature of the physical forces acting between proteins and DNA^{52, 54, 55}. With respect to a protein binding to a DNA molecule, CC theory assumes the electrostatic component of the binding free energy derives solely from the entropic entropy of mixing gained by the displacement of condensed ions from the ion cloud into the more dilute bulk solution. Upon binding, cationic side chains along a protein surface replace monovalent cations tethered to the DNA phosphate backbone. This process is inhibited by increases in the bulk salt concentration. High bulk salt reduces the ion gradient between the DNA ion cloud and bulk solution, which results in a smaller entropic gain upon protein binding. In accordance with CC theory, the expected logarithmic salt dependence of the binding affinity can be described by the following linear relationship (eq 1.8)

$$\log (K_a) = \log (K_a^{\text{non}}) - N \log [\text{salt}] \quad (1.8)$$

$$N = Z\Psi + \beta$$

where K_a^{non} represents the non-electrostatic (or salt independent) component to the binding free energy and N is the total number of counterions displaced during binding. N is a summation of the ions displaced from the DNA ($Z\Psi$) and anions (β) that are displaced

from cationic side chains of the protein. The number of DNA-associated ions that are displaced can be estimated from the number of DNA phosphate groups in contact with the bound protein (Z) and the fraction of a cation bound per phosphate group according to polyelectrolyte theory ($\Psi \sim 0.64$ for short DNA oligos)⁴⁹. A useful feature of this formalism is that the salt-dependent component drops to zero when extrapolated to 1 M salt. It is assumed that all electrostatic interactions are completely shielded at such a high salt concentration and the only contributions to the binding free energy that remain are non-electrostatic in nature.

The validity of using such a simplified model to delineate between electrostatic and nonelectrostatic interactions in a protein-DNA complex was recently evaluated in detail by Privalov⁴⁹. The components of the theory he addressed included (i) if N truly represents the number of ions displaced upon binding, (ii) what $\log K_a$ represents at 1 M salt, and (iii) if the electrostatic component to the binding free energy (ΔG_{elect}) is solely entropic. To address the first point, Privalov compared the number of observable DNA phosphate groups interacting with several proteins from atomic structures with the corresponding slope of their salt-dependent binding affinity. A plot of this data established two populations: those whose linear relationship went through the origin and those that did not. The former represents proteins that only displace DNA-bound ions and the latter are those that release anions associated with their cationic sidechains. Privalov showed that anion release from a protein can be experimentally determined simply by changing the anionic counterion of the salt in solution to one that is heavily hydrated and unlikely to interact with the protein. N has thus been established to be proportional to the number of ions displaced during a binding event. The second point was addressed by analysis of the salt-

dependent binding of different truncations of the HMG box from mLEF-1. The truncated proteins differed only in the number of residues crystallographically shown to electrostatically interact with the DNA. Their respective log-log plots differed only in slope and not in the 1 M salt extrapolated y-intercept, which lends credence to the notion that the y-intercept does not inform on any electrostatic interactions. The third point with regards to the entropic or enthalpic origin of ΔG_{elect} was addressed by simply evaluating the temperature sensitivity of salt-dependent binding. Privalov showed that the slope of the salt-dependent binding of the bZIP fragment of yeast GNC4 to its target sequence was insensitive to temperature while the y-intercept became increasingly larger as temperature rose. The temperature independence of N is consistent with a purely entropically driven displacement of ions. Privalov's comprehensive analysis demonstrates that the theoretical predictions of CC theory are validated by experimental observations.

Though simplistic in nature, CC theory provides a model by which experimentally derived interaction potentials between proteins and DNAs can be dissected in terms of their electrostatic and nonelectrostatic character. In chapters 2, 3, and 5 of this thesis, I will use this theory in a broader application to characterize the driving forces behind numerous steps in the hUNG and hOGG1 search-and-repair pathway beyond just binding to the DNA. This detailed analysis of how salt impacts various stages of protein-DNA interactions that lead to productive translocation will allow me to develop a cohesive model for how the intercellular salt concentration modulates our current understanding of facilitated diffusion.

1.7 Macromolecular Crowding: Excluded Volume and Solution Viscosity Effects

Experimental studies of proteins translocating along DNA are primarily carried out *in vitro* utilizing relatively low concentrations of macromolecular species. While this

provides simplicity in experimental design and interpretation, it ultimately ignores an essential component of the physiological environment of DNA repair: the cell is crowded. In mammalian cells, concentrations of macromolecular species range from 200-300 g/L for proteins and 50-250 g/L for nucleic acids; therefore, an astounding 10-40% of the cell volume is occupied by macromolecules and unavailable to the interacting species of interest⁵⁹. This reduction in available solution volume has profound consequences for biological processes.

The most intuitive effects of high concentrations of large species in solution revolve around excluded volume and viscosity. Reduced available volume to a protein and DNA pair would promote compact species that occupy as small a volume as possible. This favors the formation of protein-DNA complexes and disfavors free DNA and protein forms. Increased viscosity by the introduction of inert macromolecular species would also be expected to hinder diffusion driven processes in a manner described by the Stokes-Einstein equation.

Discussion of the more complex consequences of a crowded solution environment is best done using a simplified model in which intracellular macromolecules are represented as inert polymer chains. This simplification allows for theoretical prediction of solution effects at various crowding levels and also provides an experimental approach for mimicking the crowding environment of the cell using commercially available inert polymers such as dextran, ficoll, and polyethelene glycol (PEG). For the purpose of this thesis, the discussion of molecular crowding will be limited to the use of PEG as a model system. The correct size of PEG to use as an intercellular mimic is dependent on the size of the test molecule due to a unique property of some inert polymers. First noted by

Asakura and Oosawa in 1954⁶⁰, preferential interaction between PEG and water rather than a test protein leads to the formation of a “depletion layer” in which PEG is excluded from the protein surface. This hydration barrier between PEG and the test molecule is due to the polymer experiencing entropic repulsion as it approaches the protein. The consequences of this depletion layer change as a function of PEG concentration (**Figure 1.6**)⁶¹. At low concentrations, the solution is considered *dilute* and the crowding agent can be viewed as an extended sphere (coil) with a radius of gyration (R_g^{PEG}) determined by the molecular weight (M_w) of the polymer using the following relationship derived from light scattering data^{62, 63}.

$$R_g^{\text{PEG}} = 0.0215 \cdot M_w^{0.583}$$

Under these solution conditions, the depletion layer thickness scales with R_g , though the low probability of diffusive encounter between the test molecules and PEG limits any significance of the depletion layer size. As the concentration of PEG is increased beyond a defined crossover threshold (c^*)⁶⁴, the solution becomes *semi-dilute*, characterized by polymer molecules overlapping and caging the protein and DNA together in a noncovalent polymeric network with a certain average mesh size (ξ) that continues to decrease as the polymer concentration increases. The depletion layer in this scenario scales with ξ which is a function of R_g^{PEG} . In this regime, the depletion layer provides a significant benefit to the protein and DNA by enhancing attraction between the two molecules induced by the exclusion of PEG from the space between them when their separation reduces to the less than R_g^{PEG} ⁶¹. At high concentrations, the solution enters the *concentrated* regime in which polymers form a dense mesh that invades the space between the protein and DNA and inhibits their diffusive encounter. For the purpose of studying macromolecular

crowding, it is ideal to use a PEG polymer that is slightly larger than the test protein so that the depletion layer it induces is significant and at a high enough concentration to be in the *semi-dilute* regime where the depletion layer is most effective^{61, 65}.

The depletion layer generated by the exclusion of PEG from regions of solution influences not only the solution volume available to test molecules, but also has a unique consequence for viscosity. While the introduction of large PEG molecules can drastically increase the overall solution viscosity (referred to as *microviscosity*), the viscosity within the depletion layer (*nanoviscosity*) is expected to be equivalent to dilute solution in which no PEG is present⁵⁹. Therefore, a crowded solution is imbued with heterogenous viscosity and the severity of this effect is dictated by the relative size of the test molecules and PEG. Holyst rationalized this effect in the following manners: (i) when the test molecule is significantly larger than the crowding agent, the size of the depleted volume containing dilute solution is negligible and the protein experiences microviscosity only. (ii) When the test molecule is significantly smaller than the crowding agent, it is always encased in the depletion layer and experiences nanoviscosity equivalent to dilute solution. (iii) When the test molecular and crowding agent are of comparable size, the length scale of a particular interaction between test molecules will dictate the viscosity they encounter⁶⁶. Short-range motions on the order of nanometers (corresponding to rotational diffusion) experience nanoviscosity while longer-range movements (corresponding to translational diffusion) are influenced by microviscosity⁶⁷.

In chapters 4 and 5, I develop a comprehensive model for how the crowded and viscous environment of the cell nucleus can affect the individual steps of the hUNG and hOGG1 search-and-repair pathway. I show that the excluded volume effect negates the

deleterious effects of high solution viscosity and provides an environment in which facilitated diffusion can persist. Our theoretical understanding of how PEG behaves in solution as a function of size and concentration is used as the basis of our analytical interpretations.

1.8 General Summary of Thesis Chapters

My thesis work revolves around the individual and synergistic effects of ionic strength and molecular crowding on the search-and-repair pathways of both hUNG and hOGG1. In chapter 2, I present a thorough analysis of how the ionic strength of bulk solution alters the ability of hUNG to efficiently interact with both undamaged and damaged DNA molecules. This includes equilibrium binding measurements, association/dissociation kinetics, Michaelis-menten kinetics, and site transfer interpreted using CC theory. In chapter 3, I describe a complimentary study performed on the enzyme hOGG1, which reveals how structural and mechanistic differences between these enzymes results in similar damage search outcomes. In chapter 4, I present a combined study of hUNG and hOGG1 search-and-repair in the presence of a rich diversity of molecular crowding agents that probe both excluded volume and viscosity effects. Finally, in chapter 5, I detail an analysis of the combinatorial effects of salt, crowding, and bulk DNA density on the translocation probabilities of both hUNG and hOGG1 to evaluate the validity of facilitated diffusion as a search mechanism for glycosylases *in vivo*.

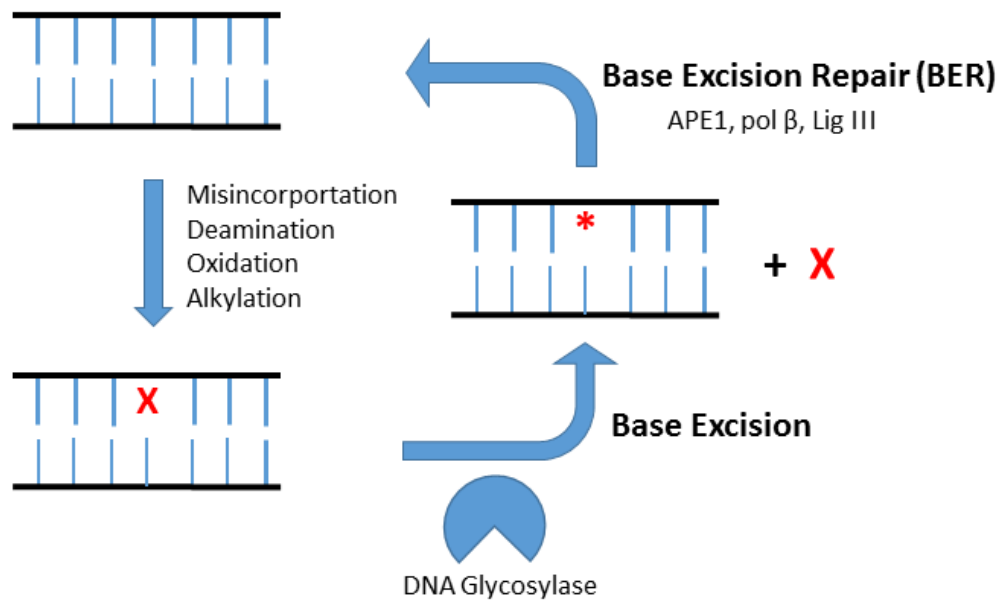


Figure 1.1. The Base Excision Repair Pathway. After DNA is damaged by any one of a variety of mechanisms, lesions (X) are recognized by specific DNA glycosylases. These enzymes catalyze cleavage of the glycosidic bond of the damage site, resulting in the free damaged base and an abasic site remaining in the DNA. This abasic site is then recognized by a cascade of enzymes responsible for correct nucleotide incorporation.

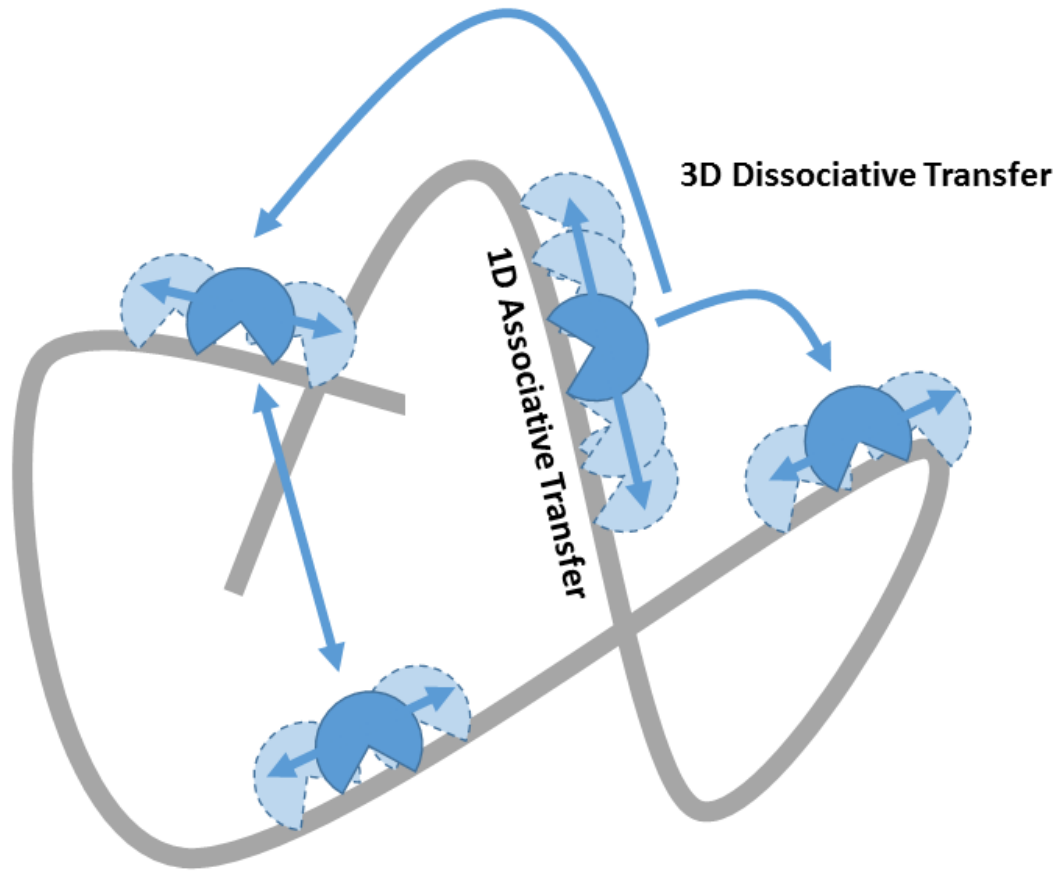


Figure 1.2. Facilitated Diffusion: Associative and Dissociative Translocation.

Increasing the rate at which glycosylase molecules can efficiently scan DNA is accomplished by two major transfer mechanisms: a 1D associative slide, in which the protein remains closely localized to the DNA, and a 3D dissociative hop which requires the enzyme to dissociate and reassociate with the DNA chain.

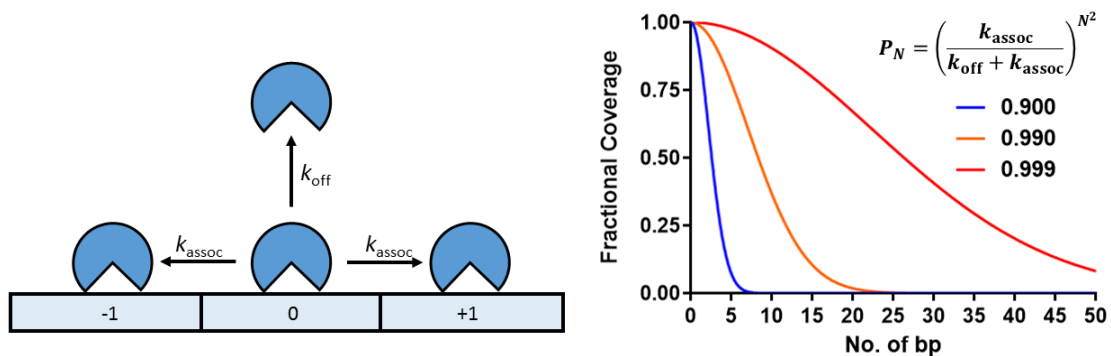


Figure 1.3. Mathematical representation of associative transfers. Modeling of associative transfer steps involves an enzyme molecule that has an equal probability of stepping to the right (+1) or to the left (-1) from its point of origin (0). The figure on the right shows simulated data representing the expecting differences in the fraction of enzyme molecules occupying sites distant from the point of origin. This fraction is heavily dependent on the rates of dissociation (k_{off}) and associative translocation (k_{assoc}). The values of $k_{\text{assoc}} / (k_{\text{off}} + k_{\text{assoc}})$ plotted are 0.900 (blue), 0.990 (orange), and 0.999 (red). As k_{off} increases, the enzyme has a lower probability of occupying distant sites on the DNA.

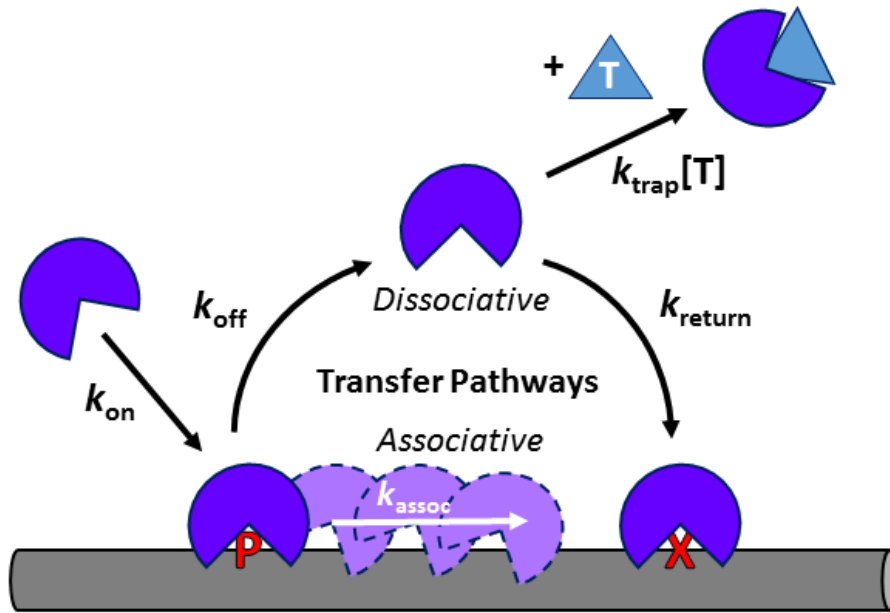


Figure 1.4. Schematic of the Molecular Clock assay. The probability of undergoing an associative transfer steps is described as an interplay between the rate of sliding (k_{assoc}) and the dissociation rate (k_{off}). Dissociated enzyme molecules can either reassociate with the same DNA (k_{return}) to complete a hopping event or become lost in bulk solution. To delineate between associate and dissociative transfer pathways, a small molecule trap is introduced in solution (T). This molecule rapidly diffuses ($k_{\text{trap}}[\text{T}]$) to the exposed active site of any dissociating enzyme molecules, which eliminates hopping steps. All transfers impenetrable to the trap are associative in nature.

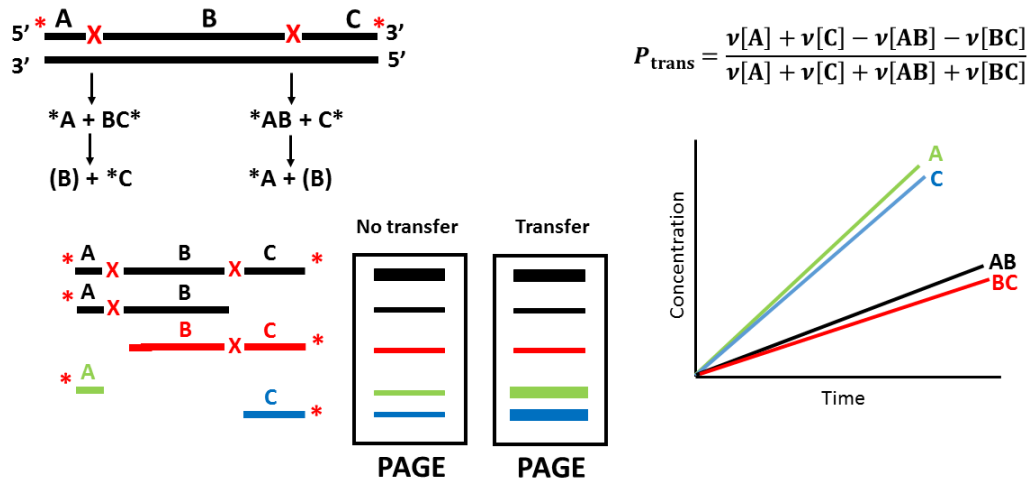


Figure 1.5. The Site Transfer assay. In order to quantify processivity of DNA glycosylases (P_{trans}), DNA containing two damage sites (X) is radiolabeled on both the 3' and 5' ends (*) and reacted with enzyme. The DNA fragments are then separated by denaturing polyacrylamide gel electrophoresis. Facilitate diffusion between sites is indicated by the excess of double cleaved fragments (A and C) over single cleaved fragments (AB and BC). If both damage sites are equivalent and the enzyme does not display translocation bias, the rates of formation should be as follows: $A = C$, $AB = BC$. P_{trans} can be calculated using the rates of formation of each fragment.

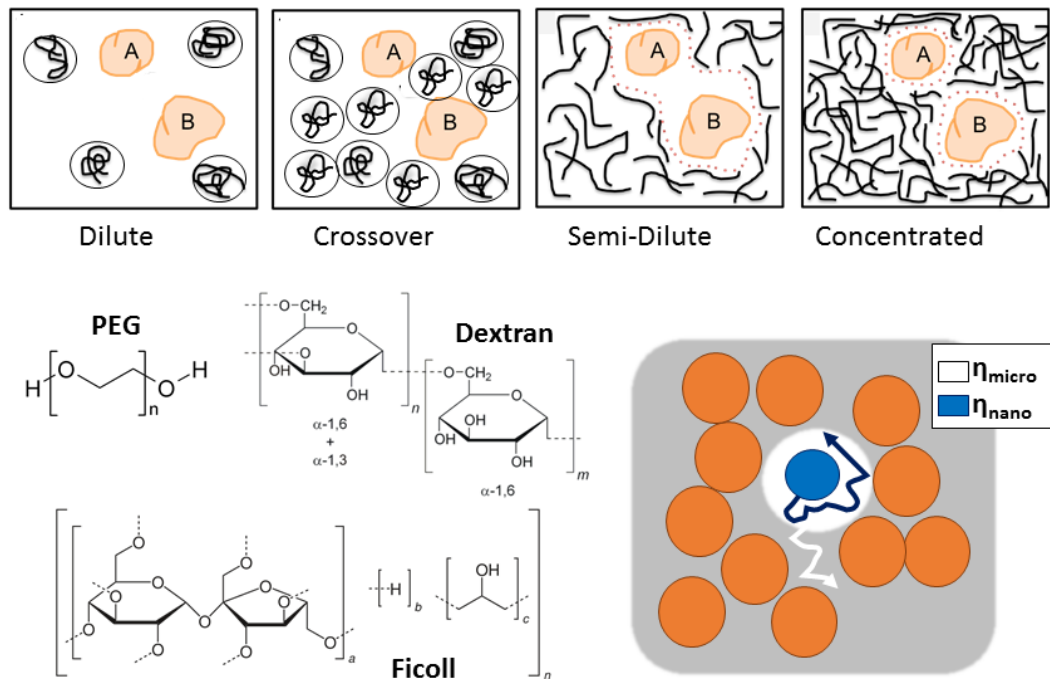


Figure 1.6. Representations of molecular crowding agents in solution. The solution characteristics of inert polymers (i.e. PEG, Dextran, Ficoll) is dependent on concentration. In the dilute regime (low concentrations), the polymer is globular and isolated. As the concentration increases, a crossover point is reached upon which the polymers will begin to interact with one another. Beyond the crossover point is the semi-dilute regime where the crowding agent has formed a mesh that cages the macromolecules (A and B) together. At high concentrations, this mesh becomes extremely dense and penetrates the space between species A and B, hindering their interactions. Exclusion of inter polymers from the surface of proteins due to entropic depletion effects generates a depletion layer (nm in diameter) of dilute solution. These pockets of dilute buffer produce heterogeneity in the viscosity of the solution that is experienced by the protein depending on the length scale of its motion. Long range motions encounter microviscosity equivalent to the bulk solution and short range motions occur in the nanoviscosity of the dilute depletion layer.

1.9. References

1. Sancar, A., Lindsey-Boltz, L. A., Unsal-Kacmaz, K., and Linn, S. (2004) Molecular mechanisms of mammalian DNA repair and the DNA damage checkpoints. *Annu. Rev. Biochem.* 73, 39-85.
2. Hoeijmakers, J. H. (2009) DNA damage, aging, and cancer. *N. Engl. J. Med.* 361, 1475-1485.
3. Seeberg, E., Eide, L., and Bjørås, M. (1995) The base excision repair pathway. *Trends Biochem. Sci.* 20, 391-397.
4. Krokan, H. E., Drablos, F., and Slupphaug, G. (2002) Uracil in DNA--occurrence, consequences and repair. *Oncogene.* 21, 8935-8948.
5. Olinski, R., Jurgowiak, M., and Zaremba, T. (2010) Uracil in DNA—Its biological significance. *Mutation Research/Reviews in Mutation Research.* 705, 239-245.
6. Mashiyama, S. T., Hansen, C. M., Roitman, E., Sarmiento, S., Leklem, J. E., Shultz, T. D., and Ames, B. N. (2008) An assay for uracil in human DNA at baseline: Effect of marginal vitamin B6 deficiency. *Anal. Biochem.* 372, 21-31.
7. Cross, D. R., Miller, B. J., and James, S. J. (1993) A simplified HPLC method for simultaneously quantifying ribonucleotides and deoxyribonucleotides in cell extracts or frozen tissues. *Cell Prolif.* 26, 327-336.
8. Horowitz, R. W., Zhang, H., Schwartz, E. L., Ladner, R. D., and Wadler, S. (1997) Measurement of deoxyuridine triphosphate and thymidine triphosphate in the extracts of thymidylate synthase-inhibited cells using a modified DNA polymerase assay. *Biochem. Pharmacol.* 54, 635-638.
9. el-Hajj, H. H., Zhang, H., and Weiss, B. (1988) Lethality of a dut (deoxyuridine triphosphatase) mutation in escherichia coli. *J. Bacteriol.* 170, 1069-1075.
10. Gadsden, M. H., McIntosh, E. M., Game, J. C., Wilson, P. J., and Haynes, R. H. (1993) dUTP pyrophosphatase is an essential enzyme in saccharomyces cerevisiae. *EMBO J.* 12, 4425-4431.
11. Seiple, L., Jaruga, P., Dizdaroglu, M., and Stivers, J. T. (2006) Linking uracil base excision repair and 5-fluorouracil toxicity in yeast. *Nucleic Acids Res.* 34, 140-151.
12. Kouzminova, E. A., and Kuzminov, A. (2004) Chromosomal fragmentation in dUTPase-deficient mutants of escherichia coli and its recombinational repair. *Mol. Microbiol.* 51, 1279-1295.
13. Kohli, R. M., and Zhang, Y. (2013) TET enzymes, TDG and the dynamics of DNA demethylation. *Nature.* 502, 472-479.
14. Parker, J. B., Bianchet, M. A., Krosky, D. J., Friedman, J. I., Amzel, L. M., and Stivers, J. T. (2007) Enzymatic capture of an extrahelical thymine in the search for uracil in DNA. *Nature.* 449, 433-437.
15. Parker, J. B., and Stivers, J. T. (2011) Dynamics of uracil and 5-fluorouracil in DNA. *Biochemistry.* 50, 612-617.
16. Neeley, W. L., and Essigmann, J. M. (2006) Mechanisms of formation, genotoxicity, and mutation of guanine oxidation products. *Chem. Res. Toxicol.* 19, 491-505.

17. Nakabeppu, Y. (2014) Cellular levels of 8-oxoguanine in either DNA or the nucleotide pool play pivotal roles in carcinogenesis and survival of cancer cells. *Int. J. Mol. Sci.* *15*, 12543-12557.
18. David, S. S., O'Shea, V. L., and Kundu, S. (2007) Base-excision repair of oxidative DNA damage. *Nature*. *447*, 941-950.
19. Hazra, T. K., Hill, J. W., Izumi, T., and Mitra, S. (2001) Multiple DNA glycosylases for repair of 8-oxoguanine and their potential in vivo functions. *Prog. Nucleic Acid Res. Mol. Biol.* *68*, 193-205.
20. Ide, H., and Kotera, M. (2004) Human DNA glycosylases involved in the repair of oxidatively damaged DNA. *Biol. Pharm. Bull.* *27*, 480-485.
21. Friedman, J. I., and Stivers, J. T. (2010) Detection of damaged DNA bases by DNA glycosylase enzymes. *Biochemistry*. *49*, 4957-4967.
22. Berg, O. G., Winter, R. B., and von Hippel, P. H. (1981) Diffusion-driven mechanisms of protein translocation on nucleic acids. 1. models and theory. *Biochemistry*. *20*, 6929-6948.
23. Schonhoft, J. D., Kosowicz, J. G., and Stivers, J. T. (2013) DNA translocation by human uracil DNA glycosylase: Role of DNA phosphate charge. *Biochemistry (N. Y.)*. *52*, 2526-2535.
24. Schonhoft, J. D., and Stivers, J. T. (2013) DNA translocation by human uracil DNA glycosylase: The case of single-stranded DNA and clustered uracils. *Biochemistry*. *52*, 2536-2544.
25. Rowland, M. M., Schonhoft, J. D., McKibbin, P. L., David, S. S., and Stivers, J. T. (2014) Microscopic mechanism of DNA damage searching by hOGG1. *Nucleic Acids Research*. *42*, 9295-9303.
26. Blainey, P. C., van Oijen, A. M., Banerjee, A., Verdine, G. L., and Xie, X. S. (2006) A base-excision DNA-repair protein finds intrahelical lesion bases by fast sliding in contact with DNA. *Proceedings of the National Academy of Sciences*. *103*, 5752-5757.
27. Blainey, P. C., Luo, G., Kou, S. C., Mangel, W. F., Verdine, G. L., Bagchi, B., and Xie, X. S. (2009) Nonspecifically bound proteins spin while diffusing along DNA. *Nat. Struct. Mol. Biol.* *16*, 1224-1229.
28. Porecha, R. H., and Stivers, J. T. (2008) Uracil DNA glycosylase uses DNA hopping and short-range sliding to trap extrahelical uracils. *Proceedings of the National Academy of Sciences*. *105*, 10791-10796.
29. Hedglin, M., and O'Brien, P. J. (2008) Human alkyladenine DNA glycosylase employs a processive search for DNA damage. *Biochemistry*. *47*, 11434-11445.
30. Leonid Mirny and Michael Slutsky and Zeba Wunderlich and Anahita Tafvizi and Jason Leith and Andrej Kosmrlj. (2009) How a protein searches for its site on DNA: The mechanism of facilitated diffusion. *Journal of Physics A: Mathematical and Theoretical*. *42*, 434013.
31. Halford, S. E., and Marko, J. F. (2004) How do site-specific DNA-binding proteins find their targets? *Nucleic Acids Res.* *32*, 3040-3052.
32. Smoluchowski, M. (1917) Mathematical theory of the kinetics of the coagulation of colloidal solutions. *Z. Phys. Chem.* *92*.

33. Riggs, A. D., Bourgeois, S., and Cohn, M. (1970) The lac repressor-operator interaction. 3. kinetic studies. *J. Mol. Biol.* 53, 401-417.
34. Richter, P. H., and Eigen, M. (1974) Diffusion controlled reaction rates in spheroidal geometry. application to repressor--operator association and membrane bound enzymes. *Biophys. Chem.* 2, 255-263.
35. Berg, O. G., and Blomberg, C. (1976) Association kinetics with coupled diffusional flows. special application to the lac repressor--operator system. *Biophys. Chem.* 4, 367-381.
36. Adam, G., and Delbruck, M. (1968) *Structural Chemistry and Molecular Biology*. W.H. Freeman, San Francisco.
37. von Hippel, P. H., and Berg, O. G. (1989) Facilitated target location in biological systems. *J. Biol. Chem.* 264, 675-678.
38. Gowers, D. M., Wilson, G. G., and Halford, S. E. (2005) Measurement of the contributions of 1D and 3D pathways to the translocation of a protein along DNA. *Proc. Natl. Acad. Sci. U. S. A.* 102, 15883-15888.
39. Slutsky, M., and Mirny, L. A. (2004) Kinetics of protein-DNA interaction: Facilitated target location in sequence-dependent potential. *Biophys. J.* 87, 4021-4035.
40. Schurr, J. M. (1979) The one-dimensional diffusion coefficient of proteins absorbed on DNA. hydrodynamic considerations. *Biophys. Chem.* 9, 413-414.
41. Bagchi, B., Blainey, P. C., and Xie, X. S. (2008) Diffusion constant of a nonspecifically bound protein undergoing curvilinear motion along DNA. *J Phys Chem B.* 112, 6282-6284.
42. Schonhofs, J. D., and Stivers, J. T. (2012) Timing facilitated site transfer of an enzyme on DNA. *Nat. Chem. Biol.* 8, 205-210.
43. Zhou, H. (2011) Rapid search for specific sites on DNA through conformational switch of nonspecifically bound proteins. *Proceedings of the National Academy of Sciences.* 108, 8651-8656.
44. Friedman, J. I., Majumdar, A., and Stivers, J. T. (2009) Nontarget DNA binding shapes the dynamic landscape for enzymatic recognition of DNA damage. *Nucleic Acids Research.* 37, 3493-3500.
45. Terry, B. J., Jack, W. E., and Modrich, P. (1985) Facilitated diffusion during catalysis by EcoRI endonuclease. nonspecific interactions in EcoRI catalysis. *J. Biol. Chem.* 260, 13130-13137.
46. Stanford, N. P., Szczelkun, M. D., Marko, J. F., and Halford, S. E. (2000) One- and three-dimensional pathways for proteins to reach specific DNA sites. *EMBO J.* 19, 6546-6557.
47. Sidorenko, V. S., and Zharkov, D. O. (2008) Correlated cleavage of damaged DNA by bacterial and human 8-oxoguanine-DNA glycosylases. *Biochemistry.* 47, 8970-8976.
48. Lodish, H., Berk, A., and Zipursky, S. L. (2000) Intracellular Ion Environment and Membrane Electric Potential, in *Molecular Cell Biology* 4th ed., W.H. Freeman, New York.

49. Privalov, P. L., Dragan, A. I., and Crane-Robinson, C. (2011) Interpreting protein/DNA interactions: Distinguishing specific from non-specific and electrostatic from non-electrostatic components. *Nucleic Acids Res.* *39*, 2483-2491.
50. Bai, Y., Das, R., Millett, I. S., Herschlag, D., and Doniach, S. (2005) Probing counterion modulated repulsion and attraction between nucleic acid duplexes in solution. *Proc. Natl. Acad. Sci. U. S. A.* *102*, 1035-1040.
51. Anderson, C. F., and Record, M. T., Jr. (1995) Salt-nucleic acid interactions. *Annu. Rev. Phys. Chem.* *46*, 657-700.
52. Record, M. T., Jr, deHaseth, P. L., and Lohman, T. M. (1977) Interpretation of monovalent and divalent cation effects on the lac repressor-operator interaction. *Biochemistry.* *16*, 4791-4796.
53. Record, M. T. (1975) Effects of Na^+ and Mg^{++} ions on the helix-coil transition of DNA. *Biopolymers.* *14*, 2137-2158.
54. Record Jr, M. T., Lohman, T. M., and Haseth, P. d. (1976) Ion effects on ligand-nucleic acid interactions. *J. Mol. Biol.* *107*, 145-158.
55. Record, M. T., Jr, Anderson, C. F., and Lohman, T. M. (1978) Thermodynamic analysis of ion effects on the binding and conformational equilibria of proteins and nucleic acids: The roles of ion association or release, screening, and ion effects on water activity. *Q. Rev. Biophys.* *11*, 103-178.
56. Anderson, C. F., and Record, M. T., Jr. (1990) Ion distributions around DNA and other cylindrical polyions: Theoretical descriptions and physical implications. *Annu. Rev. Biophys. Biophys. Chem.* *19*, 423-465.
57. Record, M. T., Woodbury, C. P., and Lohman, T. M. (1976) Na^+ effects on transitions of DNA and polynucleotides of variable linear charge density. *Biopolymers.* *15*, 893-915.
58. Manning, G. S. (1978) The molecular theory of polyelectrolyte solutions with applications to the electrostatic properties of polynucleotides. *Q. Rev. Biophys.* *11*, 179-246.
59. Theillet, F. X., Binolfi, A., Frembgen-Kesner, T., Hingorani, K., Sarkar, M., Kyne, C., Li, C., Crowley, P. B., Gierasch, L., Pielak, G. J., Elcock, A. H., Gershenson, A., and Selenko, P. (2014) Physicochemical properties of cells and their effects on intrinsically disordered proteins (IDPs). *Chem. Rev.* *114*, 6661-6714.
60. Asakura, S., and Oosawa, F. (1954) On interaction between two bodies immersed in a solution of macromolecules. *J. Chem. Phys.* *22*, 1255-1256.
61. Kozer, N., Kuttner, Y. Y., Haran, G., and Schreiber, G. (2007) Protein-protein association in polymer solutions: From dilute to semidilute to concentrated. *Biophys. J.* *92*, 2139-2149.
62. Linegar, K. L., Adeniran, A. E., Kostko, A. F., and Anisimov, M. A. (2010) Hydrodynamic radius of polyethylene glycol in solution obtained by dynamic light scattering. *Colloid Journal.* *72*, 279-281.
63. Devanand, K., and Selser, J. C. (1991) Asymptotic behavior and long-range interactions in aqueous solutions of poly(ethylene oxide). *Macromolecules.* *24*, 5943-5947.
64. de Gennes, P. (1979) *Scaling Concepts in Polymer Physics*. Cornell University Press, Ithaca, N.Y.

65. Kozer, N., and Schreiber, G. (2004) Effect of crowding on protein-protein association rates: Fundamental differences between low and high mass crowding agents. *J. Mol. Biol.* 336, 763-774.
66. Holyst, R., Bielejewska, A., Szymanski, J., Wilk, A., Patkowski, A., Gapinski, J., Zywockinski, A., Kalwarczyk, T., Kalwarczyk, E., Tabaka, M., Ziebac, N., and Wiczorek, S. A. (2009) Scaling form of viscosity at all length-scales in poly(ethylene glycol) solutions studied by fluorescence correlation spectroscopy and capillary electrophoresis. *Phys. Chem. Chem. Phys.* 11, 9025-9032.
67. Kuttner, Y. Y., Kozer, N., Segal, E., Schreiber, G., and Haran, G. (2005) Separating the contribution of translational and rotational diffusion to protein association. *J. Am. Chem. Soc.* 127, 15138-15144.

Chapter 2:

Electrostatic properties of complexes along a DNA glycosylase damage search pathway

Reproduced in part from:

Cravens, S.L., Hobson, M., Stivers, J.T.; (2014) Electrostatic properties of complexes along a DNA glycosylase damage search pathway; *Biochemistry*, 53 (48), 7680-7692

2.1. INTRODUCTION

DNA glycosylases initiate the base excision repair pathway by localizing to a specific lesion site and catalytically cleaving the glycosidic bond of a damaged base. Different glycosylases can be highly specialized for the removal of specific lesions that in some cases vary only subtly from native bases [5,6]. Achievement of high enzymatic specificity for damaged sites as well as rapid searching of abundant undamaged DNA sequences requires highly optimized thermodynamic and kinetic interactions with both specific and non-specific sequences. The basis for this statement is straightforward: if the enzyme binds too tightly to non-specific DNA sequences, the residence time will be too long to efficiently scan the entire genome before the next replication event, while if interactions are too weak, insufficient time will be spent inspecting individual DNA base pairs, leading to overlooked base lesions [7,8]. Determining the factors that contribute to the molecular recognition of both specific and non-specific DNA sequences can shed light on how these enzymes have optimized their scan-and-repair mechanisms under solution conditions found in human cells.

It is generally accepted that the DNA glycosylase damage search process involves two major modes: an *associative*¹ mode that involves tracking along the DNA using a loosely associated enzyme state (often called “sliding”) and a *dissociative* mode that involves intermittent dissociation and re-association of the enzyme with the DNA chain

¹ We use the term *dissociative* to refer to a facilitated diffusion pathway that involves dissociation of the enzyme from the DNA chain and diffusion outside of the DNA ion cloud before reassociation. The term *associative* refers to a distinct pathway where the enzyme remains associated with the DNA within the ion cloud. Historically, the terms “hopping” and “sliding” have been used to describe these two pathways for facilitated diffusion. However, recent studies with hUNG and 8-oxoguanine DNA glycosylase (hOGG1) have established aspects of the intramolecular site transfer mechanisms by these enzymes that are not consistent with the older terminology [1-3]

(“hopping”) [4,9-21]. Since most studies of the damage search mechanism have used dilute, low-salt solutions [11,12,22,23], a key unknown is how the individual non-specific and specific complexes respond to the high salt concentrations encountered in the cell nucleus. A general understanding of such electrostatic effects is important given the generally large impact salt concentration has on the kinetic and thermodynamic properties of many enzyme-DNA complexes [5,6,24-27].

Counterion condensation (CC) theory attributes the electrostatic component of the protein-DNA binding free energy to the cratic entropy of mixing. In this view, during binding to the phosphate backbone the cationic side chains of the protein displace cations from the DNA ion cloud into bulk solution [7,8,27-29]. As the bulk salt concentration is increased, the cratic entropy of mixing becomes less favorable because the ion gradient between the DNA ion cloud and bulk solution is reduced. These effects are described by **eq 2.1** [7,8,27-29], where the term $\log K_a^{\text{non}}$ accounts

$$\log (K_a) = \log (K_a^{\text{non}}) - N \log [\text{salt}] \quad (2.1)$$

$$N = Z\Psi + \beta$$

for the non-electrostatic contribution to the free energy of binding, and the second term reflects the electrostatic component, where N is the total number of counterions displaced during binding. These counterions may be cations released from the DNA ($Z\Psi$) or tightly bound anions (β) that are displaced from cationic side chains of the protein. In this formalism, Z is equal to the number of DNA phosphate groups in contact with the bound protein and Ψ is the fraction of a cation bound per phosphate group according to polyelectrolyte theory ($\Psi \sim 0.64$ for short DNA oligos) [30-32]. A feature of this model is that extrapolation of the binding energy to 1 M salt makes the electrostatic term equal to

zero, allowing the non-electrostatic free energy component to be estimated. This approach, though simplistic in terms of its dissection of the non-electrostatic and electrostatic terms [28,33,34], provides useful parameters that describe the driving forces governing the stability of various protein-DNA complexes on the damage recognition pathways of DNA glycosylases. It should be noted that CC theory focuses solely on effects derived from ion displacement and does not explicitly take into account the effect of ion concentration dependent changes in protein and DNA hydration. However, it has previously been established that changes in water activity do not occur with increasing concentrations of typical monovalent salts, and consequently, that electrostatic effects can be probed independently from changes in hydration [35].

In this study, we use CC theory to understand how each transient complex on the damage search pathway of human uracil DNA glycosylase (hUNG)¹ responds to changes in salt concentration (**Fig. 2.1**). We measured the salt concentration dependences of the thermodynamic and kinetic parameters for formation of both non-specific and specific DNA complexes and the effect of salt on steady-state catalysis by hUNG. Finally, we make the first measurements of how the electrostatic environment of DNA impacts intramolecular DNA translocation by hUNG between uracil sites separated by 20 bp. The results show that an ionic environment approximating that of the cell nucleus enhances the specificity of hUNG, but significantly diminishes the efficiency of facilitated diffusion by the dissociative (“hopping”) pathway, but not the associative (“sliding”) pathway. The implications of these findings to the damage search process in human cells are discussed.

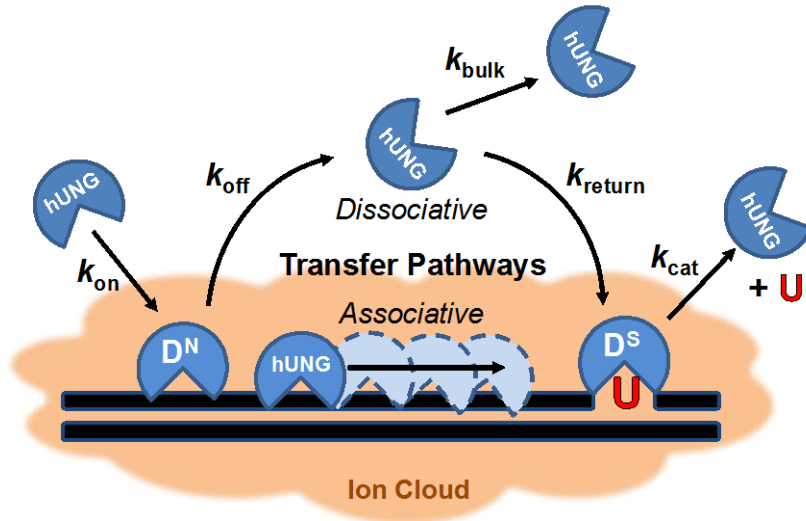


Figure 2.1. The hUNG DNA search and repair pathway. It is composed of four transient states: stationary states where the enzyme is engaged with non-specific (D^N) or specific uracilated sequences (D^S), and two mobile states where the enzyme can translocate along DNA via associative or dissociative pathways of facilitated diffusion. Non-specific and specific complexes must have distinct interactions that facilitate efficient recognition and repair (see text). The D^N complex is characterized primarily by contacts with the phosphate backbone, while the D^S complex involves additional nonpolar and hydrogen bonding interactions with the uracil base (see Figs 2A, 3A). The overall transfer probability between two uracil lesions is defined as the sum of two pathways: $P_{\text{trans}} = P_{\text{assoc}} + P_{\text{diss}}$, where P_{assoc} and P_{diss} are the probabilities of transfer via the associative and dissociative pathways, respectively. When uracils are spaced far enough apart such that all successful transfers occur via at least one dissociation event, this equation reduces to $P_{\text{trans}} = P_{\text{diss}}$. Kinetically, P_{diss} is defined as the product of two probabilities: $P_{\text{diss}} = \left(\frac{k_{\text{off}}}{k_{\text{assoc}} + k_{\text{off}}} \right) \left(\frac{k_{\text{return}}}{k_{\text{bulk}} + k_{\text{return}}} \right)$. The first term describes the probability that hUNG will dissociate from a non-specific DNA site as opposed to making an associative step along the DNA, and the second term gives the likelihood that the enzyme, once dissociated, escapes to the bulk solvent (k_{bulk}) rather than re-associating with the DNA chain (k_{return}) to complete transfer by the dissociative pathway.

2.2. RESULTS

2.2.1. Ion Effects on Non-specific DNA Binding.

The DNA binding interface of hUNG consists of a well-conserved 27 Å groove with positive electrostatic potential [38]. Despite this substantial cleft, close contact (≤ 3.3 Å) between cationic groups of hUNG and the phosphate backbone are localized to only a few sites shared in both the non-specific and specific DNA complexes (**Fig. 2.2A**) [38-40]. The relatively sparse ionic contacts between hUNG and DNA leads to the question of the nature of the thermodynamic interactions that stabilize the non-specific hUNG-DNA complex. To determine if interactions between hUNG and non-specific DNA were predominantly electrostatic or non-electrostatic in nature, the salt dependence of the non-specific equilibrium association constant (K_a^N) was measured at concentrations of potassium ions in the range 36 to 170 mM using three different counterions (Cl^- , F^- , and Glu^-). Different anions were used to determine whether there was a contribution from anion release from hUNG during formation of the non-specific complex [32]. Plots of the $\log [\text{salt}]$ against $\log K_a^N$ were used to determine the electrostatic (ΔG_{elect}) and non-electrostatic (ΔG_{non}) contributions to the binding free energy, and the number of ions (N) displaced upon hUNG-DNA association according to **eq 2.1**.

Fluorescence anisotropy measurements revealed a strong KCl dependence of hUNG binding to non-specific DNA ($N = -3.8$, **Table 2.1**). The binding affinity was 300-fold weaker when using 170 mM potassium chloride ($1/K_a^N = 360 \pm 50 \mu\text{M}$) as compared to the 36 mM potassium phosphate reference state ($1/K_a^N = 1.3 \pm 0.3 \mu\text{M}$). The presence of small anion effects was indicated by the observation that the slope of the salt dependence reduced to -3.2 and -3.0 for KGlu and KF (**Table 2.1**). For comparison, the binding

affinities in the presence of 170 mM of either salt were 3-fold lower than when the same concentration of KCl was used ($1/K_a^N = 118 \pm 5 \mu\text{M}$) (**Fig. 2.2B, Fig. 2.3, and Table 2.2**). The complete binding curves at high salt (81 – 170 mM K^+) are shown in Supplementary Figure S1.

We also evaluated whether the non-specific DNA binding affinity was affected by the addition of 500 μM MgCl_2 to the standard buffer containing 150 mM K₂Glu (This approximates the concentrations of free potassium and magnesium ions in eukaryotic cells.).[41,42] The binding affinity was only slightly weakened with the addition of magnesium [$1/K_a^N(\text{MgCl}_2) = 97 \pm 6 \mu\text{M}$, versus $1/K_a^N = 80 \pm 5 \mu\text{M}$ (no MgCl_2)], indicating that monovalent cations dominate over divalent cations under physiological conditions. Accordingly, we performed the remainder of the experiments using monovalent salts.

As expected from CC theory, a linear dependence between $\log K_a^N$ and $\log [\text{KCl}]$ was observed (**eq 2.1, Figure 2.2C**). The absolute value of the slope ($N \sim -4$) reflects the total number of ions displaced from the DNA ($Z\Psi$) and hUNG (β) upon binding ($N = Z\Psi + \beta$). This number of displaced ions is slightly greater than the number of cations that are expected to be released based on the theoretical value of $\Psi = 0.64$ cations/per DNA phosphate,[27,32] and the observation that hUNG makes ionic contacts with 5 phosphate groups within the backbone of non-specific DNA [$Z\Psi = (5)(0.64) \sim 3$ cations] [1]. This result suggested that one anion might also be displaced from hUNG during binding. Consistent with this suggestion, the slope decreased to $N \sim -3$ when K₂Glu and KF were used (**Fig. 2.2C, Table 2.1**). Thus, one chloride ion and three potassium ions are likely released from hUNG and non-specific DNA when KCl is used as the salt [32].

The above behavior of KCl, KF and KGlu salts is consistent with the fact that small ions of high charge density (such as fluoride and the carboxylate anion) interact more strongly with water than with the ammonium and guanidinium side chain atoms of hUNG. In contrast, the large weakly hydrated chloride anion forms weak interactions with water and binds tightly to these protein side chains [43,44]. Thus, the KCl data reflect the additional displacement of a chloride anion from hUNG to allow DNA phosphate binding. To focus our study on cation effects at the hUNG-DNA interface, we chose to perform all subsequent experiments using KGlu or KF.

Extrapolating the log linear data to a 1M standard state for KGlu simplifies **eq 2.1** such that only the non-electrostatic binding component remains ($\log K_a^{\text{non}}$) (**Table 2.1**). From this simplification, the non-electrostatic free energy contribution to the total binding free energy is $\Delta G_{\text{non}} = -2.0 \pm 0.2 \text{ kcal mol}^{-1}$ (**Table 2.3**). If ΔG_{non} is subtracted from the observed binding free energy at physiological salt (ΔG_{bind}), the electrostatic contribution can be estimated (i.e. $\Delta G_{\text{elec}} = \Delta G_{\text{bind}} - \Delta G_{\text{non}} = -3.5 \pm 0.5 \text{ kcal mol}^{-1}$). This analysis shows that the formation of the non-specific complex at physiological salt concentration is primarily driven by electrostatic interactions resulting in ion release.

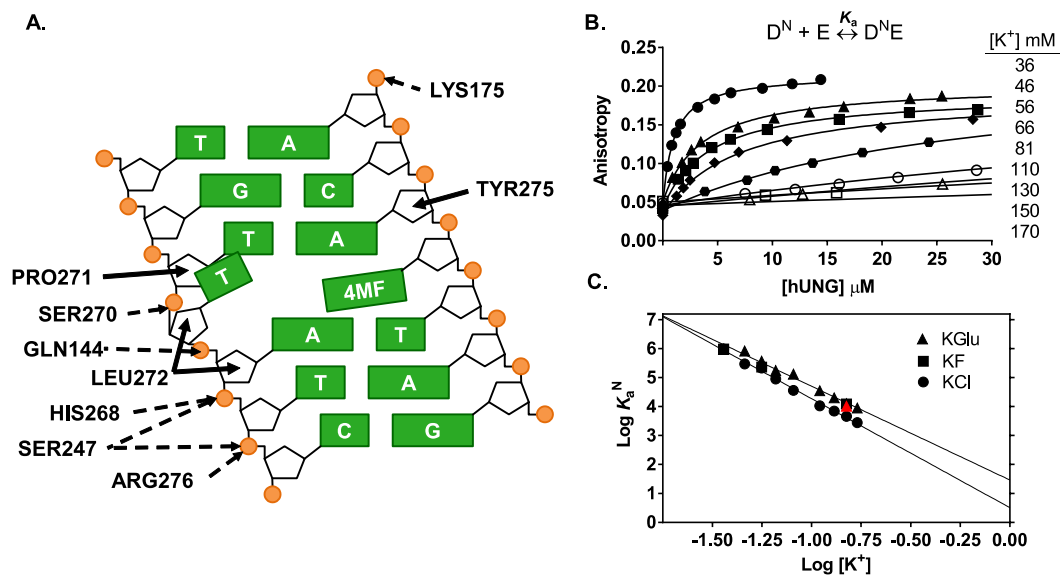


Figure 2.2. Salt dependence of the non-specific DNA (D^N) equilibrium binding affinity. (A) Schematic of electrostatic interactions implicated in ion release (dashed arrows) and the non-electrostatic (solid arrows) interactions between hUNG and non-specific DNA (Protein Data Bank entry 2OXM [40], 4MF = 4-methylindole). Using mutagenesis and NMR imino exchange methods, the partially extruded thymine residue and its interactions with the enzyme have been substantiated in solution using an hUNG-nonspecific DNA complex with central T/A base pair [73,74]. These studies showed that normal T/A base pairs (not G/C) undergo enhanced imino proton exchange when bound to hUNG and involve the residues depicted in the graphic. Electrostatic interactions are defined by nitrogen and oxygen atoms $< 3.3 \text{ \AA}$ apart from DNA phosphate oxygens, while non-electrostatic interactions are all carbon-carbon pairs $< 3.9 \text{ \AA}$ apart. An additional hydrogen bond between hUNG and the O2 of the partially extruded thymine across from 4MF was omitted in the diagram for clarity [40]. (B) Changes in fluorescence anisotropy of D^N (100 nM) as a function of hUNG concentration at varying potassium ion concentrations (36 mM – 170 mM). Full binding curves for 81 – 170 mM K^+ are provided in **Figure 2.3**. (C) Dependence of K_a on the concentrations of K⁺Glu (triangles), K⁺Cl (circles), K⁺F (squares). Inclusion of 500 μ M $MgCl_2$ at physiological K^+ (150 mM) had a negligible effect on the observed K_a (red triangle, see text).

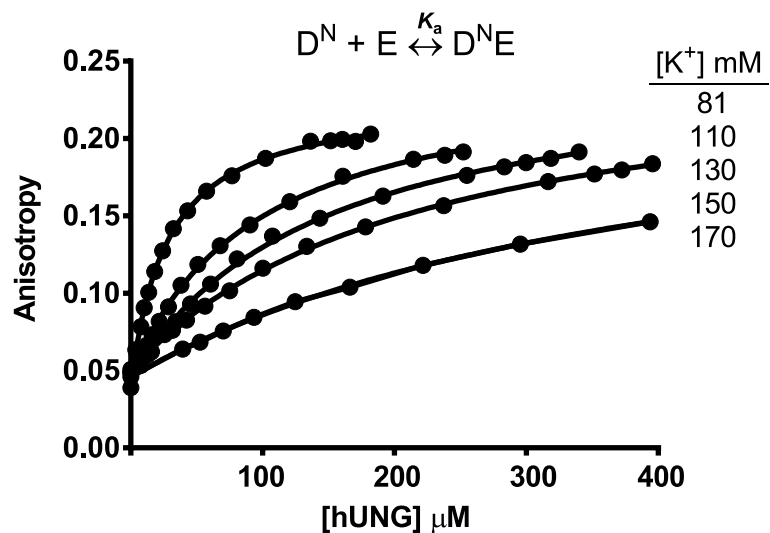


Figure 2.3. Salt dependence of the non-specific DNA (D^N) equilibrium binding affinity at high salt concentrations. Changes in fluorescence anisotropy of D^N (100 nM) are plotted as a function of hUNG concentration at varying potassium ion concentrations (81 mM – 170 mM). Data presented here is an extension of the corresponding binding curves presented in Figure 2B.

Table 2.1. Analysis of the salt dependences of the thermodynamic and kinetic parameters using **eq 2.1**^a

	Slope (N) ^b	X^{non} ^c
	-3.2 ± 0.1	$29 \pm 3 \text{ M}^{-1}$
K_a^{N}	-3.0 ± 0.1^d	$38 \pm 1 \text{ M}^{-1}{}^d$
	-3.8 ± 0.1^e	$3.2 \pm 0.7 \text{ M}^{-1}{}^e$
K_a^{S}	-2.1 ± 0.1^f	$2.29 \pm 0.05 \times 10^5 \text{ M}^{-1}{}^f$
	-2.2 ± 0.3^d	$8.9 \pm 0.5 \times 10^4 \text{ M}^{-1}{}^d$
$k_{\text{on}}^{\text{N},g}$	-1.5 ± 0.2	$6 \pm 2 \times 10^6 \text{ M}^{-1} \text{ s}^{-1}$
k_{on}^{S}	-1.5 ± 0.2	$6 \pm 2 \times 10^6 \text{ M}^{-1} \text{ s}^{-1}$
$k_{\text{off}}^{\text{N},h}$	1.4 ± 0.1	$9.5 \pm 0.2 \times 10^4 \text{ s}^{-1}$
$k_{\text{off}}^{\text{S}}$	0.5 ± 0.1	$24 \pm 2 \text{ s}^{-1}$
k_{cat}	0.9 ± 0.2	$83 \pm 12 \text{ s}^{-1}$
$1/K_m$	-2.2 ± 0.2	$1.4 \pm 0.1 \times 10^{-4} \text{ M}^d$
k_{cat}/K_m	-1.3 ± 0.2	$5.9 \pm 0.2 \times 10^5 \text{ M}^{-1} \text{ s}^{-1}$
P_{trans}^i	-1.5 ± 0.3	0.00 ± 0.05

^a All experiments were conducted using KGlu unless otherwise noted.

^b The slope (N) obtained from nonlinear regression fitting to **eq 2.1**.

^c X^{non} is the extrapolated value of the indicated parameter to the condition of 1 M $[\text{K}^+]$.

^d Determined from equilibrium binding measurements using KF.

^e Determined from equilibrium binding measurements using KCl.

^f Calculated from the ratio of the kinetic constants $k_{\text{on}}^{\text{S}}/k_{\text{off}}^{\text{S}}$.

^g k_{on}^{N} is assumed equal to k_{on}^{S} .

^h Calculated from the ratio of $k_{\text{on}}^{\text{N}}/K_a^{\text{N}}$.

ⁱ P_{trans} is defined in terms of the ratio of kinetic constants detailed in the legend to **Figure 2.1**.

Table 2.2. Binding affinities of hUNG and non-specific DNA ($1/K_a^N$) at variable salt concentration.

[K ⁺] (mM)	$1/K_a^N$ (μ M)		
	KCl	KGlu	KF
36	1.3 ± 0.3	1.3 ± 0.3	1.3 ± 0.3
46	3.4 ± 0.3	1.2 ± 0.1	-- ^a
56	5 ± 3	2.8 ± 0.7	4.3 ± 0.9
66	11.1 ± 0.9	5.7 ± 0.1	--
81	27.7 ± 0.7	7.6 ± 0.5	--
110	95 ± 5	28.1 ± 0.9	--
130	143 ± 9	50 ± 3	--
150	216 ± 8	80 ± 5	80 ± 2
170	360 ± 50	118 ± 5	--

^aData not collected at given salt concentration.

Table 2.3. Electrostatic (ΔG_{elec}) and non-electrostatic (ΔG_{non}) contributions to the binding free energy (ΔG_{bind}) for non-specific (D^{N}) and specific (D^{S}) hUNG complexes in the presence of 150 mM K^+ .^a

	D^{N}	$D^{\text{S}, b}$
ΔG_{bind}^c (kcal mol ⁻¹)	-5.5 ± 0.3	-9.4 ± 0.1
ΔG_{elec}^d (kcal mol ⁻¹)	-3.5 ± 0.5	-2.3 ± 0.2
ΔG_{non}^e (kcal mol ⁻¹)	-2.0 ± 0.2	-7.2 ± 0.1

^a All values are derived from experiments using KGlu.

^b K_a calculated from the ratio $k_{\text{on}}/k_{\text{off}}$ obtained from stopped-flow fluorescence measurements

^c Calculated $\Delta G_{\text{bind}} = -RT \ln K_a$, using K_a at 150 mM $[\text{K}^+]$.

^d $\Delta G_{\text{elec}} = \Delta G_{\text{bind}} - \Delta G_{\text{non}}$. ΔG_{elec} pertains to the condition of 150 mM K^+ .

^e $\Delta G_{\text{non}} = -RT \ln K_a$, using the measured K_a at 1M K^+ .

2.2.2. Ion Effects on the Binding Equilibrium for Specific DNA.

The electrostatic and non-electrostatic interactions predicted from the crystal structure of a specific complex between hUNG and DNA are depicted in **Figure 2.4A** [45]. In general, this complex appears to retain the electrostatic contributions that were observed in the non-specific complex (**Fig. 2.2A**), but gains substantial non-electrostatic interactions arising from flipping of the uracil base into the active site and the intercalation of a leucine side chain into the base stack. In addition, the DNA is severely bent in this structure leading to compression and expansion of the inter-phosphate distances typically seen in B DNA.

To evaluate the relative importance of these specific interactions, the salt dependence of the binding affinity for the specific substrate (D^S) was measured by monitoring the increase in 2-AP fluorescence as a function of hUNG concentration using various concentrations of potassium fluoride. These experiments used a 19 base pair duplex (D^S) that contained the fluorescent base 2-AP adjacent to U^β . This 2'-fluorinated uracil nucleotide prevents glycosidic bond cleavage during the time frame of the measurements (the fluorine is in the β anomeric configuration in this substrate analogue) [36]. Upon binding of hUNG, the uracil base is flipped into the active site, unstacking 2-AP and leading to an increase in its fluorescence intensity [36]. In these experiments KF was used because high concentrations of KGlu introduced spectral interferences that prevented reproducible fluorescence measurements. This substitution is justified because the salt dependences of non-specific DNA binding are identical in the presence of both of these salts (**Fig. 2.2C**).

For the specific substrate, a linear dependence between $\log K_a^S$ and the $\log [KF]$ was observed (**Fig. 2.4B, Fig. 2.5**), but a shallower slope was observed than for the non-

specific complex ($N = -2.1$, **Table 2.1**). Although the reduced slope may indicate that fewer ions are displaced, this conclusion is not consistent with the number of ionic contacts observed in the crystal structure (**Fig. 2.4A**). This apparent discrepancy may arise from the severe bending observed in the specific complex, which is not accounted for by simple polyelectrolyte theory where DNA is considered as a rod with identical phosphate-phosphate distances.[28,29,33] Regardless, **Table 2.3** shows that the specific complex is primarily stabilized by non-electrostatic interactions at a physiological salt concentration ($\Delta G_{\text{non}} = -7.2 \pm 0.1 \text{ kcal mol}^{-1}$, $\Delta G_{\text{elec}} = -2.2 \pm 0.2 \text{ kcal mol}^{-1}$). This is consistent with the structural findings described above where hUNG interacts extensively with the extruded uracil base and Leu272 inserts into the DNA duplex. None of these non-electrostatic interactions are observed in the non-specific complex (**Fig. 2.2A**).

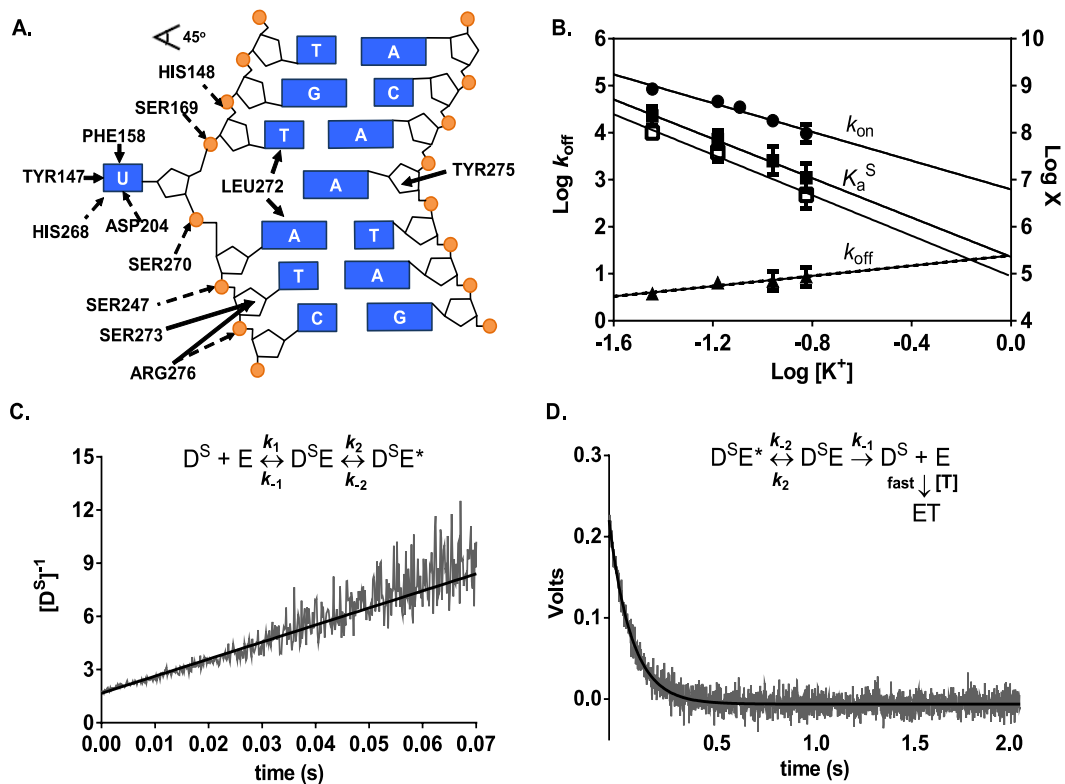


Figure 2.4. Salt dependences of the specific DNA (D^{S}) association and dissociation constants and equilibrium binding affinity determined by stopped-flow fluorescence. **(A)** Electrostatic (dashed arrows) and the non-electrostatic (solid arrows) interactions between hUNG and specific DNA (Protein Data Bank entry 1EMH[45]). **(B)** Dependence on K^+ concentration of k_{on}^{S} (circles), $k_{\text{off}}^{\text{S}}$ (triangles), the calculated K_{a}^{S} obtained from the ratio $k_{\text{off}}^{\text{S}}/k_{\text{on}}^{\text{S}}$ (solid squares), and the measured K_{a}^{S} from equilibrium fluorescence titrations using KF (open squares). $\text{Log } k_{\text{off}}^{\text{S}}$ is plotted on the left y-axis and the remaining parameters are plotted on the right y-axis [$X = K_{\text{a}}^{\text{S}}$ (M^{-1}) and k_{on}^{S} ($\text{M}^{-1} \text{s}^{-1}$)]. **(C)** Linearized kinetic trace of the second-order association of D^{S} (600 nM) with hUNG (600 nM) at 150 mM K^+ . Time dependent increase in 2-AP fluorescence was followed ($\lambda_{\text{ex}} = 310 \text{ nm}$). The line is the best-fit to a second-order rate equation. **(D)** Kinetic trace of the dissociation of hUNG from D^{S} at 150 mM K^+ . Abasic site-containing DNA (aDNA, 5 μM) was mixed with an equal volume solution containing 0.8 μM hUNG and 0.2 μM D^{S} and the time dependent decrease in 2-AP fluorescence was followed. The line is the best-fit to a single exponential decay. Controls established that the observed rate was zero-order with respect to DNA trap.

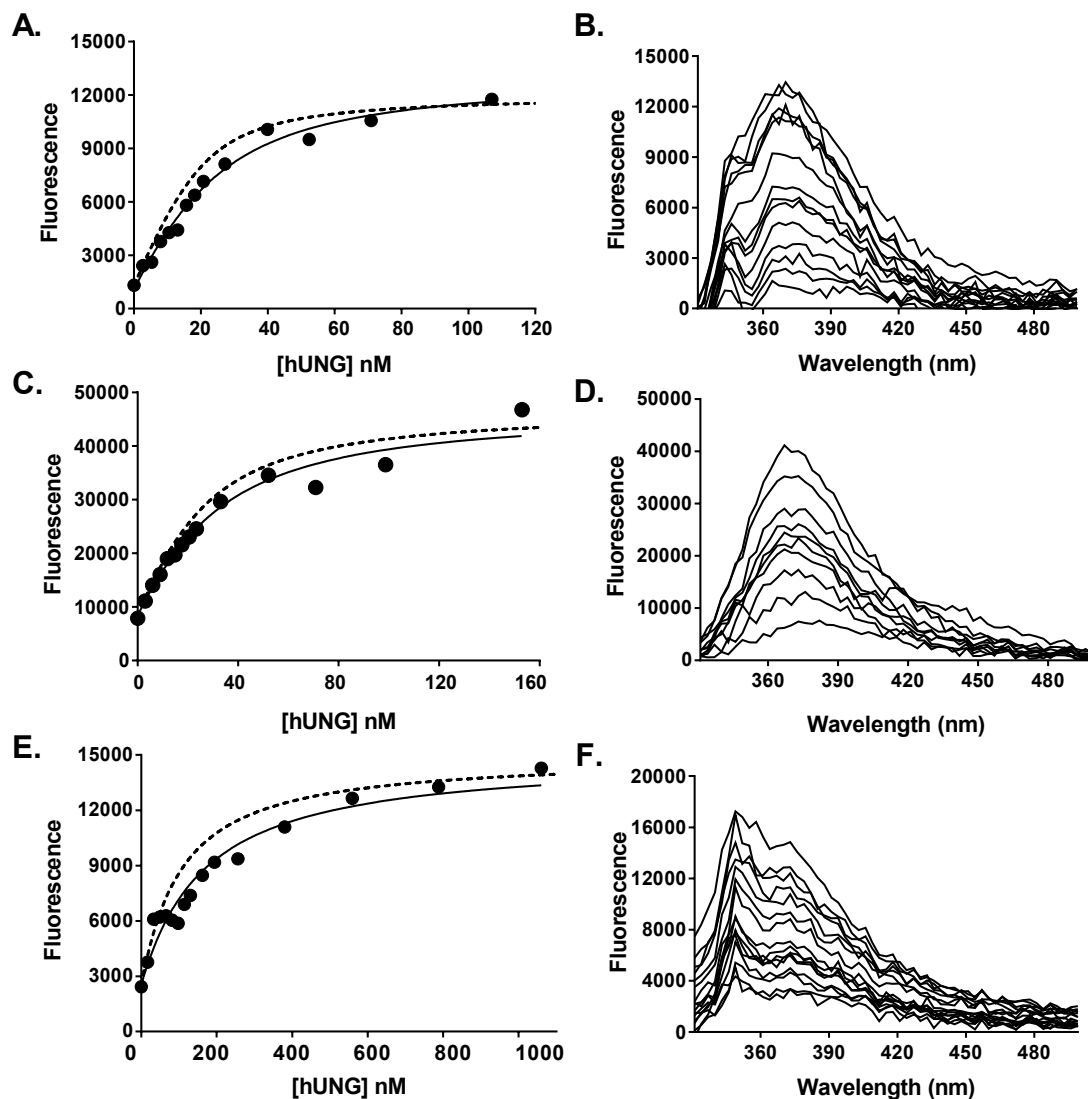


Figure 2.5. Binding affinity (K_D) of the specific substrate determined by fluorescence titration at varying salt concentrations. Comparison to the values determined by stopped-flow (dashed lines, $k_{\text{off}}^S/k_{\text{on}}^S$ ratios are reported **Table 2.4**) is included. Fluorescence intensities at 370 nm as a function of hUNG concentration (solid line) compared to the theoretical curves derived from the ratios $k_{\text{off}}^S/k_{\text{on}}^S$ (dashed lines) in the presence of (A) and (B) 36 mM KF, (C) and (D) 66 mM KF, (E) and (F) 150 mM KF. Panels B, D, and F are background corrected fluorescence emission scans. The residual peak at ~ 330 nm is due to imperfect subtraction of the intense water Raman scattering peak when using very low DNA concentrations.

2.2.3. Salt Effects on the Kinetics for Binding and Dissociation from Specific DNA.

Association and dissociation kinetics of the specific DNA complex (D^S) were measured by following the changes in 2-AP fluorescence using a stopped-flow rapid kinetic device (**Fig. 2.4C, D**). To determine the salt sensitivity of k_{on} , we monitored the increase in 2-AP fluorescence under irreversible second-order conditions, in which both the enzyme and DNA were mixed in equal molar amounts (400 or 600 nM) using increasing concentrations of KGlu (36mM – 150mM). The large signal-to-noise ratio at these high DNA concentrations significantly decreased the spectral interference from KGlu that was observed in the equilibrium binding assay, where the DNA concentration was 20-fold lower. To ensure that association was essentially irreversible for these measurements, the hUNG and DNA concentrations were kept well above the value for the equilibrium dissociation constant ($1/K_a^S$) at all salt concentrations. The irreversible conditions at high salt were confirmed by measuring k_{on} using 400 and 600 nM concentrations of both DNA and enzyme (110 mM KGlu). These conditions resulted in k_{on} values that were the same within the errors of these measurements ($1.0 \pm 0.7 \times 10^8 \text{ M}^{-1}\text{s}^{-1}$ and $1.8 \pm 0.1 \times 10^8 \text{ M}^{-1}\text{s}^{-1}$). The irreversible nature of these association reactions was further substantiated by the fact that the same change in voltage was observed at all salt concentrations tested, indicating that the same degree of saturation was reached (**Figure 2.6A**). A linearized kinetic trace at 150 mM K^+ is shown in **Figure 2.4C**, which was fitted to **eq 2.5** to obtain the association rate constant [$k_{on} = (9.6 \pm 0.4) \times 10^7 \text{ M}^{-1} \text{ s}^{-1}$]. All additional kinetic traces are shown in **Figure 2.6**. This association rate increased by an order of magnitude as the salt concentration was decreased to 36 mM [$k_{on}^S = (8.5 \pm 0.1) \times 10^8 \text{ M}^{-1} \text{ s}^{-1}$] (**Table 2.4**). We note that this represents one of the most rapid macromolecule binding reactions,

approaching the extreme of previously reported electrostatically enhanced association rates.[46]

The dissociation rates for specific DNA complexes ($k_{\text{off}}^{\text{S}}$) were also determined at increasing concentrations of potassium ions (36 mM – 150 mM) by monitoring the decrease in 2-AP fluorescence upon dissociation of hUNG from the DNA (**Fig. 2.4D, 2.6B**). To ensure that all enzyme molecules dissociated irreversibly, the dissociated enzyme was trapped with an excess of DNA containing an abasic site (aDNA). In contrast with the association rate, the first-order dissociation rate was found to increase only modestly (~2-fold) when the salt concentration was raised from 36 to 150 mM K^+ ($3.8 \pm 0.3 \text{ s}^{-1}$ to $8.7 \pm 0.7 \text{ s}^{-1}$) (**Table 2.4**). Based on comprehensive kinetic measurements with the similarly behaved *E. coli* enzyme [36,47,48], it is long-known that the single-exponential dissociation reflects rate-limiting exit of the uracil base from the enzyme active site [36,47,48]. The dissociation of the DNA from the enzyme occurs in an extremely rapid step after the slower internal steps and is not detected in the fluorescence measurements. Thus, the relative salt insensitivity of k_{off} is fully consistent with a slow internal step being overall rate limiting for dissociation of the specific DNA, while association is influenced by a different salt sensitive step.

The salt dependence of the binding kinetics to non-specific DNA was not directly addressable due to weak binding and the fast association and dissociation rates. Since non-specific binding precedes formation of the specific complex, it is reasonable to conclude that the association rates for the non-specific complex are similarly affected by salt as the specific complex (i.e. $k_{\text{on}}^{\text{N}} = k_{\text{on}}^{\text{S}}$). Using these assumed values for k_{on}^{N} , the dissociation

rates for non-specific DNA at each $[K^+]$ were calculated from the relationship $k_{\text{off}}^{\text{N}} = k_{\text{on}}^{\text{N}}/K_{\text{a}}^{\text{N}}$ using the measured equilibrium association constants at each salt concentration. The approach indicated a 7-fold increase in $k_{\text{off}}^{\text{N}}$ over the salt range tested [$k_{\text{off}}^{\text{N}}$ (calculated, 36 mM salt) = $1100 \pm 300 \text{ s}^{-1}$, $k_{\text{off}}^{\text{N}}$ (calculated, 150 mM salt) = $7700 \pm 500 \text{ s}^{-1}$], which is similar to the effect on k_{on}^{N} and k_{on}^{S} . This analysis suggests the same rate-limiting transition state is being followed in the forward and reverse directions for binding and dissociation of nonspecific DNA (i.e. two-state behavior).

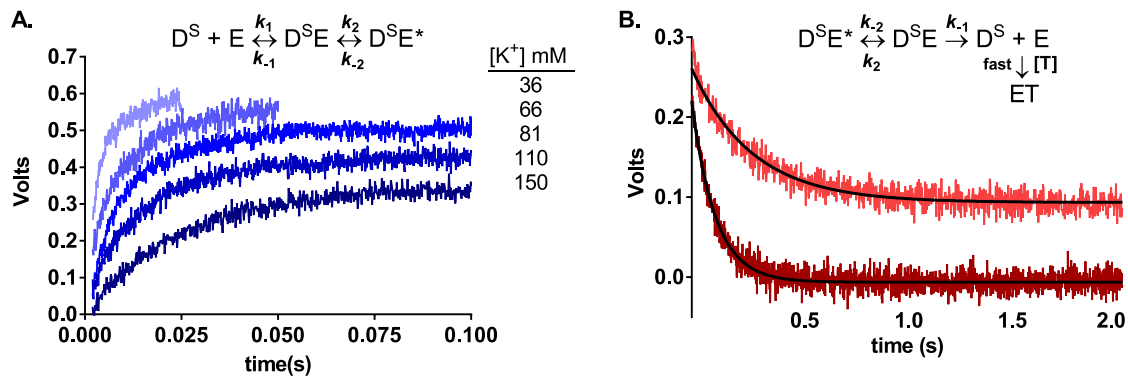


Figure 2.6. Salt dependence of the association (k_{on}) and dissociation (k_{off}) kinetics of hUNG binding to specific DNA (D^S). (A) Raw fluorescence traces of the increase in 2-AP fluorescence upon binding of hUNG under salt concentrations of 36 – 150 mM K^+ . Equal volume solutions of D^S and hUNG of equal concentration (400-600 nM) were mixed and the time dependent increase in 2-AP fluorescence was followed ($\lambda_{ex} = 310$ nm). Traces are displaced along the y-axis for ease of visualization. (B) Kinetic trace of the dissociation of hUNG from D^S at 36 mM K^+ (pink) and 150mM K^+ (red). Data for 150 mM K^+ is the same trace presented in Figure 4D. Abasic site-containing DNA (aDNA, 5 μ M) was mixed with an equal volume solution containing 0.8 μ M hUNG and 0.2 μ M D^S and the time dependent decrease in 2-AP fluorescence was followed ($\lambda_{ex} = 310$ nm). The lines are the best-fits to a single exponential decay. Traces are displaced along the y-axis for ease of visualization.

Table 2.4. Specific DNA binding affinities ($1/K_a^S$) and association (k_{on}) and dissociation (k_{off}^S) rate constants for hUNG as a function of $[K^+]$.^a

$[K^+]$ (mM)	k_{on}^S ($M^{-1} s^{-1}$)	k_{off}^S (s^{-1})	$1/K_a^S$ (nM) ^b	k_{off}^S/k_{on}^S (nM) ^c
36	$8.5 \pm 0.1 \times 10^8$	3.8 ± 0.3	10 ± 3	4.5 ± 0.4
66	$4.6 \pm 0.3 \times 10^8$	6.4 ± 0.1	26 ± 8	14 ± 1
81	$3.5 \pm 0.3 \times 10^8$	--	--	--
110	$1.8 \pm 0.1 \times 10^8$	6.9 ± 0.5	--	40 ± 5
150	$9.6 \pm 0.4 \times 10^7$	8.7 ± 0.7	260 ± 77	91 ± 11

^a All experiments were conducted using KGlu as the salt unless otherwise noted.

^b K_a measured by fluorescence titration in the presence of KF.

^c The ratio k_{off}^S/k_{on}^S was obtained from stopped-flow fluorescence measurements.

2.2.4. Salt Effects on Steady-State Kinetics of hUNG Catalyzed Uracil Excision.

Steady-state kinetic measurements used a continuous fluorescence assay and a 30 base pair oligo (PUA-30) that contained a 2-AP base adjacent to a U-A base pair [37]. The initial rate of reaction was determined by monitoring the time dependent increase in 2-AP fluorescence, which reports on hUNG catalyzed excision of the adjacent uracil base. Nonlinear regression fitting of the data to the Michaelis-Menten equation is shown in **Figure 2.7A-D**, from which k_{cat} , K_{m} , and $k_{\text{cat}}/K_{\text{m}}$ values were determined (**Table 2.5**). As shown in Figure S3, we were able to attain greater than >85% saturation of the enzyme with substrate at salt concentrations between 36 and 110 mM. However, at the highest concentration of 150 mM only 63% saturation was achieved, resulting in a larger uncertainty in k_{cat} . Nevertheless, even at this salt concentration $k_{\text{cat}}/K_{\text{m}}$ was well-determined because this second-order rate constant is also given by the initial slope of the saturation curve when $[S] \ll K_{\text{m}}$ (**Figure 2.7D**). We attempted to attain greater saturation of the enzyme at 150 mM concentration of salt, but the DNA concentration could not be increased beyond 4 μM due to apparent substrate inhibition or aggregation as the concentration was increased further.

Plots of $\log k_{\text{cat}}$, $\log 1/K_{\text{m}}$, and $\log k_{\text{cat}}/K_{\text{m}}$ against $\log [K^+]$ were all linear (**Fig. 8A, B, C**). The k_{cat} value increased 4-fold as the salt concentration was increased from 36 to 150 mM K^+ ($3.5 \pm 0.3 \text{ s}^{-1}$ and $15 \pm 2 \text{ s}^{-1}$) (**Fig. 8A**), which is a similar response as k_{off} . The slopes of the log-log plots for k_{cat} and k_{off} were slightly *positive*, implying ion uptake, with $N^{k_{\text{cat}}} = 0.9 \pm 0.2$ and $N^{k_{\text{off}}} = 0.5 \pm 0.1$ (**Table 2.1**). Since k_{cat} is limited by product release and not chemistry [49,50], and the product complex is structurally and thermodynamically similar to the substrate complex [50], it would appear that the rate-limiting transition states

for both substrate and product dissociation do not involve significant ion uptake. In contrast, the $1/K_m$ and k_{cat}/K_m values had stronger dependences on the salt concentration, with slopes resembling that of K_a^S and k_{on} , respectively ($N^{1/K_m} = -2.2$ and $N^{k_{cat}/K_m} = -1.3$, compare values in Table 1). The approximately ten-fold greater values of k_{on} as compared to k_{cat}/K_m at each salt concentration may arise from the different sequences of these specific substrates, or the presence of additional partially rate-limiting transition states that comprise k_{cat}/K_m (for instance, uracil excision occurs at a single-turnover rate $k_{ex} = 240 \text{ s}^{-1}$) [3]. Regardless, these results indicate that diffusion-controlled (or near diffusion-controlled) processes like k_{on} and k_{cat}/K_m involve transition-states that necessitate ion release.

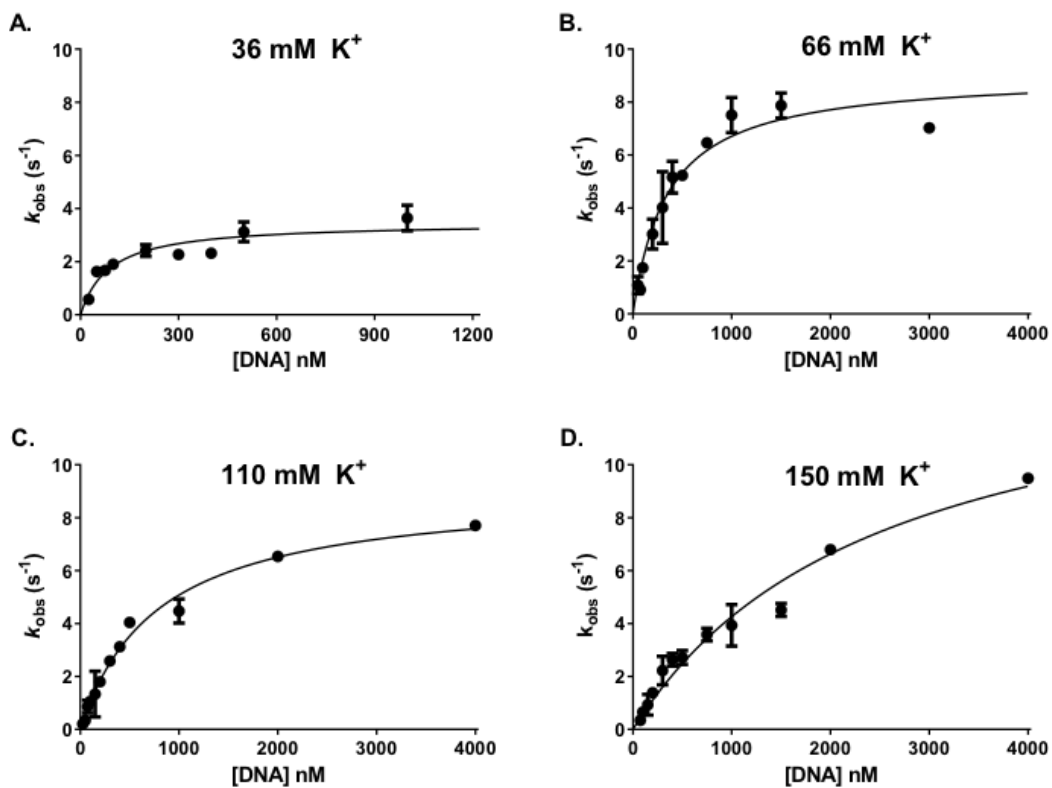


Figure 2.7. Michaelis-Menten curves of the initial rates of reaction with PUA-30 as a function of DNA concentration. The various salt concentrations are indicated in each plot (A-D). For panel (D) we attempted to attain greater saturation of the enzyme but the DNA concentration could not be increased beyond 4 μM due to apparent substrate inhibition or aggregation at higher concentrations.

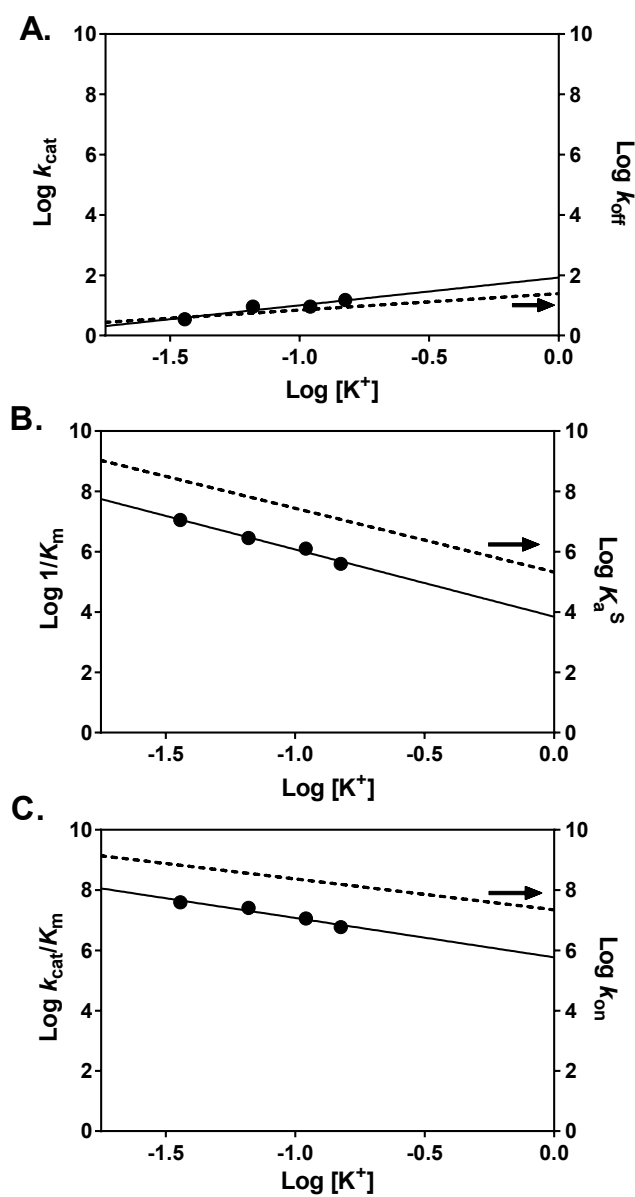


Figure 2.8. Salt dependences of k_{cat} , K_m , and k_{cat}/K_m . (A) The value for k_{cat} (circles) is limited by product release and is minimally dependent on KGlu concentration. This is similar to the behavior observed for k_{off} (dashed line). (B) The dependence of $1/K_m$ (circles) on KGlu concentration is very similar to that observed for specific DNA binding K_a^s (dashed line). (C) The dependence of k_{cat}/K_m (circles) on KGlu concentration is identical to the dependence observed for k_{on} (dashed line).

Table 2.5. Steady-state kinetic parameters of hUNG and specific DNA at various salt concentrations. ^a

[K ⁺] (mM)	<i>k</i> _{cat} (s ⁻¹)	<i>K</i> _m (M)	<i>k</i> _{cat} / <i>K</i> _m (M ⁻¹ s ⁻¹)
36	3.5 ± 0.3	9 ± 3 x 10 ⁻⁸	4 ± 2 x 10 ⁷
66	9.1 ± 0.6	3.5 ± 0.7 x 10 ⁻⁷	2.6 ± 0.7 x 10 ⁷
110	9.1 ± 0.4	7.8 ± 0.8 x 10 ⁻⁷	1.2 ± 0.1 x 10 ⁷
150	15 ± 2	2.5 ± 0.5 x 10 ⁻⁶	6 ± 2 x 10 ⁶

^a All experiments were conducted using KGlu as the salt.

2.2.5. Increased Salt Concentrations Reduce Probability of Intramolecular Site Transfer.

To characterize the salt dependence of the transition state for intramolecular translocation of hUNG between two uracil sites spaced 20 base pairs apart on the same strand in duplex DNA (S20), we used our previously developed facilitated diffusion assay [12,51]. This site spacing was chosen because all transfer events result from hUNG dissociating and re-associating with the DNA at least once (only the dissociative pathway is operational, P_{diss}) [4]. After post-reaction sample processing, the electrophoretically separated DNA fragments produced from uracil from single and double uracil excision events were quantified using phosphorimaging analysis. Intramolecular site transfer results in the production of excess A and C fragments that result from double-excision events, while single site excision produces exactly equal amounts of the A, C, AB and BC product bands (**Fig. 2.9A, B**) [21,51]. The time independent dissociative site transfer probability (P_{diss}) can be calculated precisely using **eq 2.2** by linear extrapolation of the observed transfer probabilities ($P_{\text{diss}}^{\text{obs}}$) to zero time².

$$P_{\text{diss}} = \frac{[A]^0 + [C]^0 - [AB]^0 - [BC]^0}{[A]^0 + [C]^0 + [AB]^0 + [BC]^0} \quad (2.2)$$

We measured P_{diss} in the presence of 13 to 63 mM K^+ ion, beyond which site transfer by the dissociative pathway was no longer detectable. As shown in Figure 5C, P_{diss} showed a strong dependence on salt concentration, decreasing 4-fold between 13 mM

² The uracil excision efficiency is not expected to greatly influence the salt sensitivity of the transfer probabilities (i.e. the uracil excision efficiency is the probability that once hUNG has located a uracil site it falls off the site before base excision occurs) [4]. This expectation is strongly supported by the largely salt insensitive specific substrate dissociation rates (k_{off}^S) over the salt range used in the measurements of P_{diss}

and 63 mM K^+ (**Table 2.6**). A log linear dependence was observed between 22 mM and 63 mM K^+ (**Fig. 2.9D**), which provided a slope value $N = -1.5 \pm 0.3^3$. This slope value is identical to the salt dependence of the association rate k_{on} , which suggests that hUNG molecules undergoing dissociative translocation move outside of the ion cloud, and their reassociation is influenced in the same way by the presence of bulk salt ions.

³ P_{diss} reached a plateau at salt concentrations below 22 mM (**Figure 2.9**). The basis for this effect has not been explored, but it likely arises from the kinetic definition of P_{diss} , which includes a term for k_{on} (see legend to **Figure 2.1**, where $k_{on} = k_{return}$). We speculate that when salt is reduced below 22 mM the probability of returning to the DNA could be constant and limited by the local electrostatic environment rather than the bulk salt concentration.

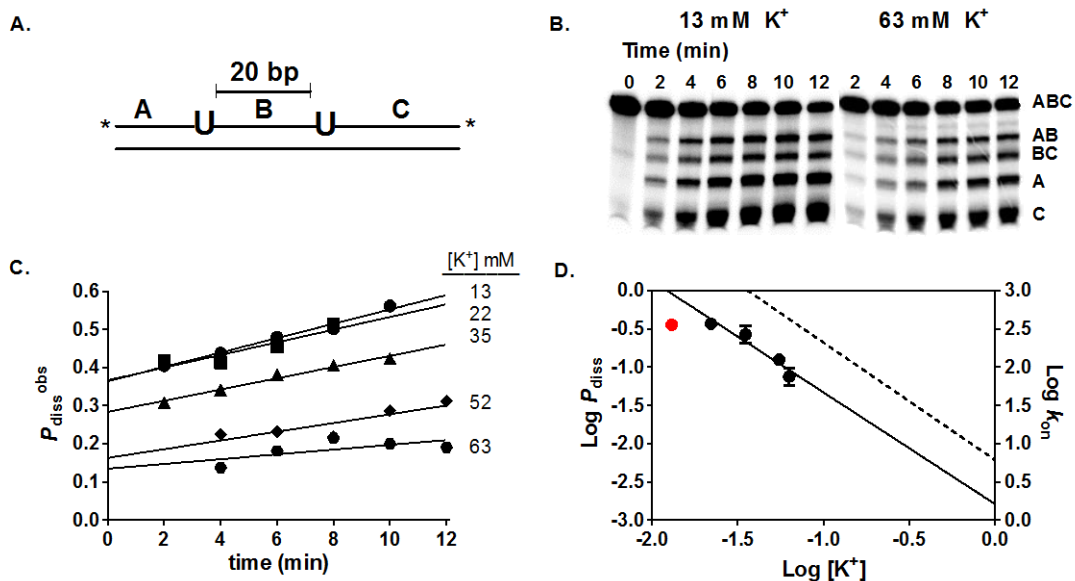


Figure 2.9. Salt dependence of the intramolecular dissociative transfer probability of hUNG between two uracil sites spaced 20 bp apart (P_{diss}). (A) Schematic of the substrate (S20) used. The asterisk denotes the location of the ^{32}P end labels. (B) Phosphorimages of the gel-resolved site transfer products derived from S20 in the presence of 13 mM and 63 mM K^+ . (C) Determination of P_{diss} at varying K^+ levels in the range 13 – 63 mM. The observed site transfer probability ($P_{\text{diss}}^{\text{obs}}$, Equation 2.2) is calculated at each time point and then linearly extrapolated to time zero to determine the true value (P_{diss}). (D) Comparison of the dependences of P_{diss} (circles) and k_{on} (dashed line) on K^+ concentration. The P_{diss} value at 13 mM (red circle) deviated negatively from the linear correlation and was omitted from the linear regression analysis (see text).

Table 2.6. Probability of site transfer (P_{trans}) between two uracils with 20 base pair spacing at varying salt concentrations.^a

[K ⁺] (mM)	P_{trans}
13	0.36 ± 0.03
22	0.37 ± 0.02
35	0.27 ± 0.07
52	0.12 ± 0.02
63	0.09 ± 0.01

^a All experiments were conducted using K₂Glu as the salt.

2.3 DISCUSSION

2.3.1. Electrostatic Contribution to Non-specific DNA Binding is Entropy Driven.

The disparate effects of salt ions on the binding of hUNG to undamaged and damaged DNA indicates that distinct thermodynamic interactions are involved in stabilizing these complexes. According to CC theory, weaker binding induced by high salt concentrations originates from a reduction in the entropy of mixing associated with expelling ions from the DNA ion cloud into bulk solution. Therefore, the electrostatic component of the binding energy is purely entropic. We confirmed this entropic expectation for the non-specific DNA complex by measuring the logarithmic salt dependence of the binding affinities at four temperatures, where the slopes of the $\log K_a$ vs. $\log [K\text{Glu}]$ plots were indistinguishable at each of the temperatures (**Fig. 2.10**) [27]. The corresponding analyses for the specific complex could not be performed because of experimental difficulties in making reliable 2-AP fluorescence measurements of equilibrium binding at low DNA concentrations at multiple temperatures.

Previous studies have shown that the complex between hUNG and non-specific DNA is held together by a handful of enzyme contacts with the phosphate backbone, with minimal distortion of the double helix (**Fig. 2.2A**) [40]. The structural view is in agreement with the present thermodynamic findings, where approximately three monovalent cations are released from the DNA upon binding, and only a small non-electrostatic contribution to the binding free energy is indicated, suggesting minimal duplex distortion (**Fig. 2.11**). These data characterize the non-specific DNA complex as a loosely associated state that is formed by virtue of the entropic effects of cation displacement from the DNA. The weak electrostatic character of the non-specific complex provides a binding mode for hUNG that

is consistent with rapid facilitated diffusion by the previously described dissociative and associative pathways (**Fig. 2.1**). A binding lifetime on non-specific DNA in the millisecond to sub-millisecond time regime has the virtue of minimizing the time spent bound to undamaged DNA sequences and provides frequent opportunities for repeated cycles of enzyme dissociation, rapid 3D diffusion and local rebinding of the DNA chain. This type of mechanism, combined with short-range associative transfers where the enzyme remains in contact with the DNA (<10 bp) [4], provides excellent search coverage at a maximum possible rate that is only bounded by the limits of diffusion.

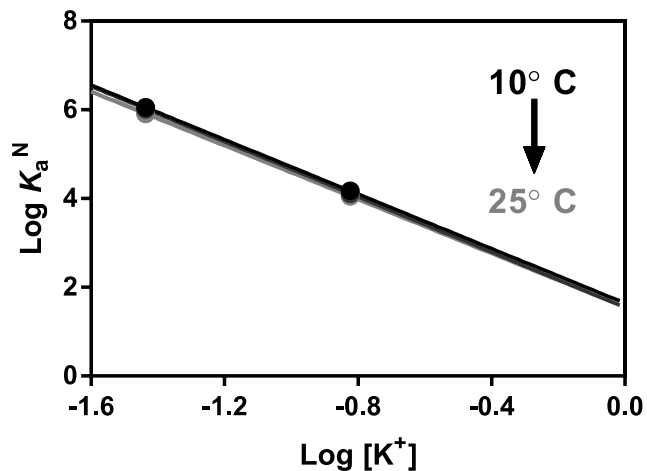


Figure 2.10. Salt dependence of the nonspecific DNA binding affinity at various temperatures. The salt effect is identical at 10, 15, 20, and 25°C (36 mM and 150 mM KGl_u). This behavior is expected from entropically driven ion displacement.

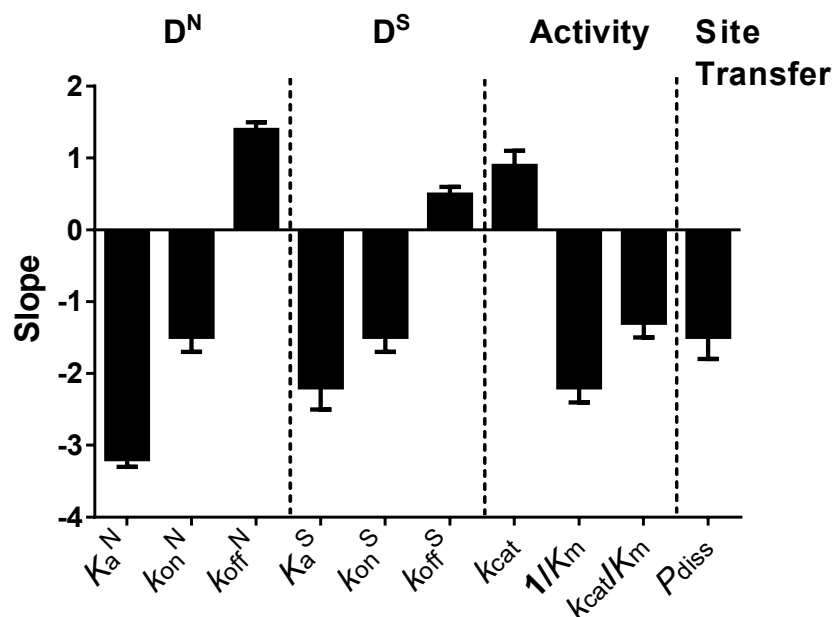


Figure 2.11. Summary of the salt dependences of each measured thermodynamic and kinetic parameter (X) (see section 2.3). The dependences are represented as the slopes of the respective $\log [\text{salt}]$ vs. $\log X$ plots. Positive slopes indicate dissociation processes resulting in ion condensation, which are facilitated by high ionic strength (k_{cat} , k_{off}). Negative slopes result from processes that involve ion displacement and are hindered by high salt concentrations.

2.3.2. Specific DNA Binding is Driven by Non-electrostatic Interactions.

In contrast with non-specific DNA, the formation of the specific complex with uracilated DNA was driven primarily by non-electrostatic forces depicted in **Figure 2.4A**. Despite the crystallographic evidence that all the ionic interactions present in the non-specific complex are preserved in the specific complex [40,52], the stability of the specific hUNG-DNA complex was less dependent on salt (**Table 2.1**). Such behavior of a specific and non-specific protein-DNA complex has been observed in studies of lac Repressor and attributed to structural differences between the two complexes that lead to changes in ion displacement stoichiometry [53-58]. For the case of hUNG, the most striking difference between the non-specific and specific complexes is the severe distortion of the helical parameters of the DNA in the latter, suggesting that similar effects of duplex deformation may be operative. In general, it is not clear how distortions of the DNA helix that are induced upon protein binding alter the surrounding ion cloud and the observed stoichiometry of ion displacement. If an increase in charge density of the phosphate backbone upon DNA bending promotes the condensation of additional cations, then the net number of ions displaced upon binding would be reduced. This potential contribution to the interpretation of ΔG_{elect} for the specific complex does not impact the primary finding that a large non-electrostatic component to the binding free energy is introduced upon formation of this complex.

Another implication of the different contributions of electrostatic and non-electrostatic binding energy terms for the non-specific and specific complexes is that binding specificity is enhanced at higher salt concentrations (defined as the ratio K_a^S/K_a^N) [35]. While this calculation is best performed for sequences of identical length and nearly

identical sequence (which is not the case for the specific and non-specific duplexes used in this study), the relative change in specificity as a function of salt is still informative. At low salt (36 mM), the specificity of hUNG for the specific DNA is 290 ± 90 while at physiological salt (150 mM), the specificity increases approximately 4-fold (1300 ± 200). The greater salt sensitivity of non-specific DNA binding and the large non-electrostatic component of the binding energy for the specific complex have the combined effect of minimizing sequestration of the enzyme on bulk undamaged DNA, while allowing the specific complex to persist long enough for efficient catalysis to take place.

2.3.3. Association of hUNG with DNA is Accelerated by Electrostatics.

Long-range electrostatic interactions are known to play a significant role in accelerating the association of proteins with various targets, and the polyanionic nature of DNA makes this effect especially significant in the case of protein-DNA association [59,60]. The acceleration provided by the electrostatic interaction will supply a biasing force that increases the basal rate of association in the absence of such a force ($k_{\text{on}}^{\text{non}}$) [46]. For modest sized enzymes such as hUNG that exhibit diffusion-controlled binding, an upper limit for $k_{\text{on}}^{\text{non}} \sim 10^6 \text{ M}^{-1} \text{ s}^{-1}$ has been estimated from theoretical considerations [61-64]. This theoretical upper limit has been achieved in some highly efficient systems (the association of barnase with its inhibitor barstar is one well-characterized example) [65]. For hUNG we estimate $k_{\text{on}}^{\text{non}} = 6 \pm 2 \times 10^6 \text{ M}^{-1} \text{ s}^{-1}$ from extrapolating the salt dependent association rates to 1 M salt (**Table 2.1**). Extrapolation from the 1 M standard state used to estimate $k_{\text{on}}^{\text{non}}$ to a physiologically relevant salt concentration of 150 mM reveals that the association rate is increased by one order of magnitude. The electrostatic contribution

towards lowering the free energy barrier for association at physiological salt may be calculated using **eq 2.3** ($G_{\text{elec}}^{\ddagger} = -1.6 \pm 0.3 \text{ kcal mol}^{-1}$).

$$G_{\text{elec}}^{\ddagger} = -RT \ln \left(\frac{k_{\text{on}}}{k_{\text{on}}^{\text{non}}} \right) \quad (2.3)$$

An electrostatic enhancement of the same magnitude is also indicated from the salt dependence of $k_{\text{cat}}/K_{\text{m}}$ (**Table 2.1**). This correspondence indicates that the rate-limiting transition state for enzyme-DNA association and steady-state turnover under limiting substrate conditions share similar electrostatic characteristics. It should be noted that $G_{\text{elec}}^{\ddagger}$ comprises all net effects arising from electrostatic interactions. This includes an increased contribution from facilitated diffusion as the salt concentration is decreased from 1 M to 0.15 M. However, a large contribution from facilitated diffusion would not be expected for the relatively small duplexes used in this study.

2.3.4. Dissociation of the Specific Complex is a Multi-step Process.

Although dissociation of the non-specific complex ($k_{\text{off}}^{\text{N}}$) was enhanced by increasing salt concentrations, the salt effect was reduced for dissociation of both the specific ($k_{\text{off}}^{\text{S}}$) and abasic product DNA complexes (using k_{cat} as a surrogate for the product k_{off}) (**Table 2.1 and Figure 2.11**). These different salt effects on the non-specific and two specific complexes can be rationalized by the crystallographic finding that extensive non-electrostatic contacts are formed in the specific complexes, which must be broken prior to dissociation (**Fig. 2.4A**) [40,45,50]. Breaking of these specific contacts must occur in a relatively salt-insensitive rate-limiting transition state that precedes dissociation. This view is consistent with previous rapid kinetic studies with UNG that have elucidated a two-step binding mechanism for formation of specific complexes [48]. In contrast, the non-

specific complex apparently forms in a salt sensitive single-step reaction, with association and dissociation occurring in the same rate-limiting transition-state. Thus, equal numbers of counter ions should be released in the forward binding direction and taken up in the reverse dissociation reaction, which is supported by the similar slopes for the salt dependences of k_{on}^{N} and $k_{\text{off}}^{\text{N}}$ in **Table 2.1** and **Figure 2.11**.

2.3.5. The Dissociative Facilitated Diffusion Pathway Involves Escape of hUNG from the DNA Ion Cloud.

We previously reported that the associative pathway for intramolecular site transfer was salt insensitive, but that the dissociative pathway was salt sensitive over the range that was studied [4]. The insensitivity of associative pathway was explained by the relatively constant nature of the ion cloud around the DNA over a wide range of salt concentrations [66-68], and the supposition that associative transfers do not lead to net ion displacement. The salt dependence of the dissociative pathway was interpreted to result from enzyme molecules diffusing beyond the ion cloud during short-range dissociation and reassociation events.

The data presented here provide further support for the conclusion that the fundamental distinction between the associative and dissociative pathways is that during dissociative transfers hUNG escapes the ion cloud prior to reassociating at a nearby position on the DNA chain. We utilized a substrate containing a uracil site spacing of 20 base pairs such that all transfers required at least one dissociation event (the associative transfer length of hUNG is only about ~5 bp) [4]. The finding that P_{diss} and k_{on} have indistinguishable dependences on salt (**Fig. 2.11**), demonstrates that the overall dissociative transfer process involves a salt sensitive step resembling that of enzyme-DNA

association from bulk solution. This interpretation is supported by the kinetic definition of the probability of dissociative transfers: $P_{\text{diss}} = \left(\frac{k_{\text{off}}}{k_{\text{assoc}} + k_{\text{off}}} \right) \left(\frac{k_{\text{return}}}{k_{\text{bulk}} + k_{\text{return}}} \right)$. The first term describes the probability that hUNG will dissociate from nonspecific DNA (k_{off}) as opposed to making an associative step along the DNA (k_{assoc}), and the second term gives the likelihood that the enzyme, once dissociated, escapes to the bulk solvent (k_{bulk}) rather than re-associating with the DNA chain to complete transfer ($k_{\text{return}} = k_{\text{on}}$). We have shown here that k_{off} is salt insensitive and we have previously shown that k_{assoc} is salt insensitive [4]. Thus, to a first approximation, the first term remains the same at all salt concentrations. In contrast, the second term contains the constant $k_{\text{return}} = k_{\text{on}}$, which is salt sensitive based on our measurements, while escape to bulk is reasonably assumed to be salt independent. Taking $k_{\text{return}} = k_{\text{on}}$ and dividing the numerator and denominator in the second term by k_{on} , gives $P_{\text{diss}} = 1/(k_{\text{bulk}}/k_{\text{on}} + 1)$ at each salt concentration. This equation predicts that P_{diss} will decrease to zero in a manner that depends on the salt concentration dependence of k_{on} , which is the basis of our assertion and interpretation.

The above result sheds light on the nature of the transition state of enzyme molecules undergoing dissociative transfer. Since the DNA ion cloud extends only a few nanometers from the DNA chain, enzyme molecules that undergo dissociative transfers must diffuse at least this distance. We have made estimates in the range 3-7 nm for the mean distance that hUNG diffuses from the DNA chain during dissociative transfers using simple Stoke-Einstein diffusion equations [4]. More recently, we developed a Monte-Carlo simulation program for the glycosylase hOGG1 that can be used to further elaborate microscopic aspects of the site transfer mechanism [4, 69-71].

The implication of the salt sensitivity of the dissociative pathway is that hUNG molecules undergoing dissociative transfers at physiological salt will suffer a decrease in productive association events. Nevertheless, the dissociated enzyme will still be positionally correlated with the departed DNA chain in both high and low salt conditions. The reduced efficiency at high salt is overcome by multiple rebinding attempts, which may result in productive binding occurring at a position along the DNA chain that is more distant from the initial position of dissociation than at low salt concentrations. When productive binding finally occurs, the salt insensitive associative search begins in the same manner as at low salt. Thus, the fundamental aspects of the transfer mechanism do not change between low and physiological concentrations of salt. What remains to be taken into consideration is the effect of other environmental factors within the nucleus, such as the macromolecular crowding, that could modulate the effects of high ion concentrations and favor the formation of compact hUNG-DNA search complexes as compared to dilute solution [46,72]. Thus, future studies will focus on increasingly realistic experimental models to understand search and repair mechanisms in physiologically relevant contexts and eventually human cells.

2.4. METHODS

2.4.1. Characterization of 1-[2-Deoxy-5-*O*-(4,4'-dimethoxytrityl)-2-fluoro-1- β -arabinofuranosyl]uracil.

The identity and purity of the previously synthesized modified uracil phosphoramidite was verified by NMR and ESI mass spectrometry. All chemical shifts,

splitting patterns, and relevant J-couplings were found to be consistent with what has been previously reported.³⁶

¹H NMR (500 MHz, CDCl₃): δ 1.02 – 1.61 [m, 12H, 2 x (CH₃)₂CH]. 2.53 (two t, 2H, CH₂CH₂CN), 3.35 – 3.70 (m, 6H, H5', 5'', CH₂CH₂CN, 2 x (CH₃)₂CH], 4.11 – 4.19 (m, 1H, H4'), 4.49 – 4.68 (m, 1H, H3'), 5.12 and 5.25 (two m, 1H, H2', J_{2',F} = 52.00 Hz), 5.59 (d, 1H, H5), 6.35 (m, 1H, H1', J_{1',F} = 18.00 Hz), 6.80 – 7.50 (m, 14H, trityl), 7.59 (dd, 1H, H6, J_{6,F} = 1.90 Hz), 8.55 (bs, 1H, NH).

³¹P NMR (CDCl₃, internal standard – TPPO in C₆D₆): δ 148.7 (s) and 149.3 (s), slower and faster migrating isomers, respectively.

ESI mass spectrometry: Mass determination was performed in the presence of LiCl, using methods previously described.^{75,76} One prominent peak was observed with m/z = 755.12, which is consistent with the expected [M+Li](+) ion (m/z = 755.72).

2.4.2. Oligonucleotide Reagents

All DNA substrates listed below (except D^S) were purchased from either Integrated DNA Technologies (www.idtdna.com) or Eurofins MWG Operon (www.operon.com). Long oligos (>20 base pairs) were purified by denaturing gel electrophoresis. For all uracil containing duplex substrates the base placed opposite the uracil is specified below. All DNAs used in this study were in the duplex form and the sequences are listed below (the sequences of the complimentary strands are not indicated).

15mer-Fluorescein labeled non-specific DNA (D^N)

5'-FAM-AGG CGC ATA GTC GCA-3'

19mer-Specific DNA (D^S), U^β -G pair

5'-GCG GCC AA PU^β A AAA AGC GC-3'

(P - 2-aminopurine)

19mer-Abasic DNA (aDNA), ϕ -A pair

5'-GCG GCC AAA ϕ AA AAA GCG C-3'

(ϕ - tetrahydrofuran abasic site mimic)

30mer-Single uracil lesion (PUA-30), U-A pair

5'-CGT AGC CAC TGC AAP UAA ACA GAG CAT AGG-3'

(P - 2-aminopurine)

90mer-20 bp U separation (S20), U-A pairs

5'-GGT ATC CGC TCA CAA TTC CAC ACA ATG CTG AGG AAT CGA U AG CTA
AGT AGG ATG AAT CGA U AG CTA AGC TGA GGC ATA CAG TGT CGA GCC-3'

2.4.3. Expression and Purification of hUNG.

The catalytic domain of wild-type, N-terminal truncated hUNG (residues 82–304) was cloned into a pET-21a vector and expressed in BL21-DE3 pLysS *E. coli* cells. Cells containing the hUNG encoding vector were grown in 2 liters of LB medium at 37 °C to an optical density (D_{600}) of 0.5, then hUNG expression was induced at 25 °C by the addition of 0.25 mM IPTG and the cells were grown at 25 °C overnight. The cells were harvested by centrifugation and frozen at -80 °C overnight. Cells were resuspended in lysis buffer (50 mM Tris-Acetate pH 7.0, 10 mM NaCl, 5% glycerol, 0.1% Triton-X-100, 1 mM EDTA, 1 mM DTT) followed by addition of lysozyme, 5 mM $MgCl_2$, and DNase1. The

supernatant was then clarified by centrifugation at 40,000g for 60 min at 4 °C and directly loaded onto an anion exchange column (UNO-Q12, BioRad) that had been preequilibrated with Buffer A (50 mM Tris-Acetate pH 7.0, 10 mM NaCl, 1 mM DTT). The flow through containing hUNG was loaded onto a Mono-S cation exchange column (GE Healthcare) preequilibrated with Buffer A. hUNG was then purified by gradient elution with Buffer A containing 800 mM NaCl. Fractions containing hUNG were dialyzed and concentrated into 10 mM sodium phosphate pH 7.5, 300 mM NaCl, 1mM EDTA, 1 mM DTT, 25% glycerol and passed through a gel filtration column using BioRad P-100 resin and eluted in 10 mM sodium phosphate pH 7.5, 150 mM NaCl. The purified protein was then diluted to final buffer conditions of 10 mM sodium phosphate, 110 mM NaCl, 20% glycerol and stored at -80 °C. The concentrations of hUNG stock solutions were determined using the absorbance at 280 nm and an extinction coefficient of 33.68 mM⁻¹ cm⁻¹.

2.4.4 Oligonucleotide Preparation.

1-[2-Deoxy-5-*O*-(4,4'-dimethoxytrityl)-2-fluoro-1- β -arabinofuranosyl]uracil was previously synthesized [4,9-21,36]. The specific substrate (D^S) was synthesized using standard phosphoramidite chemistry on an Applied Biosystems 390; however, the coupling time for the addition of the fluorinated uracil nucleoside phosphoramidite was increased to 10 min. The size, purity, and nucleotide composition of D^S were assessed by denaturing polyacrylamide gel electrophoresis with visualization by crystal violet staining and MALDI mass spectrometry. All other oligonucleotides sequences were purchased from either Integrated DNA technologies (<http://www.idtdna.com>) or Eurofin (<http://www.operon.com>) and purified in house by denaturing polyacrylamide gel

electrophoresis (PAGE). Concentrations of solutions were determined by the absorbance at 260 nm using nearest neighbor extinction coefficients.

2.4.5. Experimental Conditions.

Most experiments were conducted at 20 °C in Buffer B (20 mM potassium phosphate (pH 7.5), 0.002% Brij 35 detergent (Sigma-Aldrich), 1 mM DTT) unless otherwise stated. The potassium phosphate stock was brought to pH 7.5 using concentrated KOH; this resulted in a final potassium concentration of 36 mM. Site transfer experiments were conducted at 20 °C in Buffer C (20 mM HEPES (pH 7.5), 0.002% Brij 35 detergent (Sigma-Aldrich), 3 mM EDTA (added from a 0.5 M stock at pH 8.0), 1 mM DTT). HEPES stock was brought to pH 7.5 using concentrated KOH; this resulted in a final potassium concentration of 12 mM. Higher potassium concentrations for both buffers were achieved by addition of either KCl, KGlu, or KF.

2.4.6. Dissociation Constants for DNA Binding using Fluorescence Measurements.

Binding of hUNG to non-specific DNA (D^N) was measured by fluorescence anisotropy with a SPEX Fluoromax 3 spectrofluorometer at 20 °C (excitation wavelength of 494 nm, emission wavelength of 518 nm). Concentrated hUNG in Buffer B was titrated into a cuvette containing 100 nM of fluorescein labeled DNA in Buffer B. After each addition, the solution was allowed to equilibrate for 4 min inside the fluorometer and three measurements were averaged. For dissociation constants ($1/K_a$) of $> 6 \mu\text{M}$, values were determined by diluting a solution of concentrated hUNG and 100 nM labeled DNA in Buffer B with a solution of 100 nM labeled DNA only. Potassium concentrations were adjusted by addition of KCl, KGlu, or KF to Buffer B to sample a range of 36 – 170 mM.

Temperature dependence of the non-specific binding affinity was measured using the same experimental procedure at additional temperatures of 10, 15, and 25°C in the presence of 36 mM and 150 mM K⁺ using KGlu. All data were then fitted using **eq 2.4**, where A₀ and A_f are the minimal and maximal anisotropy values, respectively.

$$A = -\left\{\frac{(A_0 - A_f)}{2} \times [\text{DNA}]_{\text{tot}}\right\} \times \left(b - \sqrt{b^2 - 4[\text{hUNG}]_{\text{tot}}[\text{DNA}]_{\text{tot}}}\right) + A_0 \quad (2.4)$$

$$b = (1/K_a) + [\text{hUNG}]_{\text{tot}} + [\text{DNA}]_{\text{tot}}$$

Binding of hUNG to specific DNA (D^S) was followed by an increase in the fluorescence of 2-aminopurine (2-AP). Emission was recorded over the wavelength range of 330 – 500 nm using an excitation wavelength of 310 nm, 0.25 second integration time, and averaging of three scans. Background corrected fluorescence intensity at 370 nm was plotted against hUNG concentration and fitted using **equation (2.4)**. Similar results were obtained by integrating the entire emission spectrum.

2.4.7. Stopped-Flow Kinetic Measurements.

Stopped-flow fluorescence experiments were performed at 20 °C in Buffer B using an Applied Photophysics device in two-syringe mode (dead time = 2 ms). The dissociation and association kinetics for specific DNA (D^S) were followed using 2-AP fluorescence changes using an excitation wavelength of 310 nm and a 360-nm cut-on filter. Ten–fifteen kinetic traces were averaged to produce an acceptable signal-to-noise ratio. All bimolecular association reactions were performed under second-order conditions with equivalent concentrations (400 nM or 600 nM) of both the enzyme and DNA well above the 1/K_a to ensure irreversibility of the binding event. Higher specific DNA concentrations were used

at higher salt due to increased background fluorescence of KGlu. Data were linearized as a function of unbound DNA concentration and fitted using the 2nd order rate equation (eq 2.5), where A_0 and A_t are the initial and final unbound DNA concentrations, respectively.

$$\frac{1}{A_t} = k_{on}t + \frac{1}{A_0} \quad (2.5)$$

Dissociation kinetics were measured by mixing a solution containing both D^S and saturating amounts of hUNG with an equal volume of a concentrated solution of duplex DNA containing an abasic site (aDNA) to ensure irreversible trapping of dissociated enzyme molecules. Data were fitted using a single exponential decay expression $F_t = \Delta F \exp(-k_{off}t) + C$, where F_t is the voltage at time t , ΔF is the amplitude of the voltage change, and C is a constant offset. All other relevant specifications for the individual experiments are described in the figure legends and text.

2.4.8. Steady-State Kinetic Measurements.

Time-dependent increase in the steady-state fluorescence of DNA containing a uracil lesion adjacent to 2-AP (PUA-30) was followed using a SPEX Fluoromax 3 spectrofluorometer in the time base mode as previously described [37]. Emission was observed at 370 nm using an excitation wavelength of 315 nm and a sampling interval of 10s. Michaelis-Menten parameters were determined from hyperbolic fits of the initial rates as a function of DNA substrate concentration.

2.4.9. Intramolecular Site Transfer Assay.

The methods of Schonhoff and Stivers [4] were followed using a substrate with two uracil sites spaced by 20 bp such that all intramolecular site transfers occurred by the

dissociative pathway [4]. Stock solutions of DNA containing either a 5' or 3' ^{32}P end label were generated by incubation of a DNA strand with $[\gamma\text{-}^{32}\text{P}]\text{ATP}$ (Perkin-Elmer) and T4 polynucleotide kinase (New England Biolabs) or $[\alpha\text{-}^{32}\text{P}]\text{ATP}$ (Perkin-Elmer) and terminal transferase (New England Biolabs), respectively. The 5' and 3'-labeled strands were hybridized by heating to 95 °C in a heating block for 20 min and allowing the block to cool to room temperature. Unincorporated $[\gamma\text{-}^{32}\text{P}]$ and $[\alpha\text{-}^{32}\text{P}]\text{ATP}$ were removed by gel filtration.

Each reaction contained 40 nM ^{32}P -labeled duplex DNA substrate, composed of mixing equal amounts of 5' and 3'-labeled DNA, in Buffer C. Site transfer experiments were conducted in Buffer C due to the reduced intramolecular site transfer (P_{trans}) observed when phosphate buffer was used (Buffer B). We attribute this affect to competitive inhibition by phosphate dianion. The reaction was then initiated by the addition of hUNG to a final concentration of 5 pM and incubated at 20 °C. At each time point, an aliquot of the reaction mix was quenched with uracil DNA glycosylase inhibitor (UGI) at a final concentration of 0.1 U (New England Biolabs), which rapidly and efficiently quenched hUNG activity. Following reaction quenching, abasic sites were cleaved by heating each aliquot at 95 °C for 10 min in the presence of 165 mM EDA pH 8.0. Fragments were then separated on a 12% nondenaturing polyacrylamide gel. The gel was dried, exposed overnight to a storage phosphor screen and imaged with a Typhoon 8600 phosphorimager (GE Healthcare). All gel images were quantified using QuantityOne (Bio-Rad) by the box method.

2.5. REFERENCES

1. Schonhoft, J. D., Kosowicz, J. G. and Stivers, J. T. (2013) DNA Translocation by Human Uracil DNA Glycosylase: Role of DNA Phosphate Charge. *Biochemistry* 52, 2526–2535.
2. Rowland, M. M., Schonhoft, J. D., McKibbin, P. L., David, S. S. and Stivers, J. T. (2014) Microscopic mechanism of DNA damage searching by hOGG1. *Nucleic Acids Res.* 42, 9295–9303.
3. Schonhoft, J. D. and Stivers, J. T. (2013) DNA translocation by human uracil DNA glycosylase: the case of single-stranded DNA and clustered uracils. *Biochemistry* 52, 2536–2544.
4. Schonhoft, J. D. and Stivers, J. T. (2012) Timing facilitated site transfer of an enzyme on DNA. *Nat Chem. Biol.* 8, 205–210.
5. Stivers, J. T. and Jiang, Y. L. (2003) A Mechanistic Perspective on the Chemistry of DNA Repair Glycosylases. *Chem. Rev.* 103, 2729–2760.
6. Friedman, J. I. and Stivers, J. T. (2010) Detection of Damaged DNA Bases by DNA Glycosylase Enzymes. *Biochemistry* 49, 4957–4967.
7. Mirny, L., Slutsky, M., Wunderlich, Z., Tafvizi, A., Leith, J. and Kosmrlj, A. (2009) How a protein searches for its site on DNA: the mechanism of facilitated diffusion. *J. Phys. A: Math. Theor.* 42, 434013.
8. Slutsky, M. and Mirny, L. A. (2004) Kinetics of Protein-DNA Interaction: Facilitated Target Location in Sequence-Dependent Potential. *Biophys. J.* 87, 4021–4035.
9. Gowers, D. M., Wilson, G. G., Halford, S. E. and Hippel, von, P. H. (2005) Measurement of the contributions of 1D and 3D pathways to the translocation of a protein along DNA. *Proc. Natl. Acad. Sci. U.S.A.* 102, 15883–15888.
10. Hedglin, M. and O'Brien, P. J. (2010) Hopping Enables a DNA Repair Glycosylase To Search Both Strands and Bypass a Bound Protein. *ACS Chem. Biol.* 5, 427–436.
11. Blainey, P. C., Oijen, A. M. V., Banerjee, A., Verdine, G. L. and Xie, X. S. (2006) A base-excision DNA-repair protein finds intrahelical lesion bases by fast sliding in contact with DNA. *Proc. Natl. Acad. Sci. U.S.A.* 103, 5752–5757.
12. Porecha, R. H. and Stivers, J. T. (2008) Uracil DNA Glycosylase Uses DNA Hopping and Short-Range Sliding to Trap Extrahelical Uracils. *Proc. Natl. Acad. Sci. U.S.A.* 105, 10791–10796.
13. Qi, Y., Nam, K., Spong, M. C., Banerjee, A., Sung, R.-J., Zhang, M., Karplus, M. and Verdine, G. L. (2012) Strandwise translocation of a DNA glycosylase on undamaged DNA. *Proc. Natl. Acad. Sci. U.S.A.* 109, 1086–1091.
14. Setser, J. W., Lingaraju, G. M., Davis, C. A., Samson, L. D. and Drennan, C. L. (2012) Searching for DNA lesions: structural evidence for lower- and higher-affinity DNA binding conformations of human alkyladenine DNA glycosylase. *Biochemistry* 51, 382–390.
15. Dunn, A. R., Kad, N. M., Nelson, S. R., Warshaw, D. M. and Wallace, S. S. (2011) Single Qdot-labeled glycosylase molecules use a wedge amino acid to probe for lesions while scanning along DNA. *Nucleic Acids Res.* 39, 7487–7498.
16. Terakawa, T., Kenzaki, H. and Takada, S. (2012) p53 searches on DNA by rotation-uncoupled sliding at C-terminal tails and restricted hopping of core domains. *J. Am. Chem. Soc.* 134, 14555–14562.
17. Leith, J. S., Tafvizi, A., Huang, F., Uspal, W. E., Doyle, P. S., Fersht, A. R., Mirny, L. A. and van Oijen, A. M. (2012) Sequence-dependent sliding kinetics of p53. *Proc. Natl. Acad. Sci. U.S.A.* 109, 16552–16557.

18. Granéli, A., Yeykal, C. C., Robertson, R. B. and Greene, E. C. (2006) Long-distance lateral diffusion of human Rad51 on double-stranded DNA. *Proc. Natl. Acad. Sci. U.S.A.* *103*, 1221–1226.
19. Senavirathne, G., Jaszczur, M., Auerbach, P. A., Upton, T. G., Chelico, L., Goodman, M. F. and Rueda, D. (2012) Single-stranded DNA scanning and deamination by APOBEC3G cytidine deaminase at single molecule resolution. *J. Biol. Chem.* *287*, 15826–15835.
20. Hammar, P., Leroy, P., Mahmutovic, A., Marklund, E. G., Berg, O. G. and Elf, J. (2012) The lac repressor displays facilitated diffusion in living cells. *Science* *336*, 1595–1598.
21. Szczelkun, M. D., Marko, J. F. and Halford, S. E. (2000) One- and three-dimensional pathways for proteins to reach specific DNA sites. *EMBO J.* *19*, 6546–6557.
22. Blainey, P. C., Luo, G., Kou, S. C., Mangel, W. F., Verdine, G. L., Bagchi, B. and Xie, X. S. (2009) Nonspecifically bound proteins spin while diffusing along DNA. *Nat. Struct. Mol. Biol.* *16*, 1224–1229.
23. Hedglin, M. and O'Brien, P. J. (2008) Human alkyladenine DNA glycosylase employs a processive search for DNA damage. *Biochemistry* *47*, 11434–11445.
24. Record, M. T. J., Ha, J. H. and Fisher, M. A. (1991) Analysis of equilibrium and kinetic measurements to determine thermodynamic origins of stability and specificity and mechanism of formation of site-specific complexes between proteins and helical DNA. *Methods Enzymol* *208*, 291–343.
25. Record, M. T. J., Zhang, W. and Anderson, C. F. (1998) Analysis of effects of salts and uncharged solutes on protein and nucleic acid equilibria and processes: a practical guide to recognizing and interpreting polyelectrolyte effects, Hofmeister effects, and osmotic effects of salts. *Adv. Protein Chem.* *51*, 281–353.
26. Record, M. T. J., Anderson, C. F. and Lohman, T. M. (1978) Thermodynamic analysis of ion effects on the binding and conformational equilibria of proteins and nucleic acids: the roles of ion association or release, screening, and ion effects on water activity. *Q. Rev. Biophys.* *11*, 103–178.
27. Privalov, P. L., Dragan, A. I. and Crane-Robinson, C. (2011) Interpreting protein/DNA interactions: distinguishing specific from non-specific and electrostatic from non-electrostatic components. *Nucleic Acids Res.* *39*, 2483–2491.
28. Manning, G. S. (1996) Counterion condensation theory constructed from different models. *Physica A* *231*, 236–253.
29. Manning, G. S. (1978) The molecular theory of polyelectrolyte solutions with applications to the electrostatic properties of polynucleotides. *Q. Rev. Biophys.* *11*, 179–246.
30. Olmsted, M. C., Bond, J. P., Anderson, C. F. and Record, M. T. (1995) Grand canonical Monte Carlo molecular and thermodynamic predictions of ion effects on binding of an oligocation (L8⁺) to the center of DNA oligomers. *Biophys. J.* *68*, 634–647.
31. Lohman, T. M., deHaseh, P. L. and Record, M. T., Jr. (1980) Pentylsine-deoxyribonucleic acid interactions: a model for the general effects of ion concentrations on the interactions of proteins with nucleic acids. *Biochemistry* *19*, 3522–3530.
32. Dragan, A. I., Li, Z., Makeyeva, E. N., Milgotina, E. I., Liu, Y., Crane-Robinson, C. and Privalov, P. L. (2006) Forces driving the binding of homeodomains to DNA. *Biochemistry* *45*, 141–151.
33. Stigter, D. (1995) Evaluation of the counterion condensation theory of polyelectrolytes. *Biophys. J.* *69*, 380–388.
34. Satoh, M., Kawashima, T. and Komiyama, J. (1988) A new model of counterion condensation in polyelectrolyte solutions. III. Theoretical predictions of competitive condensation between counterions of different valences. *Biophys. Chem.* *31*, 209–215.

35. Jen-Jacobson, L. and Jacobson, L. A. (2008) Role of Water and Effects of Small Ions in Site-specific Protein-DNA Interactions, in *Protein-Nucleic Acid Interactions: Structural Biology*, pp 13–46. The Royal Society of Chemistry.
36. Stivers, J. T., Pankiewicz, K. W. and Watanabe, K. A. (1999) Kinetic mechanism of damage site recognition and uracil flipping by *Escherichia coli* uracil DNA glycosylase. *Biochemistry* 38, 952–963.
37. Stivers, J. T. (1998) 2-Aminopurine fluorescence studies of base stacking interactions at abasic sites in DNA: metal-ion and base sequence effects. *Nucleic Acids Res.* 26, 3837–3844.
38. Mol, C. D., Arvai, A. S., Slupphaug, G., Kavli, B., Alseth, I., Krokan, H. E. and Tainer, J. A. (1995) Crystal structure and mutational analysis of human uracil-DNA glycosylase: structural basis for specificity and catalysis. *Cell* 80, 869–878.
39. Bianchet, M. A., Seiple, L. A., Jiang, Y. L., Ichikawa, Y., Amzel, L. M. and Stivers, J. T. (2003) Electrostatic guidance of glycosyl cation migration along the reaction coordinate of uracil DNA glycosylase. *Biochemistry* 42, 12455–12460.
40. Parker, J. B., Bianchet, M. A., Krosky, D. J., Friedman, J. I., Amzel, L. M. and Stivers, J. T. (2007) Enzymatic capture of an extrahelical thymine in the search for uracil in DNA. *Nature* 449, 433–437.
41. MacDermott, M. (1990) The intracellular concentration of free magnesium in extensor digitorum longus muscles of the rat. *Exp. Physiol.* 75, 763–769.
42. Murphy, E., Freudenrich, C. C., Levy, L. A., London, R. E. and Lieberman, M. (1989) Monitoring cytosolic free magnesium in cultured chicken heart cells by use of the fluorescent indicator Fura2. *Proc. Natl. Acad. Sci. U.S.A.* 86, 2981–2984.
43. Collins, K. D. (2004) Ions from the Hofmeister series and osmolytes: effects on proteins in solution and in the crystallization process. *Methods* 34, 300–311.
44. Collins, K. D. (2006) Ion hydration: Implications for cellular function, polyelectrolytes, and protein crystallization. *Biophys. Chem.* 119, 271–281.
45. Parikh, S. S., Walcher, G., Jones, G. D., Slupphaug, G., Krokan, H. E., Blackburn, G. M. and Tainer, J. A. (2000) Uracil-DNA glycosylase-DNA substrate and product structures: conformational strain promotes catalytic efficiency by coupled stereoelectronic effects. *Proc. Natl. Acad. Sci. U.S.A.* 97, 5083–5088.
46. Schreiber, G., Haran, G. and Zhou, H.-X. (2009) Fundamental aspects of protein-protein association kinetics. *Chem. Rev.* 109, 839–860.
47. Jiang, Y. L. and Stivers, J. T. (2002) Mutational analysis of the base-flipping mechanism of uracil DNA glycosylase. *Biochemistry* 41, 11236–11247.
48. Krosky, D. J., Song, F. and Stivers, J. T. (2005) The origins of high-affinity enzyme binding to an extrahelical DNA base. *Biochemistry* 44, 5949–5959.
49. Fitzgerald, M. E. and Drohat, A. C. (2008) Coordinating the initial steps of base excision repair. Apurinic/apyrimidinic endonuclease 1 actively stimulates thymine DNA glycosylase by disrupting the product complex. *J. Biol. Chem.* 283, 32680–32690.
50. Parikh, S. S., Mol, C. D., Slupphaug, G., Bharati, S., Krokan, H. E. and Tainer, J. A. (1998) Base excision repair initiation revealed by crystal structures and binding kinetics of human uracil-DNA glycosylase with DNA. *EMBO J.* 17, 5214–5226.
51. Terry, B. J., Jack, W. E. and Modrich, P. (1985) Facilitated diffusion during catalysis by EcoRI endonuclease. Nonspecific interactions in EcoRI catalysis. *J. Biol. Chem.* 260, 13130–13137.
52. Zharkov, D. O., Mechetin, G. V. and Nevinsky, G. A. (2010) Uracil-DNA glycosylase: Structural, thermodynamic and kinetic aspects of lesion search and recognition. *Mutat. Res.* 685, 11–20.

53. Record, M. T., Anderson, C. F., Mills, P., Mossing, M. and Roe, J. H. (1985) Ions as regulators of protein-nucleic acid interactions in vitro and in vivo. *Adv. Biophys.* 20, 109–135.
54. Record, M. T., deHaseth, P. L. and Lohman, T. M. (1977) Interpretation of monovalent and divalent cation effects on the lac repressor-operator interaction. *Biochemistry* 16, 4791–4796.
55. Winter, R. B. and Hippel, von, P. H. (1981) Diffusion-driven mechanisms of protein translocation on nucleic acids. 2. The Escherichia coli repressor--operator interaction: equilibrium measurements. *Biochemistry* 20, 6948–6960.
56. Barkley, M. D., Lewis, P. A. and Sullivan, G. E. (1981) Ion effects on the lac repressor--operator equilibrium. *Biochemistry* 20, 3842–3851.
57. Roe, J. H., Burgess, R. R. and Record, M. T. (1985) Temperature dependence of the rate constants of the Escherichia coli RNA polymerase-lambda PR promoter interaction. Assignment of the kinetic steps corresponding to protein conformational change and DNA opening. *J. Mol. Biol.* 184, 441–453.
58. Record, M. T., Mazur, S. J., Melançon, P., Roe, J. H., Shaner, S. L. and Unger, L. (1981) Double helical DNA: conformations, physical properties, and interactions with ligands. *Annu. Rev. Biochem.* 50, 997–1024.
59. Alsallaq, R. and Zhou, H.-X. (2008) Electrostatic rate enhancement and transient complex of protein–protein association. *Proteins* 71, 320–335.
60. Zhou, H.-X. (2001) Disparate ionic-strength dependencies of on and off rates in protein-protein association. *Biopolymers* 59, 427–433.
61. Northrup, S. H. and Erickson, H. P. (1992) Kinetics of protein-protein association explained by Brownian dynamics computer simulation. *Proc. Natl. Acad. Sci. U.S.A.* 89, 3338–3342.
62. Zhou, H.-X. (1997) Enhancement of protein-protein association rate by interaction potential: accuracy of prediction based on local Boltzmann factor. *Biophys. J.* 73, 2441–2445.
63. Camacho, C. J., Kimura, S. R., DeLisi, C. and Vajda, S. (2000) Kinetics of desolvation-mediated protein-protein binding. *Biophys. J.* 78, 1094–1105.
64. Schlosshauer, M. and Baker, D. (2004) Realistic protein-protein association rates from a simple diffusional model neglecting long-range interactions, free energy barriers, and landscape ruggedness. *Protein Sci.* 13, 1660–1669.
65. Schreiber, G. and Fersht, A. R. (1996) Rapid, electrostatically assisted association of proteins. *Nat. Struct. Biol.* 3, 427–431.
66. Anderson, C. F., Record, M. T. and Hart, P. A. (1978) Sodium-23 NMR studies of cation-DNA interactions. *Biophys. Chem.* 7, 301–316.
67. Bleam, M. L., Anderson, C. F. and Record, M. T., Jr. (1983) Sodium-23 nuclear magnetic resonance studies of cation-deoxyribonucleic acid interactions. *Biochemistry* 22, 5418–5425.
68. Bleam, M. L., Anderson, C. F. and Record, M. T. (1980) Relative binding affinities of monovalent cations for double-stranded DNA. *Proc. Natl. Acad. Sci. U.S.A.* 77, 3085–3089.
69. Long, H., Kudlay, A. and Schatz, G. C. (2006) Molecular dynamics studies of ion distributions for DNA duplexes and DNA clusters: salt effects and connection to DNA melting. *J. Phys. Chem. B* 110, 2918–2926.
70. Montoro, J. and Abascal, J. (1995) Ionic distribution around simple DNA models. I. Cylindrically averaged properties. *J. Chem. Phys.* 103, 8273.
71. Millett, I. S., Doniach, S., Finkelstein, K. D. and Herschlag, D. (2003) Counterion distribution around DNA probed by solution X-ray scattering. *Phys. Rev. Lett.* 90, 188103.

72. Zhou, H.-X., Rivas, G. and Minton, A. P. (2008) Macromolecular crowding and confinement: biochemical, biophysical, and potential physiological consequences. *Annu. Rev. Biophys.* 37, 375–397.
73. Cao, C., Jiang, Y. L., Stivers, J. T. and Song, F. (2004) Dynamic opening of DNA during the enzymatic search for a damaged base. *Nat. Struct. Mol. Biol.* 11, 1230–1236.
74. Cao, C., Jiang, Y. L., Krosky, D. J. and Stivers, J. T. (2006) The catalytic power of uracil DNA glycosylase in the opening of thymine base pairs. *J. Am. Chem. Soc.* 128, 13034–13035.
75. Kupihar, Z., Timar, Z., Dellinger, D. J., and Caruthers, M. H. (2005) Accurate mass analysis of phosphoramidites by electrospray mass spectrometry. *Nucleosides Nucleotides Nucleic Acids* 24, 663–666.
76. Kele, Kupihar, Kovacs, Janaky, Szabo. (1999) Electrospray mass spectrometry of phosphoramidites, a group of acid-labile compounds. *J Mass Spectrom* 34, 1317–1321.

Chapter 3:

Consequences of limited electrostatic interactions between repair enzymes and undamaged DNA: The case of human 8-oxoguanine DNA glycosylase

Reproduced in part from:

Cravens, S.L., Stivers, J.T.; (2016), Comparative Effects of Ions, Molecular Crowding, and Bulk DNA on the Damage Search Mechanisms of hOGG1 and hUNG. *Submitted*.

3.1 INTRODUCTION

Numerous crystal structures of different DNA glycosylases have been solved in the presence and absence of DNA targets, which allows for a classification of these enzymes based on the architecture of their fold^{1,2,3,4,5,6}. The three most common families have been designated as helix-hairpin-helix (HhH), helix-two turn-helix, and uracil DNA glycosylase (UDG). While structure does not provide mechanistic details of how enzymes from different classifications perform a uniform function, it can illuminate differences between the enzyme families that have potentially profound consequences for steps of the DNA search-and-repair pathway. In order to evaluate how structural differences between glycosylase families impact DNA repair, we have chosen to study human uracil DNA glycosylase (hUNG) and human 8-oxoguanine DNA glycosylase (hOGG1), which hail from the UDG and HhH superfamilies, respectively.

The structure of hUNG is best characterized as a single domain, classic α/β fold with a central 4-stranded parallel β sheet surrounded by eight α helices^{1,3}. The multilayered structure produces regions of buried hydrophobic aromatic clusters between the α helices and β strands. Along one end of the β sheet is a ridge 27 Å long and 21 Å in diameter, which is approximately equal to the diameter of a DNA double helix. This groove is rich in basic amino acids that imbue the area with a positive electrostatic potential fit for binding DNA¹. As shown in Chapter 2, hUNG binds to DNA using three loops known as the 5'-side backbone compression loop (res. 165-PPPPS-169), the uracil recognition region (res. 199-GVLLLN-204), and the 3'-side backbone compression loop (res. 246-GS-247). Numerous contacts with the phosphate backbone stabilize the DNA helix in the binding ridge. The loops compress the backbone and bend the DNA at a 45° angle upon

intercalation of the minor groove by an additional loop (res. 268-HPSPS-273). The insertion of Leu-272 stabilizes the displacement of uracil into the hUNG active site where it is recognized by specific hydrogen bonding partners.

The structure of hOGG1 is far more complex and consists of multiple domains with unique folds^{2,6}. As with all members of the HhH family, hOGG1 contains a unique helix-hairpin-helix motif, followed by a Gly/Pro-rich loop. The overall fold of the enzyme contains two α -helix domains and an additional antiparallel β -sheet that is only shared with the alkyl DNA glycosylase AlkA⁷. hOGG1 binds to 8-oxoguanine containing DNA much like hUNG with uracil sites. The 8-oxoguanine is flipped out into the active site and recognized with a single hydrogen bond (Gly-42), backbone is bent at a severe 70° angle, and Asn-149 wedges through the minor groove to stabilize the displaced base conformation⁶. Unlike hUNG and most other DNA-binding proteins, hOGG1's DNA-binding interface is lacking in positive electrostatic potential. Amino acid groups in close proximity to the DNA backbone are essentially all uncharged with the exception of a single basic residue His-270. Stabilization of the charged DNA is believed to originate from dipole electrostatic contact by orientation of the N-termini of the many α -helices in hOGG1's structure toward the DNA⁷.

Though hUNG and hOGG1 both distort damaged DNA in similar ways, it is arguable that the more relevant binding partner for both of these enzymes is undamaged DNA. DNA lesions are infrequent and occur on the order of every million base pairs; therefore, it is more likely that hOGG1 and hUNG will spend the majority of their time bound to nonspecific DNA while on the hunt for a damage site. Understanding how their

unique structures provide a binding platform for undamaged DNA is essential to fully comprehend how these enzymes translocate along DNA and rapidly discriminate between nontarget and target sequences. Previously published crystal structures of both enzymes bound to undamaged DNA paints a rather stunning difference between them^{2,3}. As detailed in Chapter 2, hUNG makes primarily electrostatic contact with the phosphate backbone and does not deform the over B-form structure of the DNA, which distinguishes it from the distorted specific complex and imbues it with a rather dramatic salt sensitivity. In contrast, the nonspecific complex of hOGG1 is very similar to its specific complex. Undamaged guanine is extruded from the DNA helix into an ‘exo site’ neighboring the active site. This is accomplished by inducing an 80° bend in the helix and a rotation over the helical axis by 20°. The heavy distortion of the DNA actually makes some of the phosphate groups inaccessible to hydrogen bonds that are present in the specific complex (His-270 and Asn-150). AlkA has also been observed to interact with nonspecific DNA in this rather interrogative manner that distinguishes the HhH superfamily from UDG⁴. The relatively sparse ionic contacts between hOGG1 and DNA leads to the question of the nature of the thermodynamic interactions that stabilize the non-specific hOGG1-DNA complex. Differences in the electrostatic and nonelectrostatic character of hOGG1-DNA complexes from those of hUNG could have a dramatic difference in the response of hOGG1’s search-and-repair mechanism to the cellular environment.

As was detailed in Chapter 2, we have carried out a thorough investigation of how the nonspecific interactions between hUNG and DNA can influence its ability to target uracil damage. A similar study has yet to be conducted with hOGG1. Due to experimental limitations with hOGG1, we have restricted our investigation to the most poignant steps in

the search-and-repair pathway that could be influenced by hOGG1's unique DNA-binding interface: nonspecific and specific DNA binding. We provide a quantified delineation of the thermodynamic driving forces that stabilize both complexes utilizing counter-ion condensation (CC) theory^{8,9,10}. Our analysis of how hOGG1 interacts with multiple DNA binding partners under physiological salt will inform later experiments presented in Chapter 5, which involve the consideration of combinatorial effects of salt, crowder, and bulk DNA density.

3.2. RESULTS

3.2.1. Structural Aspects of Non-specific and Specific hOGG1-DNA Complexes.

Crystal structures of complexes of hOGG1 with undamaged and damaged DNA have provided a detailed model of the binding interface, which provides a useful starting place for understanding the effects of solution ions on binding of non-specific and specific DNA (PDB entries 1YQR and 1EBM, respectively; **Figure 3.1A, 3.1B**). The binding interfaces in these structures encompass over 2,200 Å² of surface area and include a peripheral 'exo' binding site that can accommodate an undamaged guanine base in the non-specific complex (**Figure 3.1A**) and the catalytic active site, which is specific for 8-oxoG (**Figure 3.1B**)^{2,6}. Unlike most DNA-binding proteins, the DNA binding site of hOGG1 is lacking in charged residues with the possible exception of a single basic residue, H270, which is implicated in the discrimination between guanine and 8-oxoguanine^{6,11}. Upon binding to an undamaged DNA segment (**Figure 3.1A**), hOGG1 induces a pronounced bend (~ 80°) and rotation of the DNA (~20° about the helix axis), which apparently precludes the formation of potential ionic interactions between protein residues and the

phosphate backbone of the DNA. This structure also suggests that non-electrostatic binding energy might be gained by displacement of an undamaged guanine residue from the base stack into the ‘exo’ guanine binding site. The distorted DNA helix is apparently stabilized by insertion of an asparagine into the space vacated by the guanine base.

When hOGG1 binds to 8-oxoG-containing DNA, all of the contacts in the non-specific complex are maintained (**Figure 3.1B**). However, the reduced bend angle of the DNA helix positions the phosphate backbone in close proximity to two side chains that form unique hydrogen bonds with the phosphate backbone (His270 and Asn150) and also allows positioning of the 8-oxoG base deep into the active site with the formation of additional non-ionic interactions. We note that the severely bent non-specific DNA complex of hOGG1 and DNA differs considerably from the relatively unperturbed B duplex structure of non-specific DNA bound to hUNG, even though hUNG partially extrudes normal thymine bases into a similar exo-site bound conformation during its search for uracils in the context of U/A base pairs^{2, 3}. In contrast, the specific complex of hUNG with damaged DNA shows significant bending similar to that of hOGG1¹².

3.2.2. Ion Effects on Binding of hOGG1 to Undamaged DNA.

We were interested in whether the structural differences between hOGG1 and hUNG led to distinct electrostatic and non-electrostatic contributions to their binding energies for damaged and undamaged DNA. As in a previous study with hUNG,¹³ we used fluorescence anisotropy to measure the equilibrium association constants between hOGG1 and non-specific DNA (K_a^N) under a range of potassium ion concentrations (30 mM – 300 mM) using acetate as the counterion. We also explored several DNA sequences to probe whether the G-C content of the DNA affected the binding energetics of hOGG1. The

different DNA sequences were designed to contain a random distribution of A-T and G-C base pairs (D^N), no G-C base pairs (D^{TATA}), a single G-C base pair (D^{GC}), or entirely G-C base pairs (D^{GCGC}) (**Figure 3.1A**). A fluorescein label was attached to the 5' end of one DNA strand to follow the increase in fluorescence anisotropy that accompanied hOGG1 binding (**Figure 3.2A**). The logarithm of the binding affinities of hOGG1 for each duplex was plotted against the logarithm of the salt concentration present in the binding reaction (**Figure 3.2C**). The slopes (N) and intercepts of these plots were then used to determine the electrostatic (ΔG_{elect}) and non-electrostatic (ΔG_{non}) contributions to the binding free energies as previously described^{10, 13}. Binding affinities at all salt concentrations for D^N are listed in **Table 3.1**.

Regardless of the DNA sequence, the salt dependence of the association constants for hOGG1-DNA complexes was small compared to analogous studies with hUNG, indicating a smaller electrostatic component to binding of hOGG1 [$N^{\text{hOGG1}} = -0.9$ to -2.0 ; $N^{\text{hUNG}} = -3.8$] (**Table 3.2**)¹³. Within this series of DNA sequences, the binding of D^N (35% G/C content) was about three to ten times less sensitive to a ten-fold increase in salt concentration than the other DNA sequences (**Figure 3.3 and Table 3.3**). The different slopes for the various duplex sequences (**Table 3.2**) suggests subtle differences in the electrostatic components of the binding free energies that may in turn stem from differences in the structures of these complexes. Sequence dependent salt effects on binding may arise from differences in the heterogeneous ion density around the free duplexes and/or differential reorganization of the ion cloud arising from structural differences between hOGG1 and these non-specific DNA sequences. It is therefore unwarranted to use simple

polyelectrolyte theory to calculate numbers of ions that are released to bulk solution upon complex formation as we did previously with hUNG binding to non-specific DNA^{8, 10, 13}.

The non-electrostatic contributions to the binding free energies for these duplexes (ΔG_{non}) may be obtained from extrapolation of the linear salt dependences to a standard state of 1M salt^{8, 10, 13, 14}. Under these conditions the equation reduces to $\log K_a = \log K_a^{\text{non}}$ (with $\Delta G_{\text{non}} = -RT \ln K_a^{\text{non}}$) (**Tables 3.2 and 3.4**). Using this formalism, DNA sequences with G/C content in the range 35 to 100% had non-electrostatic contributions to their binding free energies that were about -0.8 to -1.7 kcal/mol more favorable as compared to sequences containing a single G/C or no G/C base pairs (**Table 3.4**).

The electrostatic contribution to the binding free energy of hOGG1 with non-specific DNA (ΔG_{elect}) at a physiological salt concentration of 150 mM was obtained by subtracting ΔG_{non} from the observed binding free energy. As detailed in **Table 3.4**, the values for the various sequences fell in the range $\Delta G_{\text{elect}} = -1$ to -2.5 kcal/mol. The enhanced electrostatic terms for the low or no-G/C sequences allows these sequences to bind hOGG1 with nearly the same affinity as the two G/C-rich sequences under physiological salt concentrations, despite the more favorable ΔG_{non} binding terms for the G/C-rich sequences. Thus even though the energetic basis for the binding of these duplex sequences differs, the observed affinity with hOGG1 is very similar under physiological conditions (see ΔG_{bind} in **Table 3.4**).

The major conclusions from the above data are that binding of hOGG1 to non-specific DNA is (i) less driven by electrostatic effects than for hUNG, (ii) subject to sequence dependent differences in the non-electrostatic and electrostatic binding terms, and (iii) largely independent of sequence context at physiological salt concentrations.

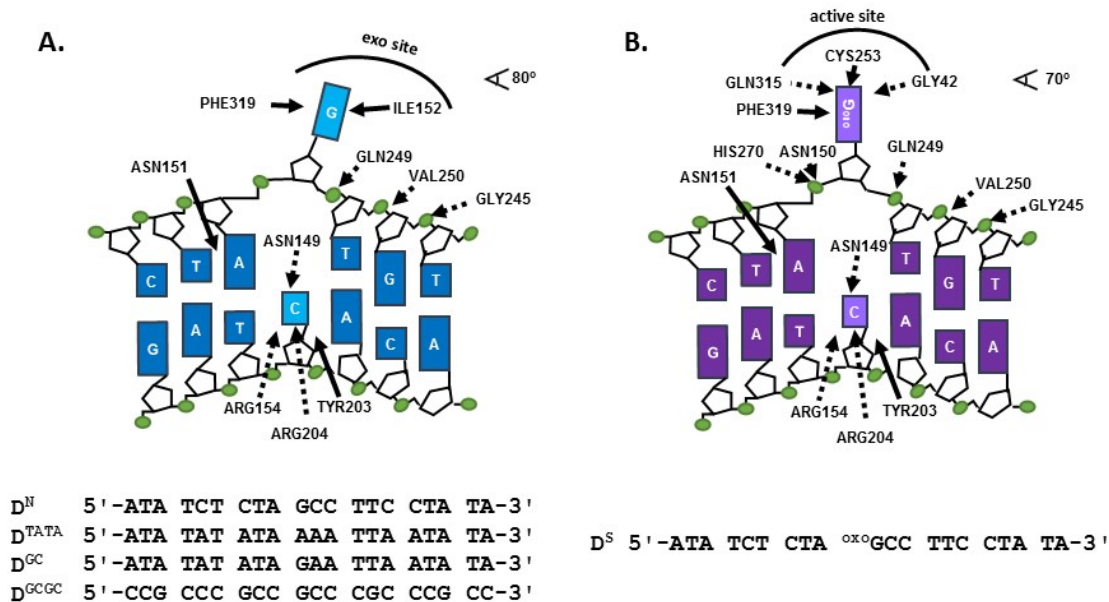


Figure 3.1. Schematics of undamaged and damaged DNA bound to hOGG1. (A) Depiction of electrostatic (dashed lines) and non-electrostatic (solid lines) contacts between undamaged DNA and WT hOGG1 (Protein Data Bank entry 1YQK²). The top strands of all undamaged DNA sequences used in this study are listed. A fluorescein label (not shown) is attached to the 5' end of each strand. Full sequences are listed in **Methods, Section 3.4.** **(B)** Schematic of electrostatic (dashed arrows) and the non-electrostatic (solid arrows) interactions between hOGG1 and specific DNA (Protein Data Bank entry 1EMB⁶). The top strand of the specific DNA sequence used in this study is shown. A 5' fluorescein label was attached to the complementary strand (not shown, see **Methods, Section 3.4**). Electrostatic interactions are defined by nitrogen and oxygen atoms of the enzyme within 3.3 Å of DNA phosphate oxygens or heteroatoms on the bases, while non-electrostatic interactions are defined as any enzyme carbon atom within 3.9 Å of a DNA carbon. Hydrogen bonds with the cytosine on the complementary strand are not expected to result in ion displacement.

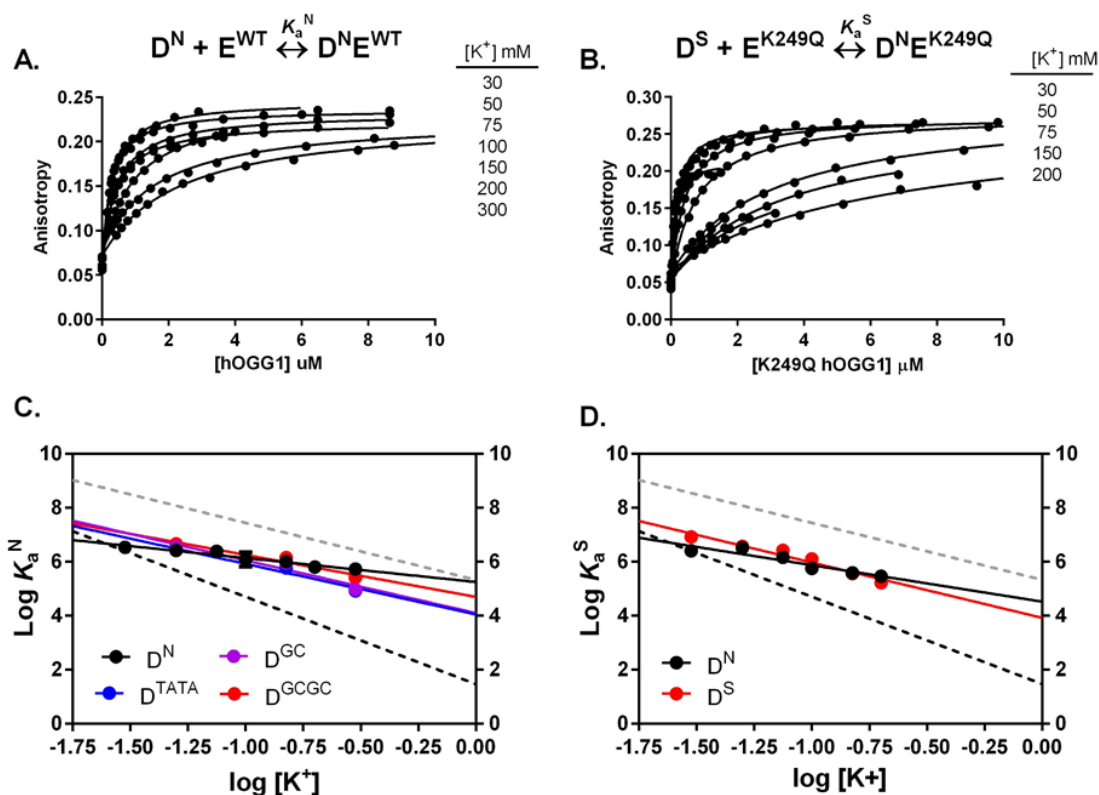


Figure 3.2. Salt dependence of the non-specific and specific DNA binding affinity determined by fluorescence anisotropy measurements at 20°C. (A) Changes in fluorescence anisotropy of the non-specific DNA ($D^N = 25 \text{ nM}$) as a function of hOGG1 concentration at varying potassium ion concentrations (30 mM – 300 mM). Binding curves for the additional non-specific DNA oligos are provided in **Fig. 3.3**. (B) Changes in fluorescence anisotropy of the specific DNA ($D^S = 10 \text{ nM}$) as a function of K249Q concentration at various potassium ion concentrations (30 mM – 200 mM). (C) Dependence of non-specific association constant (K_a^N) on the concentration of potassium acetate for D^N (black), D^{TATA} (blue), D^{GC} (purple), and D^{GCGC} (red). (D) Salt dependence of the non-specific (K_a^N) (black, left y-axis) and specific association constants (K_a^S) (red, right y-axis) for K249Q binding to D^N and D^S . For comparison, black and grey dashed lines in C and D show the published salt dependences for non-specific and specific DNA binding by hUNG¹³.

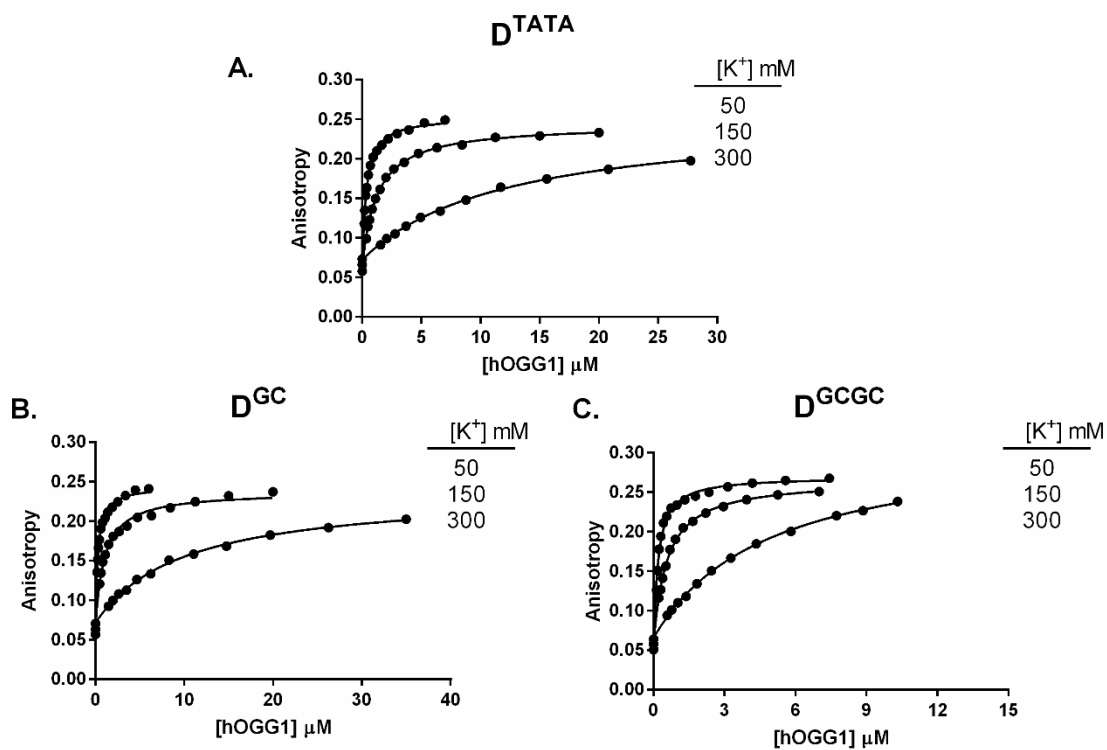


Figure 3.3. Salt dependence of the non-specific DNA binding affinity of hOGG1 at various salt concentrations using the indicated DNA sequences. Increases in fluorescence anisotropy of (A) D^{TATA} , (B) D^{GC} and (C) D^{GCGC} are plotted as a function of hOGG1 concentration at each potassium ion concentrations (50 mM – 300 mM). Data presented here correspond to the linear plot presented in **Figure 3.2C**.

Table 3.1. Binding affinities ($K_D = 1/K_a$) of hOGG1 for nonspecific DNA and specific DNA sequences at various concentrations of potassium ions.

[K ⁺] (mM)	1/ K_a (μ M)	
	D ^N	D ^S ^a
30	0.29 \pm 0.03	0.12 \pm 0.05
	0.48 \pm 0.15 ^a	
50	0.38 \pm 0.17	0.22 \pm 0.04
	0.31 \pm 0.02 ^a	
75	0.41 \pm 0.03	0.38 \pm 0.02
	0.69 \pm 0.05 ^a	
100	0.9 \pm 0.4	0.78 \pm 0.03
	1.8 \pm 0.6 ^a	
150	1.01 \pm 0.06	3.2 \pm 0.1
	2.6 \pm 0.4 ^a	
200	1.6 \pm 1	6.3 \pm 0.3
	3.5 \pm 0.4 ^a	
300	1.9 \pm 0.4	-- ^b

^a These values were determined using K249Q hOGG1.

^b Not determined.

Table 3.2. Analysis of the salt dependences of non-specific and specific binding of hOGG1.^a

	Slope (N) ^b	K_a^{non} (M ⁻¹) ^c
K_a^{N}	-0.9 \pm 0.1	1.8 \pm 0.1 $\times 10^5$
	-1.3 \pm 0.3 ^d	2.5 \pm 0.2 $\times 10^5$ ^d
K_a^{TATA}	-2.0 \pm 0.5	8.4 \pm 0.9 $\times 10^3$
K_a^{GC}	-2.0 \pm 0.6	1.3 \pm 0.2 $\times 10^4$
K_a^{GCGC}	-1.7 \pm 0.4	3.4 \pm 0.3 $\times 10^4$
K_a^{S}	-2.2 \pm 0.2 ^d	1.6 \pm 0.1 $\times 10^4$ ^d

^a All experiments were conducted using WT hOGG1 unless otherwise noted.

^b The slope (N) obtained from nonlinear regression fitting to eq 1.

^c K_a^{non} is the extrapolated value of the K_a to the condition of 1 M [K⁺].

^d These values were determined using K249Q hOGG1.

Table 3.3. Binding affinities ($K_D = 1/K_a$) of hOGG1 for multiple nonspecific DNA sequences at various concentrations of potassium ions.

[K ⁺] (mM)	1/ K_a (μ M)		
	D ^{TATA}	D ^{GC}	D ^{GCGC}
30	-- ^c	--	--
50	0.38 ± 0.06	0.28 ± 0.03	0.20 ± 0.02
75	--	--	--
100	--	--	--
150	1.8 ± 0.7	1.1 ± 0.2	0.7 ± 0.2
200	--	--	--
300	12 ± 2	10.8 ± 0.8	4.0 ± 0.9

^aNot determined.

Table 3.4. Electrostatic (ΔG_{elec} and non-electrostatic (ΔG_{non}) contributions to the binding free energy (ΔG_{bind}) for non-specific (D^N, D^{TATA}, D^{GC}, D^{GCGC}) and specific (D^S) hOGG1 complexes in the presence of 150 mM K⁺.^a

	D ^N	D ^{TATA}	D ^{SGC}	D ^{GCGC}	D ^S
ΔG_{bind}^b (kcal mol ⁻¹)	-8.0 ± 0.1 -7.5 ± 0.3 ^e	-7.7 ± 0.2	-8.0 ± 0.1	-8.2 ± 0.2	-7.4 ± 0.4 ^e
ΔG_{elec}^c (kcal mol ⁻¹)	-1.0 ± 0.2 -1.3 ± 0.7 ^e	-2.4 ± 0.3	-2.5 ± 0.2	-2.1 ± 0.4	-2.3 ± 0.8
ΔG_{non}^d (kcal mol ⁻¹)	-7.0 ± 0.1 -6.2 ± 0.4 ^e	-5.3 ± 0.1	-5.5 ± 0.1	-6.1 ± 0.2	-5.1 ± 0.4

^a All values are derived from experiments using KOAc.

^b Calculated $\Delta G_{\text{bind}} = -RT \ln K_a$, using K_a at 150 mM [K⁺].

^c $\Delta G_{\text{elec}} = \Delta G_{\text{bind}} - \Delta G_{\text{non}}$. ΔG_{elec} pertains to the condition of 150 mM [K⁺].

^d $\Delta G_{\text{non}} = -RT \ln K_a$, using the measured K_a at 1M [K⁺].

^e These values were determined using K249Q

3.2.3. Ion Effects on Binding of hOGG1 to DNA containing 8-oxoguanine.

A quantitative evaluation of the energetic contributions of these additional backbone interactions in the specific complex was performed by measuring the binding affinity for 8-oxoG-containing DNA (D^S) at a range of salt concentrations (30 mM - 200 mM K^+) (**Figure 3.2B**). These experiments required the use of a catalytically inactive form of hOGG1 containing a K249Q mutation (**Figure 3.4**)^{6, 15, 16}. To ensure that this active site mutation did not disrupt the ability of hOGG1 to bind to DNA, we confirmed that the salt dependence of non-specific binding for K249Q was similar to that of WT hOGG1 (**Figure 3.4B, Table 3.3**). While the salt sensitivity of K249Q and WT hOGG1 were essentially identical, K249Q was found to bind slightly more weakly to nonspecific DNA. Accordingly, the binding affinity K249Q for undamaged DNA is used as the basis for comparison with the specific complex to avoid small differences arising from the mutation.

The salt dependence of the binding affinity for specific DNA ($N = -2.2 \pm 0.2$) was similar to what was observed for undamaged DNA ($N = -1.3 \pm 0.3$). The slightly steeper salt dependence for the specific complex may arise from two additional contacts made with a phosphate group neighboring the 8-oxoG site (**Figure 3.2C, 3.2D**), which could result in the displacement of an additional ion. The apparent lack of thermodynamic discrimination between undamaged and 8-oxoguanine-containing DNA at physiological salt is consistent with the structural similarities between the non-specific and specific complexes (see Discussion). All of the binding affinities determined using K249Q are reported in **Table 3.1**.

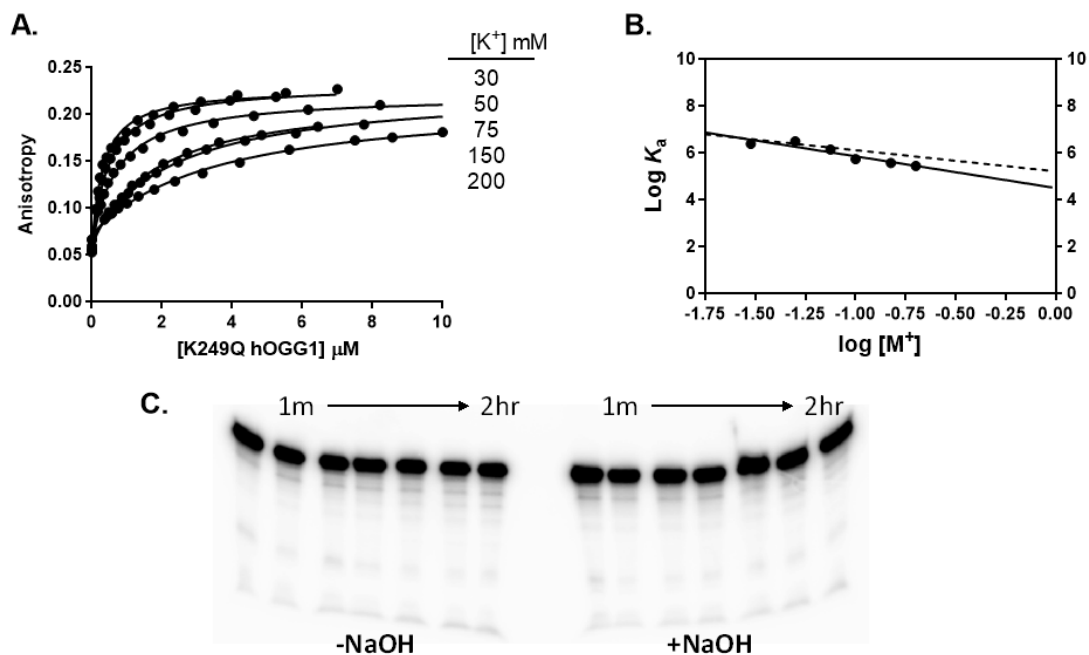


Figure 3.4. Salt dependence of the non-specific DNA binding affinity of K249Q at various salt concentrations. (A) Changes in fluorescence anisotropy of D^N as a function of K249Q concentration using potassium ion concentrations in the range 30 mM to 300 mM. (B) Dependence of K_a of K249Q for non-specific DNA (D^N) on the concentration of KOAc. For comparison, the dashed line shows the salt dependence of K_a of hOGG1 for D^N from the data shown in Figure 1D. (C) Phosphorimages of gels corresponding to an 8-oxoG excision assay performed using K249Q. Twenty-five nanomolar of a 31mer containing a single ^{oxo}G site ($S0^{oxoG}$) was incubated with 1 μ M K249Q for 2 hours at 25°C. Time points were quenched and heated at 95°C for 15 min in formamide with and without 100 mM NaOH to probe potential lyase and glycosylase activity, respectively. No reaction was observed under either condition, verifying that K249Q is an inactive mutant of hOGG1.

3.3. DISCUSSION

3.3.1. Salt Effects on DNA Binding in the Absence of Crowding or Bulk DNA.

One of the significant differences between hOGG1 and hUNG is their response to physiological concentrations of monovalent ions, which can be attributed to their different structural modes of interacting with undamaged DNA sequences (**Figure 3.1** and references 25 and 32). The binding of uracil DNA glycosylase to undamaged DNA has a large salt effect, leading to weak binding at 150 mM K^+ ($\Delta G_{\text{bind}}^{150} = -5.5$ kcal/mol). In contrast, binding of hOGG1 is comparatively salt resistant ($\Delta G_{\text{bind}}^{150} = -8$ kcal/mol). Thus, hOGG1 binds to nonspecific DNA about -2.5 kcal/mol more tightly than hUNG at 150 mM K^+ . The energetic basis for these differences has been assigned to the greater electrostatic term in the binding free energy of hUNG and the larger non-electrostatic term for hOGG1 (**Table 3.4**). Structurally, these energetic differences can be attributed to the greater number of electrostatic interactions in the hUNG-DNA complex and the nonpolar interactions in the hOGG1 complex that arise from the DNA distortion and docking of guanine into the exo-site (**Figure 3.1**).

3.3.2. Relating Salt Effects to the Efficiency of Damage Recognition.

The respective weak and stronger interactions hUNG and hOGG1 with non-specific DNA and their different electrostatic attributes are suited to the catalytic properties of these two enzymes and the nature of the DNA damage that these enzymes must recognize. Uracil DNA glycosylase is a highly active enzyme capable of flipping and excising uracil from the DNA duplex on a millisecond timescale^{3, 17, 18}. Thus, if the lifetime of hUNG on non-

specific DNA sites were significantly longer than milliseconds, its search and repair efficiency would be diminished. The millisecond timescale for hUNG binding and catalysis are also consistent with the rapid sub-millisecond intrinsic breathing dynamics of base pairs containing uracil or thymidine^{3, 19}. These motions allow the enzyme to inspect T/A and U/G base pairs by taking advantage of their frequent excursions from the base stack without severely distorting the DNA^{3, 19, 20}. Distortion of an undamaged DNA duplex by hUNG would likely lead to greater non-electrostatic interactions (as observed with hOGG1) and a non-productive increase in hUNG's bound lifetime. Thus, a physiological salt concentration facilitates the hUNG reaction by decreasing its lifetime on non-specific DNA and intrinsic base pair breathing precludes the requirement for DNA distortion until a uracil base is detected and flipped into the enzyme active site²⁰. Consistent with the above proposal, the hUNG specific DNA complex is severely distorted and displays a +1 kcal/mol smaller electrostatic binding term and a -5 kcal/mol more favorable non-electrostatic binding term than the non-specific complex¹³.

In contrast, hOGG1 excises 8-oxoG on a time scale of seconds^{21, 22, 23}, which requires a greater lifetime on non-specific DNA to allow damage recognition to occur efficiently. The lower rates of base pair breathing for G/C and 8-oxoG/C pairs as compared to those of uracil and thymidine^{19, 24, 25}, and the requirement for a longer extrahelical lifetime to allow excision, may have driven the evolution of an active base flipping mechanism for hOGG1. This requirement for damage recognition would give rise to hOGG1's primarily non-electrostatic DNA binding mode for both undamaged and damaged DNA. Thus unlike hUNG, hOGG1 is not imbued with salt dependent DNA binding specificity. It is important to point out that most specificity for damaged bases

occurs in the transition state for base excision by both hUNG and hOGG1^{22,26}. For instance, the transition state specificity for uracil as opposed to thymine or cytosine has been estimated to be at least 10⁵-fold for hUNG^{20,26}.

The implication of the difference in the salt sensitivities of hUNG and hOGG1 with regards to undamaged DNA binding could be profound in the context of translocation. The ability of a glycosylase to diffuse along a DNA chain is heavily dictated by its interaction with the noncognate sequences flanking the lesion sites. These enzymes have evolved with different sensitivities to the high ionic strength encountered in the cell, which could manifest as a difference in their mechanistic approach to DNA repair under physiologically relevant conditions. Chapter 5 will explore how these differing salt effects influence productive repair by hUNG and hOGG1.

3.4. METHODS

3.4.1. Experimental Conditions. All experiments with hOGG1 were performed in buffer containing 15 mM potassium phosphate pH 7.5, 1 mM EDTA, and 0.1 mg/mL BSA. This buffer contained a total of 30 mM K⁺ originating from pH adjustment of potassium phosphate and EDTA. Increasing ionic strength measurements were made by supplementing the buffer with potassium acetate (KOAc). All experiments with hUNG were performed in a buffer consisting of 20 mM HEPES pH 7.5, 3 mM EDTA, 1 mM DTT, 0.002% Brij 35. This buffer contained a total of 22 mM K⁺ originating from pH adjustment of the HEPES and EDTA stock solutions. The catalytic domain of recombinant hUNG, WT hOGG1 and the K249Q mutant hOGG1 were purified as previously described²⁷. All oligonucleotides were purchased from either Integrated DNA Technologies or Eurofin and

purified in-house by denaturing PAGE. PEG 8K was purchased from Sigma Chemical and was purified by overnight treatment with activated carbon (0.1g/mL) and filtered to remove UV absorbing impurities. Salmon sperm DNA (salDNA) was purchased from ThermoFisher Scientific.

3.4.2. Oligonucleotide Reagents

All DNA substrates listed below were purchased from either Integrated DNA Technologies (www.idtdna.com) or Eurofins MWG Operon (www.operon.com). Long oligos (>20 base pairs) were purified by denaturing gel electrophoresis. For all DNA duplex substrates, uracil bases were paired with adenine and 8-oxoguanine bases were paired with cytosine. All DNAs used in this study were in the duplex form and the sequences are listed below (the sequences of the complimentary strands for the two-site substrates are not shown).

20mer DNA substrates

D^N : Randomized nonspecific sequence

```
5' -FAM-ATA TCT CTA GCC TTC CTA TA-3'
3' -      TAT AGA GAT CGG AAG GAT AT-5'
```

D^{TATA} : Nonspecific sequence with no GC base pairs

```
5' -FAM-ATA TAT ATA AAA TTA ATA TA-3'
3' -      TAT ATA TAT TTT AAT TAT AT-5'
```

D^{GC} : Same nonspecific sequence as D^{TATA} with a central GC pair

```
5' -FAM-ATA TAT ATA GAA TTA ATA TA-3'
3' -      TAT ATA TAT CTT AAT TAT AT-5'
```

D^{GCGC}: Nonspecific sequence with no TA base pairs

5' -FAM-CCG CCC GCC GCC CGC CCG CC-3'
3' - GGC GGG CGG CGG GCG GGC GG-5'

D^S: Specific DNA containing 2-aminopurine (P) paired with T

5' -ATA TCT CTP °G CCT TCC TAT A-3'
3' -TAT AGA GAT C GGA AGG ATA T-FAM-5'

hOGG1 Activity Test substrate

S0^{oxoG}: 31mer with single 8-oxoguanine

5' -ATG CTG AGG AAT TTC °G CTC CTT GTA GGA TGA-3'
3' -TAC GAC TCC TTA AAG C GAG GAA CAT CCT ACT-5'

3.4.3. hOGG1 Equilibrium DNA Binding Measurements.

Binding of WT and K249Q hOGG1 to a non-specific 5' fluorescein-labeled 20mer DNA duplexes was measured by fluorescence anisotropy using a SPEX Fluoromax-3 spectrofluorometer at 20 °C (excitation wavelength of 494 nm, emission wavelength of 518 nm). All anisotropy values were corrected for the spectral G factors. Experiments were performed in a back-titration mode by diluting a solution of concentrated hOGG1 containing 25 nM labeled DNA with increasing volumes of a solution containing 25 nM labeled DNA only. After each addition, the solution was allowed to equilibrate for 4 min inside the fluorometer and three anisotropy measurements were averaged. All data were fitted to **eq 2.2 (Chapter 2)** using the software Prism. While the full final anisotropy change was not attainable for the higher salt titrations due to limits of protein solubility, we achieved 75% or greater saturation for all experiments. Further, all of the binding curves

extrapolated to the same final anisotropy when this parameter was used as a floating variable in the curve fitting process.

The binding affinity of hOGG1 for specific, 8-oxoguanine-containing DNA (K_D^S) was determined via a fluorescence anisotropy following the same back titration procedure described above and all data was fit using eq 1. A 10 nM solution of specific DNA (D^S) containing a single 8-oxoguanine and a 5'-FAM label on the complimentary strand was mixed with catalytically inactive K249Q hOGG1.

3.4.4. Salt Dependence of DNA Binding.

An evaluation of the electrostatic and non-electrostatic contributions to the binding free energy of both nonspecific and specific complexes formed by hOGG1 was carried out utilizing counter-ion condensation theory⁸. The log of the binding affinity was plotted against the log of the corresponding salt concentration and the data were fit using linear regression (eq 3.1)

$$\log (K_a) = \log (K_a^{\text{non}}) - N \log [\text{salt}] \quad (3.1)$$

$$N = \alpha\Psi + \beta$$

where the slope N may be interpreted as the number of ions displaced from the DNA upon protein binding, α is the number of phosphate groups in contact with the protein, Ψ represents the average number of monovalent counterions around each phosphate (0.64 for a short oligo¹⁰), and β is the number of ions displaced from the protein upon binding¹⁰. The second term in eq 3.1 becomes zero when $[\text{salt}] = 1 \text{ M}$; and accordingly, the first term reports on the binding affinity at a 1 M standard state of salt (i.e. when the electrostatic contribution to binding energy is removed). Thus, the free energy of non-electrostatic

interactions that do not involve ion displacement are obtained from the equation $\Delta G_{\text{non}}(1\text{ M}) = -RT\ln K_a^{\text{non}}$. The electrostatic contribution to the observed binding free energy at physiological salt concentration (taken as 150 mM K^+) may be obtained from **eq 3.2**.

$$\Delta G_{\text{elect}} = \Delta G_{\text{bind}} - \Delta G_{\text{non}} \quad (3.2)$$

3.4.5. K249Q Activity Assay.

To ensure that the K249Q mutation rendered hOGG1 catalytically inactive, a 25 nM solution of a 5' ^{32}P -labeled 31mer duplex containing a single 8-oxoG site (S0^{oxoG}) was incubated with 3 μM enzyme for 2 hours at 20°C in buffer containing 150 mM K^+ . These conditions were chosen to ensure that no appreciable amount of DNA was cleaved within the 2 hours it took to complete the specific DNA binding experiments. Samples were quenched with formamide and heated at 95°C for 30 min in the presence and absence of 100 mM NaOH. DNA fragments were separated using a denaturing 10% polyacrylamide gel and the gels were dried and exposed overnight to a storage phosphor screen and imaged with a Typhoon 8600 phosphorimager (GE Healthcare). All gel images were quantified by box method using QuantityOne (Bio-Rad). Background correction was made by subtracting the intensity of the gel directly below each band from the intensity of the corresponding band.

3.5. REFERENCES

1. Mol, C. D., Arvai, A. S., Slupphaug, G., Kavli, B., Alseth, I., Krokan, H. E., and Tainer, J. A. (1995) Crystal structure and mutational analysis of human uracil-DNA glycosylase: Structural basis for specificity and catalysis. *Cell*. *80*, 869-878.
2. Banerjee, A., Yang, W., Karplus, M., and Verdine, G. L. (2005) Structure of a repair enzyme interrogating undamaged DNA elucidates recognition of damaged DNA. *Nature*. *434*, 612-618.
3. Parker, J. B., Bianchet, M. A., Krosky, D. J., Friedman, J. I., Amzel, L. M., and Stivers, J. T. (2007) Enzymatic capture of an extrahelical thymine in the search for uracil in DNA. *Nature*. *449*, 433-437.
4. Hollis, T., Ichikawa, Y., and Ellenberger, T. (2000) DNA bending and a flip-out mechanism for base excision by the helix-hairpin-helix DNA glycosylase, *Escherichia coli* AlkA. *EMBO J*. *19*, 758-766.
5. Maiti, A., Noon, M. S., MacKerell, A. D., Pozharski, E., and Drohat, A. C. (2012) Lesion processing by a repair enzyme is severely curtailed by residues needed to prevent aberrant activity on undamaged DNA. *Proceedings of the National Academy of Sciences*. *109*, 8091-8096.
6. Bruner, S. D., Norman, D. P., and Verdine, G. L. (2000) Structural basis for recognition and repair of the endogenous mutagen 8-oxoguanine in DNA. *Nature*. *403*, 859-866.
7. Koval, V. V., Knorre, D. G., and Fedorova, O. S. (2014) Structural features of the interaction between human 8-oxoguanine DNA glycosylase hOGG1 and DNA. *Acta Naturae*. *6*, 52-65.
8. Manning, G. S. (1978) The molecular theory of polyelectrolyte solutions with applications to the electrostatic properties of polynucleotides. *Q. Rev. Biophys*. *11*, 179-246.
9. Record Jr, M. T., Lohman, T. M., and Haseth, P. d. (1976) Ion effects on ligand-nucleic acid interactions. *J. Mol. Biol*. *107*, 145-158.
10. Privalov, P. L., Dragan, A. I., and Crane-Robinson, C. (2011) Interpreting protein/DNA interactions: Distinguishing specific from non-specific and electrostatic from non-electrostatic components. *Nucleic Acids Res*. *39*, 2483-2491.
11. Blainey, P. C., van Oijen, A. M., Banerjee, A., Verdine, G. L., and Xie, X. S. (2006) A base-excision DNA-repair protein finds intrahelical lesion bases by fast sliding in contact with DNA. *Proceedings of the National Academy of Sciences*. *103*, 5752-5757.
12. Parikh, S. S., Walcher, G., Jones, G. D., Slupphaug, G., Krokan, H. E., Blackburn, G. M., and Tainer, J. A. (2000) Uracil-DNA glycosylase-DNA substrate and product structures: Conformational strain promotes catalytic efficiency by coupled stereoelectronic effects. *Proceedings of the National Academy of Sciences*. *97*, 5083-5088.
13. Cravens, S. L., Hobson, M., and Stivers, J. T. (2014) Electrostatic properties of complexes along a DNA glycosylase damage search pathway. *Biochemistry*. *53*, 7680-7692.
14. Jen-Jacobson, L., and Jacobson, L. A. (2008) Chapter 2 Role of Water and Effects of Small Ions in Site-Specific Protein-DNA Interactions, in pp 13-46, The Royal Society of Chemistry, .

15. Nash, H. M., Lu, R., Lane, W. S., and Verdine, G. L. (1997) The critical active-site amine of the human 8-oxoguanine DNA glycosylase, hOgg1: Direct identification, ablation and chemical reconstitution. *Chem. Biol.* *4*, 693-702.
16. Chen, L., Haushalter, K. A., Lieber, C. M., and Verdine, G. L. (2002) Direct visualization of a DNA glycosylase searching for damage. *Chem. Biol.* *9*, 345-350.
17. Friedman, J. I., and Stivers, J. T. (2010) Detection of damaged DNA bases by DNA glycosylase enzymes. *Biochemistry.* *49*, 4957-4967.
18. Krosky, D. J., Song, F., and Stivers, J. T. (2005) The origins of high-affinity enzyme binding to an extrahelical DNA base. *Biochemistry.* *44*, 5949-5959.
19. Parker, J. B., and Stivers, J. T. (2011) Dynamics of uracil and 5-fluorouracil in DNA. *Biochemistry.* *50*, 612-617.
20. Stivers, J. T., and Jiang, Y. L. (2003) A mechanistic perspective on the chemistry of DNA repair glycosylases. *Chem. Rev.* *103*, 2729-2759.
21. Dherin, C., Radicella, J. P., Dizdaroglu, M., and Boiteux, S. (1999) Excision of oxidatively damaged DNA bases by the human alpha-hOgg1 protein and the polymorphic alpha-hOgg1(Ser326Cys) protein which is frequently found in human populations. *Nucleic Acids Res.* *27*, 4001-4007.
22. Kuznetsov, N. A., Kuznetsova, A. A., Vorobjev, Y. N., Krasnoperov, L. N., and Fedorova, O. S. (2014) Thermodynamics of the DNA damage repair steps of human 8-oxoguanine DNA glycosylase. *PLoS ONE.* *9*, e98495.
23. Leipold, M. D., Workman, H., Muller, J. G., Burrows, C. J., and David, S. S. (2003) Recognition and removal of oxidized guanines in duplex DNA by the base excision repair enzymes hOGG1, yOGG1, and yOGG2. *Biochemistry.* *42*, 11373-11381.
24. Crenshaw, C. M., Wade, J. E., Arthanari, H., Frueh, D., Lane, B. F., and Nunez, M. E. (2011) Hidden in plain sight: Subtle effects of the 8-oxoguanine lesion on the structure, dynamics, and thermodynamics of a 15-base pair oligodeoxynucleotide duplex. *Biochemistry.* *50*, 8463-8477.
25. Every, A. E., and Russu, I. M. (2013) Opening dynamics of 8-oxoguanine in DNA. *J. Mol. Recognit.* *26*, 175-180.
26. Stivers, J. T., Pankiewicz, K. W., and Watanabe, K. A. (1999) Kinetic mechanism of damage site recognition and uracil flipping by escherichia coli uracil DNA glycosylase. *Biochemistry.* *38*, 952-963.
27. Cravens, S. L., Schonhoft, J. D., Rowland, M. M., Rodriguez, A. A., Anderson, B. G., and Stivers, J. T. (2015) Molecular crowding enhances facilitated diffusion of two human DNA glycosylases. *Nucleic Acids Res.* *43*, 4087-4097.

Chapter 4:

Molecular crowding enhances facilitated diffusion of two human DNA glycosylases

Reproduced in part from:

Cravens, S. L., Schonhofs, J. D., Rowland, M. M., Rodriguez, A. A., Anderson, B. G., and Stivers, J. T. (2015) Molecular crowding enhances facilitated diffusion of two human DNA glycosylases. *Nucleic Acids Res.* *43*, 4087-4097

4.1 INTRODUCTION

A significant triumph in biochemistry over the last twenty years was the ability to isolate human DNA repair enzymes and study their *in vitro* properties using defined DNA substrates containing damaged sites. Typically, these studies have been performed using dilute conditions, where the concentration of the enzyme, DNA and buffer components were low compared to the concentration of water. Although a wealth of insights into the thermodynamic, kinetic and structural properties of enzymes have resulted from such approaches (1-7), DNA repair enzymes act in a crowded cellular environment with quite different physical properties (8, 9). Thus, an open question is how the complex intracellular milieu affects the ability of enzymes to locate and repair damage sites embedded in a large polymeric DNA substrate.

The human intracellular environment has numerous physical properties that could dramatically affect enzyme activity. These include high inorganic ion and metabolite concentrations (10, 11), lower dielectric properties (12-14), higher bulk viscosity (15, 16), and the presence of high concentrations of macromolecules which consume available volume (“molecular crowding”) (17, 18). Indeed, the concentration of macromolecules in human cells is an astounding ~100 to 300 mg/mL (9, 19), which means that 10 to 40% of the total cellular volume is consumed by large molecules (often called the *excluded volume*). Taken together, these parameters could affect association of an enzyme with its target in complex ways. For instance, high ion concentrations are expected to shield electrostatic interactions between an enzyme and its highly charged DNA substrate (10, 20, 21), while a lower dielectric constant could have an opposite effect. Increases in macroscopic viscosity will slow the translational movement of macromolecules and due to

entropic effects, crowded environments will push macromolecular association when the complex consumes a smaller volume than the free component species (9, 22, 23).

Although volume exclusion largely explains the effects of crowded environments on binding equilibria, crowding has been reported to have a surprisingly small effect on the diffusion-controlled association kinetics of macromolecules (24). Indeed, it has been observed that some diffusion-controlled association reactions occur at nearly the same rates in crowded solutions and in cells as they do in dilute solution (24, 25). These kinetic effects are counterintuitive, but can be understood by considering that macromolecular crowders alter the macroscopic viscosity and available volume in crowded solutions, but do not change the microscopic viscosity (26, 27). Thus, over short nanometer distances, the rotational and translational diffusion of proteins is not greatly affected by crowding because the protein only feels the microscopic viscosity of the solvent that is present in the spaces between the larger crowding molecules (28). Over larger distances, hard sphere repulsion between the protein and crowding molecules increases the effective viscosity and slows translational diffusion (8, 28, 29). When two binding partners approach one another, they are captured within a low viscosity (high mobility) cage created by the larger crowding molecules, which increases the probability for a productive encounter event. Surprisingly, the capture of two binding partners within a high mobility cage can in some cases offset all of the negative effects of high viscosity on the overall association rate (29).

The above considerations raise the interesting question of what effect molecular crowding has on enzyme association with DNA, and in particular, the property of facilitated diffusion along a DNA chain? Facilitated diffusion on the DNA chain

(“translocation”) is a distinct process that involves transient states of an enzyme and DNA that are not directly observable in equilibrium binding, steady-state or rapid kinetic measurements (1-4, 30). Here we measure the effect of inert crowding agents on the probability that the DNA repair enzymes uracil and 8-oxoguanine DNA repair glycosylase will successfully translocate between two damaged sites in a DNA chain. We find that crowding increases the likelihood that each enzyme will successfully translocate between their respective target sites without dissociation to bulk solution and also increases the average translocation distance. For both enzymes, crowding biases the damage search process towards a chain tracking search mode rather than a 3D search mode. Such a crowder-induced transition in the search mode could significantly impact the effectiveness of the damage search in a crowded nuclear environment. These enzymes represent two of the largest superfamilies of glycosylases and their similar behavior in these studies suggests that the findings will be general for other related glycosylases.

4.2. RESULTS

4.2.1. Crowding Effects on DNA Translocation.

We first probed the effects of solution viscosity and excluded volume on translocation of hUNG between its target uracil sites in DNA, using our previously described site transfer assay (3, 30). Translocation between two uracil sites embedded in a single DNA chain can occur by an *associative* pathway that involves movement of a loosely associated enzyme molecule on the surface of the DNA chain, or a *dissociative* pathway that involves reversible short-range excursions from the DNA surface (**Figure 4.1A**). The overall probability of transferring between uracil sites (P_{trans}) is the sum of the

probabilities of transferring by each individual pathway (i.e. $P_{\text{trans}} = P_{\text{assoc}} + P_{\text{diss}}$) and those enzyme molecules that fail to transfer are lost to bulk solution after reacting at only a single site. The contribution of the associative pathway in isolation can be determined by adding a small molecule active site trap to the transfer reaction (**T**, **Figure 4.1A**). High concentrations of trap serve to capture all enzyme molecules undergoing dissociative excursions, which selectively blocks this transfer pathway, while leaving the associative pathway intact (30, 31). P_{trans} is calculated from the relative amounts of DNA product fragments that result from uracil excision at only a single site (fragments AB and BC), and the double site cleavage events that reflect successful intra-site transfer (resulting in fragments A and C). These 5' and 3' ^{32}P end-labeled DNA fragments are electrophoretically separated on a denaturing polyacrylamide gel and quantified by phosphorimaging as shown in **Figure 4.1B** (see **Methods** and **eq 4.1** for further details). It is useful to note that intramolecular site transfer gives rise to more A and C transfer products relative to the AB and BC single site excision products, which can be discerned by simple visual inspection of the band intensities at low extents of reaction (**Figure 4.1B**).

We initially explored how P_{trans} was affected by 0 – 30% (w/v) ethylene glycol (EG), PEG 600, 1500, 3350, and 8K using a DNA substrate that contained two uracil sites spaced 20 bp apart (**Figure 4.1B**). Varying the polymer size and concentration allowed us to probe both viscosity and crowding effects, with the latter effect expected to become more significant with larger polymers (29, 35). Representative data in the presence of 20% PEG 8K are shown in **Figure 4.1B**, where a large increase in P_{trans} is apparent in the presence and absence of the uracil trap (compare A and C bands in the buffer only and PEG 8K lanes in **Figure 4.1B**). P_{trans} was found to increase and then plateau as the concentration

reached about 15% (w/v), regardless of the PEG polymer that was used (**Figure 4.2A**). In contrast, the small molecule viscogen EG showed no effect on P_{trans} over the concentration range 0 – 30% (w/v) (**Figure 4.2B**). It is important to point out that the large increases in P_{trans} for PEG polymers excludes the possibility of strong interactions of these polymers with either the DNA or the enzyme (36).

Given that both transfer pathways involve diffusional processes, which should be slowed in a linear fashion by increases in bulk solution viscosity (**Figure 4.1A**), we explored whether the transfer probability changed linearly with respect to the relative viscosity of the polymer solutions ($\eta^{\text{rel}} = \eta^{\text{crowd}}/\eta^{\text{buffer}}$) (**Figure 4.1C**). In this analysis, the relative viscosity values (**Table 4.1**) were obtained from the literature (29). While P_{trans} did initially increase with viscosity in the range $\eta^{\text{rel}} < 4$, it eventually showed downward curvature and reached a plateau level of $P_{\text{trans}} \sim 0.8$. In the presence of 20% PEG 8K, nearly every enzyme molecule that reacted at one site made it to the second site 20 bp away, as compared to only 1 in 3 molecules in dilute buffer (**Table 4.2**). In contrast, P_{trans} was unchanged when the concentration of the small EG viscogen was increased to 30% (w/v) ($\eta^{\text{rel}} = 2.2$) (**Figure 4.2B**). These findings indicate that viscosity changes alone cannot account for the increases in P_{trans} , and that the enhancement of P_{trans} requires high molecular weight polymers (i.e. crowding).

Control experiments were performed to explore other possible effects of PEG polymers that were unrelated to viscosity and crowding effects. First, we confirmed that other structurally distinct crowding agents (Dextran 25K and Ficoll 70) also increased P_{trans} in a concentration dependent fashion and approached the same plateau value at high concentrations and viscosity observed with PEG polymers (**Figures 4.2C and 4.2D**). Thus,

the general observations are independent of the chemical structure and size of large crowders. We also investigated whether the results might arise from large changes in the Na^+ ion activity by PEG polymers. However, using a sodium ion-selective electrode, we found that the activity of Na^+ decreased only minimally upon addition of 20% PEG 8K ($49 \pm 1 \text{ mV}\cdot\text{M}^{-1}$ in buffer and $41 \pm 3 \text{ mV}\cdot\text{M}^{-1}$ in 20% PEG 8K) (**Methods and Table 4.3**). Based on our previous studies on the salt dependence of P_{trans} (10), a small $\sim 15\%$ reduction in the sodium ion activity would not have any significant effect on P_{trans} and would have no effect on P_{assoc} , which is resistant to changes in salt concentration (30).

We point out that the reported P_{trans} values are not corrected for the kinetic efficiency (E) at which hUNG excises uracil once a site is encountered (30). Thus, the observed $P_{\text{trans}} = E \times P_{\text{trans}}^{\text{true}}$ reports on the combined effects of crowding arising from viscosity, molecular crowding, as well as any changes in the excision efficiency once the site is reached. In the context of this work, corrections for the excision efficiency changes are superfluous because the excision efficiency in dilute buffer is already large ($E = 0.81 \pm 0.16$) (30) and the excision efficiency in the presence of 20% PEG 8K is even larger based on the maximum P_{trans} values reported in Table S3 ($E \geq 0.92$). The maximal change in excision efficiency is therefore only 10-11%, which is within experimental error of excision efficiency measurements. Furthermore, the following site spacing studies are performed with a single concentration of PEG 8K, which makes the data entirely independent of any changes in the excision efficiency.

Given the representative behavior of PEG polymers and the large body of useful polymer theory that has focused on PEG (35, 37-40), we performed all additional experiments using 20% PEG 8K. The use of 20% PEG 8K as the standard crowding

condition allowed us to further probe both viscosity and molecular crowding effects on the site spacing dependence of site transfer. Importantly, the relative viscosity of 20% PEG 8K is nearly 13-fold greater than water (29) and its larger radius of gyration as compared to hUNG would be expected to produce significant volume exclusion effects (29, 35).

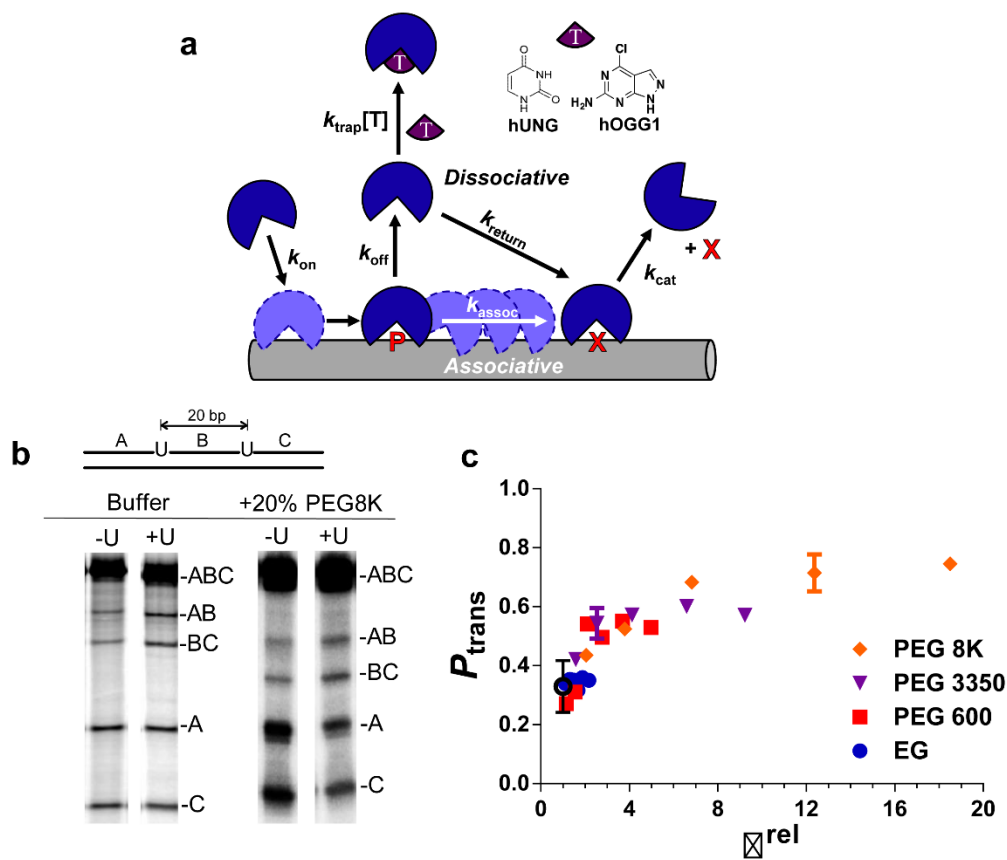


Figure 4.1. Approach for measuring site transfer probabilities of hUNG and hOGG1.

A) The search and repair pathway used by DNA glycosylases. The site transfer method has been modified to include a “molecular clock” where a small molecule trap [T = U for hUNG, or I for hOGG1] is used to block the dissociative pathway. **B)** Phosphorimages of the products derived from reaction of hUNG with a 90mer substrate (S20^U) with two uracils 20bp apart in dilute buffer and +20% PEG 8K (+/-U denotes the presence and absence of uracil trap). The increased transfers in the presence of 20% PEG 8K are indicated by the increased levels of the A and C bands (double excision fragments) as compared to AB and BC bands (single excision fragments). **c)** The transfer probabilities between uracil sites spaced 20 bp apart (measured at 37 °C) as a function of relative viscosity ($\eta^{rel} = \eta^{crowder}/\eta^{buffer}$) for a series of PEG polymers. Relative viscosities of these cosolutes were obtained from reference (29). The P_{trans} value for buffer alone is indicated by the black open circle.

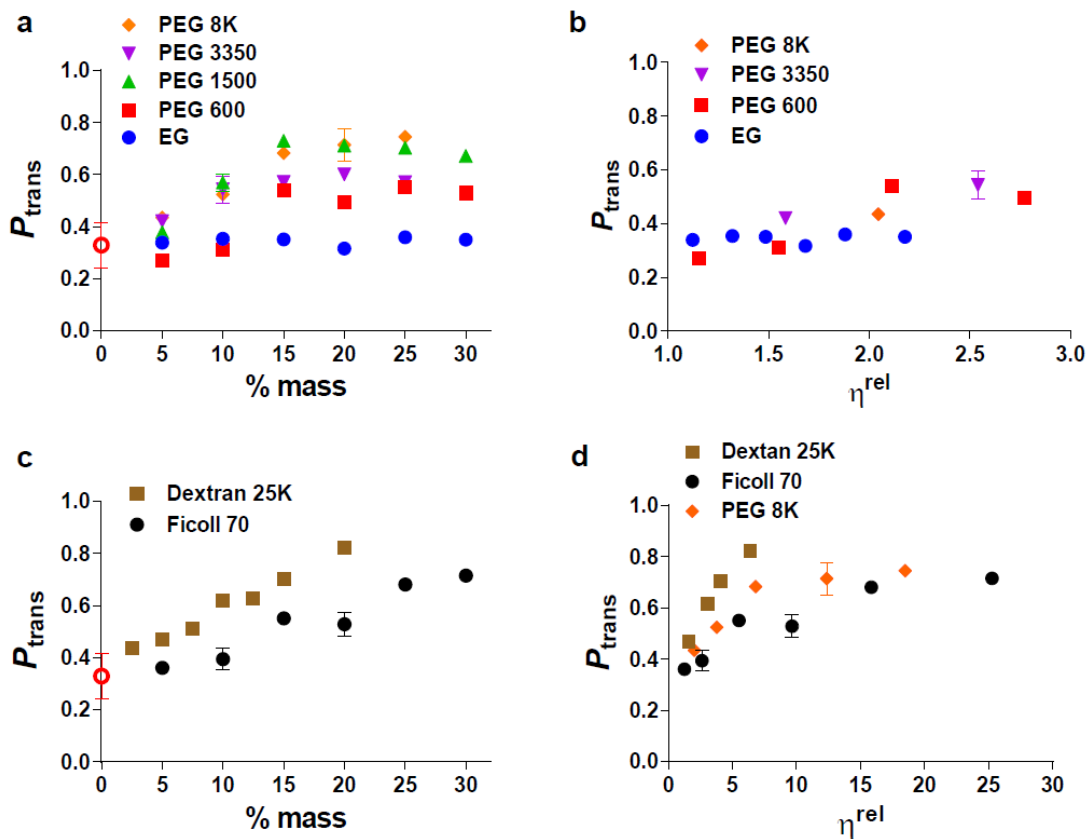


Figure 4.2. Effect of molecular crowding agents on the site transfer probability (P_{trans}) of hUNG between uracil lesions spaced 20 bp apart. (A) Overall site transfer probabilities (P_{trans}) plotted as a function of % mass for ethylene glycol (EG) and other high MW PEG polymers. (B) Expansion of Figure 1c to highlight the minimal changes in P_{trans} at low relative solution viscosities ($\eta^{\text{rel}} = \eta^{\text{crowd}}/\eta^{\text{buffer}}$). (C) P_{trans} as a function of increasing amounts of Dextran 25K and Ficoll 70. (D) P_{trans} for Dextran 25K, Ficoll 70 (Figure 4.3C), and PEG 8K (Figure 4.3A) plotted as a function of relative solution viscosity. Relative viscosities for were taken from the literature ((59) for Dextran 25K and (60) for Ficoll 70). Only the data corresponding to solution conditions equivalent to those from the literature sources were used.

Table 4.1. Solution viscosities at 25 °C for varying amounts of EG, PEG 600, PEG 3350, and PEG 8K (literature values) (29).

% mass (w/v)	$\eta^{\text{crowd}}/\eta^{\text{buffer}}$			
	EG	PEG 600	PEG 3350	PEG 8K
5	1.12	1.15	1.57	2.04
10	1.32	1.55	2.54	3.79
15	1.48	2.11	4.12	6.83
20	1.68	2.77	6.60	12.37
25	1.88	3.69	-- ^a	--
30	2.18	4.98	--	--
40	2.93	--	--	--

^aValue could not be determined from literature source.

Table 4.2. P_{trans} , P_{assoc} , and P_{diss} for hUNG in the presence and absence of 20% PEG 8K

Site Spacing (bp)	P_{trans}		P_{assoc}^a		P_{diss}^b	
	Buffer	20% PEG 8K	Buffer	20% PEG 8K	Buffer	20% PEG 8K
	5	0.60 ± 0.04	0.92 ± 0.06	0.37 ± 0.06	0.61 ± 0.09	0.23 ± 0.07
10	0.45 ± 0.04	0.91 ± 0.06	0.03 ± 0.04	0.44 ± 0.08	0.46 ± 0.04	0.5 ± 0.1
20	0.33 ± 0.09	0.71 ± 0.06	0.02 ± 0.07	0.26 ± 0.03	0.33 ± 0.09	0.45 ± 0.07
55	0.21 ± 0.06	0.50 ± 0.08	-0.08 ± 0.07	0.14 ± 0.06	0.21 ± 0.06	0.4 ± 0.1

^a P_{assoc} was determined by performing the site transfer experiment in the presence of 10 mM uracil and was independent of uracil concentration in the range 10 to 20 mM.

^b Calculated from $P_{\text{diss}} = P_{\text{trans}} - P_{\text{assoc}}$

Table 4.3. Sodium ion activity in the presence and absence of 20% PEG 8K

Na⁺ Activity	
(mV·M⁻¹)	
Buffer	49 ± 1
20% PEG 8K	41 ± 3

4.2.2. Crowding Primarily Enhances the Associative Transfer Pathway.

To investigate the fundamental basis for the observed polymer induced enhancements of P_{trans} , we made site transfer measurements using substrates with site spacings in the range 5 to 55 bp in the presence and absence of the uracil trap so that the relative contributions of the associative and dissociative pathways could be determined. Controls established that the observed transfer probabilities in the presence of the uracil trap (10 or 20 mM) were independent of trap concentration even in the presence of 20% PEG 8K (**Figure 4.2**).

In the absence of the uracil trap, the overall site transfer probabilities for all site spacings increased significantly in the presence of 20% PEG 8K (**Figure 4.4A**, compare red and black data, see also **Table 4.2**). The dramatic increases in the transfer probabilities also persisted in the presence of the uracil trap (**Figure 4.4B**), indicating that the overall effect was dominated by an increase in associative transfers. Strikingly, introduction of 20% PEG 8K resulted in the persistence of associative transfers for uracils site spacings as large as 55 bp, whereas in dilute buffer solution the associative pathway was abolished for site spacings ≥ 10 bp (**Figure 4.4B**). This indicates that hUNG can traverse a larger linear distance on the DNA chain in the presence of crowding. In contrast, only a small increase in P_{diss} was observed in the presence of 20% PEG 8K (**Figure 4.4C**).

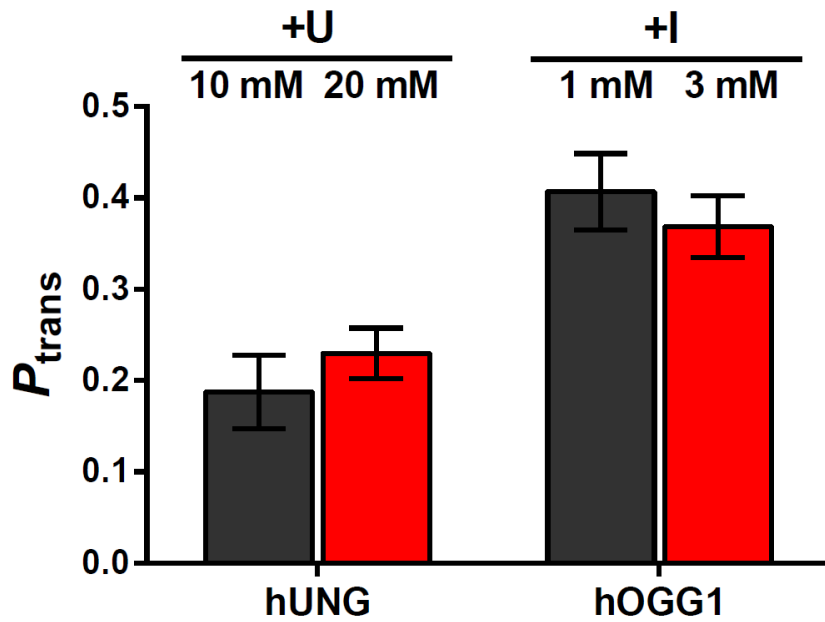


Figure 4.3. Molecular trap concentration control. The amount of associative transfers between lesions spaced 20 bp apart measured in the presence of PEG 8K are independent of the trap concentration for both hUNG and hOGG1. Both uracil and the hOGG1 inhibitor (I) precipitate when higher concentrations are used (30, 31).

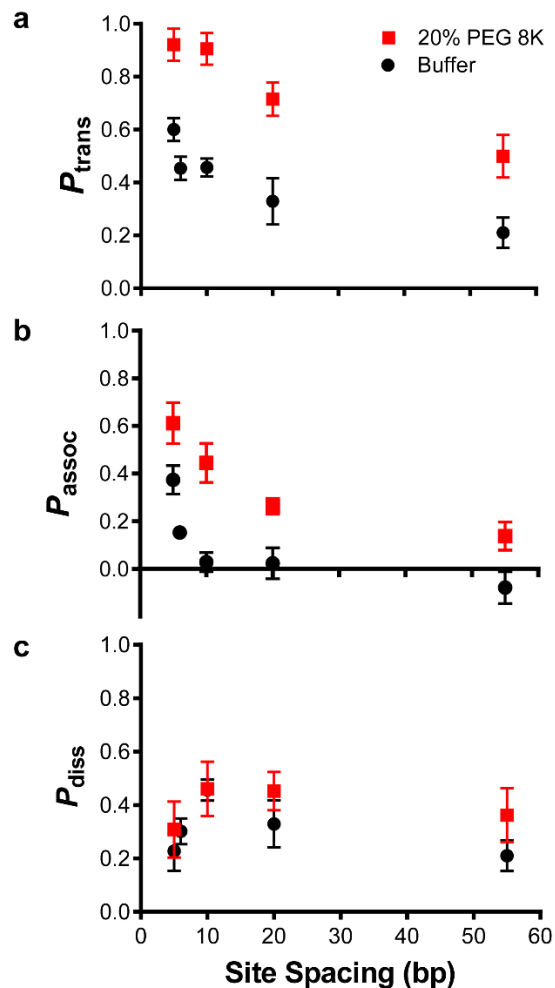


Figure 4.4. Effect of 20% PEG 8K on the intramolecular site transfer probability between uracil sites of variable spacing. All data obtained from dilute buffer conditions (black) have been previously reported and are displayed here for comparison (30). **a)** Overall site transfer probabilities (P_{trans}) as a function of spacing length between uracil sites in the presence (red) and absence (black) of PEG 8K. **b)** The increased contribution of the associative transfer pathway (P_{assoc}) and the longer associative transfer distances in the presence of PEG 8K were determined using high concentrations of uracil trap (10 and 20 mM). **c)** A smaller increase in the probability of dissociative transfers ($P_{diss} = P_{trans} - P_{assoc}$) was observed for all site spacings in the presence of PEG 8K.

4.2.3. Crowding Effects on Translocation of hOGG1.

We were interested in whether the above effects of crowding agents on DNA translocation were specific to hUNG, or alternatively, might reflect a more general property that extended to other DNA glycosylases. Thus we explored the general effects of crowding agents on the site transfer mechanism of hOGG1, a representative enzyme from the large HhH superfamily of DNA glycosylases that removes the oxidized base 8-oxoguanine from DNA (41). We previously determined the site transfer properties of hOGG1 using the same approach as used with hUNG, except that an 8-oxoG analogue (2-amino-6-chloropurine) was used as the small molecule trap (**Figure 4.1A**) (31). In initial kinetic experiments using a 31mer DNA duplex containing a single 8-oxoguanine site, we found that 20% PEG 8K reduced the steady-state turnover rate of hOGG1 by approximately 8-fold as compared to buffer (**Figure 4.5**). An inhibitory effect of 20% PEG 8K on the uracil excision rate was also observed with hUNG under k_{cat} conditions. Similar to hUNG, the overall site transfer probability (P_{trans}) of hOGG1 over a site spacing of 20 bp increased in the presence of 20% PEG 8K ($P_{\text{trans}}^{\text{buffer}} = 0.34 \pm 0.09$, $P_{\text{trans}}^{\text{PEG8K}} = 0.50 \pm 0.03$).

We were curious if the origin of the effect on the overall P_{trans} for hOGG1 arose from enhanced probability of transfer by the associative pathway as seen with hUNG (**Figure 4.6**). This indeed turned out to be the case as associative transfers of hOGG1 increased by ~3-fold in the presence of 20% PEG 8K, while change in the probability of dissociative transfers was negligible (**Figure 4.6, Table 4.4**). In control experiments we established that the level of associative transfers in the presence of PEG 8K was independent of the trap concentration (**Figure 4.3**). The fact that the magnitude of the effects on P_{trans} and P_{assoc} are not as pronounced for hOGG1 as they are for hUNG is

consistent with an excluded volume effect. The significance of volume exclusion can be estimated by the size differential between the proteins of interest and the crowding agent (29). Since hOGG1 is larger than hUNG we would predict reduced impact from the crowding agent on hOGG1 translocation.

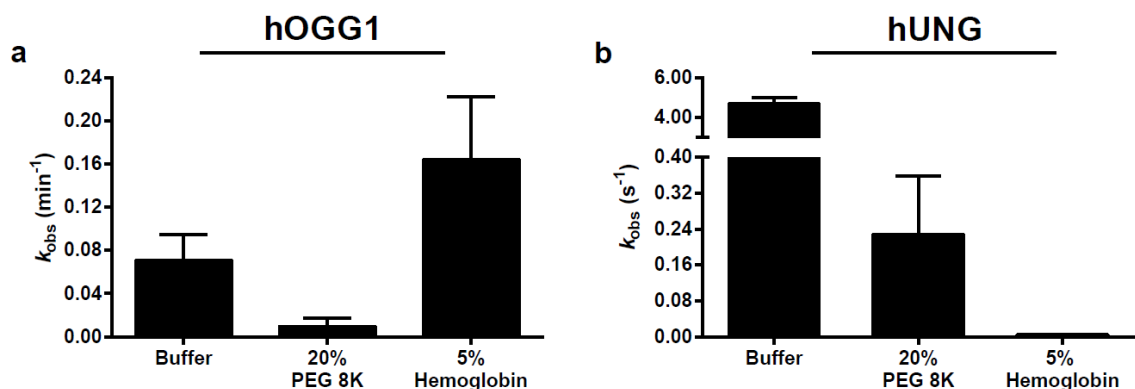


Figure 4.5. Reaction rates in dilute buffer, 20% (w/v) PEG 8K, and 5% (w/v) hemoglobin. **A)** Rates determined by quantifying the amount of product formed as a function upon mixing 1 nM of hOGG1 with 20 nM ^{32}P labeled S0^{G} 31mer substrate (Buffer: $0.07 \pm 0.02 \text{ min}^{-1}$, 20% PEG 8K: $0.010 \pm 0.008 \text{ min}^{-1}$, 5% Hemoglobin: $0.16 \pm 0.06 \text{ min}^{-1}$). **B)** Reaction rates estimated by determining the rate of total product formation when hUNG was reacted with 40 nM of ^{32}P labeled S20^{U} 90mer substrate in the site transfer assay (**Figures 4.1 and 4.11**) (Buffer: $4.7 \pm 0.3 \text{ s}^{-1}$, 20% PEG 8K: $0.2 \pm 0.1 \text{ s}^{-1}$, 5% Hemoglobin: $0.003 \pm 0.001 \text{ s}^{-1}$). Linear reaction rates were measured for both enzymes under conditions of less than 30% product formation.

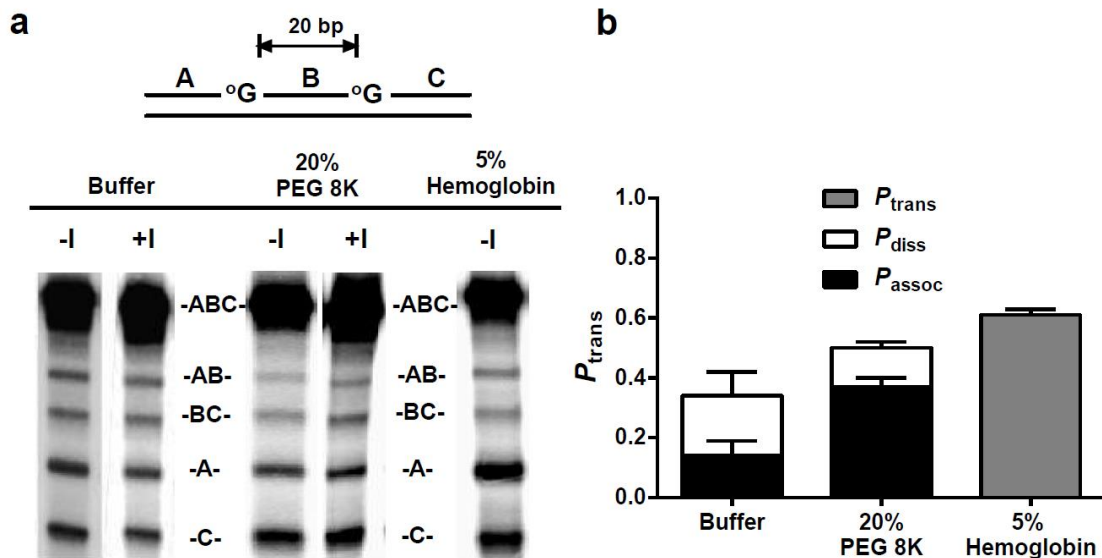


Figure 4.6. Effect of 20% PEG 8K and 5% hemoglobin on the site transfer probability of hOGG1 over a 20 bp spacing (P_{trans}). **A)** Phosphorimages of polyacrylamide gels showing the separation of the reaction products generated from excision of 8-oxoG. The presence or absence of the molecular trap (Figure 1) is indicated by +/- I. **B)** Partitioning of the total transfers between the associative (P_{assoc}) and dissociative (P_{diss}) pathways. Error bars show the SD of three replicate determinations of P_{trans} . Overall P_{trans} was found to increase when PEG 8K was added, primarily due to an increase in the relative contribution of the associative pathway. A similar increase in P_{trans} was observed upon addition of hemoglobin, though the contributions of P_{assoc} and P_{diss} could not be discerned due to precipitation upon addition of the trap.

Table 4.4. Effect of 20% PEG 8K on P_{trans} , P_{assoc} , and P_{diss} for hOGG1 (S20^{oG}).

Site	P_{trans}		P_{assoc}^a		P_{diss}^b	
	Buffer	20% PEG 8K	Buffer	20% PEG 8K	Buffer	20% PEG 8K
Spacing (bp)						
20	0.34 ± 0.09	0.50 ± 0.03	0.14 ± 0.05	0.37 ± 0.03	0.20 ± 0.11	0.13 ± 0.02

^a P_{assoc} was determined by performing the site transfer experiment in the presence of 3 mM trap.

^b Calculated from $P_{\text{diss}} = P_{\text{trans}} - P_{\text{assoc}}$

^cData has been previously published and is presented here for comparison (12).

4.2.4. Effects of a Protein Crowder on Translocation.

The interesting consequences of inert polymer crowders on the translocation of both glycosylases begged the question if the effect can be extended to protein crowders. After a survey of possible protein crowding agents, we chose hemoglobin because it is large enough to exclude significant volume, and it has a favorably low number of ionic groups that helped minimize changes in ionic strength upon addition of high hemoglobin concentrations. In our buffer conditions, hemoglobin was soluble up to 50 mg/ml [5% (w/v)] and this concentration was used in these experiments. Much like 20% PEG 8K, P_{trans} for hOGG1 was found to increase in the presence of hemoglobin (**Figure 4.6**). The larger increase in P_{trans} observed in 5% hemoglobin as compared to 20% PEG 8K bolsters our conclusion that the effect is not due simply to viscosity since the hemoglobin solution is significantly less viscous (42). We could not partition this effect into contributions from associative and dissociative transfers because addition of the trap caused gross precipitation.

Similar experiments using hUNG produced more complex results than with hOGG1. First, 50 mg/ml hemoglobin inhibited the steady-state rate of hUNG by ~1,000-fold, while having only a negligible effect on hOGG1 (**Figure 4.5**). This significant effect on the reaction rate precluded any definitive conclusions on translocation (**Figure 4.11**). We have provided a reasonable analysis of this data in the **Methods Section 4.4.11**, but do not include it in our global conclusions about the effect of crowding on translocation due to the specific inhibition by hemoglobin. The disparities in the effects of hemoglobin on P_{trans} and the reaction rates for hUNG and hOGG1 indicate the limitations of using protein crowding agents, which are clearly not inert in every context and have the potential to mask

viscosity and molecular crowding effects by interacting with the macromolecules of interest.

4.2.5. Crowding Decreases Turnover of hUNG with Large DNA Substrates.

The similar effects of molecular crowding agents on DNA translocation by hUNG and hOGG1 suggests that it is a general mechanism that facilitates DNA chain surveillance by DNA glycosylases. Since the mechanism of facilitated diffusion depends on the thermodynamic and kinetic stability of intermediate states along the search and repair pathway (**Figure 4.1**), we sought to dissect the effects of PEG polymers on each microscopic step of the hUNG reaction as described below.

We first investigated the effect of increased associative transfers on the steady-state kinetic parameters for uracil excision from short and long DNA substrates (**Fig. 4.7 A-D**). In these studies we used (i) a molecular beacon hairpin DNA construct ($6U^{11}$) that contained six closely spaced uracils within an 11 bp stem, allowing continuous fluorescence measurement of the steady-state rates, (ii) a 30mer with a single central uracil ($1U^{30}$), and (iii) a 90mer duplex with a single central uracil ($1U^{90}$). Taking advantage of the convenient fluorescence assay available with $6U^{11}$ (see **Methods**), the k_{cat} , K_m and k_{cat}/K_m values were determined in the presence of dilute buffer, 5 – 20% PEG 8K, and 20 – 40% EG. For $1U^{30}$ and $1U^{90}$, the same parameters were measured in discontinuous assays using $5' \text{-}^{32}\text{P}$ labeled DNA using dilute buffer and a single concentration of 20% PEG 8K. The kinetic parameters for these substrates under the various conditions are summarized in **Table 4.5**.

The use of EG as a small molecule viscogen resulted in apparent inhibition of hUNG. This effect was manifested most prominently in a 7-fold increase in K_m and an order-of-magnitude reduction in k_{cat}/K_m (**Figure 4.7B, Table 4.5**). Such inhibition by EG is not entirely unexpected because the related molecule glycerol has been shown to bind to the UNG active site in the position occupied by the uracil base and inhibit the reaction (43). In addition, inhibitory effects of EG have been observed previously in the context of protein-protein association and have been attributed to preferential hydration of proteins in EG solutions, resulting in slowed association rates due to increased difficulty of stripping away additional water molecules (24).

The most salient findings from the kinetic studies utilizing 20% PEG 8K were that (i) k_{cat} and K_m values for both 6U¹¹ and 1U³⁰ were decreased by ~4-fold, such that the k_{cat}/K_m values were only slightly lower than dilute buffer, and (ii) 1U⁹⁰ exhibited a much larger 20-fold decrease in k_{cat} and a 10-fold decrease in k_{cat}/K_m (**Figure 4.7E, Table 4.5**). We note that the origin of the apparent inhibitory effect of PEG for the 1U⁹⁰ substrate is almost entirely on k_{cat} , requiring that it arises from a step involving the ES complex, but not the free enzyme (this is distinct from the inhibition by EG, which primarily binds to free E). Further, the step must occur before or after glycosidic bond cleavage, because the chemical step is very rapid for all of these substrates ($k_{cl} = 240 \text{ s}^{-1}$) (30). Thus, the only fundamental difference between the ES complex for 1U⁹⁰ and the shorter substrates is the presence of additional non-specific flanking DNA.

This viewpoint led us to hypothesize that the slow turnover of 1U⁹⁰ was due to increased time spent by hUNG in repetitive associative and dissociative transfers on non-specific DNA prior to reaching the target site for protein molecules that associate far from

the uracil site, in addition to transfers along the flanking DNA after uracil excision. We tested this proposal by measuring the effect of 20% PEG 8K on the k_{cat} values for the 1U^{30} and 1U^{90} substrates in the presence of a higher salt concentration that is known to disrupt non-specific DNA binding (10). The expectation was that the k_{cat} effect would be equalized under such conditions if turnover was indeed limited by the time spent in associative transfers on the non-specific DNA sequences within 1U^{90} . This expectation was confirmed because the effect of PEG 8K on the k_{cat} value of 1U^{90} was reduced to 2-fold, which is indistinguishable from the 2-fold effect seen with 1U^{30} at high-salt (**Figure 4.7F**). We conclude that crowding increases the time spent in associative transfers on DNA and that these transfers can greatly reduce steady-state turnover when the DNA chains are long.

Figure 4.7. The effect of molecular crowding agents on the steady-state kinetics of hUNG acting on short and long duplex DNA substrates. (A) Effect of 5 – 20% PEG 8K on the initial rates of reaction of hUNG with a DNA hairpin containing an 11 bp stem ($6U^{11}$). (B) Effect of 20 – 40% EG on the initial reaction rates of hUNG with $6U^{11}$. The dashed blue line is the curve for dilute buffer shown in panel A. (C) Effect of 20% PEG 8K (black) on the initial reaction rates of hUNG with a 30 mer duplex ($1U^{30}$) in comparison to dilute buffer (blue). (D) Initial rates of uracil excision from the 90 mer duplex ($1U^{90}$) in the presence of 20% PEG 8K. (E) The relative effect of 20% PEG 8K on the steady-state kinetic parameters (X^{rel}) for hUNG acting on short ($6U^{11}$ and $1U^{30}$) and long ($1U^{90}$) duplex DNA substrates. X^{rel} is defined as the kinetic parameter obtained in the presence of PEG 8K divided by that obtained in buffer alone (see **Table 4.5**). (F) The salt-dependent change in k_{cat} for 30 bp ($1U^{30}$) and 90 bp ($1U^{90}$) DNA substrates in the presence of molecular crowding agents. The effect of 20% PEG 8K on k_{cat} for both substrates was determined in presence of high salt (75 mM total cation concentration, grey bars). For comparison, the black bars show the k_{cat} values determined at low salt (22 mM cation concentration, see **Figure 4.8**). The parameter k_{cat}^{rel} is defined as the k_{cat} value determined in the presence of 20% PEG 8K divided by the value obtained using buffer alone. The k_{cat} values for both $1U^{30}$ and $1U^{90}$ dropped ~2-fold upon addition of 20% PEG 8K ($1U^{30}$): k_{cat} decreased from $2.1 \pm 0.9 \text{ s}^{-1}$ to $1.2 \pm 0.5 \text{ s}^{-1}$; $1U^{90}$ k_{cat} decreased from $10.5 \pm 0.4 \text{ s}^{-1}$ to $5 \pm 2 \text{ s}^{-1}$. The similar effect of PEG 8K for both substrates at high, but not low salt, supports the proposal that rate-limiting associative transfers limit turnover of the large substrate at low salt. The differences in the absolute k_{cat} values for each substrate are due to sequence dependent differences in the steady-state turnover rate (5, 49).

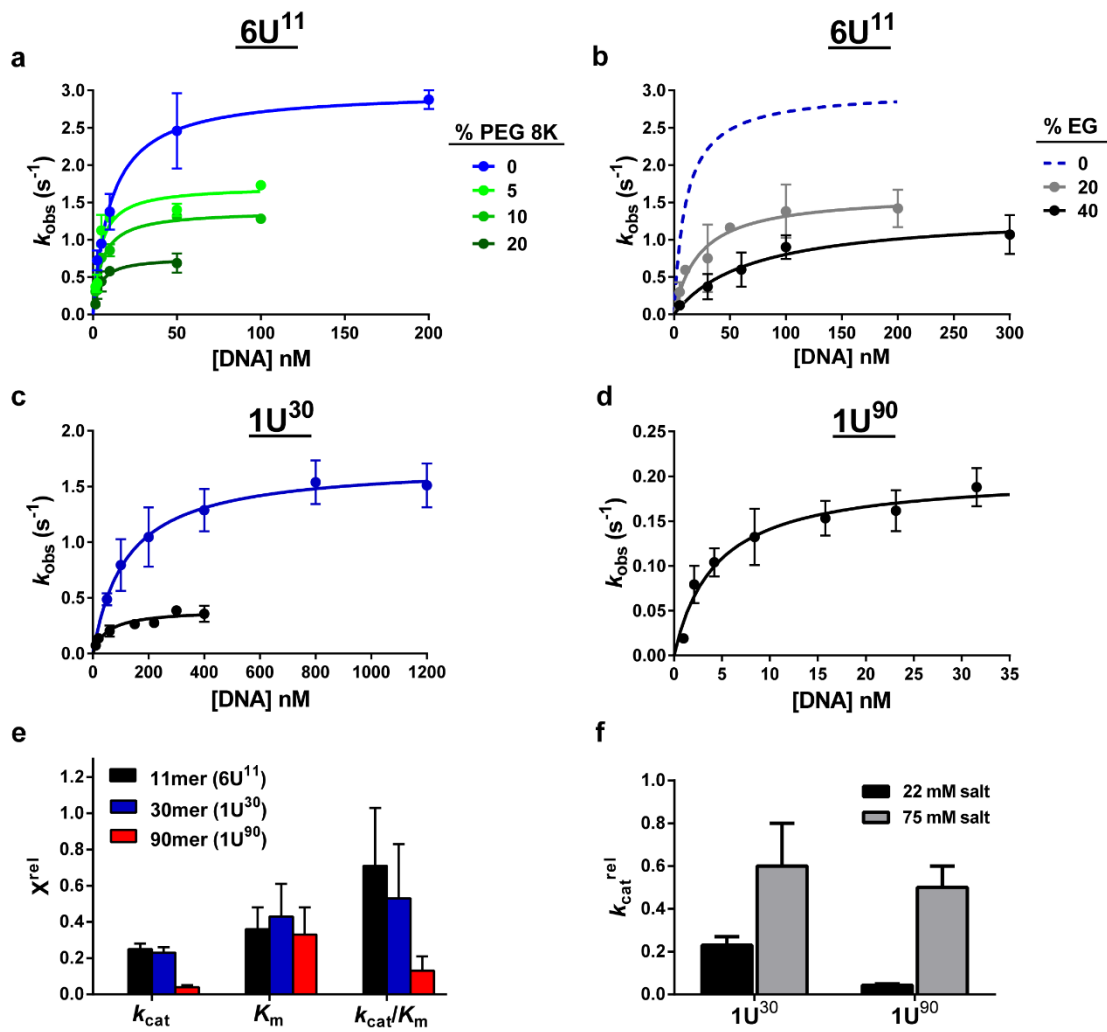


Figure 4.7.

Table 4.5. Effects of EG and PEG 8K on the steady-state kinetic parameters of hUNG with short and long DNA substrates.^a

DNA Substrate		k_{cat} (s ⁻¹)	K_m (M)	k_{cat}/K_m (M ⁻¹ s ⁻¹)
6U¹¹ (11mer) ^b	Buffer	3.0 ± 0.1	11 ± 1 × 10 ⁻⁹	2.8 ± 0.3 × 10 ⁸
	20% EG	1.6 ± 0.1	23 ± 6 × 10 ⁻⁹	7 ± 2 × 10 ⁷
	40% EG	1.4 ± 0.2	70 ± 30 × 10 ⁻⁹	2 ± 1 × 10 ⁷
	5% PEG 8K	1.7 ± 0.2	4 ± 1 × 10 ⁻⁹	5 ± 2 × 10 ⁸
	10% PEG 8K	1.39 ± 0.05	5.2 ± 0.7 × 10 ⁻⁹	3.2 ± 0.5 × 10 ⁸
	20% PEG 8K	0.76 ± 0.06	3 ± 1 × 10 ⁻⁹	1.9 ± 0.8 × 10 ⁸
1U³⁰ (30mer)	Buffer ^c	1.70 ± 0.04	120 ± 10 × 10 ⁻⁹	1.4 ± 0.2 × 10 ⁷
	20% PEG 8K	0.39 ± 0.06	50 ± 20 × 10 ⁻⁹	8 ± 3 × 10 ⁶
1U⁹⁰ (90mer)	Buffer ^c	4.7 ± 0.3 ^c	13 ± 3 × 10 ^{-9^c}	4 ± 1 × 10 ^{8^c}
	20% PEG 8K	0.20 ± 0.02	4 ± 2 × 10 ⁻⁹	5 ± 3 × 10 ⁷

^aThe substrates used for the kinetic measurements have different sequences surrounding the uracil sites, which gives rise to modest differences in the kinetic parameters arising from sequence (5, 49). Thus, the fold changes in the kinetic parameters resulting from the addition of PEG are the most relevant parameters to compare.

^bThe kinetic parameters for this substrate reflect the excision of multiple uracils in a single encounter event that then result in a fluorescence increase due to hairpin destabilization. Thus, the rate units are oligonucleotide reacted per second rather than sites excised per unit time.

^cData has been previously published and is presented here for comparison (30).

4.2.6. Crowding has Little Effect on Non-specific DNA Binding.

To understand the basis for the effects of crowding on P_{trans} , it is useful to interrogate the equilibrium effects on non-specific DNA binding because translocation involves non-specific DNA interactions. To explore this property, binding measurements were made by following the increases in fluorescence anisotropy that accompanied hUNG binding to a 5'-fluorescein end-labeled non-specific 15mer duplex DNA (D^{N}) (**Figure 4.8**). In contrast with the large increase in the associative transfer distances in the presence of 20% PEG 8K (**Figure 4.4B**), we measured only a 2-fold increase in the non-specific equilibrium dissociation constant ($K_{\text{D}}^{\text{N}} = 1.3 \pm 0.5 \mu\text{M}$ in buffer; $K_{\text{D}}^{\text{N}} = 2.3 \pm 0.5 \mu\text{M}$ in 20% PEG 8K). Thus, the presence of 20% PEG 8K slightly disfavors equilibrium binding.

The different effects of crowding on binding and site transfer indicates that the major ground states involved in equilibrium binding measurements do not share the same DNA interactions as the transient enzyme states involved in site transfer (**Figure 4.1A**). This result and interpretation is consistent with previous findings where methylphosphonate backbone substitutions and high salt concentrations produced large increases in K_{D}^{N} , but did not alter P_{assoc} (44). Nevertheless, the K_{D} places an important thermodynamic constraint on the system that must be compatible with the kinetic and P_{trans} measurements.

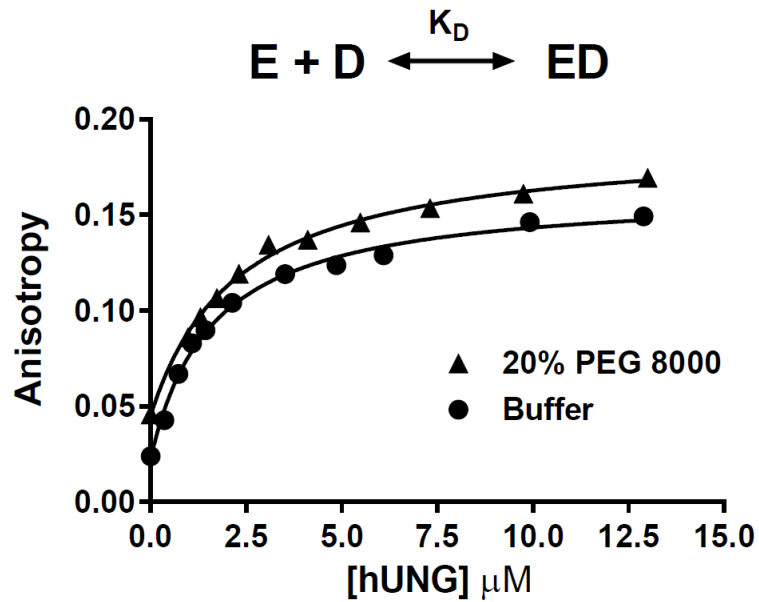


Figure 4.8. Binding affinity (K_D) of hUNG for nonspecific DNA (D^N , 100 nM) in the presence and absence of 20% PEG 8K. The binding affinity was measured by changes in fluorescence anisotropy as a function of hUNG concentration. Inclusion of 20% PEG 8K moderately increases the K_D from $1.3 \pm 0.5 \mu\text{M}$ to $2.3 \pm 0.5 \mu\text{M}$.

4.2.7. Crowding Effects on the Association Rate with a Specific Site.

In order to determine the origin of the minimal effect of crowding agents on DNA binding, we first investigated how the presence 20% PEG 8K alters the association rate (k_{on}) of hUNG using a specific substrate analog by stopped-flow fluorescence methods (**Figure 4.9A**). These experiments used a 19mer duplex (D^S) that contained a fluorescent 2-aminopurine (2-AP) base adjacent to a 2'-fluorinated deoxyuridine nucleotide (U^β). The U^β nucleotide is resistant to glycosidic bond cleavage during the time frame of the measurements (45). Upon binding of hUNG, the uracil base of U^β is flipped into the active site, unstacking the 2-AP base and leading to an increase in its fluorescence intensity at 370 nm. Association rates were determined using second-order irreversible binding conditions in which equal molar amounts of hUNG and DNA (200 nM) were rapidly mixed in the presence of increasing amounts of PEG 8K (0 – 20%) and the kinetic traces were fit to eq 4.2 (see **Methods**). As shown in **Figure 4.9A** and reported in **Table 4.6**, k_{on} decreased markedly from $2.7 \times 10^9 \text{ M}^{-1}\text{s}^{-1}$ to $3 \times 10^8 \text{ M}^{-1}\text{s}^{-1}$ as the PEG 8K concentration was increased from 0 to 20%. The irreversibility of the association reactions was substantiated by the similar k_{on} values obtained using 100 nM concentrations of enzyme and DNA using dilute buffer or 20% PEG 8K conditions ($k_{\text{on}} = 3.5 \pm 0.7 \times 10^9 \text{ M}^{-1}\text{s}^{-1}$ for dilute buffer; $k_{\text{on}} = 2.9 \pm 0.5 \times 10^8 \text{ M}^{-1}\text{s}^{-1}$ for 20% PEG 8K). The association rate measured in dilute buffer approaches the fastest known rate constants for protein-DNA association (46) and requires that the steps subsequent to association leading to the 2-AP fluorescence increase are extremely rapid (i.e. base flipping and DNA/enzyme conformational changes) (5, 45, 47). Thus, binding of hUNG to this DNA in the absence of crowding is essentially encounter controlled.

We were curious as to whether the association rate attenuations observed with various concentrations of PEG 8K could be explained solely by the increases in relative viscosity (η^{rel}) as the PEG 8K concentration was increased. To address this question we plotted the relative association times at each concentration of PEG 8K ($\tau^{\text{rel}} = \tau^{\text{crowd}}/\tau^{\text{buffer}}$) against the relative viscosities (η^{rel}) (29). We also performed the same plots using 20 – 40% EG and 5 – 30% PEG 600 to ascertain whether polymer size played a role (**Figure 4.9B**). These plots were compared with the expected linear correlation between τ^{rel} and η^{rel} predicted from the Stokes-Einstein (SE) equation (i.e. $\tau^{\text{rel}} = \eta^{\text{rel}}$, black line, **Figure 4.9B**). For EG (black squares), τ^{rel} increased in a steep parabolic fashion that deviated positively from the SE line at concentrations higher than 20% (positive deviations indicated slower association than expected from viscosity alone). This suggested inhibitory interactions of EG with hUNG when its concentration exceeds 20% (**Figure 4.9B**), which is consistent with what was observed in the steady-state kinetic measurements. In contrast, τ^{rel} for increasing concentrations of PEG 600 (purple circles), showed no significant deviation from SE behavior, indicating ideal viscogen behavior for this moderately small PEG polymer. Finally, τ^{rel} for increasing concentrations of PEG 8K (green diamonds) traced a concave curve that deviated negatively from the SE line (faster association than would be expected from viscosity alone).

Figure 4.9. Influence of PEG 8K on association kinetics of hUNG from specific DNA (D^S) determined by stopped-flow 2-aminopurine fluorescence measurements at 20 °C.

a) Kinetic traces for the second-order association of hUNG (200nM) with D^S (200nM) in dilute buffer (blue) and in the presence of 5 – 20% PEG 8K. Traces are displaced along the y-axis for clarity. The second-order rate constants (k_{on}) are reported in **Table 4.5**. **b)** Effect of relative viscosity ($\eta^{rel} = \eta^{crowder}/\eta^{buffer}$) on the relative association times ($\tau_{rel} = \tau^{crowder}/\tau^{buffer}$, where $\tau = 1/k_{on}$) for hUNG and specific DNA (D^S). The data points correspond to dilute buffer (blue) and increasing concentrations of EG (black), PEG 600 (purple), and PEG 8K (green). Relative viscosities of these cosolutes were obtained from reference (29). The theoretical line shows the expected dependence of the association times based solely on the increases in the relative viscosity of the solutions as expected from Stokes-Einstein behavior. **c)** Effect of PEG 8K on the dissociation rate of hUNG from a specific site (D^S). Kinetic traces are shown in a semi-log format. The dissociation kinetics follow a single exponential in buffer alone (blue), and a double exponential in the presence of 15% (light green) and 20% PEG 8K (dark green). The second slower exponential that appears in the presence of PEG 8K is deemed a fluorescence artifact as detailed in the Supplemental Methods. The kinetic parameters are reported in **Table 4.6**.

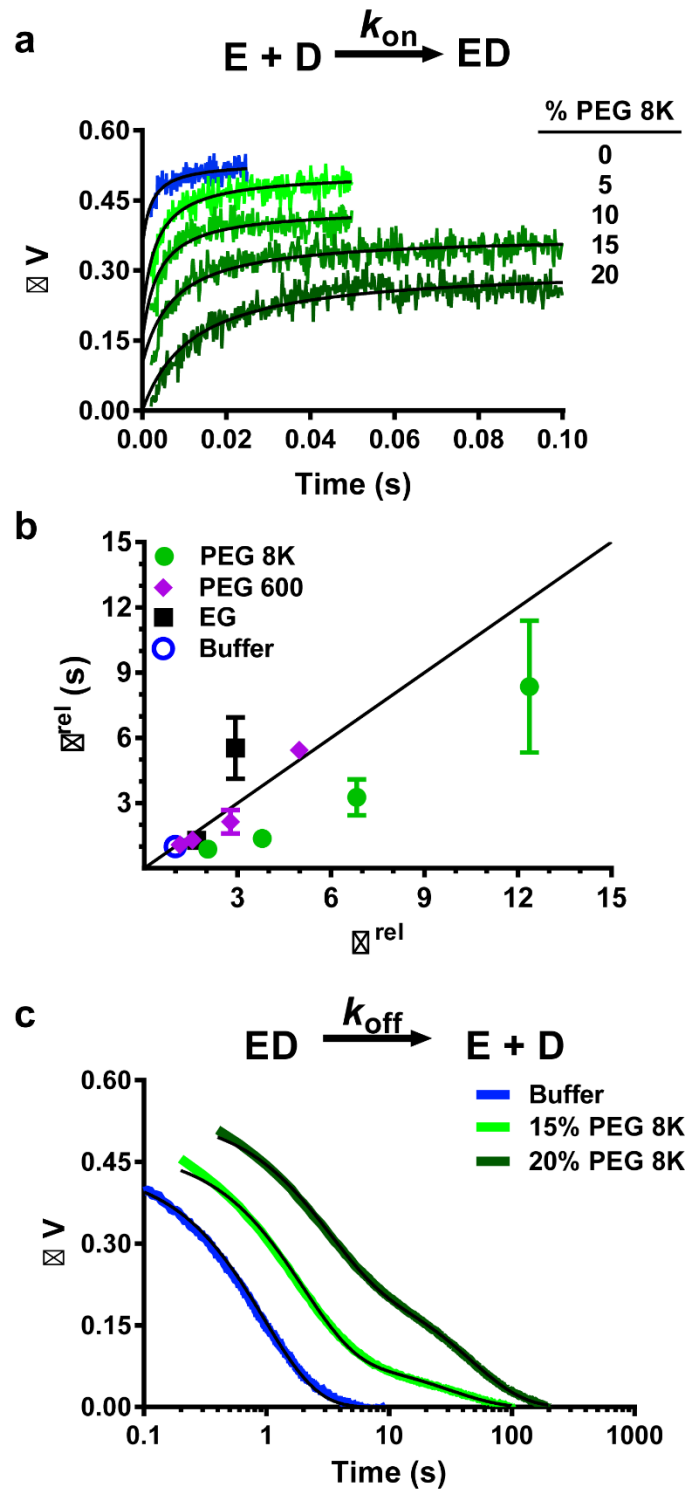


Figure 4.9.

Table 4.6. Specific DNA association rates (k_{on}) for hUNG in the presence of a variety of molecular crowding agents compared to the predicted rate from the Stokes-Einstein relation ($k_{\text{on}}^{\text{SE}}$).

		5%		10%		15%		20%		30%		40%	
	k_{on}^a	k_{on}	$k_{\text{on}}^{\text{SE},b}$	k_{on}	$k_{\text{on}}^{\text{SE}}$	k_{on}	$k_{\text{on}}^{\text{SE}}$	k_{on}	$k_{\text{on}}^{\text{SE}}$	k_{on}	$k_{\text{on}}^{\text{rel}}$	k_{on}	$k_{\text{on}}^{\text{SE}}$
Buffer	27 ± 7	-- ^c	--	--	--	--	--	--	--	--	--	--	--
EG	--	--	--	--	--	--	--	20 ± 1	18 ± 5	--	--	4.8 ± 0.4	11 ± 3
PEG 600	--	25 ± 8	23 ± 6	21 ± 1	17 ± 5	--	--	12.6 ± 0.4	10 ± 3	5.0 ± 0.4	7 ± 2	--	--
PEG 8K	--	31 ± 1	13 ± 3	20 ± 9	7 ± 2	8 ± 3	4 ± 1	3 ± 1	2.2 ± 0.6	--	--	--	--

^a k_{on} has units of $10^8 \text{ M}^{-1}\text{s}^{-1}$.

$$^b k_{\text{on}}^{\text{SE}} = k_{\text{on}}^{\text{buffer}} / \eta^{\text{rel}}$$

^cNot determined.

4.2.8. Crowding Effects on the Dissociation Rate from a Specific Site (D^S).

The effects of 5 to 20% PEG 8K on the dissociation rate from a specific site were determined by following the decrease in 2-AP fluorescence that accompanies hUNG dissociation from D^S (**Figure 4.9C**). In these experiments, an excess amount of DNA containing a high affinity abasic site (ϕ DNA) was rapidly mixed with a pre-incubated solution of hUNG and D^S to ensure that all dissociated enzyme molecules were rapidly and irreversibly trapped (two ϕ DNA concentrations were used to confirm this requirement). Although the dissociation rate in buffer alone was well fit to a single exponential decay with a rate constant $k_{\text{off}} = 1.01 \pm 0.05 \text{ s}^{-1}$ (**Figure 4.9C, Table 4.7**), the presence of PEG 8K resulted in double-exponential decays of the fluorescence (**Figure 4.9C**). Both the rate and amplitude of the first rapid phase decreased with increasing PEG 8K concentrations (**Table 4.7**). At the final concentration of 20% PEG 8K, the rate of the fast transient ($k_{\text{off}}^{\text{PEG}} = 0.35 \text{ s}^{-1}$) was ~ 3 -fold less than the buffer only value and the amplitude was reduced by 40%. The rate constant for the slower phase ($k_{\text{slow}} = 0.024 \text{ s}^{-1}$) was 50-fold smaller than the value for k_{off} in buffer only, and the amplitude of the slower kinetic phase increased with PEG 8K concentration to a final value that was 44% of the total fluorescence change (**Figure 4.9C, Table 4.7**).

We conducted a number of experimental and theoretical evaluations to determine if the slower kinetic transient for dissociation of D^S in the presence of PEG 8K reflected an important aspect of the dissociation reaction, or alternatively, was an artefactual 2-AP fluorescence change resulting from the presence of the PEG polymer. We excluded the possibility that 20% PEG 8K produced detectable 2-AP or hUNG tryptophan fluorescence changes by mixing the enzyme or D^S DNA alone with the ϕ DNA trap in the stopped flow

device and following the fluorescence emission at 370 nm over time. Although this control did not reveal any detectable fluorescence changes, as observed when enzyme and D^S were mixed, the 50-fold slower kinetic transient in the traces shown in **Figure 4.9C** is not compatible with many other measurements contained in this study. One inconsistency is that an exceedingly slow transient in the presence of 20% PEG 8K should reduce the net rate of substrate dissociation and also reduce K_m , yet only a 4-fold decrease in K_m was observed for a substrate of similar length as D^S (1U³⁰). Also, we have previously found that the kinetic process and conformational changes for UNG dissociation from a substrate analogue site and a product site are very similar, which suggests that k_{cat} is a good surrogate for the product dissociation rate (6, 10, 57, 58). Accordingly, the ~4-fold decreases in k_{cat} that were observed for the short substrates 1U³⁰ and 6U¹¹, more closely resemble the 3-fold reduction in the fast kinetic phase for dissociation of D^S in **Figure 4.9C**, and not the 50-fold slower kinetic phase. Finally, if the dissociation rate of D^S is assumed to be equivalent to the fast kinetic phase, the calculated K_D^S in the presence of 20% PEG 8K is $k_{off}^{PEG}/k_{on}^{PEG} = 1.2 \pm 0.5 \times 10^{-9}$ M, which is about 3-fold greater than K_D^S in the absence of PEG 8K (**Table 4.6**). This effect of PEG 8K on specific binding is similar to the ~2-fold increase in K_D observed for non-specific binding and the modest ~3-fold increases in the substrate K_m values. We thus conclude that the significantly slower phase observed in the presence of PEG 8K does not reflect on the dissociation rate of hUNG from a specific site on DNA.

Given that the slow kinetic transient can only reasonably be attributed to a fluorescence artifact unrelated to the dissociation rate of hUNG from D^S, we only consider the $k_{off}^{PEG} = 0.35 \text{ s}^{-1}$ in our analyses of the effects of 20% PEG 8K on DNA binding and translocation.

Table 4.7. Rate constants and amplitudes for slow and fast kinetic phases for the biphasic dissociation of hUNG from specific DNA in the presence of various amounts of PEG 8K.

	$k_{\text{off}}^{\text{buffer } a}$ (s ⁻¹)	$k_{\text{off}}^{\text{PEG}}$ (s ⁻¹)	k_{slow}^b (s ⁻¹)	$A^{\text{PEG}, c}$	$A^{\text{slow}, c}$	$K_D^{S^d}$ (nM)
Buffer	1.01 ± 0.05	-- ^e	--	--	--	0.4 ± 0.1
5%	--	0.97 ± 0.05	0.048 ± 0.009	0.84	0.16	0.31 ± 0.02
10%	--	0.48 ± 0.01	0.022 ± 0.001	0.78	0.22	0.2 ± 0.1
15%	--	0.57 ± 0.02	0.035 ± 0.003	0.81	0.19	0.7 ± 0.3
20%	--	0.35 ± 0.02	0.024 ± 0.004	0.56	0.44	1.2 ± 0.5

^a k_{off} is a single exponential in the absence of PEG 8K.

^b k_{slow} is attributed to an artifact resulting from 2-AP fluorescence interference by PEG 8K.

^c Fractional amplitudes of each kinetic phase.

^d Calculated based on $K_D = k_{\text{off}}^{\text{PEG}}/k_{\text{on}}$.

^e Not applicable

4.3. DISCUSSION

In this study, we have developed an *in vitro* model that approximates some aspects of the crowded environment of the cell nucleus in order to explore how molecular crowding affects the DNA damage search and repair pathway of two human DNA glycosylases. The extensive results can be largely explained by considering both the macroscopic and microscopic effects of large polymers on solution viscosity and excluded volume. These effects are depicted in **Figure 4.10** for the search coordinate of hUNG, which will be the focus of the following discussion given that the bulk of the experiments were performed on this enzyme. While we have not explicitly determined the effects for each step of the search coordinate of hOGG1, the generality of the conclusions are inferred based on the similarities of the effects of molecular crowding on facilitated diffusion of both enzymes. Below, we interpret the results based on the sequential steps shown in **Figure 4.10** (left to right), beginning with bulk diffusion of the enzyme to the DNA chain and ending with its departure to bulk solution after encountering the specific site. For hUNG, the forward steps leading to excision of the uracil base are much faster than dissociation from the specific site (45); these steps are not shown in **Figure 4.10** for clarity.

4.3.1 Translational Diffusion from Bulk Solution to DNA.

Addition of PEG 8K resulted in the attenuation of the bimolecular encounter rates compared to buffer ($k_{on}, k_{cat}/K_m$), but to a lesser extent than expected from viscosity changes alone (**Figure 4.9B**). Association of hUNG with a large DNA chain requires long-range translation through solution, which will be slowed by macroscopic viscosity according to the Stokes-Einstein (SE) relation $D_t = k_B T / 6\pi\eta R$, where η is the solution viscosity and R is the hydrodynamic radius of the diffusing species. However, the diffusion limit imposed

by viscosity can be substantially reduced when the cosolute is a crowder that occupies a solution volume larger than the diffusing species (8). This effect arises from the preferential interaction of water with the protein (and DNA) resulting in a hydration layer in which the crowder is excluded (termed the “depletion layer”). For PEG and other random coil polymers, the depletion layer scales as a function of the radius of gyration of the polymer (R_g) (35). (The basis for the depletion layer sizes that we use in our qualitative analysis is found in **Methods, Section 4.4.10.**) Accordingly, the depletion layer for PEG 8K (~4.1 nm) is calculated as approximately 4.5-fold larger than PEG 600 (~0.9 nm) (29, 48). The comparatively large depletion layer for PEG 8K indicates that when the centers of mass of hUNG and the DNA approach within ~11 nm of each other (see **Methods, Section 4.4.10.**), binding will efficiently ensue, partially ameliorating the effects of bulk viscosity on translational diffusion. The significantly thinner depletion layer of PEG 600 (**Figure 4.9B**) accounts for its adherence to SE behavior because hUNG and the DNA must come in much closer proximity before the low viscosity depletion zone is formed. We conclude that the kinetic effects of PEG 600 and PEG 8K on bimolecular encounter are accounted for by viscosity alone (PEG 600), or antagonistic viscosity and caging effects derived from the large depletion layer of PEG 8K.

4.3.2. Associative Transfer Steps.

A major finding was that crowding agents dramatically increased the probability and mean distance for associative transfers on the DNA chain (**Figure 4.4B**). We propose that this effect derives from two distinct properties (i) the fact that associative transfers occur with the enzyme still located within the ion cloud of the DNA (< 2 nm) (30), and therefore, also within the low viscosity depletion layer, and (ii) the caging effect of

crowders that would tend to reflect the enzyme back to the DNA chain during dissociation attempts. The increased time spent in associative transfers would allow for more comprehensive local damage surveillance, but at the expense of moving frequently to other DNA chains. This comprises the basis for why removal of uracils embedded in a population of long 1U⁹⁰ substrate molecules is slowed significantly in the presence of crowding, but smaller DNA substrates do not show the same behavior (**Figure 4.7E**, **Table 4.5**). Such a local search mechanism is highly appropriate for the human cell nucleus because glycosylases are typically abundant enzymes (>100,000 copies per nucleus) (7), and each enzyme only needs to scan less than 20,000 base pairs of DNA on average. Thus, there is no great need for individual enzyme molecules to move through a large volume to affect repair.

4.3.3. Dissociative Transfer Steps.

In contrast with the substantial enhancement of the associative transfer pathway in the presence of 20% PEG 8K, only a small effect was observed for the dissociative pathway (P_{diss}). This result may be rationalized using the kinetic definition of $P_{\text{diss}} = [k_{\text{off}}/(k_{\text{off}}+k_{\text{assoc}})][(k_{\text{return}}/(k_{\text{return}}+k_{\text{bulk}})]$ (30). The first term describes the likelihood that an enzyme molecule will dissociate from the DNA as opposed to proceeding through an associative step (the inverse of the kinetic definition of P_{assoc}). For the same reasons discussed above for associative transfers, this first term would be reduced in the presence of crowders. The second term describes the probability that a dissociated enzyme molecule will return to the DNA chain (k_{return}) or become lost to bulk solution (k_{bulk}). Since the low viscosity depletion layer extends to ~10 nm we expect that the majority of the dissociated enzyme molecules will return to the DNA chain, and we also surmise that escape to bulk

will be impeded in heavily crowded and viscous solutions. Thus, the second term of this expression is expected to increase. We propose that opposing changes in the first and second terms nearly cancel, resulting in the overall small change in P_{diss} that is observed.

4.3.4. Departure to Bulk Solution.

The presence of PEG 8K resulted in similar decreases (3 to 4-fold) in the dissociation rates from a specific site ($k_{\text{off}}^{\text{PEG}}$) and product sites derived from the 6U¹¹ and 1U³⁰ substrates (in this comparison we use k_{cat} as a surrogate for the dissociation rate from the product site) (**Figure 4.9C, Table 4.7**). These common decreases are likely the result of increased solution viscosity and/or inefficient escape of the enzyme from the depletion layer around the DNA chain due to collision with the polymer cage. Finally, the 2-3 fold increases in K_{D}^{NS} , K_{D}^{S} and the substrate K_{m} values in the presence of 20% PEG 8K are accounted for by the compensatory changes in the association rate (a decrease of ~10-fold, **Table 4.6**) and dissociation rate (a decrease of ~3-fold, **Table 4.7**).

4.3.5. Damage Search and Repair in the Cell Nucleus.

This study moves us one step closer to understanding how environmental factors within the human cell nucleus could modulate the activity of DNA repair enzymes. While further *in vitro* experiments will be designed to even more closely mimic the nuclear environment, our clearest understanding of DNA search and repair will ultimately require measurements in human cells. Nevertheless, the systematically studied *in vitro* behaviors will be essential for useful interpretation of the behaviors observed in the context of a complex nuclear milieu.

Figure 4.10. General schematic of how the introduction of molecular crowders can influence individual steps in the DNA glycosylase damage search pathway. These steps including the rate of diffusion to the DNA chain (k_{on}), the lifetime of nonspecific ($1/k_{\text{off}}^{\text{N}}$) and specific ($1/k_{\text{off}}^{\text{S}}$) DNA complexes, the probability of associative and dissociative transfers between damage sites, and changes in the rate of product release (rate-limiting for k_{cat}). Dashed lines represent the sizes of the depletion layers surrounding the protein and DNA where the PEG 8K polymer (orange lines), but not solvent, is excluded. For large DNA molecules, association is limited by translation of the protein through the crowded solution ($k_{\text{on}}^{\text{bulk}}$) until their depletion layers overlap and association proceeds within a low viscosity environment. Also depicted are highly dynamic closed-to-open conformational changes in hUNG and hOGG1 that accompany nonspecific DNA binding (50, 51); only the open state is viewed competent for translocation (50). Release of each enzyme from the product requires an even larger closed-to-open transition that has been shown to be at least partly rate-limiting for turnover of hUNG (k'_{open}) (45). Image is drawn to scale using a DNA duplex of 2 nm as a scale reference. The depletion layer size in the dilute regime for PEG 8K is shown (equivalent to $R_{\text{g}}^{\text{PEG}}$, see **Methods, Section 4.4.10**).

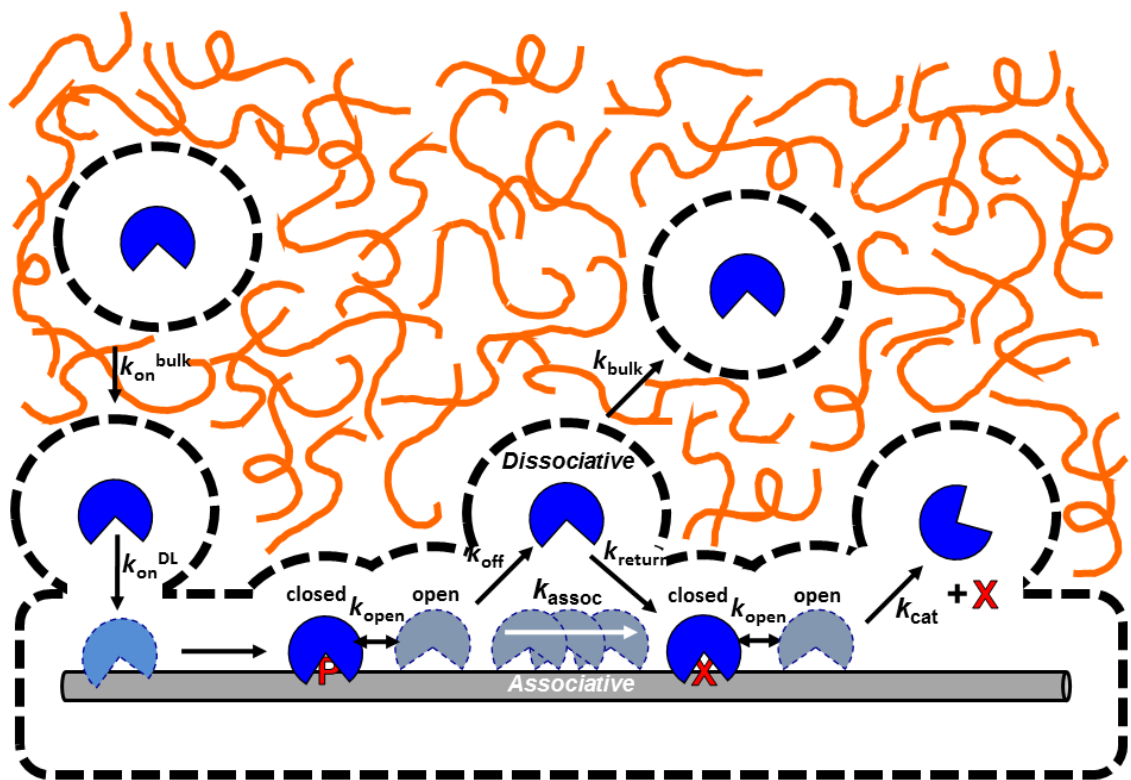


Figure 4.10.

4.4. METHODS

4.4.1. Experimental Conditions.

All experiments with hUNG were performed in a buffer consisting of 20 mM HEPES pH 7.5, 3 mM EDTA, 1 mM DTT, 0.002% Brij 35. This buffer contained a total of 22 mM Na⁺ originating from pH adjustment of the HEPES and EDTA stock solutions. All experiments with hOGG1 were performed in buffer containing 20 mM TrisCl pH 8.0, 1 mM EDTA, and 1 mM DTT, 17 mM NaCl, and 0.1 mg/mL BSA. The catalytic domain of recombinant hUNG was purified as previously described (10) and a detailed description of recombinant hOGG1 purification can be found below. The specific DNA (D^S) containing a non-hydrolyzable deoxyuridine analogue (2'-β-fluoro-2-deoxyuridine) was synthesized in-house as the phosphoramidite form and incorporated during solid phase DNA synthesis as previously described (10). All other oligonucleotides were purchased from either Integrated DNA Technologies or Eurofin and purified in-house by denaturing PAGE. All DNA sequences are listed in below. Ethylene glycol, PEG 600, PEG 1500, PEG 3350, and PEG 8K were purchased from Sigma Chemical. To remove UV absorbing impurities, these reagents were purified by overnight treatment with activated carbon (0.1g/mL) and filtered. Dextran 25K and Ficoll 70 were purchased from GE Healthcare.

4.4.2. hOGG1 Expression and Purification.

E. coli BL21(DE3) Trigger Factor cells were transformed with pET30a(+) (Novagen) plasmid encoding wild type hOGG1 (residues 1-345) with an N-terminal His₆ tag. Expressions used 2 liters of LB containing 40 μg/mL kanamycin and 34 μg/mL chloramphenicol. Culture broth was inoculated with the transformed cells and then

incubated at 37 °C until $OD_{600} = 0.6$. hOGG1 expression was induced by the addition of 0.5 mM IPTG and the culture was further incubated at 16 °C overnight. Cells were then harvested by centrifugation and frozen at -80 °C overnight. Cells were resuspended in lysis buffer (50 mM Tris pH 7.5, 300 mM NaCl, 5% glycerol, 0.1% Triton-X 100, 1 mM EDTA, 1 mM DTT, 0.25 mg/mL lysozyme). The supernatant was clarified by centrifugation at 40,000g for 40 min at 4 °C and then batch bound to 3 mL of Ni-NTA agarose (Qiagen) by rocking the lysate (supplemented with 5 mM imidazole) and column resin for 1 hour at 4 °C. The resin was pelleted by centrifugation at 4,000x rpm for 10 min and the supernatant was discarded. The column was rocked for 10 min at 4 °C with buffer A (20 mM Tris-Cl, pH 7.5, 1 mM DTT, 10% glycerol) containing 5 mM imidazole to remove any nonspecifically bound protein. After pelleting the resin and discarding the supernatant, the resin was rocked for 10 min at 4 °C with buffer A containing 500 mM imidazole to remove all specifically bound protein. The resin was pelleted and the supernatant was diluted 3-fold and poured directly onto a Mono-S cation exchange column (GE Healthcare) preequilibrated in buffer A. hOGG1 was then purified by gradient elution with buffer A containing 1 M NaCl. Fractions containing hOGG1 were pooled and diluted to final buffer conditions of 20 mM Tris-Cl pH 7.5, 300 mM NaCl, 1 mM DTT, 20% glycerol and stored at -80 °C. The N-terminal His₆ tag was not removed given previous reporting in the literature that removal of the His₆ tag resulted in no difference in single-turnover rate constants (52). Purification yielded protein that was 30–50% active, determined by single-turnover active site titrations. All hOGG1 protein concentrations reported correspond to active enzyme concentrations.

4.4.3 Measurement of hOGG1 Reaction Rates.

Stock solutions of hOGG1 must be diluted carefully to obtain reproducible kinetic measurements. Empirically we have found that the following procedure provides reproducible results. hOGG1 stock (6 μM) can be stored at $-80\text{ }^{\circ}\text{C}$ for at least several months without any observed decrease in activity. 2 μL of a 6 μM hOGG1 stock in storage buffer (20mM Tris-HCl pH 7.5, 300mM NaCl, 20% glycerol) was diluted to 20 μL using buffer B (20 mM Tris-HCl pH7.5, 500 mM NaCl, 20% glycerol, and 150 $\mu\text{g}/\text{mL}$ BSA). The resulting enzyme solution was incubated at room temperature for 5 min before 12-fold dilution in buffer B to give a final concentration of 50 nM. One-microliter of this diluted enzyme solution was used to initiate each 50 μL reaction (final [hOGG1] = 1 nM). hOGG1 (1 nM) was reacted with 20 nM ^{32}P -labeled substrate ($\text{S}0^{\text{G}}$) in buffer A at $37\text{ }^{\circ}\text{C}$. As needed, the buffer contained 20% (w/v) PEG 8K or 5% (w/v) of Hemoglobin in a total volume of 50 μl . At 2, 4, 6, 8, and 10 min, 6 μL portions of the reaction mixtures were quenched with 20 μL of formamide loading buffer and heated for 10 min at $95\text{ }^{\circ}\text{C}$ to generate a 15mer cleavage product that could be visualized after electrophoretic separation using a 10% polyacrylamide gel containing urea. The fractional extent of reaction at each time was quantified by phosphorimaging of the gels and the reaction rates were determined from the linear slopes of plots of product concentration against time using Prism and averaging over three trials.

4.4.4 Site Transfer Assay.

Site transfer assays were performed as previously reported (30) and the general procedure is recapitulated here. To initiate the reactions, hUNG (20-900 pM) was mixed

with a dual uracil ^{32}P labeled DNA substrate (40 nM) at 37 °C in the presence and absence of varying amounts of PEG 8K, 3350, 1500, 600, ethylene glycol, and hemoglobin. At the indicated times, aliquots of the reaction mixture were quenched with Uracil DNA Glycosylase Inhibitor protein (UGI, New England Biolabs) and the abasic sites were cleaved by heating in the presence of ethylene diamine. For hUNG experiments using hemoglobin, the same procedure was followed with the following exceptions: 1) aliquots were quenched in 28 uL of formamide buffer and 2) abasic sites were cleaved by heating at 95 °C for 90 minutes. For experiments using hOGG1, 1 nM of enzyme was added to 20 nM ^{32}P -labeled S20^{oG} in the presence and absence of 20% PEG 8K and 5% hemoglobin. At the denoted times, aliquots of the reaction were quenched with 20 μL formamide loading buffer and heated for 10 min at 95 °C. For both enzymes, the discrete DNA fragments generate by heating were resolved by electrophoresis on a denaturing 10% PAGE gel containing 7 M urea. All gels were dried, exposed overnight to a storage phosphor screen and imaged with a Typhoon 8600 phosphorimager (GE Healthcare). All gel images were quantified using QuantityOne (Bio-Rad) by the box method. The time independent overall site transfer probability (P_{trans}) was calculated using eq 4.1 by linear extrapolation of the observed transfer probabilities ($P_{\text{trans}}^{\text{obs}}$) to zero time. For experiments involving the use of uracil trap for hUNG, an aliquot of a 10 mM uracil stock solution in water was dried and then reconstituted in reaction buffer such that the final reaction concentration was 10 mM. For experiments involving the use of the 2-amino-6-chloropurine trap (Sigma-Aldrich) trap for hOGG1, a final concentration of 3 mM was added to each reaction from a stock solution prepared in DMSO. Reactions were carried out in 15% DMSO to ensure solubility of the trap. We have shown previously that DMSO does not alter translocation of hOGG1 on

DNA (31). Controls established that transfer probabilities in the presence of the hUNG trap (10 and 20 mM) and hOGG1 trap (1 and 3 mM) were independent of trap concentration in the presence and absence of 20% PEG 8K. The intramolecular transfer assay was then performed as described above.

$$P_{\text{trans}} = \frac{[A]^0 + [C]^0 - [AB]^0 - [BC]^0}{[A]^0 + [C]^0 + [AB]^0 + [BC]^0} \quad (4.1)$$

4.4.5. hUNG Equilibrium DNA Binding Measurements.

Binding of hUNG to a nonspecific 5' fluorescein-labeled 15mer DNA duplex (D^N) was measured by fluorescence anisotropy using a SPEX Fluoromax-3 spectrofluorometer at 20 °C (excitation wavelength of 494 nm, emission wavelength of 518 nm). All anisotropy values were corrected for the spectral G factors. Experiments were performed in a back-titration mode by mixing a solution of concentrated hUNG containing 100 nM labeled DNA with increasing volumes of a solution containing 100 nM labeled DNA only. Experiments were performed with the above buffer in the absence and presence of 20% (w/v) PEG 8K. After each addition, the solution was allowed to equilibrate for 4 min inside the fluorometer and three anisotropy measurements were averaged. All data were fitted to eq 2.2 (Chapter 2) using the software Prism.

4.4.6. hUNG Stopped Flow Measurements.

To measure the association and dissociation rates of a specific site, a 19mer duplex DNA substrate (D^S) was used that contained a non-hydrolyzable analog of uracil ($U^\beta = 2'$ - β -fluoro-2-deoxyuridine) adjacent to the environmentally sensitive reporter base 2-aminopurine (2-AP) (32). Association rates were measured under second-order conditions

by mixing 400 nM D^S with 400 nM of hUNG in equal volumes using an Applied Photophysics 720 stopped-flow device in two-syringe mode. The 2-AP fluorescent signal was recorded using a 360 nm long-pass emission filter and a 310 nm excitation wavelength at a temperature of 20 °C. Higher temperatures could not be used because the association rates exceeded the time resolution of the instrument. These experiments were conducted in the presence and absence of varying amounts (w/v) of PEG 8K (5%, 10%, 15%, 20%), PEG 600 (5%, 10%, 20%, 30%), and ethylene glycol (20%, 40%).

Since the concentrations of each species were equal ($[DNA]_0 = [hUNG]_0$) and much greater than the K_D for the interaction at a specific site ($K_D = 0.3$ nM), the rate of association (k_{on}) was determined by fitting the fluorescent traces to eq 4.2, where Y_0 is the initial fluorescence intensity (33).

$$Y(t) = Y_f - Y_0 \left(1 - \frac{1}{k_{on}[P] + 1} \right) t \quad (4.2)$$

To measure dissociation rates, equal volumes of a pre-incubated solution of hUNG and D^S (800 nM and 200 nM final concentrations) were rapid mixed with a trap solution containing 5 μM of a 19mer DNA with a high affinity tetrahydrofuran abasic site mimic (ϕDNA). This trap ensures irreversible trapping of the dissociated enzyme molecules. The kinetic constants were the same when either 5 or 10 μM of the trap was used, establishing that trapping was not rate-limiting. These experiments were conducted in the presence and absence of varying amounts (w/v) of PEG 8K (5%, 10%, 15%, 20%). The resultant curves were fit to either a single or a double exponential decay equation as required (see **Results, Section 4.2.8.**).

4.4.7. hUNG Steady-State Kinetic Measurements.

Equal volumes of hUNG (30 pM final concentration) and a 5' ³²P-labeled 90mer DNA substrate containing a single uracil (1U⁹⁰) (1 nM – 32 nM final concentration) were mixed in the standard buffer at 37° C. At various times, 4 μL portions were removed and quenched with 4 μL UGI (0.2 units/μL). Sample treatment and gel procedures were identical to what is described above for the site transfer assay. The same procedure was used to determine the steady-state kinetic parameters of the 5' ³²P-labeled 30mer DNA substrate containing a single uracil (1U³⁰) (10 nM – 400 nM final concentration) at 25 °C. Initial rates for both substrates were determined by linear regression using plots of product concentration against time and the software program Prism (Graphpad Software, Inc.). The experiments were performed in the presence and absence of 20% (w/v) PEG 8K.

The k_{cat} values for 1U⁹⁰ and 1U³⁰ at 75 mM total cation concentration in the presence and absence of 20% PEG 8K were measured essentially as described above for 1U⁹⁰. The 75 mM total cation concentration was established by adding 53 mM KGlu to the standard reaction buffer and gels for separating the products derived from 5' FAM-labeled 1U³⁰ were imaged with a Typhoon 8600 phosphorimager (GE Healthcare) without drying. Bands were quantified by histogram volume analysis using QuantityOne (Bio-Rad). The values for k_{cat} were obtained by using high substrate concentrations such that the rate was independent of concentration. This condition was confirmed by measuring identical rates at two substrate concentrations in the range 0.4 to 3 μM. The reported k_{cat} values are an average of the rates determined at the two substrate concentrations.

Kinetic measurements on a short hairpin substrate containing 6 U/A pairs within the 11 bp stem region (6U¹¹) were performed using a continuous fluorescence assay (34). Fluorescein emission ($\lambda_{\text{ex}} = 494 \text{ nm}$, $\lambda_{\text{em}} = 518 \text{ nm}$) was monitored at 10 s time intervals using a SPEX Fluoromax-3 spectrofluorometer at 25 °C using excitation and emission slit widths of 1 nm and 2 nm, respectively. The experiment was performed in the presence and absence of PEG 8K [5%, 10% and 20% (w/v)] and ethylene glycol [20% and 40% (w/v)].

4.4.8. Ion Activity Measurements.

The sodium ion activity in the presence of 20% (w/v) PEG 8K was determined using a Cole-Parmer Sodium Ion Selective Electrode (ISE). Standard sodium solutions were made over the range of 2 – 1000 ppm in the presence and absence of 20% PEG 8K. An ionic strength adjuster (ISA, 4M NH₄Cl / 4M NaOH) was added to each standard in a 1:50 dilution and a magnetic stirrer was used to ensure a constant stirring rate during ion potential readings. The potential was recorded for each solution using an Accumet AR25 Dual Channel pH/Ion Meter (Fischer Scientific) in mV mode. The electrode was thoroughly rinsed with a 1:50 solution of ISA in distilled water and dried between readings. The slopes of a semi-log plot of the mV reading (linear axis) against the sodium concentration (log axis) were used to determine the sodium ion activity coefficients in aqueous solution and 20% PEG 8K.

4.4.9. DNA Sequences.

All DNA's are double stranded with the exception of the hairpin 6U¹¹. The complimentary strand sequences are implied based on normal Watson-Crick pairing but not shown below. All uracils and tetrahydrofuran residues are paired with A on the opposite

strand, except where indicated, and 2-aminopurine is paired with T. 8-oxoG is always paired with C on the complimentary strand.

hUNG

D^N: 5'-FAM-AGG CGC ATA GTC GCA-3'

D^S: 5'-GCG GCC AA PU^βA AAA AGC GC-3'

(U^β/G mismatch; P - 2-aminopurine)

ϕDNA: 5'-GCG GCC AAA ϕ AA AAA GCG C-3' (ϕ - tetrahydrofuran; *ϕ-A pair*)

Substrates for Steady-State Kinetics

6U¹¹ (hairpin): 5'-FAM-GCA UUA AGA AGA AG-(PEG)₆-CUU CUU AAT TGC-BHQ-3'

1U⁹⁰ (90mer): 5' - GTT ATC CGC TCA CAA TTC CAC ACA ATG CTG AGG AAT CGA UAG CTA AGT AGG ATG TTA GCT ATC GAT TCA TCC TCA GCA CAG TGT CGA GCC - 3'

1U³⁰ (30mer): 5' - CGT AGC CAC TGC AAP UAA ACA GAG CAT AGG - 3'

Two-Site Substrates

S10^U (90mer): 5' - GGT ATC CGCT AGT CAC AAT TCC ACA CAATGC TGA GGA ATC GA U AG CTA AT CGA U AGC TAA GCT GAG GCATAC AGG ATC AAT TGT CGA GCC-3'

S20^U (90mer): 5'-GGT ATC CGC TCA CAA TTC CAC ACA ATG CTG AGG AAT
CGA U AG CTA AGT AGG ATG AAT CGA U AG CTA AGC TGA GGC ATA CAG
TGT CGA GCC - 3'

S55^U (125mer): 5'-GGT ATC CGC TCA CAA TTC CAC ACA ATG CTG AGG AAT
CGA U AGC TAA GTG AAT CTC TCA CGT CAC ATC GTC CGC ACT AGC ACA
TGG AAT GAA TCG A U AGC TAA GCT GAG GCA TAC AGT GTC GAG CC - 3'

hOGG1

S0^G (31mer): 5'-ATG CTG AGG AAT TTC °GCT CCT TGT AGG ATG A-3'

S20^G (90mer): 5'-GGT ATC CGC TCA CAA TTC CAC ACA ATG CTG AGG AAT
TTC °GCT CCT TGT AG G ATG A AT TTC °GCT CCT TGC TGA GGC ATA CAG
TGT CGA GCC-3'

4.4.10 Calculation of Depletion Layer Sizes.

In the dilute regime, polymers can be considered as non-interactive random coils with a defined radius of gyration (R_g^{PEG}) that is dependent on the molecular weight (M_w) of the polymer ($R_g^{\text{PEG}} = 0.0215 \cdot M_w^{0.583}$) (53, 54). The depletion layer surrounding the protein and DNA in this regime is considered equivalent to R_g^{PEG} (29, 35). As the concentration of polymer is increased beyond a defined crossover threshold (c^*) (35), the solution enters the semi-dilute regime, where polymer molecules overlap and the protein and DNA are embedded in a noncovalent polymeric network with a certain average mesh size (ξ) that continues to decrease as the polymer concentration increases. The depletion layer around the protein and DNA also decreases with the mesh size, which is a complex

function of R_g^{PEG} (35). For simplicity, we chose to calculate the relative sizes of the depletion layers generated by semi-dilute solutions of PEG using the simple approximations for the dilute regime (4.1 nm for PEG 8K and 0.9 nm for PEG 600). Using this model, the depletion layers surrounding the protein and DNA would overlap when centers of mass of both species reach a distance equal to the combined radii of the two depletion layers ($2 \times R_g^{\text{PEG}}$) plus the sum of the Stokes radii for the protein and DNA ($R_{\text{Stokes}}^{\text{hUNG}} + R^{\text{DNA}}$, where $R_{\text{Stokes}}^{\text{hUNG}} = 2.3$ nm (55) and $R^{\text{DNA}} \sim 1$ nm for B-form DNA). While it is true that the depletion layer would begin to decrease in the semi-dilute regime as concentration of PEG was increased, the depletion layer for PEG 8K would still be larger than PEG 600 in this regime. Our qualitative analysis is not dependent on whether the depletion layer sizes for PEG solutions are precisely known.

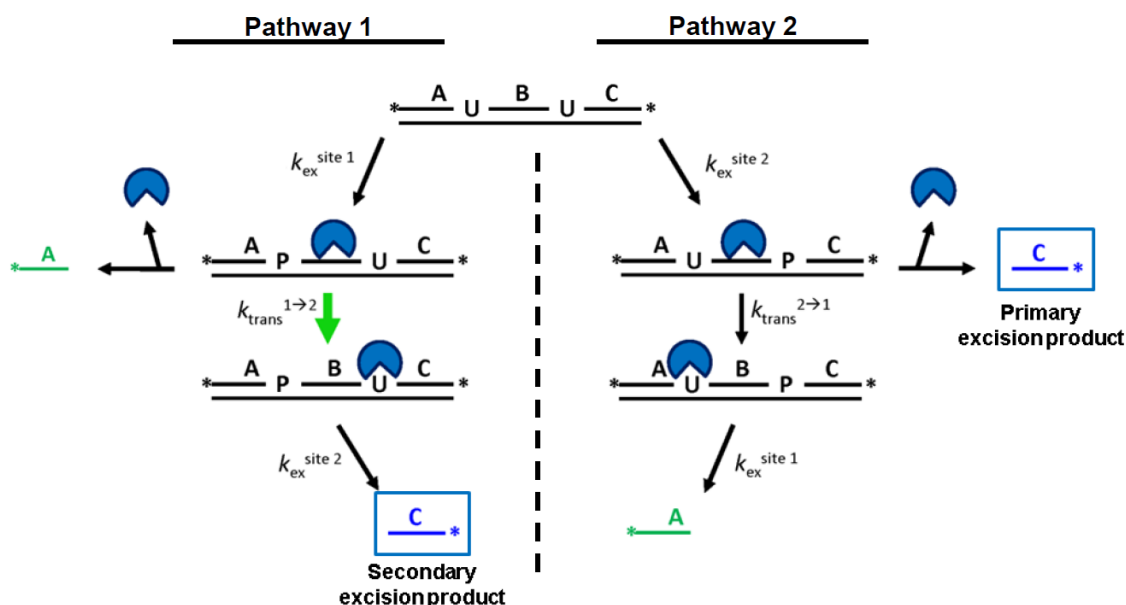
4.4.11. Effect of Hemoglobin on Translocation of hUNG.

Site transfer experiments conducted with hUNG were complicated by a dramatic reduction in the reaction rate of uracil excision in the presence of 5% (w/v) hemoglobin (see **Results (Section 4.3), Figure 4.11**). Despite this non-ideality, the data revealed an apparent directional bias for transfer of hUNG along the DNA, which can be discerned by the enhanced production of the double cleavage product band C relative to A (see analysis below and **Figure 4.11**). We ensured this result was not due to hemoglobin altering the electrophoretic migration of the DNA through the gel by control experiments that verified equivalent amounts of intact, single, and double cleaved DNA fragments were observed on a gel when loaded in the presence and absence of hemoglobin.

Analysis of the reaction velocities for each product band revealed a burst phase followed by a slower linear rate (**Figure 4.11B**). The amplitude of the burst phase was

independent of [hUNG] in the range 100 to 500 pM hUNG, indicating that it does not arise from slow ES turnover in the presence of hemoglobin. The burst phase likely results from slow onset inhibition of hUNG upon its addition to the solution containing hemoglobin, resulting in a steady-state level of free E that is maintained over the remaining course of the reaction. In contrast, the linear steady-state rates were about 10 times slower when 100 pM hUNG was used as compared to 500 pM.

We analyzed the site excision data in the presence of hemoglobin using the model shown in **Scheme 1**.



Scheme 4.1. Site transfer mechanism consistent with hUNG behavior in the presence of hemoglobin. k_{ex} is the initial rate of primary excision events at either uracil site, which may then result in dissociation of the enzyme before encounter of the second site, or alternatively, transfer to that site (k_{trans}). The biased directionality of site transfers is indicated by arrows. Thick, green arrows indicate steps favored in the presence of hemoglobin and the color-coding of DNA fragments coincides with **Figure 4.11**. The major C product fragment is boxed for clarity.

Although we have previously established that it is not possible to distinguish whether apparent directional bias in site transfer arises from differences in the excision rates at each site (k_{ex}) or true directionality to site transfer (56), we believe the current results are most reasonably interpreted in terms of transfer effects. Our reasoning is that it seems highly unlikely that hemoglobin would give rise to different effects on site excision because both sites are identical. Using the reasonable assumption that k_{ex} is the same for both sites, then the high levels of fragment C in **Figure 4.11A** (derived from pathways 1 and 2 in **Scheme 1**) may be explained using eq 4.1, where the fragment concentrations are obtained by extrapolation to zero time (**Fig. 4.11C**). This equation

$$P_{\text{trans}}^{1 \rightarrow 2} = \frac{[A]_0 - [BC]_0}{[A]_0} \quad (4.3)$$

isolates how much fragment C was generated via pathway 1 by consumption of fragment BC after translocation of the enzyme from site 1 \rightarrow 2 (**Scheme 4.1**). Although fragment A can also be made by secondary excision via pathway 2, this cannot be a significant occurrence because fragment AB is always present at a much higher level than BC. The observed $P_{\text{trans}}^{1 \rightarrow 2}$ value of 0.56 ± 0.05 is higher than P_{trans} determined in buffer (0.33 ± 0.09) and was unchanged in the presence of 20 mM uracil trap ($P_{\text{trans}} = 0.64 \pm 0.02$), suggesting that the biased transfers are associative in nature (**Figure 4.11C**). Although these data can be interpreted in terms of biased transfer in the presence of hemoglobin, we concede that the data could arise from unknown complications and are therefore unable to definitely conclude that a protein crowder increases hUNG translocation.

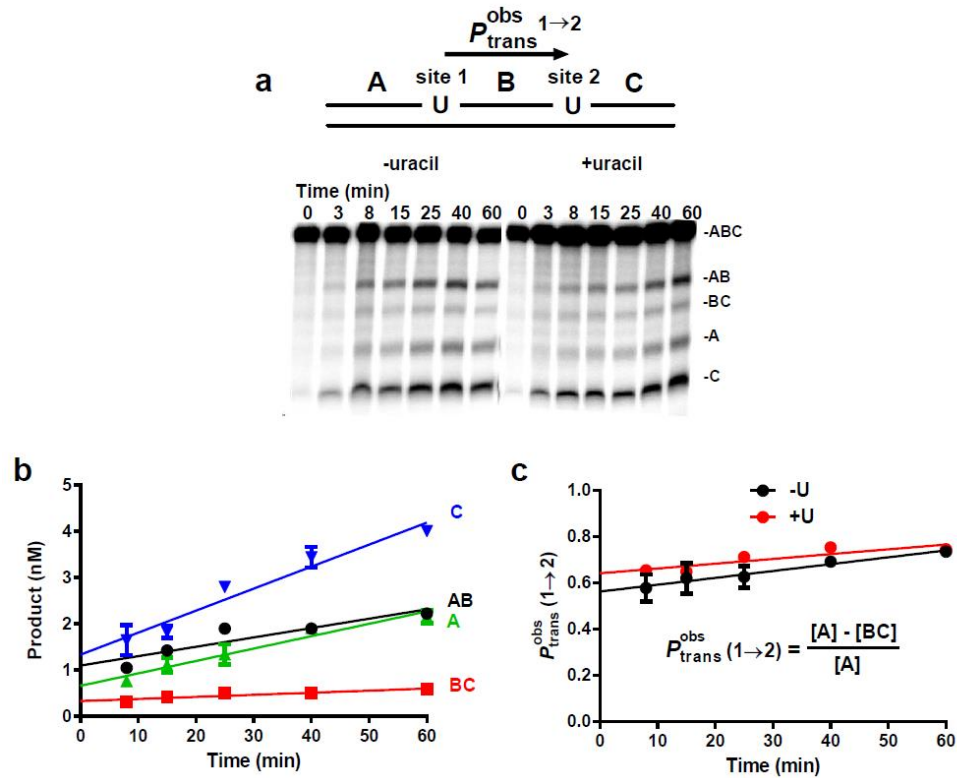


Figure 4.11 Effect of hemoglobin on the site transfer probability (P_{trans}) of hUNG between uracil lesions spaced 20 bp apart. A) Phosphorimages of reactions of hUNG with 40 nM of S20^U in buffer containing 5% hemoglobin in the presence and absence of 20 mM uracil trap. Concentrations of hUNG of 500 and 900 pM were used in the absence and presence of the trap. **B)** Velocities of formation of individual fragments derived from S20^U in the absence of uracil trap. Y-intercepts unequal to zero indicate that a burst kinetic phase occurs in the presence of hemoglobin followed by a slower steady-state rate. **C)** Observed probability of biased transfers from site 1 to 2 in the presence (red) and absence (black) of 20 mM uracil trap. This equation makes the assumption that fragment A is only generated by primary excision events. This assumption is supported by the observation that fragment AB is always present at a high levels indicating poor transfer from site 2→1.

4.5. REFERENCES

1. Blainey, P.C., Oijen, A.M.V., Banerjee, A., Verdine, G.L. and Xie, X.S. (2006) A base-excision DNA-repair protein finds intrahelical lesion bases by fast sliding in contact with DNA. *Proc. Natl. Acad. Sci. U.S.A.*, **103**, 5752–5757.
2. Blainey, P.C., Luo, G., Kou, S.C., Mangel, W.F., Verdine, G.L., Bagchi, B. and Xie, X.S. (2009) Nonspecifically bound proteins spin while diffusing along DNA. *Nat. Struct. Mol. Biol.*, **16**, 1224–1229.
3. Porecha, R.H. and Stivers, J.T. (2008) Uracil DNA glycosylase uses DNA hopping and short-range sliding to trap extrahelical uracils. *Proc. Natl. Acad. Sci. U.S.A.*, **105**, 10791–10796.
4. Hedglin, M. and O'Brien, P.J. (2008) Human alkyladenine DNA glycosylase employs a processive search for DNA damage. *Biochemistry*, **47**, 11434–11445.
5. Krosky, D.J., Song, F. and Stivers, J.T. (2005) The origins of high-affinity enzyme binding to an extrahelical DNA base. *Biochemistry*, **44**, 5949–5959.
6. Parker, J.B., Bianchet, M.A., Krosky, D.J., Friedman, J.I., Amzel, L.M. and Stivers, J.T. (2007) Enzymatic capture of an extrahelical thymine in the search for uracil in DNA. *Nature*, **449**, 433–437.
7. Friedman, J.I. and Stivers, J.T. (2010) Detection of Damaged DNA Bases by DNA Glycosylase Enzymes. *Biochemistry*, **49**, 4957–4967.
8. Theillet, F.-X., Binolfi, A., Frembgen-Kesner, T., Hingorani, K., Sarkar, M., Kyne, C., Li, C., Crowley, P.B., Gierasch, L., Pielak, G.J., et al. (2014) Physicochemical Properties of Cells and Their Effects on Intrinsically Disordered Proteins (IDPs). *Chem. Rev.*, **114**, 6661–6714.
9. Ellis, R.J. (2001) Macromolecular crowding: obvious but underappreciated. *Trends Biochem. Sci.*, **26**, 597–604.
10. Cravens, S.L., Hobson, M. and Stivers, J.T. (2014) Electrostatic Properties of Complexes along a DNA Glycosylase Damage Search Pathway. *Biochemistry*, **53**, 7680–7692.
11. Wishart, D.S., Jewison, T., Guo, A.C., Wilson, M., Knox, C., Liu, Y., Djoumbou, Y., Mandal, R., Aziat, F., Dong, E., et al. (2013) HMDB 3.0--The Human Metabolome Database in 2013. *Nucleic Acids Res.*, **41**, D801–7.
12. Müller-Spätth, S., Soranno, A., Hirschfeld, V., Hofmann, H., Rügger, S., Reymond, L., Nettels, D. and Schuler, B. (2010) Charge interactions can dominate the dimensions of intrinsically disordered proteins. *Proc. Natl. Acad. Sci. U.S.A.*, **107**, 14609–14614.
13. Uversky, V.N. and Dunker, A.K. (2010) Understanding protein non-folding. *Biochim. Biophys. Acta*, **1804**, 1231–1264.
14. Mao, A.H., Crick, S.L., Vitalis, A., Chicoine, C.L. and Pappu, R.V. (2010) Net charge per residue modulates conformational ensembles of intrinsically disordered proteins. *Proc. Natl. Acad. Sci. U.S.A.*, **107**, 8183–8188.
15. Banipal, T.S., Kaur, D. and Banipal, P.K. (2004) Apparent Molar Volumes and Viscosities of Some Amino Acids in Aqueous Sodium Acetate Solutions at 298.15 K. *J. Chem. Eng. Data*, **49**, 1236–1246.
16. Jenkins, H.D.B. and Marcus, Y. (1995) Viscosity B-Coefficients of Ions in Solution. *Chem. Rev.*, **95**, 2695–2724.
17. Cheung, M.C., LaCroix, R., McKenna, B.K., Liu, L., Winkelman, J. and Ehrlich, D.J. (2013) Intracellular protein and nucleic acid measured in eight cell types using deep-ultraviolet mass mapping. *Cytometry Part A*, **83A**, 540–551.
18. Zeskind, B.J., Jordan, C.D., Timp, W., Trapani, L., Waller, G., Horodincu, V., Ehrlich, D.J. and Matsudaira, P. (2007) Nucleic acid and protein mass mapping by live-cell deep-ultraviolet microscopy. *Nat Meth*, **4**, 567–569.

19. Minton, A.P. (2001) The Influence of Macromolecular Crowding and Macromolecular Confinement on Biochemical Reactions in Physiological Media. *Journal of Biological Chemistry*, **276**, 10577–10580.
20. Alsallaq, R. and Zhou, H.-X. (2008) Electrostatic rate enhancement and transient complex of protein–protein association. *Proteins*, **71**, 320–335.
21. Zhou, H.-X. (2001) Disparate ionic-strength dependencies of on and off rates in protein-protein association. *Biopolymers*, **59**, 427–433.
22. Minton, A.P. (2013) Quantitative assessment of the relative contributions of steric repulsion and chemical interactions to macromolecular crowding. *Biopolymers*, **99**, 239–244.
23. Zhou, H.-X., Rivas, G. and Minton, A.P. (2008) Macromolecular Crowding and Confinement: Biochemical, Biophysical, and Potential Physiological Consequences. *Annu Rev Biophys*, **37**, 375–397.
24. Phillip, Y., Sherman, E., Haran, G. and Schreiber, G. (2009) Common crowding agents have only a small effect on protein-protein interactions. *Biophysical Journal*, **97**, 875–885.
25. Phillip, Y., Harel, M., Khait, R., Qin, S., Zhou, H.-X. and Schreiber, G. (2012) Contrasting factors on the kinetic path to protein complex formation diminish the effects of crowding agents. *Biophysical Journal*, **103**, 1011–1019.
26. Qvist, J., Persson, E., Mattea, C. and Halle, B. (2009) Time scales of water dynamics at biological interfaces: peptides, proteins and cells. *Faraday Discuss.*, **141**, 131–144.
27. Jasnin, M., Stadler, A., Tehei, M. and Zaccai, G. (2010) Specific cellular water dynamics observed in vivo by neutron scattering and NMR. *Phys. Chem. Chem. Phys.*, **12**, 10154–10160.
28. Kuttner, Y.Y., Kozer, N., Segal, E., Schreiber, G. and Haran, G. (2005) Separating the Contribution of Translational and Rotational Diffusion to Protein Association. *J. Am. Chem. Soc.*, **127**, 15138–15144.
29. Kozer, N., Kuttner, Y.Y., Haran, G. and Schreiber, G. (2007) Protein-protein association in polymer solutions: from dilute to semidilute to concentrated. *Biophysical Journal*, **92**, 2139–2149.
30. Schonhofs, J.D. and Stivers, J.T. (2012) Timing facilitated site transfer of an enzyme on DNA. *Nat Chem Biol*, **8**, 205–210.
31. Rowland, M.M., Schonhofs, J.D., McKibbin, P.L., David, S.S. and Stivers, J.T. (2014) Microscopic mechanism of DNA damage searching by hOGG1. *Nucleic Acids Res.*, **42**, 9295–9303.
32. Stivers, J.T. (1998) 2-Aminopurine fluorescence studies of base stacking interactions at abasic sites in DNA: metal-ion and base sequence effects. *Nucleic Acids Res.*, **26**, 3837–3844.
33. Fersht, A. (1999) Structure and mechanism in protein science: a guide to enzyme catalysis and protein folding. W.H. Freeman and Company, New York, NY.
34. Weil, A.F., Ghosh, D., Zhou, Y., Seiple, L., McMahon, M.A., Spivak, A.M., Siliciano, R.F. and Stivers, J.T. (2013) Uracil DNA glycosylase initiates degradation of HIV-1 cDNA containing misincorporated dUTP and prevents viral integration. *Proc. Natl. Acad. Sci. U.S.A.*, **110**, E448–57.
35. Gennes, P.G.D. (1979) Scaling Concepts in Polymer Physics. Cornell University Press, Ithaca, NY.
36. Knowles, D.B., LaCroix, A.S., Deines, N.F., Shkel, I. and Record, M.T. (2011) Separation of preferential interaction and excluded volume effects on DNA duplex and hairpin stability. *Proc. Natl. Acad. Sci. U.S.A.*, **108**, 12699–12704.
37. Hermans, J. (1982) Excluded-volume theory of polymer–protein interactions based on polymer chain statistics. *J. Chem. Phys.*, **77**, 2193.
38. Knoll, D. and Hermans, J. (1983) Polymer-protein interactions. Comparison of experiment and excluded volume theory. *J. Biol. Chem.*, **258**, 5710–5715.

39. Arakawa, T. and Timasheff, S.N. (1985) Mechanism of polyethylene glycol interaction with proteins. *Biochemistry*, **24**, 6756–6762.
40. Atha, D.H. and Ingham, K.C. (1981) Mechanism of precipitation of proteins by polyethylene glycols. Analysis in terms of excluded volume. *J. Biol. Chem.*, **256**, 12108–12117.
41. Boiteux, S. and Radicella, J.P. (2000) The Human OGG1 Gene: Structure, Functions, and Its Implication in the Process of Carcinogenesis. *Archives of Biochemistry and Biophysics*, **377**, 1–8.
42. Derham, B.K. and Harding, J.J. The effect of the presence of globular proteins and elongated polymers on enzyme activity. *Biochimica et Biophysica Acta (BBA) - Proteins and Proteomics*, **1764**, 1000–1006.
43. Xiao, G., Tordova, M., Jagadeesh, J., Drohat, A.C., Stivers, J.T. and Gilliland, G.L. (1999) Crystal structure of Escherichia coli uracil DNA glycosylase and its complexes with uracil and glycerol: structure and glycosylase mechanism revisited. *Proteins*, **35**, 13–24.
44. Schonhoft, J.D., Kosowicz, J.G. and Stivers, J.T. (2013) DNA Translocation by Human Uracil DNA Glycosylase: Role of DNA Phosphate Charge. *Biochemistry*, **52**, 2526–2535.
45. Stivers, J.T., Pankiewicz, K.W. and Watanabe, K.A. (1999) Kinetic mechanism of damage site recognition and uracil flipping by Escherichia coli uracil DNA glycosylase. *Biochemistry*, **38**, 952–963.
46. Schreiber, G., Haran, G. and Zhou, H.-X. (2009) Fundamental aspects of protein-protein association kinetics. *Chem. Rev.*, **109**, 839–860.
47. Jiang, Y.L. and Stivers, J.T. (2002) Mutational analysis of the base-flipping mechanism of uracil DNA glycosylase. *Biochemistry*, **41**, 11236–11247.
48. Linegar, K.L., Adeniran, A.E., Kostko, A.F. and Anisimov, M.A. (2010) Hydrodynamic radius of polyethylene glycol in solution obtained by dynamic light scattering. *Colloid J*, **72**, 279–281.
49. Ye, Y., Stahley, M.R., Xu, J., Friedman, J.I., Sun, Y., McKnight, J.N., Gray, J.J., Bowman, G.D. and Stivers, J.T. (2012) Enzymatic excision of uracil residues in nucleosomes depends on the local DNA structure and dynamics. *Biochemistry*, **51**, 6028–6038.
50. Friedman, J.I., Majumdar, A. and Stivers, J.T. (2009) Nontarget DNA binding shapes the dynamic landscape for enzymatic recognition of DNA damage. *Nucleic Acids Res.*
51. Bruner, S.D., Norman, D.P. and Verdine, G.L. (2000) Structural basis for recognition and repair of the endogenous mutagen 8-oxoguanine in DNA. *Nature*, **403**, 859–866.
52. Leipold, M.D., Workman, H., Muller, J.G., Burrows, C.J. and David, S.S. (2003) Recognition and Removal of Oxidized Guanines in Duplex DNA by the Base Excision Repair Enzymes hOGG1, yOGG1, and yOGG2 †. *Biochemistry*, **42**, 11373–11381.
53. Linegar, K.L., Adeniran, A.E., Kostko, A.F. and Anisimov, M.A. (2010) Hydrodynamic radius of polyethylene glycol in solution obtained by dynamic light scattering. *Colloid J*, **72**, 279–281.
54. Devanand, K. and Selser, J.C. (1991) Asymptotic behavior and long-range interactions in aqueous solutions of poly(ethylene oxide). *Macromolecules*, **24**, 5943–5947.
55. Timchenko, A.A., Kubareva, E.A., Volkov, E.M., Voronina, O.L., Lunin, V.G., Gonchar, D.A., Degtyarev, S.K., Timchenko, M.A., Kihara, H. and Kimura, K. (2006) Structure of Escherichia coli uracil-DNA glycosylase and its complexes with nonhydrolyzable substrate analogues in solution studied by synchrotron small-angle X-ray scattering. *Biophysics*, **51**, 1–7.
56. Schonhoft, J.D. and Stivers, J.T. (2013) DNA translocation by human uracil DNA glycosylase: the case of single-stranded DNA and clustered uracils. *Biochemistry*, **52**, 2536–2544.

57. Parikh, S.S., Mol, C.D., Slupphaug, G., Bharati, S., Krokan, H.E. and Tainer, J.A. (1998) Base excision repair initiation revealed by crystal structures and binding kinetics of human uracil-DNA glycosylase with DNA. *EMBO J.*, **17**, 5214–5226.
58. Parikh, S.S., Walcher, G., Jones, G.D., Slupphaug, G., Krokan, H.E., Blackburn, G.M. and Tainer, J.A. (2000) Uracil-DNA glycosylase-DNA substrate and product structures: conformational strain promotes catalytic efficiency by coupled stereoelectronic effects. *Proc. Natl. Acad. Sci. U.S.A.*, **97**, 5083–5088.
59. Goins, A.B., Sanabria, H. and Waxham, M.N. (2008) Macromolecular Crowding and Size Effects on Probe Microviscosity. *Biophysical Journal*, **95**, 5362–5373.
60. Georgalis, Y., Philipp, M., Aleksandrova, R. and Krüger, J.K. Light scattering studies on Ficoll PM70 solutions reveal two distinct diffusive modes. *Journal of Colloid and Interface Science*, **386**, 141–147.

Chapter 5:

Differential Effects of Ions, Molecular Crowding, and Solution DNA Density on the Damage Search Mechanism of hOGG1 and hUNG

Reproduced in part from:

Cravens, S.L., Stivers, J.T.; (2016), Comparative Effects of Ions, Molecular Crowding, and Bulk DNA on the Damage Search Mechanisms of hOGG1 and hUNG. *Submitted.*

5.1. INTRODUCTION

DNA is subjected to an array of chemical modifications (oxidation, deamination, alkylation) that result in a diversity of damaged bases. Although these DNA lesions are rare in the context of the billions of bases that make up the human genome, they can have devastating consequences if allowed to persist into S phase where their deleterious effects on the genetic code are made permanent by DNA replication errors^{1, 2}. DNA base excision repair glycosylases are charged with the task of searching the genome for damaged bases and initiating repair by cleaving the glycosidic bond connecting the base and sugar^{3, 4}. The efficiency of the search process relies on the fraction of the total search time that the enzyme remains in the vicinity of DNA as opposed to diffusing through regions of the nucleus that do not contain potential damage sites. The localization of glycosylases to the vicinity of DNA chains involves both intrinsic properties of the enzyme (such as electrostatic or non-electrostatic interaction energies)^{5, 6, 7, 8}, as well as properties of the nuclear environment (such as molecular crowding) that tend to favor the formation of DNA-protein complexes^{9, 10, 11, 12, 13}. An important property that affects the search time is the binding lifetime of a DNA glycosylase with undamaged DNA. This lifetime must be sufficiently long to permit recognition of damage when it is encountered, yet short enough to allow dissociation events that facilitate movement of the enzyme to other DNA chains^{14, 15, 16}. Thus, two fundamental questions are the nature of the energetic interactions of DNA glycosylases with undamaged and damaged DNA and the contribution of the nuclear environment to the search time and recognition mechanism.

We have undertaken a detailed analysis of the effects of key solution parameters (i.e. ion concentration and crowding agents) on the specificity of human uracil DNA

glycosylase (hUNG) for undamaged and uracil containing DNA^{8,9}. This work has shown that the positively charged DNA binding site of hUNG promotes weak electrostatic interactions with undamaged DNA chains. These weak interactions facilitate two general types of translocation events along DNA chains: *associative translocations* where the enzyme remains within the DNA ion cloud and moves relatively short <10bp distances and *dissociative translocations* where the enzyme diffuses outside of the local ion environment of the DNA, but eventually rebinds to the same DNA chain^{17, 18, 19, 20, 21}. The two mechanisms work cooperatively to maximize the search coverage and minimize the search time^{17, 19, 21}. Although the specific complex between hUNG and uracil-containing DNA retains the non-specific electrostatic binding energy, specific binding is enhanced by an additional non-electrostatic free energy component ($\Delta G_{\text{non}} = -7.2$ kcal/mol; at a 1 M standard state of [KCl]), which derives from unique interactions with the extrahelical uracil base in the specific complex^{8,22}. This additional term enhances specificity for uracil sites at physiological ion concentrations⁸.

In addition to the above intramolecular translocation events, frequent dissociative transfers also provide an opportunity for the enzyme to move away from the original DNA chain and encounter a new DNA chain (intermolecular transfers). In dilute aqueous solutions where diffusion is not hindered, these events serve to enhance global repair in a population of damaged DNA molecules by allowing the enzyme to move rapidly between DNA chains^{8,17}. However, in the presence of molecular crowding (i.e. 20% PEG8000), the rate of global repair is decreased because the crowding macromolecule increases the time that hUNG spends translocating along individual DNA chains, thereby hindering its rapid movement to other damaged DNA chains⁹. These key observations concerning the effect

of crowded environments on the efficiency of global DNA repair suggested that efficient repair in the crowded cell nucleus is facilitated by the high hUNG copy number in dividing cells ($\sim 10^5$ molecules/nucleus)²³. Thus on average, individual enzyme molecules can be charged with efficient scanning of fairly small 15kb DNA domains, forgoing the requirement for global coverage by a limited number of enzyme molecules. A remaining question is whether these mechanistic determinants of hUNG transpose to other DNA repair glycosylases?

In humans, oxidative damage to guanine bases is primarily repaired by 8-oxoguanine DNA glycosylase (hOGG1)²⁴. This glycosylase is a classic member of the Helix-hairpin-Helix Gly/Pro/Asp (HhH-GPD) superfamily and differs significantly from hUNG in overall structure, charge distribution across its active site, and its propensity to deform both damaged and undamaged DNA^{25, 26}. The marked differences between these two enzymes raised the distinct possibility that different mechanisms might be used to solve the search and recognition problem. To investigate this issue, we now describe a comparative study of the factors that govern the activity of hUNG and hOGG1 with damaged and undamaged DNA. In particular, we explore the consequences of three key solution variables that are relevant to the cell nucleus: monovalent ions, molecular crowding, and high solution densities of undamaged DNA chains.

5.2. RESULTS

5.2.1. Environmental Effects on DNA Translocation by hOGG1.

A number of environmental factors in the cell nucleus could modulate the efficiency by which hOGG1 uses translocation along a single DNA chain to locate 8-oxoG

residues. Three major factors to consider are the physiological salt composition⁸, molecular crowding by nuclear proteins⁹, and the local density of DNA chains. Although it is not possible to completely mimic the nuclear environment in a test tube, the response of hOGG1 and hUNG to these variables provides a useful basis set for understanding future measurements in cells.

hOGG1 DNA translocation experiments were carried out with 90mer substrates containing two 8-oxoG residues positioned 10bp and 20bp apart on the same DNA strand (S10^{8oxoG} and S20^{8oxoG})²⁷. As previously described, translocation between two damage sites within the context of a single DNA chain can occur by either an associative or dissociative pathway^{19, 20, 21, 27, 28}. The associative pathway involves movement of a loosely bound enzyme along the surface of the DNA and the dissociative pathway involves short-range dissociation and diffusion outside of the DNA ion cloud before reassociation with the DNA chain (**Figure 5.1A**). The overall probability of an enzyme molecule transferring between damage sites (P_{trans}) is the sum of the probabilities of transferring by each pathway. The enzyme molecules that do not translocate successfully are lost to bulk solution after reacting at only a single site. As described in previous studies^{28, 29}, P_{trans} is calculated by determining the relative amounts of DNA product fragments that result from base excision at a single site only (producing fragments AB or BC), as compared both sites in a single encounter event (producing fragments A and C).

The ³²P end-labeled DNA fragments resulting from base excision are separated on a denaturing polyacrylamide gel and quantified by phosphorimaging (**Figure 5.1B**). Productive intramolecular site transfer results in more A and C products relative to the AB and BC products, which can be discerned by visual comparison of the band intensities at

low fractional extents of reaction (**Figure 5.1B**). We have shown that for both hOGG1 and hUNG, associative transfers dominate when damage sites are closely spaced (<10 bp separation) and that dissociative transfers dominate for spacings much greater than 20 bp^{27, 28}. Therefore, to probe the effects of the cellular environment on the two modes of translocation, we used sequences that are primarily repaired through associative transfer (S10^{oxoG}) or dissociative transfers (S20^{oxoG}).

We first investigated the effects of molecular crowding and the presence of bulk non-specific DNA using a buffer containing 30 mM K⁺ (**Figure 5.1C**, red bars). Crowding was introduced with the use of 20% (w/v) polyethylene glycol (PEG) 8K, which we have previously used to introduce excluded volume and viscosity effects on DNA translocation⁹. For the first time, we now also include two high concentrations of non-specific DNA that bracket the expected density of 30 bp DNA binding sites in the cell nucleus. These concentrations are based on an average nuclear volume of 4200 μm^3 and the size of the human diploid genome (~ 7 billion bp)²⁹ and were achieved by the addition of salmon sperm DNA (salDNA) at 0.10 mM and 1 mM [bp]. The possible effect of chromatinized DNA is best explored in the context of experiments performed in human cells.

At a low 30 mM salt concentration introduction of the crowding agent doubled the translocation efficiency of hOGG1 over a site spacing of 20bp ($P_{\text{trans}}^{\text{buffer}} = 0.26 \pm 0.04$; $P_{\text{trans}}^{\text{PEG}} = 0.50 \pm 0.03$). Interestingly, the same increase was not observed for a 10 bp spacing ($P_{\text{trans}}^{\text{buffer}} = 0.46 \pm 0.01$; $P_{\text{trans}}^{\text{PEG}} = 0.45 \pm 0.01$) (**Figure 5.1C**, red bars). The basis for this result is not known but may arise from the possibility that translocation of hOGG1 over such short distances may be inhibited by the time it takes for the bent DNA to relax its normal structure, which may force the enzyme to dissociate and rebind before reaching

the second site²⁷. The further addition of 0.1 and 1 mM salDNA to the crowded solution containing S20^{oxoG} reduced P_{trans} by about 50 and 100%, respectively. The concentration dependence of bulk DNA indicates that the local density of exposed DNA chains in a heterogeneous nuclear environment could dramatically impact the efficiency of translocation on single DNA chains. In contrast, addition of 1 mM salDNA to a crowded reaction solution containing S10^{oxoG} only decreased P_{trans} by 40% (**Figure 5.1C**, red bars). These effects suggest that crowding agents and bulk DNA chain density have reduced effects on short-range translocation where the associative pathway dominates. All low salt P_{trans} values are reported in **Table 5.1**.

As previously reported, increasing the salt concentration to 150 mM completely abolished site transfer by hOGG1 for the substrates with 10 and 20 bp site spacings (black and red bars in **Figure 5.1C**)²⁷, but addition of the crowder nearly restored the translocation efficiencies to the levels observed in the absence of salt (**Figure 5.1C**). The beneficial effect of the crowder on DNA translocation in the presence of high salt is most likely attributed to an increased lifetime of hOGG1 on the DNA chain⁹. In other words, the crowder serves to reflect hOGG1 back to the DNA chain, whereas in its absence, hOGG1 dissociation is made irreversible by the rapid condensation of salt ions around the enzyme and DNA. The addition of salDNA reduced translocation across the 10 and 20bp site spacings in a concentration dependent manner like that observed for the low salt conditions. However, residual translocation was still observed for the short 10bp spacing even at 1 mM salDNA ($P_{\text{trans}} \sim 0.15$)(**Figure 5.1C**, black bar). We conclude that short-range transfers are possible under conditions of physiological concentrations of salt, crowding and dense concentrations of decoy DNA chains. All high salt P_{trans} values are reported in **Table 5.2**.

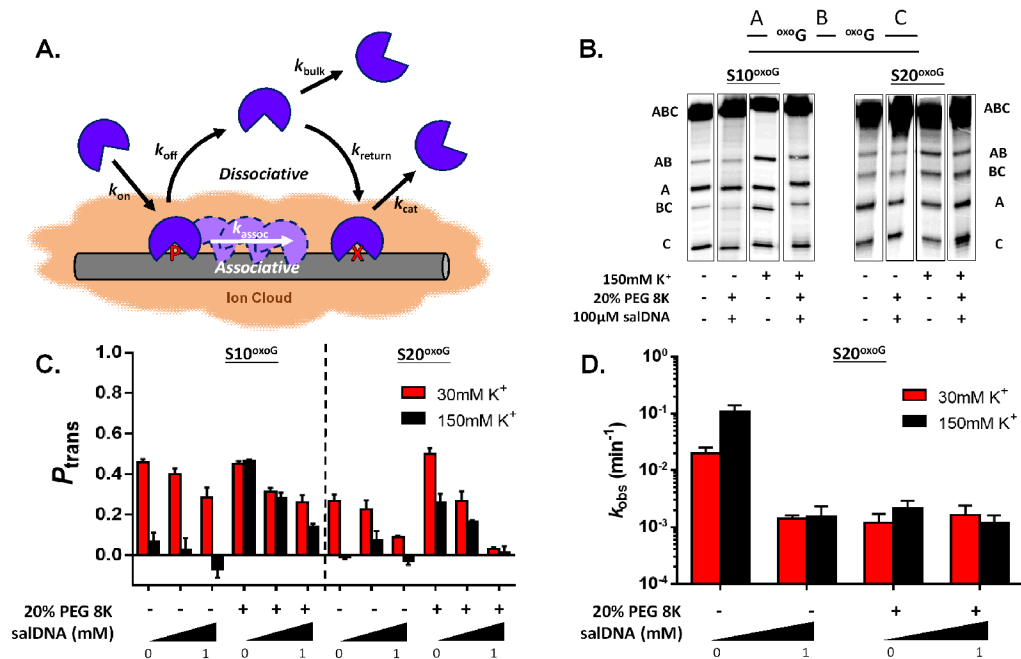


Figure 5.1. Site transfer probabilities and kinetic activity of hOGG1 in the presence of variable cosolutes. (A) The multistep search and repair pathway of DNA glycosylases involves associative and dissociative translocation along the DNA chain (see text). (B) Phosphorimages of the products derived from reaction of hOGG1 with two 90mer substrates (S20^{oxoG} and S10^{oxoG}) with two ^{oxoG} residues positioned 10 and 20bp apart. Solution conditions and co-solutes are indicated under each lane of the gel images. (C) The transfer probabilities between ^{oxoG} sites in S10^{oxoG} and S20^{oxoG} in the presence of variable cosolutes using 30 mM (red) and 150 mM salt (black) ($T = 37^\circ\text{C}$). (D) Effects of salt, 20% PEG 8K, and salDNA on the observed rate of 8-oxoG excision from S20^{oxoG}.

Table 5.1. Effect of 20% PEG 8K, and salmon sperm DNA (salDNA) on the site transfer probability (P_{trans}) of hOGG1 at 30 mM potassium ions.

	30 mM K⁺	
	S20^{oxoG}	S10^{oxoG}
	<i>P_{trans}</i>	<i>P_{trans}</i>
Buffer	0.26 ± 0.04	0.46 ± 0.01
100 μM salDNA	0.22 ± 0.04	0.40 ± 0.03
1 mM salDNA	0.09 ± 0.01	0.29 ± 0.05
20% PEG 8K	0.50 ± 0.03	0.45 ± 0.01
20% PEG 8K + 100 μM salDNA	0.27 ± 0.05	0.31 ± 0.02
20% PEG 8K + 1 mM salDNA	0.03 ± 0.01	0.26 ± 0.04

Table 5.2. Effect of 20% PEG 8K, and salmon sperm DNA (salDNA) on the site transfer probability (P_{trans}) of hOGG1 at 150 mM potassium ions.

	150 mM K⁺	
	S20^{oxoG}	S10^{oxoG}
	<i>P_{trans}</i>	<i>P_{trans}</i>
Buffer	-0.01 ± 0.01	0.07 ± 0.04
100 μM salDNA	0.07 ± 0.05	0.03 ± 0.06
1 mM salDNA	-0.03 ± 0.02	-0.07 ± 0.04
20% PEG 8K	0.26 ± 0.04	0.47 ± 0.01
20% PEG 8K + 100 μM salDNA	0.16 ± 0.01	0.28 ± 0.03
20% PEG 8K + 1 mM salDNA	0.01 ± 0.03	0.14 ± 0.01

5.2.2. Environmental Effects on Steady-State Turnover of hOGG1.

The effect of the same environmental factors on the steady-state rate of 8-oxoG excision from S20^{oxo-G} was investigated (**Figure 5.1D**). Under low salt conditions, the addition of 20% PEG8K reduced the enzyme turnover by about one-order of magnitude, and the further addition of salDNA had no appreciable effect on the rate (**Figure 5.1D**). The adverse effect of the crowder on steady-state turnover is attributed to (i) its trapping of hOGG1 on abasic product sites, from which the enzyme releases very slowly^{30, 31}, and (ii) the increased time spent translocating on DNA chains, rather than cycling through the population of DNA molecules by rapid 3D diffusive steps. This leads to reduced turnover of the 8-oxoG sites in the population of DNA molecules (a similar effect has been previously reported with hUNG)⁹.

The addition of 150 mM salt had little effect on the rate of hOGG1 turnover as compared to low salt, regardless of the presence of crowder or bulk DNA (compare red and black bars in **Figure 5.1D**)(**Table 5.3, Figure 5.2**). This finding indicates that the rate-limiting step leading to product release is salt-independent. We hypothesize that the overall rate-limiting step for turnover involves resolution of the covalent Schiff base linkage between hOGG1 and the abasic sugar product or a slow conformational change prior to enzyme release from the product³². Neither of these steps would be expected to be strongly dependent on bulk salt concentration.

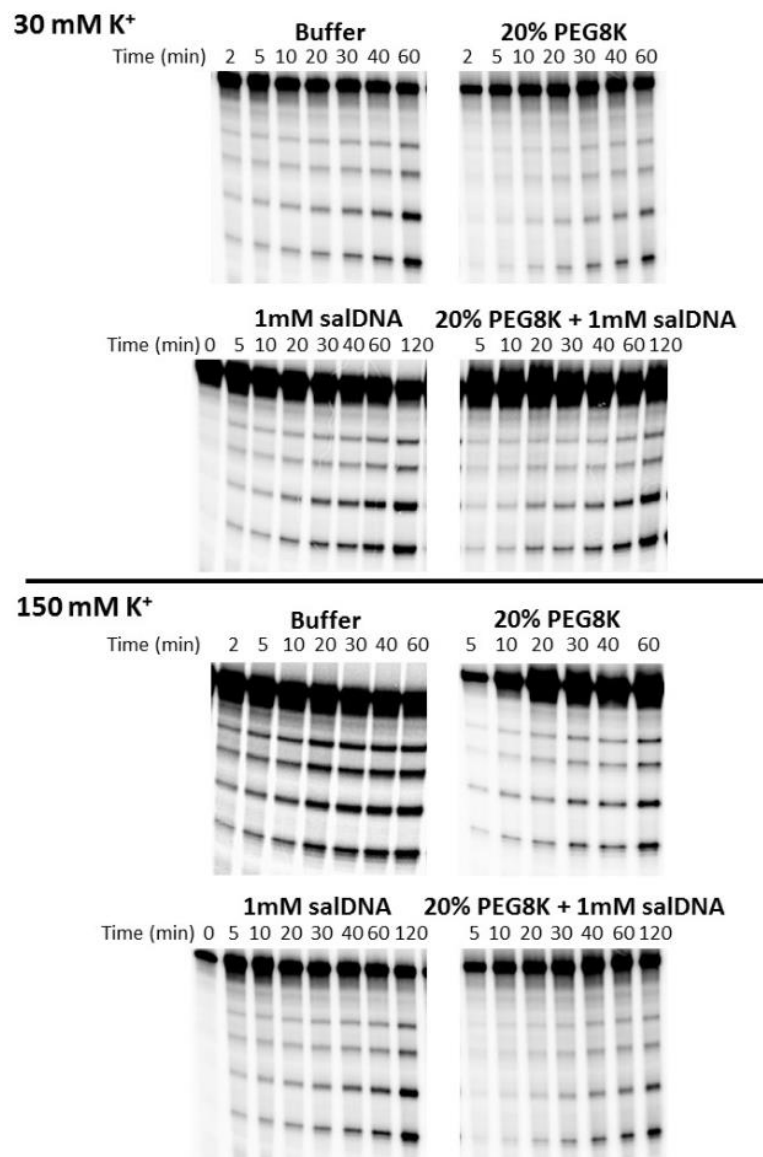


Figure 5.2. Example gels of hOGG1 reacting with S20^{oxoG} under various solution conditions. All experiments contained 20 nM DNA and a hUNG concentration that ranged from 1 nM – 40 nM. Gel bands were quantified as a function of time to determine P_{trans} and turnover rate.

Table 5.3. Reaction rates (k_{obs}) with S20^{oxoG} in the presence of salt, 20% PEG 8K, and salmon sperm DNA (salDNA) for hOGG1.

	S20 ^{oxoG}	
	30mM K ⁺	150 mM K ⁺
	k_{obs} (min ⁻¹)	k_{obs} (min ⁻¹)
Buffer	0.020 ± 0.005	0.11 ± 0.03
1 mM salDNA	0.0014 ± 0.0002	0.0015 ± 0.0008
20% PEG 8K	0.0012 ± 0.0005	0.0022 ± 0.0007
20% PEG 8K + 1 mM salDNA	0.0016 ± 0.0008	0.0012 ± 0.0003

5.2.3. Environmental Effects on DNA Translocation of hUNG.

We performed the same experiments with human uracil DNA glycosylase (hUNG) to determine if the effects of salt, molecular crowding, and bulk DNA density are common between the two enzymes. We have previously characterized hUNG with respect to the variables of high salt and molecular crowding^{8,9}, but the effects of bulk decoy DNA have not yet been addressed. This question is interesting because hUNG binds to non-specific DNA using primarily electrostatic interactions and uses non-electrostatic interactions to enhance its specificity for specific DNA at physiological salt concentrations⁸.

The site spacings chosen for measuring DNA translocation by hUNG were five (S5^U) and twenty base pairs (S20^U) in order to satisfy the condition of testing site spacings where uracil excision occurred by primarily associative or dissociative transfers (**Figure 5.3A**)²⁸. The low salt condition employed 22 mM KOAc to be consistent with previous measurements^{8,9,28}. Translocation by hUNG at low salt was greatly enhanced by the presence of 20% PEG 8K for both site spacings (red bars, **Figure 5.3B**)(**Table 5.4**). The addition 0.1 and 1 mM salDNA to the crowded solution modestly reduced P_{trans} for both substrates. Comparing the trends in P_{trans} for the 20bp spacing between hOGG1 and hUNG reveals similar trends with respect to the effects of the crowding agent and salDNA (compare red bars in **Figure 5.1C** and **5.3B**).

The introduction of 150 mM salt reduced or eliminated DNA translocation over the 5 and 20bp spacings in the absence of crowding (compare red and black bars in **Figure 5.3B**)(**Table 5.5**)⁸. As seen with the low salt condition, the addition of crowder to the high salt solution increased P_{trans} by at least 8-fold for the S20^U substrate (black bars, in **Figure 5.3B**). The further introduction of salDNA to the crowded solution reduced, but did not

eliminate transfers over the 20bp spacing. Once again, these effects of crowder and salDNA broadly parallel those of hOGG1, even though the enzymes have different driving forces for interacting with non-specific DNA.

Although similar effects of salt, crowding and bulk DNA were observed for the 5bp spacing, the translocation events were biased in the direction of site 2 \rightarrow 1 in the presence of high, but not low salt (**Figure 5.3B**). Such an effect leads to an atypical product fragment distribution as seen in **Figure 5.3A** and described previously (see also **Methods Section 5.4.5 and Figure 5.4**)^{9, 33}. Although we cannot ascertain the detailed basis for this effect, we have speculated that it arises from an asymmetric interaction of the enzyme with the DNA that is manifested under select conditions³³. The $P_{\text{trans}}^{2 \rightarrow 1}$ values that we report in **Figure 5.3B** reflect this directional bias.

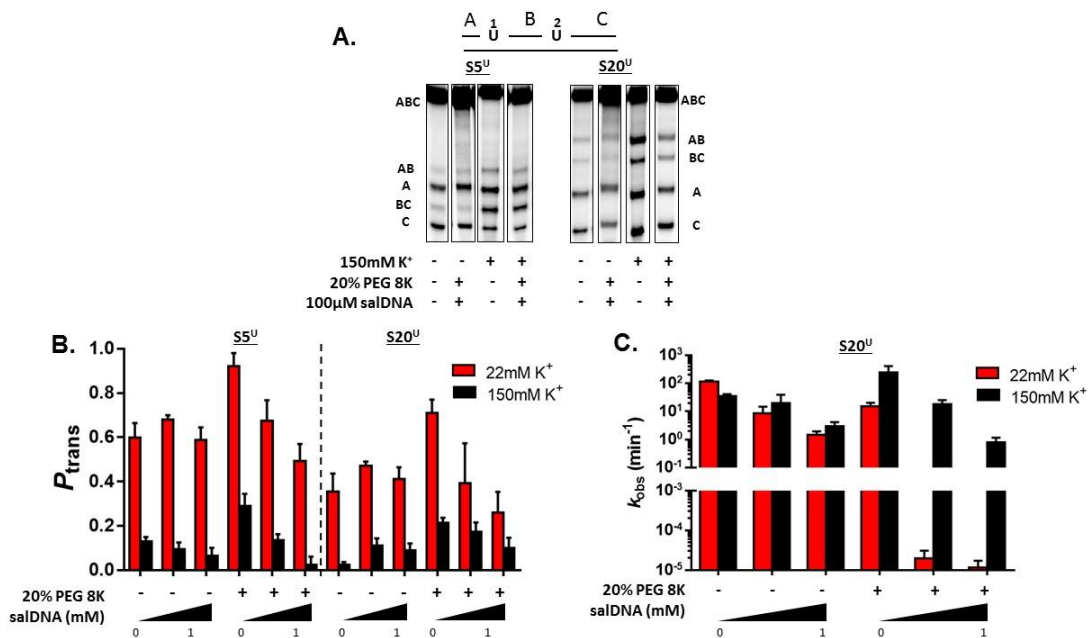


Figure 5.3. Site transfer probabilities and kinetic activity of hUNG in the presence of variable cosolutes. (A) Phosphorimages of the products derived from reaction of hUNG with two 90mer substrates (S5^U and S20^U) with two uracil residues spaced 5 (black) and 20bp (red) apart. Solution conditions and co-solutes are indicated under each lane of the gel images. The P_{trans} values for S5^U reflect directional bias as indicated by the low population of the single excision AB fragment. (B) The transfer probabilities between uracil sites in S5^U and S20^U in the presence of various co-solutes at 22 (red) and 150 mM salt (black) ($T = 37^{\circ}\text{C}$). The P_{trans} values for S5^U at 150 mM salt represent unidirectional site transfer from site 2 to site 1 ($P_{\text{trans}}^{2 \rightarrow 1}$). (C) Effects of salt, 20% PEG 8K, and salDNA on the observed rate of 8-oxoG excision from S20^U. P_{trans} and reaction rate data for 22 mM K⁺ in the presence of 20% PEG 8K has been published and is shown here for comparison⁹.

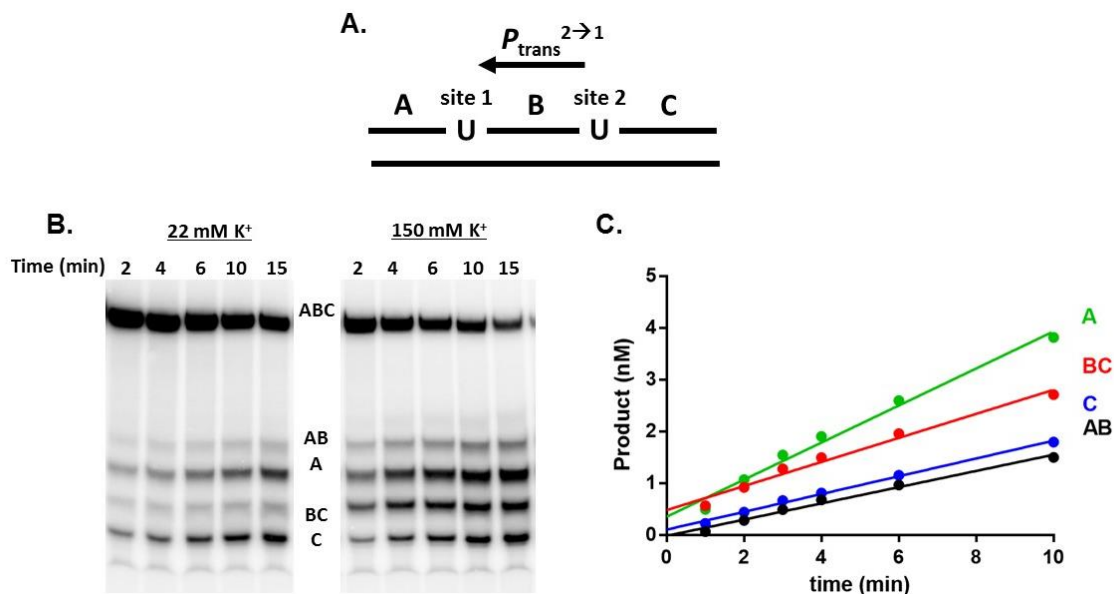


Figure 5.4. Effect of salt concentration on the site transfer probability of hUNG between uracil lesions spaced 5 bp apart. (A) Schematic of proposed site 2→1 biased transfer mechanism. (B) Phosphorimages of products derived from reaction of hUNG with 40 nM of the 90mer substrate ($S5^U$) in low salt and high salt buffer. At low salt, directionally unbiased chain transfer is indicated by equal amounts of single cleaved fragments AB and BC and equivalent (but larger) amounts of double cleaved fragments A and C. Unequal distribution of band intensities at high salt indicates directional transfer bias (see Supplemental Discussion). (C) Velocities of formation of individual fragments derived from $S5^U$ at high salt. Directionally biased transfers from site 1 to site 2 are supported by the observation that fragment BC is always present at a high levels indicating poor transfer from site 2→1.

Table 5.4. Effect of salt, 20% PEG 8K, and salmon sperm DNA (salDNA) on the site transfer probability (P_{trans}) of hUNG at 22 mM potassium ions.

	22 mM K⁺	
	S20^U	S5^U
	P_{trans}	P_{trans}
Buffer	0.36 ± 0.08	0.60 ± 0.07
100 μM salDNA	0.47 ± 0.02	0.68 ± 0.02
1 mM salDNA	0.41 ± 0.05	0.59 ± 0.06
20% PEG 8K	0.71 ± 0.06^a	0.92 ± 0.06^a
20% PEG 8K + 100 μM salDNA	0.39 ± 0.18	0.67 ± 0.09
20% PEG 8K + 1 mM salDNA	0.26 ± 0.09	0.49 ± 0.08

^a Data has been previously published and is presented here for comparison.

Table 5.5. Effect of salt, 20% PEG 8K, and salmon sperm DNA (salDNA) on the site transfer probability (P_{trans}) of hUNG at 150 mM potassium ions.

	150 mM K⁺	
	S20^U	S5^U
	P_{trans}	$P_{\text{trans}}^{2 \rightarrow 1}{}^a$
Buffer	0.02 ± 0.01	0.13 ± 0.02
100 μM salDNA	0.11 ± 0.03	0.09 ± 0.03
1 mM salDNA	0.09 ± 0.03	0.07 ± 0.04
20% PEG 8K	0.21 ± 0.02	0.29 ± 0.05
20% PEG 8K + 100 μM salDNA	0.17 ± 0.04	0.14 ± 0.03
20% PEG 8K + 1 mM salDNA	0.10 ± 0.05	0.03 ± 0.03

^a $P_{\text{trans}}^{2 \rightarrow 1}$ represents biased transfer from site 2 to site 1 and is derived from $P_{\text{trans}}^{2 \rightarrow 1} = ([C]_o - [AB]_o)/[C]_o$.

5.2.4. Environmental Effects on Steady-State Turnover of hUNG.

As with hOGG1, the effect of solution environment on the steady-state rate of uracil excision was determined. Under low salt conditions, the introduction of 20% PEG 8K caused an ~10-fold reduction in turnover of S20^U (red bars, **Figure 5.3C**). This reduction was previously attributed to the crowding agent trapping hUNG on non-specific DNA, thereby increasing the amount of time the enzyme spends translocating on DNA chains at the expense of diffusing rapidly through bulk solution to new chains⁹. Addition of 0.1 or 1 mM salDNA to the crowded low salt solution resulted in turnover rates that were suppressed by ~10⁵-fold relative to buffer alone (**Figure 5.3C, Table 5.6, and Figure 5.5**). This rate reduction is attributed to competitive binding of the vast excess of non-specific DNA sites, which is driven by electrostatic interactions with hUNG at low salt concentration. Remarkably, the slow turnover in the presence of salDNA is restored by a factor of 10⁴ to 10⁵ by the addition of high salt (black bars, **Figure 5.3C**). These substantial salutary effects of high salt on the steady-state turnover of hUNG in the presence of crowding and decoy DNA are accounted for by reduced electrostatic binding to non-specific DNA sites and the enhanced uracil site specificity at high salt provided by the non-electrostatic binding energy for specific sites⁸.

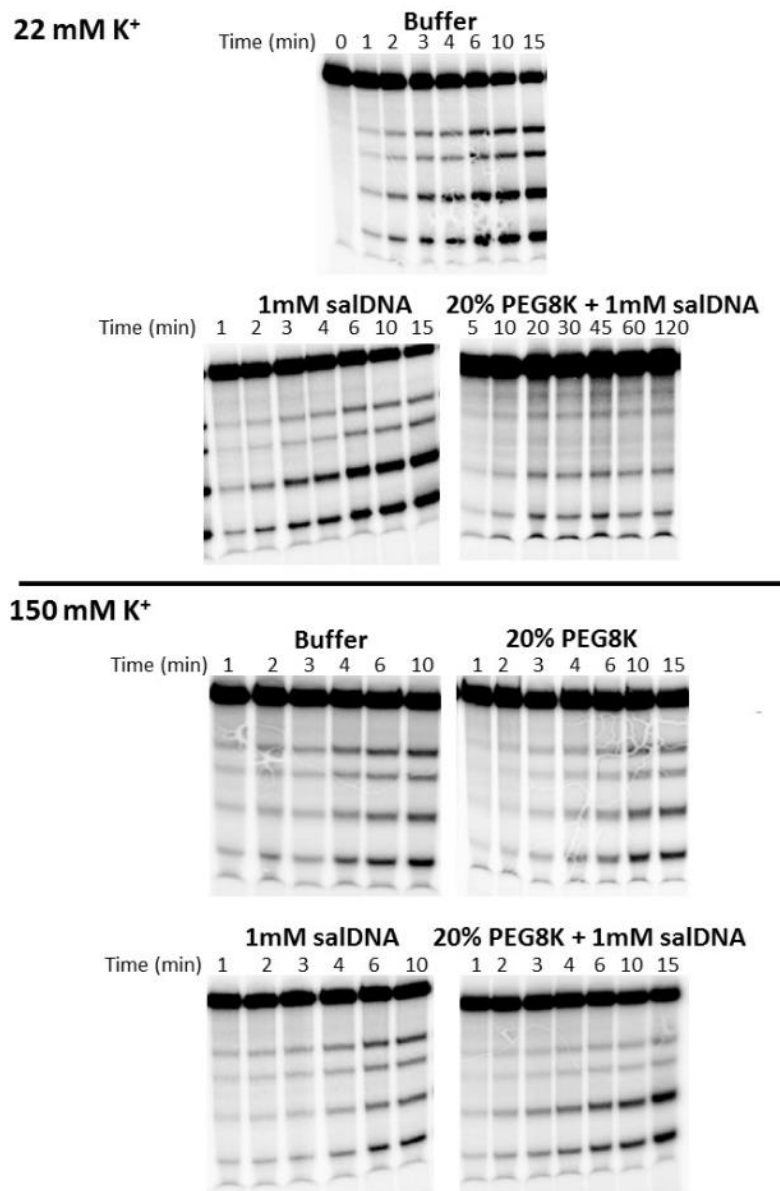


Figure 5.5. Example gels of hUNG reacting with S20^U under various solution conditions. All experiments contained 40 nM DNA and a hUNG concentration that ranged from 20 pM – 190 nM. Gel bands were quantified as a function of time to determine P_{trans} and turnover rate.

Table 5.6. Reaction rates (k_{obs}) in the presence of salt, 20% PEG 8K, and salmon sperm DNA (salDNA) for hUNG.

	S20^U	
	22 mM K⁺	150 mM K⁺
	k_{obs} (min ⁻¹)	k_{obs} (min ⁻¹)
Buffer	115 ± 10	35 ± 6
100 μM salDNA	9 ± 6	19 ± 5
1 mM salDNA	1.8 ± 0.1	3 ± 1
20% PEG 8K	14.9 ± 0.1	240 ± 160
20% PEG 8K + 100 μM salDNA	2 ± 1 x 10 ⁵	18 ± 6
20% PEG 8K + 1 mM salDNA	1.1 ± 0.6 x 10 ⁵	0.8 ± 0.4

5.3. DISCUSSION

The general question of whether DNA glycosylases from distinct fold families use different energetic and kinetic mechanisms to locate rare damaged DNA bases in a densely crowded nuclear environment is largely unexplored. The present study utilizes a simple *in vitro* model that consists of an inert crowding agent, physiological concentrations of potassium acetate and high concentrations of bystander DNA chains to mimic the nuclear environment. The common and unique aspects of the mechanisms utilized by hUNG and hOGG1 are discussed below and summarized in **Figure 5.6**. In **Figure 5.6A**, the observed “salt effect” (X^{150}/X^{LS}) is indicated for each solution condition we have explored. The salt effect is defined as the value of a given measurement (K_D , P_{trans} or k_{obs}) at 150 mM salt (X^{150}) to the same measurement at low salt (X^{LS}). **Figure 5.6A** facilitates comparison of the salt effect in dilute buffered solution as compared to when 20% PEG8K, 1 mM bulk DNA, or both are present. **Figure 5.6B** presents a reasonable model for the combined effects of salt, crowding and bulk DNA chains on enzyme-DNA binding and chain translocation (see below).

5.3.1. Salt Effects on DNA Translocation in the Absence of Crowding or Bulk DNA.

Physiological salt concentration also diminishes the translocation efficiency (P_{trans}) of hUNG and hOGG1 in the absence of crowding and bulk DNA chains (**Figures 5.1C, 5.3B, 5.6A**). For both enzymes, P_{trans} is reduced to zero for the substrates with a 10 to 20bp site spacing. For hUNG, the effects of salt on P_{trans} can be rationalized in much the same way as the antagonistic effects of salt on non-specific DNA binding. That is, when hUNG makes a dissociative step away from the DNA and escapes the DNA ion cloud, the presence of high bulk salt takes away the entropic advantage of rebinding the same DNA chain.

Thus, more enzyme molecules are lost to bulk solution when attempting to transfer between the sites. However, at a shorter five base pair spacing hUNG can still transfer in the presence of 150 mM K^+ , which is attributed to the increased use of the associative pathway that is more salt resistant²⁸. The antagonistic effect of salt on P_{trans} of hOGG1 may also arise from similar entropic effects even though its non-specific DNA binding is far less sensitive to salt concentration than hUNG. For hOGG1, the 3 to 5-fold decrease in its non-specific binding affinity as the salt is increased from 30 to 150 mM is apparently sufficient to ablate effective translocation between sites. In addition, the relative efficiency of transfer of hOGG1 and hUNG between sites will be affected by the average number of microscopic dissociative steps that are taken by each enzyme during the transfer. In other words, each dissociative step introduces a probability where the enzyme may reassociate with the same DNA chain or escape to bulk solution. Even a relatively small salt effect on several dissociative steps would increase the escape probability multiplicatively, leading to a significant reduction in successful site transfers^{8,20}.

5.3.2. Salt Effects on Turnover in the Absence of Crowding or Bulk DNA.

A physiological concentration of salt can also increase or decrease the catalytic turnover of an enzyme if there are salt sensitive rate-limiting steps along the reaction coordinate⁸. If salt sensitive binding steps are involved, an increased salt concentration will reduce the entropic driving force for ion release in the transition state for binding^{6,8}, and facilitate the same transition state in the reverse direction (by microscopic reversibility). For the turnover studies performed here in the absence of crowding or bulk DNA, the kinetic effects of salt are modest and reflect the net effect on the binding steps

and product release (see k_{obs} , **Figure 5.6A**). Below we return to discuss the major effect of salt, which becomes profoundly important when crowding and bulk DNA are introduced.

5.3.3. Impacts of Inert Macromolecule Crowding on the Salt Effect.

The addition of 20% PEG8K to the aqueous buffer substantially enhances the translocation efficiency for both hOGG1 and hUNG (see P_{trans} , **Figure 5.1C** and **5.3B**). The effect is especially impactful at physiological salt concentration using the longer site spacing of 20bp, where P_{trans} is increased from essentially zero to around 0.25-0.3 for both enzymes. This appears to be a general effect of crowding that derives from increased sequestration of the enzymes in the vicinity of the DNA chain by the polymer cage. Thus, the partitioning of dissociated enzyme molecules to bulk solution is disfavored, which dramatically attenuates the effect of high salt for both enzymes. The other effect of crowding is to reduce the observed rate of reaction by about 10-fold for both enzymes when low salt conditions are used (**Figure 5.1D** and **5.3C**). For hUNG, we have previously attributed the cause of this effect to the increased time spent translocating on long (but not short) DNA chains before and after uracil excision⁹. The increased time spent translocating on DNA chains reduces opportunities for rapid 3D diffusion steps, which is the most efficient mechanism for rapid sampling all DNA chains in the population^{17-21, 28, 34}. For hUNG, the inhibitory effect of crowding on the rate is strikingly relieved when a physiological salt concentration is used (**Figure 5.3C**, see k_{obs} **Figure 5.6A**). This effect is reasonably attributed to an increase in the dissociation frequency from both non-specific DNA and the product complex, which provides more opportunities for escape of the enzyme from the polymer cage around the DNA^{8,9}. For hOGG1, the same salutary effect of increased ions on the rate is not observed (**Figure 5.5A**), which is reasonably attributed

to its weaker electrostatic binding component to non-specific DNA and the very slow nature of product release, which likely involves salt independent resolution of the covalent Schiff base linkage with the abasic sugar aldehyde^{32, 35}.

5.3.4. Bulk DNA Effects on Translocation and Turnover.

In the absence of crowding, the general effect of a high density of bulk DNA chains on hOGG1 and hUNG activity is to reduce P_{trans} and enzyme turnover regardless of the monovalent cation concentration (**Figure 5.6A**), which is attributed to bulk DNA trapping of dissociated enzymes molecules in the process of translocating between two sites and equilibrium competitive inhibition, respectively. Trapping of translocating enzymes by bulk DNA chains is entirely plausible because at a 1 mM salDNA concentration a single bp of salDNA would be located an average of ~10 nm from a substrate DNA molecule. This separation is close to the mean distance for diffusion of these enzymes from the substrate DNA chain during a single productive dissociative transfer step (~7 nm), suggesting a high probability of being captured by the DNA trap (**Figure 5.6B**)^{27, 28}.

The antagonistic effect of bulk DNA chains on P_{trans} is greatly attenuated in the presence of crowding, regardless of the monovalent ion concentration (**Figure 5.1C** and **5.3C**). This effect of crowding may arise from the individual substrate and bulk DNA chains being sequestered in their own polymer cages (**Figure 5.6B**), which would tend to diminish trapping by bulk DNA chains near the site of a translocating enzyme independent of salt effects. The data also indicate that P_{trans} decreases as the bulk DNA concentration is increased when crowding is held constant. This effect may arise from merging of the bulk and substrate DNA polymer cages and the tendency of DNA chains to interact at high DNA concentrations and in the presence of Coulombic shielding effects provided by of high salt

concentrations (**Figure 5.6B**)³⁶. Thus, the combined effects of crowding and high salt may allow intermolecular DNA complexes to form between bulk and substrate DNA chains and populate the microscopic region where the enzyme is translocating. This would lead to the observed reduction in P_{trans} (**Figure 5.1C** and **5.3B**)^{37,38}.

The introduction of high salt results in a profound increase in the exceedingly slow turnover rate of hUNG under conditions of crowding and high bulk DNA concentration (**Figure 5.6A**). No such effect of salt was observed with hOGG1 (**Figure. 5.1D**). The beneficial kinetic effect of 150 mM salt on turnover of hUNG but not hOGG1 under these conditions is reasonably attributed to the larger electrostatic contribution to non-specific DNA binding by hUNG, the expected enhanced specificity for uracil sites under such conditions, and the previously reported accelerating effects of salt on the product release step (**Chapter 3, Table 3.4**). For hOGG1, the same stimulatory effect of high monovalent ions would not be expected because of its smaller non-electrostatic binding free energy and its rate-limiting product release step is not stimulated by salt ions. In summary, monovalent cations are required for hUNG to maintain high turnover in the presence of high concentrations of bulk DNA chains, whereas hOGG1 avoids this problem by avoiding strong electrostatic interactions with non-specific DNA.

Figure 5.6. Summary of the effects of salt, molecular crowding, and bulk DNA on each measured thermodynamic and kinetic parameter. (A) The salt effect (X^{150}/X^{LS}) indicated for each solution condition we have explored. This is defined as the value of a measurement (K_D , P_{trans} or k_{obs}) at 150 mM salt (X^{150}) divided by the value at low salt (X^{LS}). This panel compares the salt effect in dilute solution as compared to when 20% PEG8K, 1 mM bulk DNA, or both are present. Salt effects falling below the dashed line are reduced by high ionic strength and those above are enhanced. hUNG and hOGG1 respond differently to the introduction of salt with respect to non-specific DNA binding (K_D^N) and kinetic activity in the presence of crowder and salDNA. (B) General model for the effects of molecular crowders (orange lines) and bulk DNA (purple bars) on DNA translocation at a physiological salt concentration. The image is drawn to scale using a DNA duplex of with a 2 nm diameter as a scale reference. Dashed lines depict the depletion layer where the PEG 8K polymer is excluded around the protein and DNA macromolecules (see **Chapter 4**). The depletion layer and polymer cage are very effective at enhancing DNA translocation by keeping dissociated enzyme molecules in the vicinity of the substrate DNA chain. Two effects of bulk DNA chains (dark gray) are also depicted. In the first scenario, the bulk DNA chain is enclosed in its own depletion layer and separated from the substrate DNA chain at a distance determined by the bulk DNA chain concentration. Such bulk DNA chains would be hindered from trapping translocating enzyme molecules compared to the absence of crowding. In the second scenario, the depletion layers of the bulk and substrate DNA have overlapped, which is facilitated by the reduced volume of complexation and shielding of the repulsive phosphate charge at high salt^{36, 38}.

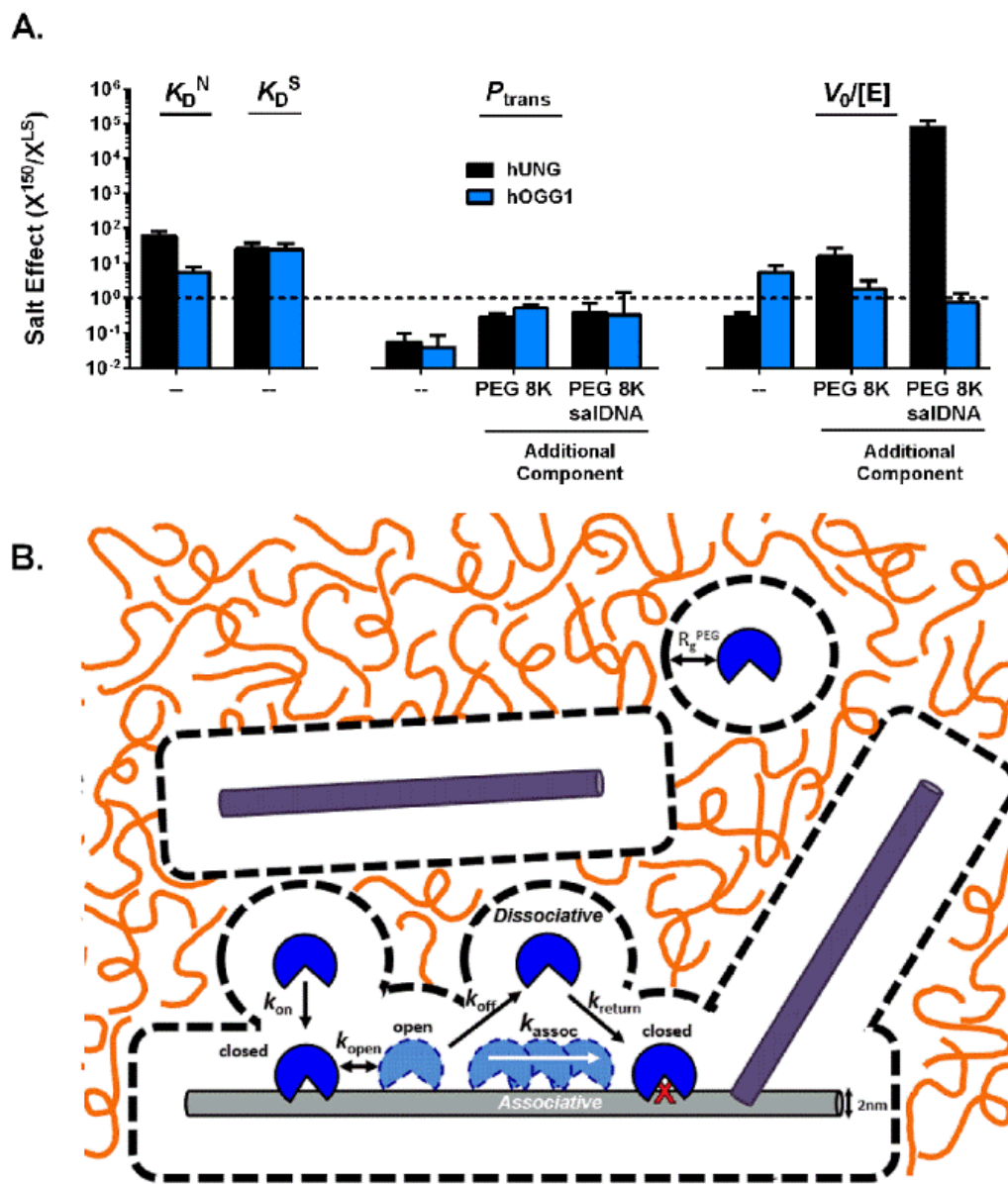


Figure 5.6.

5.3.5. Glycosylase Activity in a Cellular Environment.

It is abundantly clear that monovalent ions, molecular crowding, and high-densities of bulk DNA have profound effects on the activities of hUNG and hOGG1. It is also clear that the individual effects of these solution components, which can either enhance or antagonize a given activity parameter, can be significantly altered when all three components are present simultaneously. Remarkably, we find that the basic features of the damage search and repair process that have been previously determined at low salt concentrations or in the presence of a crowding agent only^{9, 27, 28}, persist under conditions that more closely mimic the nuclear environment. These features include short-range associative translocations over ~10bp distances and frequent dissociative transfers that allow rapid 3D diffusion to new positions on the same DNA chain or to new DNA chains when the chain density is high. A new finding in the current work is that the caging effect of macromolecular crowding agents and the electrostatic effects of monovalent cations can act cooperatively to retain an efficient search mechanism in the presence of high concentrations of bulk DNA chains. Thus, the caging effect of the crowder counteracts the antagonistic effect of high monovalent ion concentrations on DNA translocation, and high monovalent ion concentrations promote dissociation of enzyme molecules from non-specific DNA chains providing more opportunities for escape from the polymer cage. For hUNG, these effects lead to retention of an efficient search mechanism even in the presence of high concentrations of bulk DNA. Despite the different energetic basis for the interaction of hOGG1 with DNA, it also shows the same general trends with respect to DNA translocation. However, the exceptionally slow release of hOGG1 with its reaction product is exacerbated in a crowded environment under all conditions studied (**Figure**

5.1D). This observation must be taken into the context that hOGG1 turnover has been shown to be greatly accelerated by the next enzyme in the base excision repair pathway, AP endonuclease 1 (APE1)^{40, 41}. Based on the expectation that crowding agents shift binding equilibria towards the formation of lower volume protein complexes as opposed to the free species^{12, 42, 43}, we speculate that APE1-facilitated release of hOGG1 from its product complex will be promoted in a crowded nuclear environment.

5.4. METHODS

5.4.1. Experimental Conditions.

All experiments with hOGG1 were performed in buffer containing 15 mM potassium phosphate pH 7.5, 1 mM EDTA, and 0.1 mg/mL BSA. This buffer contained a total of 30 mM K⁺ originating from pH adjustment of potassium phosphate and EDTA. Increasing ionic strength measurements were made by supplementing the buffer with potassium acetate (KOAc). All experiments with hUNG were performed in a buffer consisting of 20 mM HEPES pH 7.5, 3 mM EDTA, 1 mM DTT, 0.002% Brij 35. This buffer contained a total of 22 mM K⁺ originating from pH adjustment of the HEPES and EDTA stock solutions. The catalytic domain of recombinant hUNG, WT hOGG1 and the K249Q mutant hOGG1 were purified as previously described⁹. All oligonucleotides were purchased from either Integrated DNA Technologies or Eurofin and purified in-house by denaturing PAGE. PEG 8K was purchased from Sigma Chemical and was purified by overnight treatment with activated carbon (0.1g/mL) and filtered to remove UV absorbing impurities. Salmon sperm DNA (salDNA) was purchased from ThermoFisher Scientific.

5.4.2. Oligonucleotide Reagents

All DNA substrates listed below were purchased from either Integrated DNA Technologies (www.idtdna.com) or Eurofins MWG Operon (www.operon.com). Long oligos (>20 base pairs) were purified by denaturing gel electrophoresis. For all DNA duplex substrates, uracil bases were paired with adenine and 8-oxoguanine bases were paired with cytosine. All DNAs used in this study were in the duplex form and the sequences are listed below (the sequences of the complimentary strands for the two-site substrates are not shown).

Two-site 90mer substrates

S10^{oxoG}

5' -GGT ATC TGT AG G ATG CGC TCA CAA TTC CAC ACA ATG CTG AGG
AAT TTC °G CT CCT AT TTC oxoG CT CCT TGC TGA GGC ATA CAG TGT
CGA GCCA-3'

S20^{oxoG}

5' -GGT ATC CGC TCA CAA TTC CAC ACA ATG CTG AGG AAT TTC oxoG
CT CCT TGT AG G ATG A AT TTC °G CT CCT TGC TGA GGC ATA CAG
TGT CGA GCC-3'

S5^U

5' -GGT ATC CGC TGA AGT AGT CAC AAT TCC ACA CAA TGC TGA GGA
ATC GA U AGC GA U AGC TAA GCT GAG GCA TAC AGG ATC AAT TGT CGA
GCC-3'

S20^U

5' -GGT ATC CGC TCA CAA TTC CAC ACA ATG CTG AGG AAT CGA U AG
CTA AGT AGG ATG AAT CGA U AG CTA AGC TGA GGC ATA CAG TGT
CGA GCC-3'

5.4.3. Site Transfer Assay.

Site transfer assays were performed as previously reported and the general procedure is recapitulated here^{27, 28, 29}. To initiate the reactions, hUNG (20 pM - 190 nM) was mixed with a dual uracil ³²P labeled DNA substrate (40 nM) at 37 °C using the buffer noted above supplemented with all combinations of the following solution components: 22 mM potassium from buffer pH adjustment, 150 mM potassium by addition of 128 mM KOAc, 20% PEG 8K, 100 μM salmon sperm DNA (salDNA), and 1 mM salDNA. The 190 nM concentration of hUNG was only used with buffer containing 22 mM K⁺, 20% PEG 8K, and either 100 μM or 1 mM salDNA due to extreme inhibition of the enzyme in these solution conditions. In the presence of 0.1 or 1 mM salDNA, most hUNG is bound and the free enzyme concentration is low enough to maintain, the initial rate, single encounter conditions required for site transfer experiments. At various times, aliquots of the reaction mixture were quenched with Uracil DNA Glycosylase Inhibitor protein (UGI, New England Biolabs) and the abasic sites were cleaved by heating at 95°C in the presence of 100 mM KOH for 30 minutes. For experiments using hOGG1, enzyme (1 to 40 nM) was added to 20 nM ³²P-labeled S20^{oxoG} in the presence of all solution conditions noted above. Concentrations of hOGG1 > 5 nM were only used in experiments containing salDNA for the same reasons outlined above for hUNG. Aliquots of the reaction were quenched with 20 μL formamide loading buffer and heated for 15 min at 95 °C. For both enzymes, the discrete DNA fragments generate by heating were resolved by electrophoresis on a denaturing 10% PAGE gel containing 7 M urea. All gels were dried, exposed overnight to a storage phosphor screen and imaged with a Typhoon 8600 phosphorimager (GE Healthcare). All gel images were quantified using QuantityOne (Bio-Rad) by the box

method and background corrected as described above. The time independent overall site transfer probability (P_{trans}) was calculated using eq 5.1 by linear extrapolation of the observed transfer probabilities ($P_{\text{trans}}^{\text{obs}}$) to zero time.

$$P_{\text{trans}} = \frac{[A]^0 + [C]^0 - [AB]^0 - [BC]^0}{[A]^0 + [C]^0 + [AB]^0 + [BC]^0} \quad (5.1)$$

The fractional extent of reaction at each time was quantified by phosphorimaging of the gels and the reaction rates for both hUNG and hOGG1 under all tested conditions were determined from linear slopes of plots of product concentration versus time in Prism.

5.4.4. Turnover Rate Determination.

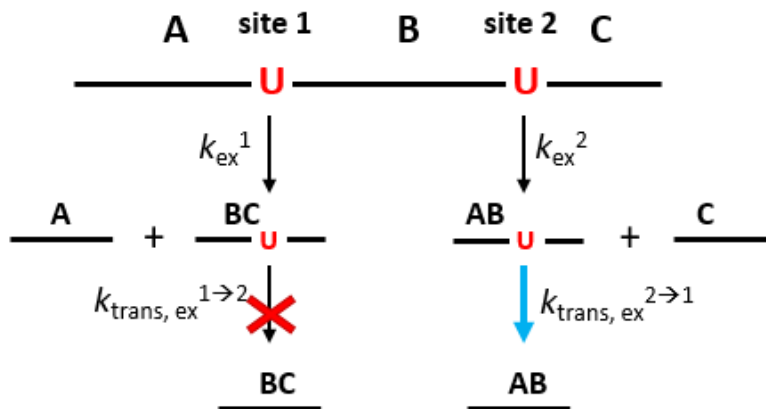
The observed turnover rates of hUNG and hOGG1 under various solution conditions were determined using the S20^U and S20^{oxoG} substrates, respectively. For hUNG, the rate was calculated utilizing the same data that was used to determine P_{trans} . The fraction reaction at each time point was calculated from the ratio of the summed intensities of all product bands to the summed intensity of substrate and product bands. The fraction reaction was plotted as a function of time and the rates (slopes) were obtained by linear regression fitting (<30% reaction). The slopes were converted to observed rate constants by multiplying by the total DNA concentration ($[S20^U] = 40 \text{ nM}$ in all experiments) and dividing by the enzyme concentration ($[hUNG] = 20 \text{ pM}$ to 190 nM depending on conditions). Because of day-to-day variability in the activity of hOGG1, we compared the turnover rates under various conditions using a single stock of enzyme on the same day. The rate data were quantified as described above for hUNG ($[S20^{\text{oxoG}}] = 20 \text{ nM}$; $[hOGG1] = 1 \text{ nM}$ to 40 nM).

5.4.5. hUNG Transfer Bias at High Salt. The atypical distribution of product fragments observed for SU⁵ at high salt suggests biased transfer in the direction site 2→1 (**Figure 5.4**). We previously established that an apparent transfer bias could arise from two possible mechanisms^{9, 33}. The first mechanism is true directional bias and the second involves different uracil excision rates at each site (k_{ex}). We excluded the possibility of different excision rates at the two sites in earlier studies, which is the expected result since the DNA substrates were originally designed to have identical sequences surrounding the uracil sites². For the above reasons we analyze the data in terms of biased transfer (eq 5.2 and Scheme S1). Equation S1 quantifies the fraction of the excision events at site 2 (producing fragments C and AB) that result in successful translocation and excision at site 1 (thereby generating fragment A by consumption of fragment AB). The zero subscripts in eq 5.2 indicate that the fragment concentrations are extrapolated to zero time:

$$P_{trans}^{2 \rightarrow 1} = \frac{[C]_0 - [AB]_0}{[C]_0} \quad (5.2)$$

Equation 5.2 may be rationalized in the following way. Since $[C]_0 = [AB]_0$ in the absence of site 2→1 translocation, then the difference in the numerator of eq S1 is zero in the absence of translocation. In the presence of translocation, $[C]_0 > [AB]_0$ and the difference $[C]_0 - [AB]_0$ calculates how much fragment A was produced from consumption of AB. The fundamental requirement in order to use eq S1 is that no fragment C can be produced by excision of fragment BC after translocation in the site 1→2 direction. In the present data this pathway cannot be significant because we observe a persistent level of the BC fragment that always greatly exceeds the amount of fragment AB. The persistence of the BC fragment excludes significant translocation and excision in the direction site 1→2.

The observed $P_{\text{trans}}^{2 \rightarrow 1}$ values for all solution conditions tested are reported in **Table 5.3** and **Figure 5.6**.



Scheme 5.1. Directionally biased site transfer mechanism for substrate $S5^U$ in the presence of 150 mM K^+ . k_{ex} is the initial rate of first excision event (at either site 1 or site 2), which then results in either translocation or dissociation of the enzyme before reaching the second site (k_{trans}). The observed biased directionality of site transfers is indicated by the thick blue arrow.

5.5. REFERENCES

1. Hoeijmakers, J. H. (2009) DNA damage, aging, and cancer. *N. Engl. J. Med.* 361, 1475-1485.
2. Sancar, A., Lindsey-Boltz, L. A., Unsal-Kacmaz, K., and Linn, S. (2004) Molecular mechanisms of mammalian DNA repair and the DNA damage checkpoints. *Annu. Rev. Biochem.* 73, 39-85.
3. Stivers, J. T., and Jiang, Y. L. (2003) A mechanistic perspective on the chemistry of DNA repair glycosylases. *Chem. Rev.* 103, 2729-2759.
4. Seeberg, E., Eide, L., and Bjørås, M. (1995) The base excision repair pathway. *Trends Biochem. Sci.* 20, 391-397.
5. Alsallaq, R., and Zhou, H. X. (2008) Electrostatic rate enhancement and transient complex of protein-protein association. *Proteins.* 71, 320-335.
6. Privalov, P. L., Dragan, A. I., and Crane-Robinson, C. (2011) Interpreting protein/DNA interactions: Distinguishing specific from non-specific and electrostatic from non-electrostatic components. *Nucleic Acids Res.* 39, 2483-2491.
7. Zhou, H. (2001) Disparate ionic-strength dependencies of on and off rates in protein-protein association. *Biopolymers.* 59, 427-433.
8. Cravens, S. L., Hobson, M., and Stivers, J. T. (2014) Electrostatic properties of complexes along a DNA glycosylase damage search pathway. *Biochemistry.* 53, 7680-7692.
9. Cravens, S. L., Schonhoft, J. D., Rowland, M. M., Rodriguez, A. A., Anderson, B. G., and Stivers, J. T. (2015) Molecular crowding enhances facilitated diffusion of two human DNA glycosylases. *Nucleic Acids Res.* 43, 4087-4097.
10. Ellis, R. J. (2001) Macromolecular crowding: Obvious but underappreciated. *Trends Biochem. Sci.* 26, 597-604.
11. Minton, A. P. (2001) The influence of macromolecular crowding and macromolecular confinement on biochemical reactions in physiological media. *J. Biol. Chem.* 276, 10577-10580.
12. Phillip, Y., Sherman, E., Haran, G., and Schreiber, G. (2009) Common crowding agents have only a small effect on protein-protein interactions. *Biophys. J.* 97, 875-885.
13. Zhou, H. X., Rivas, G., and Minton, A. P. (2008) Macromolecular crowding and confinement: Biochemical, biophysical, and potential physiological consequences. *Annu. Rev. Biophys.* 37, 375-397.
14. Parker, J. B., Bianchet, M. A., Krosky, D. J., Friedman, J. I., Amzel, L. M., and Stivers, J. T. (2007) Enzymatic capture of an extrahelical thymine in the search for uracil in DNA. *Nature.* 449, 433-437.
15. Krosky, D. J., Song, F., and Stivers, J. T. (2005) The origins of high-affinity enzyme binding to an extrahelical DNA base. *Biochemistry.* 44, 5949-5959.
16. Veksler, A., and Kolomeisky, A. B. (2013) Speed-selectivity paradox in the protein search for targets on DNA: Is it real or not? *J Phys Chem B.* 117, 12695-12701.
17. Gowers, D. M., Wilson, G. G., and Halford, S. E. (2005) Measurement of the contributions of 1D and 3D pathways to the translocation of a protein along DNA. *Proc. Natl. Acad. Sci. U. S. A.* 102, 15883-15888.
18. Halford, S. E., and Marko, J. F. (2004) How do site-specific DNA-binding proteins find their targets? *Nucleic Acids Res.* 32, 3040-3052.
19. Leonid Mirny and Michael Slutsky and Zeba Wunderlich and Anahita Tafvizi and Jason Leith and Andrej Kosmrlj. (2009) How a protein searches for its site on DNA: The mechanism of facilitated diffusion. *Journal of Physics A: Mathematical and Theoretical.* 42, 434013.

20. Stanford, N. P., Szczelkun, M. D., Marko, J. F., and Halford, S. E. (2000) One- and three-dimensional pathways for proteins to reach specific DNA sites. *EMBO J.* 19, 6546-6557.
21. von Hippel, P. H., and Berg, O. G. (1989) Facilitated target location in biological systems. *J. Biol. Chem.* 264, 675-678.
22. Parikh, S. S., Walcher, G., Jones, G. D., Slupphaug, G., Krokan, H. E., Blackburn, G. M., and Tainer, J. A. (2000) Uracil-DNA glycosylase–DNA substrate and product structures: Conformational strain promotes catalytic efficiency by coupled stereoelectronic effects. *Proceedings of the National Academy of Sciences.* 97, 5083-5088.
23. Friedman, J. I., and Stivers, J. T. (2010) Detection of damaged DNA bases by DNA glycosylase enzymes. *Biochemistry.* 49, 4957-4967.
24. David, S. S., O'Shea, V. L., and Kundu, S. (2007) Base-excision repair of oxidative DNA damage. *Nature.* 447, 941-950.
25. Banerjee, A., Yang, W., Karplus, M., and Verdine, G. L. (2005) Structure of a repair enzyme interrogating undamaged DNA elucidates recognition of damaged DNA. *Nature.* 434, 612-618.
26. Bruner, S. D., Norman, D. P., and Verdine, G. L. (2000) Structural basis for recognition and repair of the endogenous mutagen 8-oxoguanine in DNA. *Nature.* 403, 859-866.
27. Rowland, M. M., Schonhoft, J. D., McKibbin, P. L., David, S. S., and Stivers, J. T. (2014) Microscopic mechanism of DNA damage searching by hOGG1. *Nucleic Acids Research.* 42, 9295-9303.
28. Schonhoft, J. D., and Stivers, J. T. (2012) Timing facilitated site transfer of an enzyme on DNA. *Nat. Chem. Biol.* 8, 205-210.
29. Porecha, R. H., and Stivers, J. T. (2008) Uracil DNA glycosylase uses DNA hopping and short-range sliding to trap extrahelical uracils. *Proceedings of the National Academy of Sciences.* 105, 10791-10796.
30. Leipold, M. D., Workman, H., Muller, J. G., Burrows, C. J., and David, S. S. (2003) Recognition and removal of oxidized guanines in duplex DNA by the base excision repair enzymes hOGG1, yOGG1, and yOGG2. *Biochemistry.* 42, 11373-11381.
31. Dherin, C., Radicella, J. P., Dizdaroglu, M., and Boiteux, S. (1999) Excision of oxidatively damaged DNA bases by the human alpha-hOgg1 protein and the polymorphic alpha-hOgg1(Ser326Cys) protein which is frequently found in human populations. *Nucleic Acids Res.* 27, 4001-4007.
32. Kuznetsov, N. A., Kuznetsova, A. A., Vorobjev, Y. N., Krasnoperov, L. N., and Fedorova, O. S. (2014) Thermodynamics of the DNA damage repair steps of human 8-oxoguanine DNA glycosylase. *PLoS ONE.* 9, e98495.
33. Schonhoft, J. D., and Stivers, J. T. (2013) DNA translocation by human uracil DNA glycosylase: The case of single-stranded DNA and clustered uracils. *Biochemistry.* 52, 2536-2544.
34. Berg, O. G., Winter, R. B., and von Hippel, P. H. (1981) Diffusion-driven mechanisms of protein translocation on nucleic acids. 1. models and theory. *Biochemistry.* 20, 6929-6948.
35. Fromme, J. C., Bruner, S. D., Yang, W., Karplus, M., and Verdine, G. L. (2003) Product-assisted catalysis in base-excision DNA repair. *Nat. Struct. Biol.* 10, 204-211.
36. Bai, Y., Das, R., Millett, I. S., Herschlag, D., and Doniach, S. (2005) Probing counterion modulated repulsion and attraction between nucleic acid duplexes in solution. *Proc. Natl. Acad. Sci. U. S. A.* 102, 1035-1040.
37. Kombrabail, M. H., and Krishnamoorthy, G. (2005) Fluorescence dynamics of DNA condensed by the molecular crowding agent poly(ethylene glycol). *J. Fluoresc.* 15, 741-747.
38. Vasilevskaya, V. V., Khokhlov, A. R., Matsuzawa, Y., and Yoshikawa, K. (1995) Collapse of single DNA molecule in poly(ethylene glycol) solutions. *J. Chem. Phys.* 102, 6595-6602.

39. de Gennes, P. (1979) *Scaling Concepts in Polymer Physics*. Cornell University Press, Ithaca, N.Y.
40. Vidal, A. E., Hickson, I. D., Boiteux, S., and Radicella, J. P. (2001) Mechanism of stimulation of the DNA glycosylase activity of hOGG1 by the major human AP endonuclease: Bypass of the AP lyase activity step. *Nucleic Acids Res.* *29*, 1285-1292.
41. Hegde, M. L., Hazra, T. K., and Mitra, S. (2008) Early steps in the DNA base excision/single-strand interruption repair pathway in mammalian cells. *Cell Res.* *18*, 27-47.
42. Kozer, N., and Schreiber, G. (2004) Effect of crowding on protein-protein association rates: Fundamental differences between low and high mass crowding agents. *J. Mol. Biol.* *336*, 763-774.
43. Kozer, N., Kuttner, Y. Y., Haran, G., and Schreiber, G. (2007) Protein-protein association in polymer solutions: From dilute to semidilute to concentrated. *Biophys. J.* *92*, 2139-2149.

Chapter 6:

Concluding Remarks

The question of whether or not facilitate diffusion persists as a relevant mechanism by which glycosylases search DNA in the wake of a complex solution environment has been thoroughly addressed. Despite the vast differences between hUNG and hOGG1, both enzymes are capable of undergoing measurable amounts of facilitated diffusion in a nuclear environment mimicked through the use of high salt, molecular crowding agents, and bulk DNA. This suggests that the cell acts as an equalizer in which microscopic disparities in how hUNG and hOGG1 interact with damaged and undamaged DNA do not manifest into macroscopic changes in their search pathway. A combinatorial effect between salt and crowder provides a means by which the most beneficial aspects of ionic strength and excluded volume dominate and support a rapid search model. It is clear that the major effects of the solution environment are on the overall rate of global damage repair and the range over which facilitated diffusion is relevant. A model that involves rapid searching of short DNA segments and sequestering of the enzyme to sites nearby the initial target before eventual escape would be of great utility in the context of an actual nucleus (**Figure 6.1**). Genomic DNA is compacted in a conglomerate involving histone complexes, which limit the amount of exposed DNA to search enzymes. The dynamic nature of sequence exposure and the high density of DNA provided by the close proximity of nucleosome core particles creates an environment most logically searched through repeated encounter events.

In this thesis, I have provided comprehensive evidence detailing the individual and combinatorial effects of ionic strength, crowding, and solution DNA density on the ability of DNA glycosylases to efficiently interact with their targets. Chapter 2 and 3 provide evidence for how differences in the thermodynamic nature of protein-DNA complex stability can enhance specificity or promote a sustained lifetime on DNA regardless of the

sequence context. These two scenarios aid in the recognition of DNA lesions that have disparate behavior in the context of a duplex. The specificity of hUNG is greatly enhanced by physiological salt and its lifetime bound to undamaged DNA is greatly ablated. This effect would facilitate the rapid search required by an enzyme that recognizes lesions that flip out of the DNA helix at an accelerated rate (sub-millisecond) relative to their undamaged counterparts. Conversely, for an enzyme like hOGG1 which must distinguish a DNA lesion that behaves identically to undamaged DNA, a prolonged lifetime on undamaged DNA provides a means by which the glycosylase can interrogate the sequence with high fidelity. In Chapter 4, I expand our knowledge of facilitated diffusion to a crowded environment and perform the first analysis of molecular crowding on DNA glycosylase translocation. Unlike the response to ionic strength, both hUNG and hOGG1 behave similarly in the presence of molecular crowding agents. Reduced available volume favors the formation of a compact complex between these enzymes and DNA, which promotes an enhanced bound lifetime. This long-lived state of the enzyme allows for long range associative transfers to occur at the expense of global repair. The crowded environment promotes the search of relatively small fragments of the genome by each glycosylase molecule rather than a large diffusive search, which is entirely plausible given the high copy number of these enzymes in the cell.

With a final study presented in Chapter 5, I show that, remarkably, the historic model of facilitated diffusion withstands the test of a more physiologically relevant environment for both hUNG and hOGG1. In fact, the combination of salt, molecular crowding agents, and excess DNA provides a path for efficient repair. The reduced lifetime of the bound enzyme and inefficient base excision by high salt is rescued with the

introduction of crowding agents. These inert polymers sequester the enzyme molecules to their initial DNA target, but the degree to which they inhibit global repair is limited by high salt. High ionic strength allows the crowding effect to still enhance facilitated diffusion without the detrimental effects on turnover. This creates an environment in which hUNG and hOGG1 can efficiently sample surrounding DNA sites in close spatial proximity in combination with short, interrogative associative slides to reach the target lesion.

The work I present in this thesis serves to fill a gap in our understanding of facilitated diffusion and builds on the previously established models of associative and dissociative transfers by hUNG and hOGG1. With our new knowledge of how individual aspects of the cellular environment modulate DNA repair both in isolation and in combination, we have an analytical framework for understanding cell based assays. These new experiments will either validate this model or provide new insight into how the cellular environment finely tunes DNA repair beyond what can be recapitulated *in vitro*. We are now poised to move our investigation of facilitated diffusion from test tube to the human cell nucleus.

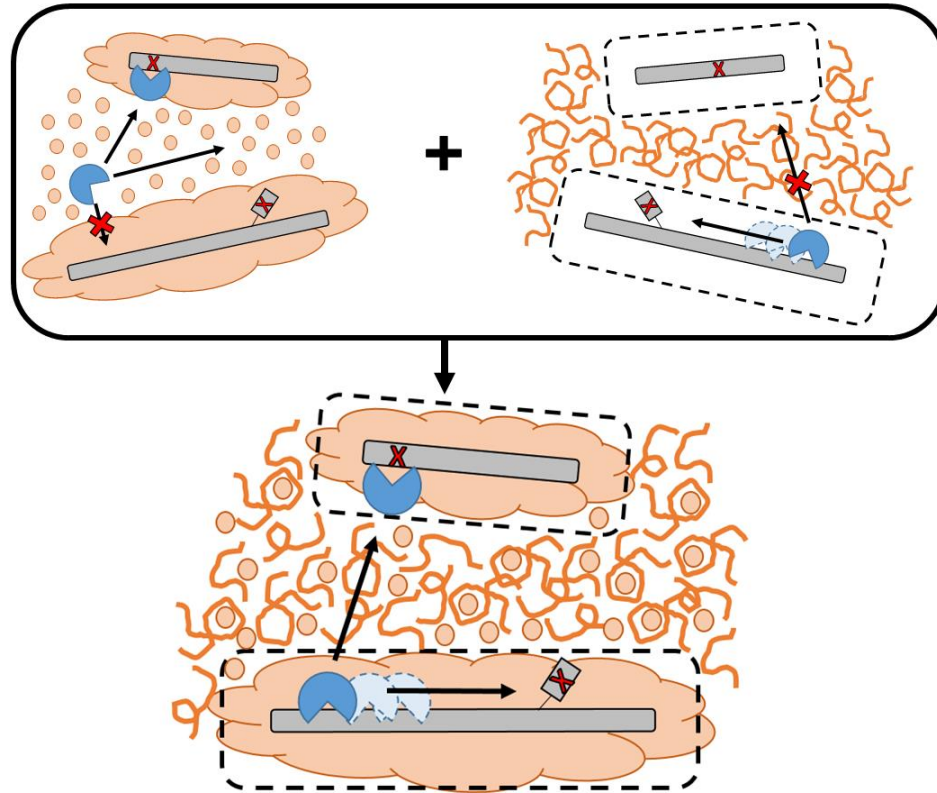


Figure 6.1. Model of the DNA Search-and-Repair Pathways of hUNG and hOGG1 in the Cellular Environment. High salt impedes facilitated diffusion through an ablation of nonspecific binding affinity (hUNG) or excision efficiency (hOGG1) (Chapters 2 and 3). This results in a search mechanism dominated by uncorrelated 3D diffusion. Molecular crowding compacts the environment experienced by the enzyme molecules, reduces translational diffusion, and facilitates associative translocation along initially encountered substrates (Chapter 4). This results in a 1D local searching mechanism and hinders global repair. The combined solution environment. Provides a means for a productive local search induced by crowding in conjunction with a sufficient turnover rate facilitated by high salt to allow for efficient global repair.

Chapter 7:

Appendix

7.1. Overview of hOGG1+APE1 investigation

Human 8-oxoguanine DNA glycosylase (hOGG1) recognizes and excises the abundant oxidative lesion 8-oxoguanine (8-oxoG) when paired with cytosine in DNA. Due to potential mispairing with adenine during replication, efficient repair of 8-oxoG lesions is essential to reduce the probability of mutagenesis. Eventual data collected for this project will entail pre-steady state, steady state, and single turnover kinetics to show that the multiple-turnover excision of 8-oxoG is slowed by detrimental inhibition of hOGG1 by the abasic site product formed, which is only mildly alleviated under physiological salt. This activity can be rescued in the presence of AP endonuclease (APE1), the primary enzyme for processing abasic sites within DNA in human cells, with no effect on single-turnover excision. By monitoring the stability of the covalent complex formed between hOGG1 and lesioned DNA, we show that the presence of APE1 shifts the equilibrium population of hOGG1 toward “free enzyme” that is able to initiate additional catalytic cycles. We provide evidence that APE1 facilitates the turnover of hOGG1 without forming a ternary complex with the bound glycosylase. Despite the stimulatory effects of APE1, we find that under physiological conditions of high salt, crowding, and large DNA density, the presence of APE1 does not facilitate the translocation of hOGG1 between lesion sites. These results suggest a model in which efficient turnover of hOGG1 is expedited by the binding of APE1 to the abasic product site during transient displacement of hOGG1 from the DNA, preventing inhibitory rebinding of the glycosylase.

7.2. Literature Review of hOGG1 interactions with APE1

Previous experiments between hOGG1 and APE1 reveal an enhancement of hOGG1 activity similar to what is investigated here in greater detail. In the presence of 75 mM NaCl, APE1 has been shown to increase the multiple turnover rate of hOGG1¹. This is true even when an inactive mutant (D210N) of APE1 is used. An effect on hOGG1's lyase activity was investigated by separating 5' cleaved and 3' cleaved abasic site fragments. APE1 is known to cleave 5' to the abasic site, while hOGG1 initiates 3' cleavage. Vidal *et al* claim that APE1 does not interfere with the lyase function of hOGG1, though their data is poorly resolved. The only conclusion I have drawn is that APE1 efficiently competes out the lyase activity of hOGG1 and is primary source of abasic site cleavage when in solution¹.

Two potential mechanisms for APE1 mediated turnover of hOGG1 have been proposed: (i) a kinetic model - product sequestration where APE1 binds to abasic DNA upon transient dissociation by hOGG1 or (ii) a structural model - APE1 actively displaces hOGG1 by forming a ternary complex with the bound glycosylase. Vidal *et al.* claim that APE1 facilitation of hOGG1 activity is carried out through product sequestration¹. This was tested by pre-incubating hOGG1 with product DNA and then adding an excess of unlabeled substrate to trap any dissociating enzyme. This was done with and without APE1. The rate at which the hOGG1:DNA complex decreased was the same, which supports the kinetic model. Sidorenko *et al.* contradicted this result through the observation of a ternary complex formed between APE1 and hOGG1 crosslinked to abasic DNA². This leaves the actual mechanism of hOGG1 stimulation by APE1 as an unresolved debate.

7.3. Preliminary Data

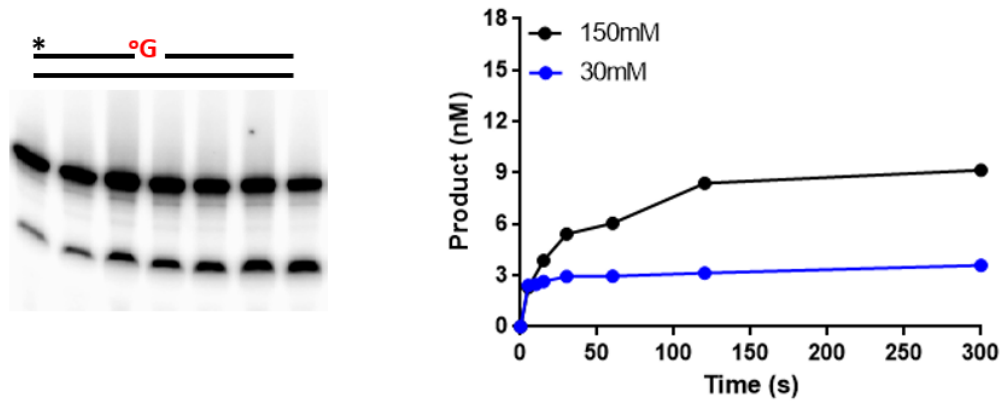


Figure 7.1. hOGG1 remains tightly bound to product DNA. 20 nM of 5' ^{32}P -labeled 31mer DNA (sequence is S0^{oxoG} in Chapter 5) with 1 nM hOGG1. Fragments were separated on 10% denaturing PAGE. The introduction of salt minimally raises the steady-state turnover rate of hOGG1. Fit displayed is not quantitative.

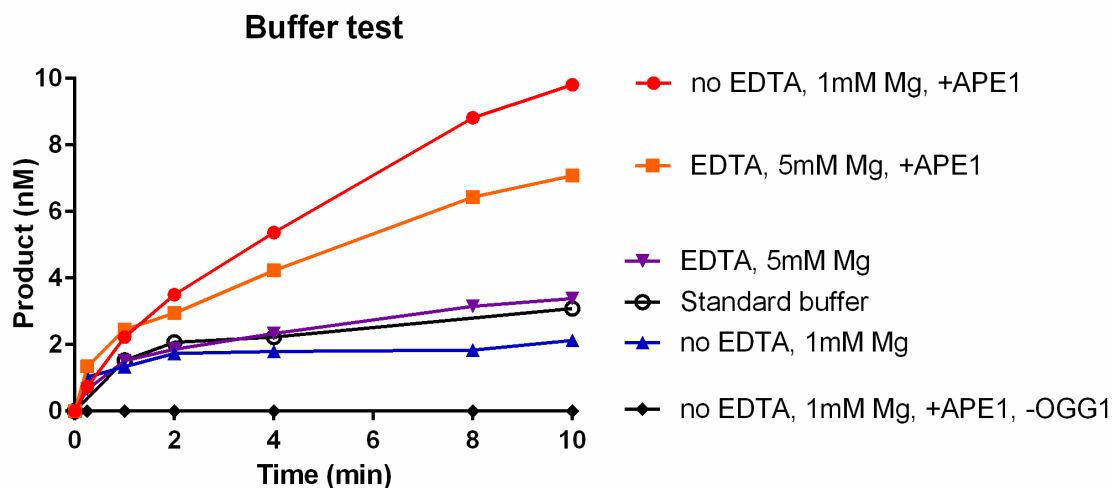


Figure 7.2. Reactions containing APE1 require buffer devoid of EDTA and a minimum of 1mM MgCl₂. 20 nM of S^{0oxoG} reacted with 1 nM hOGG1 in the presence and absence of 10 nM APE1 under the listed modifications of the standard reaction buffer used in Chapter 5 (EDTA concentration was 1mM if used). Removal of EDTA and addition of 1 mM MgCl₂ had no effect on the reaction by hOGG1 (compare blue triangles to black open circles), but was essential for a maximal effect by APE1 (compare red circles to orange squares). Additional of MgCl₂ and APE1 does not generate any background reaction in the absence of hOGG1 (black diamonds). Experiments without APE1 will use the standard reaction buffer and those with APE1 will have no EDTA and 1 mM MgCl₂.

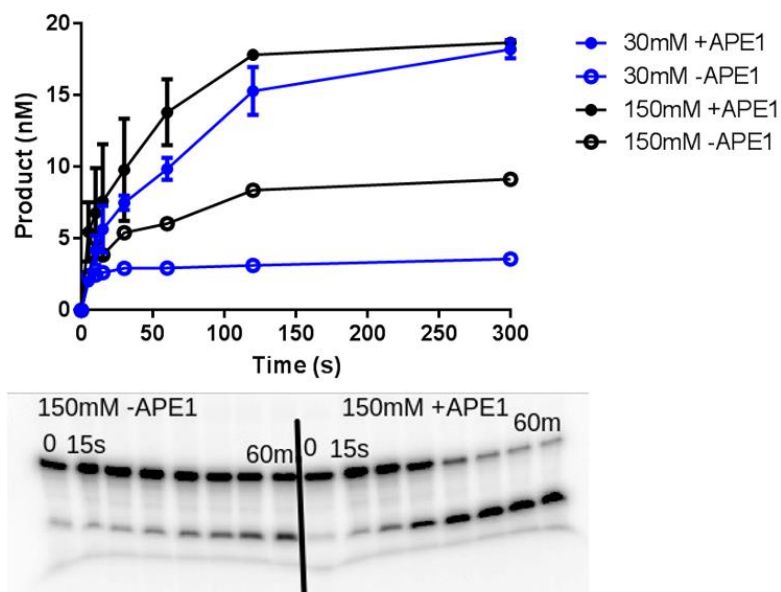


Figure 7.3. Addition of APE1 rescues hOGG1 regardless of ionic strength. 1 nM hOGG1 was spiked into a solution containing 20 nM $S0^{oxoG}$ pre-mixed with 100nM APE1. The burst height observed in the absence of APE1 disappears in the presence of APE1, indicating that APE1 prevents hOGG1 from remaining bound to its product site. The fits here are not quantitative given the large rate of reaction captured in the time course.

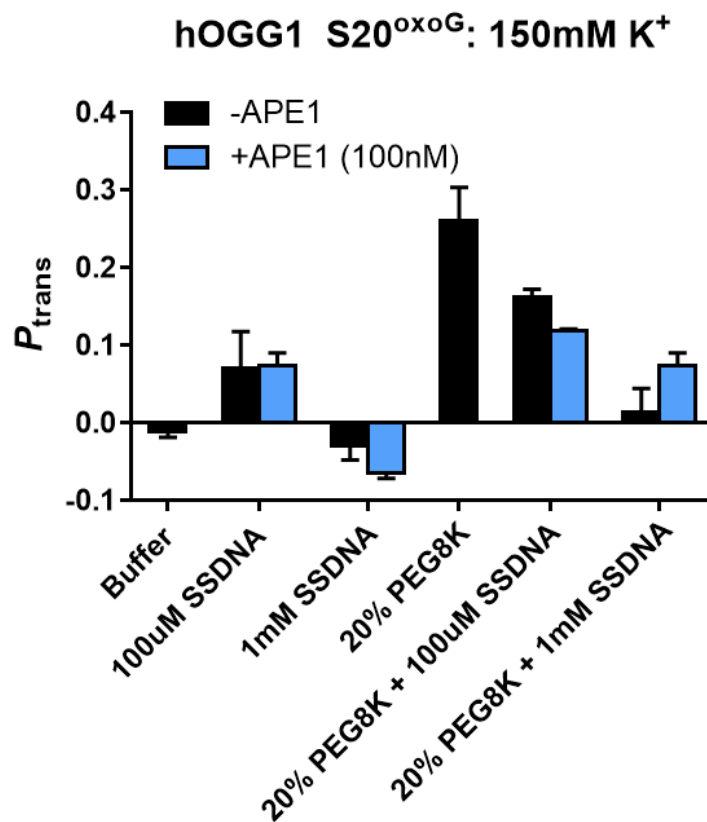


Figure 7.4. Addition of APE1 has no effect on P_{trans} . Addition of 10 nM APE1 had no effect on the ability of hOGG1 to translocate along S20^{oxoG} in 150mM K⁺ buffer containing either ssDNA alone or in addition to 20% PEG 8K. APE1 enhances the reaction rate, but does not actively participate in hOGG1's facilitated diffusion mechanism.

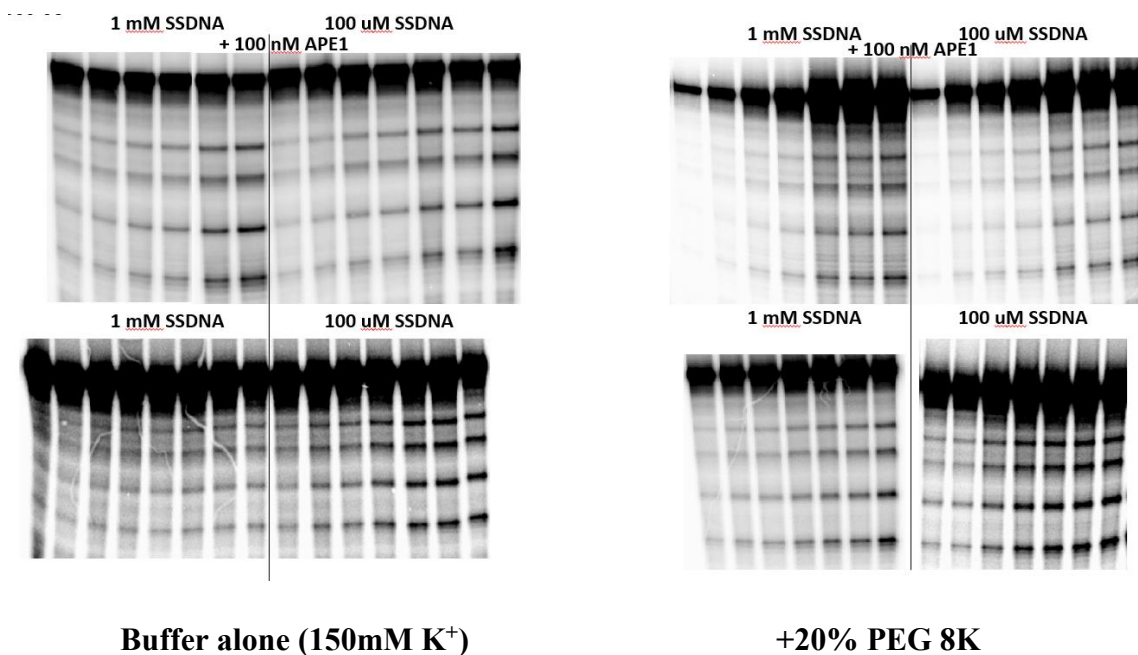


Figure 7.5. Example gels of hOGG1 reacting with S20^{oxoG} with and without the addition of APE1. hOGG1 was spiked into a solution containing S20^{oxoG} pre-mixed with APE1. Time points (min): 5, 10, 20, 30, 40, 60, 120.

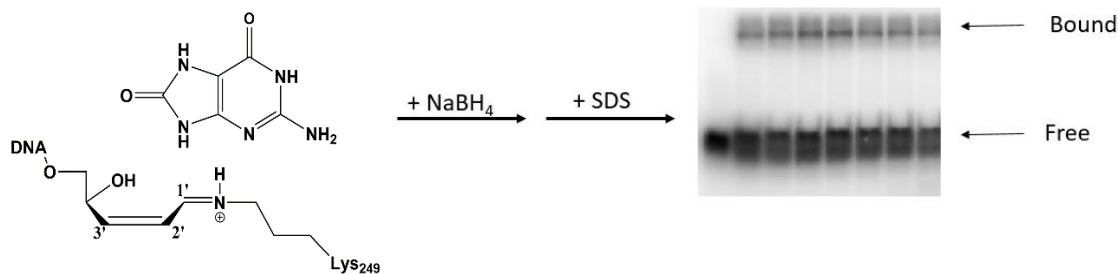


Figure 7.6. Reaction scheme for hOGG1-DNA covalent complex trapping. Reactions are carried out using 5' ³²P-labeled 20 nM S0^{oxoG} and 10 nM hOGG1 and are initiated by addition of an equal volume of hOGG1 for instantaneous mixing. Mixtures are incubated at 37°C and the covalent complex is reduced by mixing of a 6 uL aliquot with 6 uL of 200 mM NaBH₄ at various time points. Reduction is quenched by addition of an equal volume (12 uL) of standard SDS loading dye after 15 minutes. A 10% SDS-PAGE was pre-run at 150 V for 25 min, samples were loaded without heating, and run on the gel at 150 V for 25 min. Gels were dried (30 min per gel) and exposed overnight.

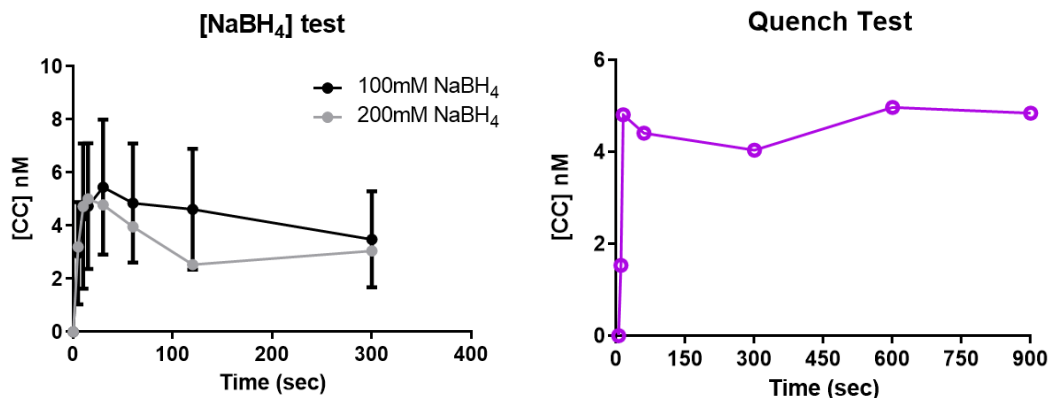


Figure 7.7. Controls to determine appropriate NaBH₄ concentration and timing of SDS quench addition. All reactions were performed with 20 nM S⁰_{oxoG} and 10 nM hOGG1 in 30 mM K⁺ buffer. 100 mM NaBH₄ is sufficient for reducing all covalent complexes formed in solution as shown by identical amounts captured by 100 mM and 200 mM NaBH₄ on the left. The quench test on the right was performed by initiating 6 separate reactions and adding 100 mM NaBH₄ after 20 seconds. Reactions were quenched at the indicated times with SDS loading dye. Test reveals that the quench should be added at least 10 seconds after NaBH₄ and quenching can be delayed for at least 15 min without an effect on the amount of covalent complex trapped.

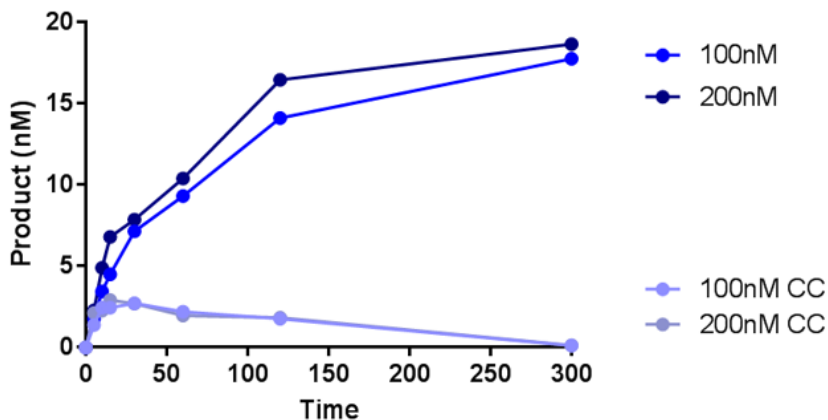


Figure 7.8. Addition of 100 nM APE1 is sufficient for maximal effect on hOGG1. Data represents reaction with $S^{0\text{oxoG}}$ (20nM) and hOGG1 (1nM) in 30 mM K^+ buffer. “100nM” and “200 nM” data are from denaturing PAGE and quantification of total product formation in the presence of 100 nM and 200 nM APE1, respectively. “100 nM CC” and “200 nM CC” are SDS-PAGE covalent complex trapping experiments in which the y-axis represents the amount of covalent complex formed at each time point in the presence of 100 nM and 200 nM APE1, respectively.

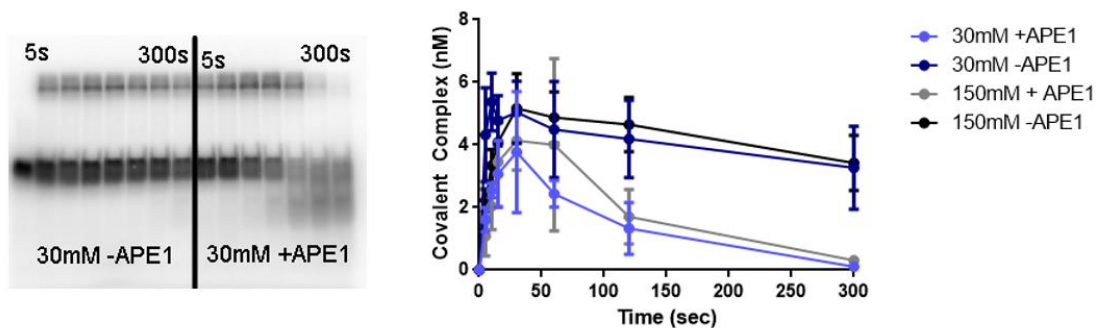


Figure 7.9 Addition of APE1 reduces the lifetime of the hOGG1 covalent complex. An example gel on the left shows the amount of covalent complex (top band) between 10 nM hOGG1 and formed in the presence and absence of 100 nM APE1. On the right are the quantified amounts of complex. Without APE1, an equilibrium is established between free and trapped hOGG1, which appears impervious to salt. The trapped enzyme is rescued by addition APE1.

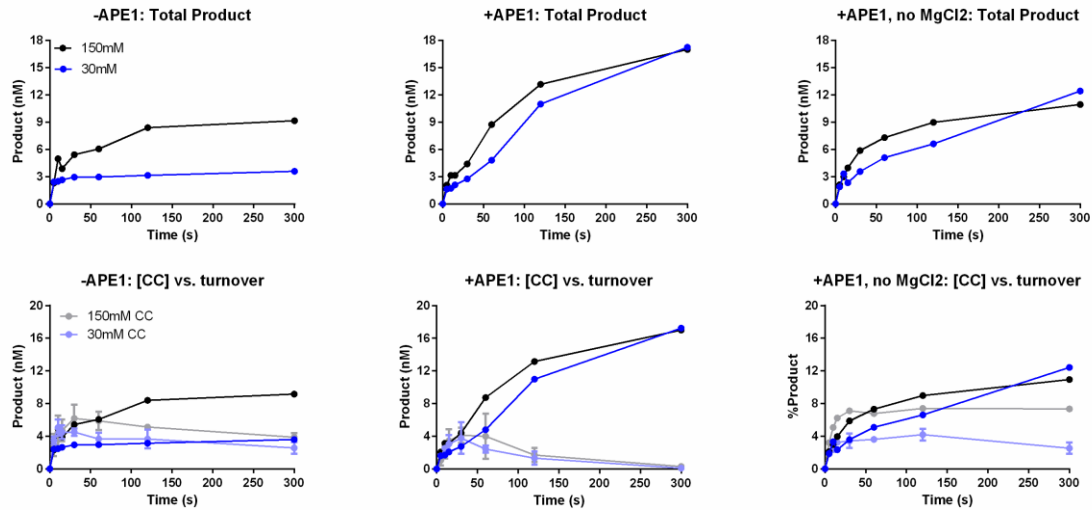


Figure 7.10. Effect of active and inactive APE1 on turnover and covalent complex lifetime. The top left panel is a recapitulation of the data in Figure 7.1 and the bottom left shows that data superimposed with the amount of covalent complex formed without APE1 (Figure 7.9). There is only a minor benefit to turnover and no effect on the covalent complex by addition of salt. The middle panel are the same conditions with the addition of 100 nM APE1. APE1 stimulates turnover of hOGG1 (top) and significantly reduces the lifetime of the covalent complex (bottom) regardless of salt concentration. The right panel shows the effect of inactive APE1 (no MgCl₂). APE1 can still facilitate turnover, but has a more pronounced effect at low salt. This is most likely due to tighter nonspecific binding of APE1 to the abasic DNA at low salt, which more efficiently prevents hOGG1 from rebinding. The amount of covalent complex sustained in the presence of inactive APE1 is lower at low salt.

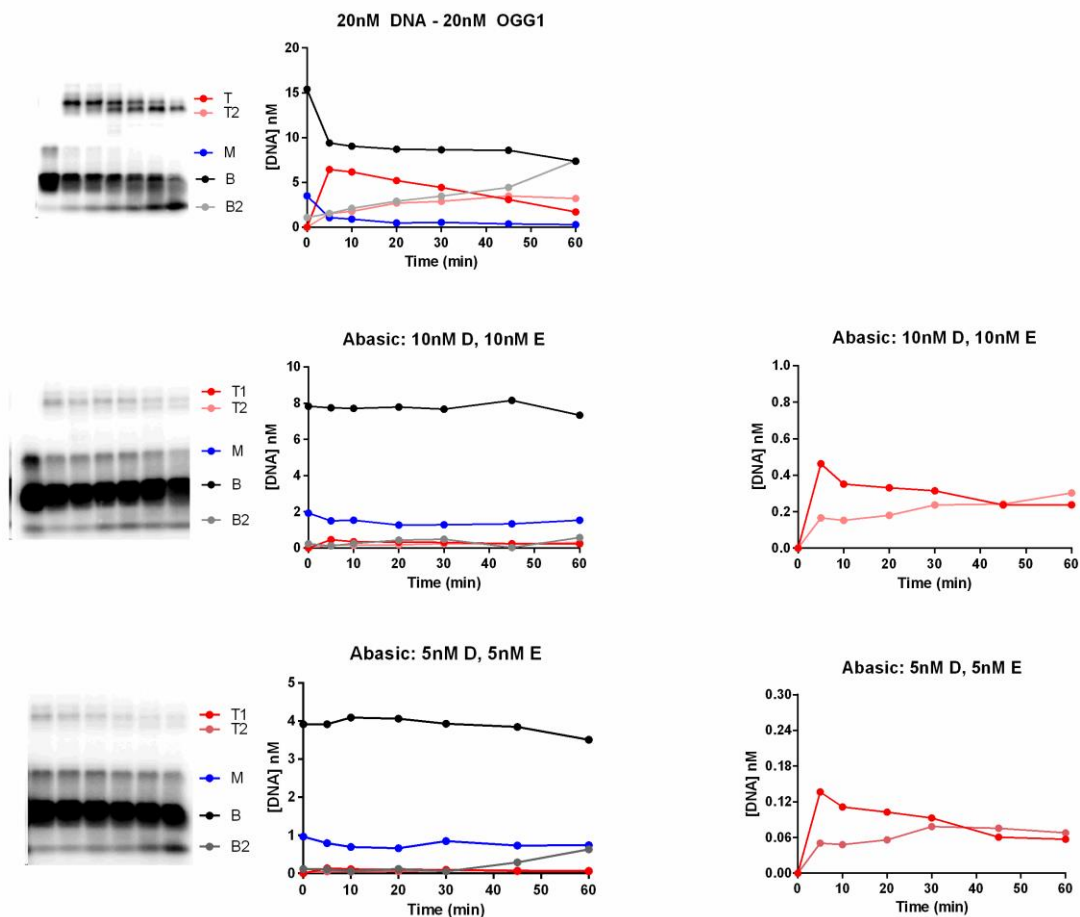


Figure 7.11. Covalent complex trapping using hOGG1 and pre-formed abasic DNA.

Abasic DNA was generated by using a modified version of $S0^{oxoG}$ containing a U-C pair instead of an $oxoG$ -C pair. 20 – 40 nM of the DNA was incubated with 250 pM hUNG at 37°C for 40 min. This was sufficient for hUNG to cleave all of the uracil from the DNA. The DNA was then mixed with an equal volume of hOGG1 to generate mixed solutions with the final concentrations noted above. Covalent complex trapping was quenched by addition of SDS buffer after 15 min. Multiple trapped bands are detectable, which could indicate lyase activity by hOGG1, but this has yet to be confirmed.

7.4. Generation of inducible hOGG1 cell line

For the purpose of future *in vivo* investigations into facilitated diffusion of hOGG1, an inducible cell line was generated. The purpose of this cell line was to allow for control of expression of hOGG1 both in terms of when it is expressed and how much of it is expressed. The cell line was generated using a knock-out HAP1 cell line purchased from Haplogen.

1. hOGG1 gene was ligated into the pENTR4 entry vector (Sall and BamHI sites).
2. hOGG1 gene was transferred to the pCW57.1 destination vector using a homologous recombination kit.
3. Vector was digested to confirm the presence of the hOGG1 gene. (Figure 7.12)
Insert removed from pCW57.1 is the same size as the hOGG1 gene, so a triple digest was done.
4. Lenti-virus was generated using the pCW57.1-hOGG1 vector.
5. 7 serial dilutions of virus were used to spin infect cells.
6. Selection was carried out for ~1 week in the presence of 1 $\mu\text{g}/\text{mL}$ puromycin. The cells infected with the 4 highest concentrations of virus survived.
7. Inducible expression test was successfully carried out using doxycycline (Figure 7.13).

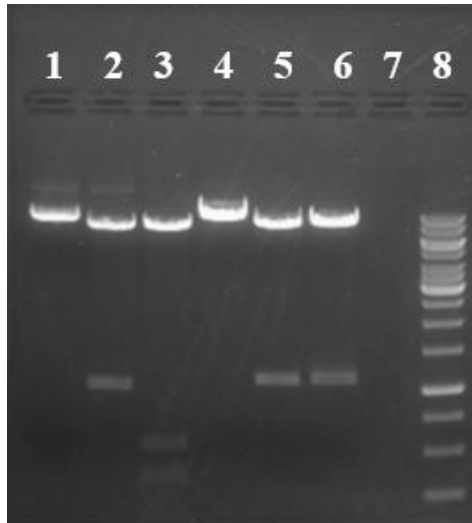


Figure 7.12. Digestion of pCW57.1 before and after homologous recombination step. Sequential triple digest was performed to verify presence of the hOGG1 gene. Digestion was performed on pCW57.1 after recombination with pENTR4-hOGG1 and before. PstI was used to cleave the hOGG1 gene at two sites in order to distinguish it from the pCW57.1 fragment that is removed by BamHI and SalI. Lanes: (1-3 are pENTR4-hOGG1) 1: +SalI, 2: +SalI and BamHI, 3: +SalI, BamHI, and PstI; (4-6 are pENTR4) 4: +SalI, 5: +SalI and BamHI, 6: +SalI, BamHI, and PstI; 7: empty lane; 8: ladder.

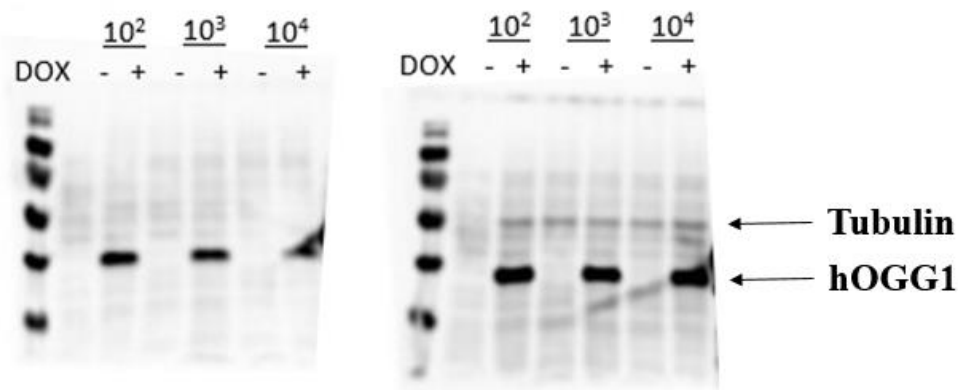


Figure 7.13. Test induction of hOGG1 expression using doxycycline. Three cell lines generated from the 2nd, 3rd, and 4th highest concentrations of virus (10², 10³, 10⁴) were grown up in Tet-free media. Cells were split into two flasks with and without 1 µg/mL doxycycline (DOX) was added to one flask. Cells were lysed after 48 hours. 7.8 µg of total protein was added to each lane. Samples were run on a 12% SDS-PAGE at 220V for 48 min. After transfer to a nitrocellulose membrane, membrane was blocked overnight at 4°C. 1:10,000 of primary antibody Rb OGG1 and 1:2,000 of secondary antibody goat polyclonal anti-rabbit were used. The top gel was also mixed with the tubulin primary antibody of the same dilution.

7.5. REFERENCES

1. Vidal, A. E., Hickson, I. D., Boiteux, S., and Radicella, J. P. (2001) Mechanism of stimulation of the DNA glycosylase activity of hOGG1 by the major human AP endonuclease: Bypass of the AP lyase activity step. *Nucleic Acids Res.* 29, 1285-1292.
2. Sidorenko, V. S., Nevinsky, G. A., and Zharkov, D. O. (2007) Mechanism of interaction between human 8-oxoguanine-DNA glycosylase and AP endonuclease. *DNA Repair (Amst).* 6, 317-328.

Curriculum vitae

Shannen L. Cravens

Birth: July 25th, 1989 Laguna Hills, CA

Education:

- 2011 - Current **Johns Hopkins University School of Medicine**
Program in Molecular Biophysics
Ph.D. Advisor: James T. Stivers
Thesis Title: From test tube to the human cell nucleus: The nature of “invisible” damage search transition states of human DNA glycosylases
- 2007 - 2011 **University of San Diego**
Department of Chemistry and Biochemistry
Research Advisors: Tammy J. Dwyer, Deborah C. Tahmassebi
Topic: NMR structural studies of Actinomycin D bound to non-natural DNA
- 2010 **University of Washington**
Department of Chemistry
Research Advisor: Gabriele Varani
Topic: NMR structural studies of microRNA-21 and 18a

Peer Reviewed Publications

1. **Cravens, S.L.**, Schonhoft, J.D., Rowland, M.M., Rodriquez, A.A., Anderson, B.G., Stivers, J.T., “Molecular crowding enhances facilitated diffusion of two human DNA glycosylases,” *Nucleic Acids Research*, **2015**, *43* (8), 4087-4097.
2. **Cravens, S.L.**, Hobson, M., Stivers, J.T., “Electrostatic properties of complexes along a DNA glycosylase damage search pathway,” *Biochemistry*, **2014**, *53* (48), 7680-7692.
3. Hansen, E. C., Seamon, K. J., **Cravens, S. L.**, Stivers, J. T., "GTP activator and dNTP substrates of HIV-1 restriction factor SAMHD1 generate a long-lived activated state," *PNAS*, **2014**, *11* (8), E1843-E1851.
4. **Cravens, S.L.**; Navapanich, A.C.; Geierstanger, B.H.; Tahmassebi, D.C.; Dwyer, T.J.; “NMR Solution Structure of a DNA-Actinomycin D Complex Containing a Non-Hydrogen Bonding Pair in the Binding Site”, *J. Am. Chem. Soc.*, **2010**, *132* (49), 17588-17598.

Awards and Fellowships

1. **National Institute of Health National Research Service Award**, 2015-2016
2. **National Science Foundation Graduate Fellowship Honorable Mention**, 2013
3. **Owen Graduate Fellowship**, Johns Hopkins University, 2011 – 2014
4. **Outstanding Senior Academic Award**, University of San Diego, 2011
5. **Research Excellence Award**, University of San Diego, 2011
6. **Dr. Eugene Labovits Award for Academics**, University of San Diego, 2011
7. **Student Leadership Award**, American Chemical Society, 2010
8. **Gladys Anderson Emerson Scholarship**, Iota Sigma Pi, 2010
9. **Barry M. Goldwater Scholarship Nominee**, University of San Diego, 2009 and 2010
10. **Alice B. Hayes Scholarship**, University of San Diego, 2009
11. **CRC Press Freshman Achievement Award**, University of San Diego, 2008

Research Conference Presentations

1. “Differential Effects of Ions, Molecular Crowding, and Solution DNA Density on the Damage Search Mechanisms of hOGG1 and hUNG.” **Cravens, S.L.**, Stivers, J.T., *Biophysical Society Annual Meeting*, Los Angeles, CA, 2016
2. “Molecular crowding enhances facilitated diffusion of two human DNA glycosylases.” **Cravens, S.L.**, Schonhoft, J.D., Rowland, M.M., Rodriguez, A.A., Stivers, J.T., *Biophysical Society Annual Meeting*, Baltimore, MD, 2015.
3. “NMR and computational studies of DNA duplexes containing the guanine isostere 4-fluoro-6-methylbenzimidazole.” Navapanich, A.C., Sadler, H., **Cravens, S.L.**, Sacknoff, S., Dwyer, T.J., Tahmassebi, D.C., *241st ACS National Meeting*, Anaheim, CA, 2011.
4. “NMR solution structure of an actinomycin D:DNA complex containing a non-hydrogen bonding pair in the binding site.” **Cravens, S.L.**, Navapanich, A.C., Dwyer, T.J., Tahmassebi, D.C., *239th ACS National Meeting*, San Francisco, CA, 2010.

Teaching Experience

- **Johns Hopkins Preparing Future Faculty Teaching Academy (Fall 2014-15)**
 - Instructor of Record for semester-long undergraduate level “Chemistry with Problem Solving” course (*Fall 2015*)
 - Summer Teaching Institute 3-day workshop (*May 27 – 29, 2015*)
 - An Introduction to Evidence-Based Undergraduate STEM Teaching Course, (*Oct. – Nov. 2014*) Center for the Integration of Research, Teaching, and Learning (CIRTL)